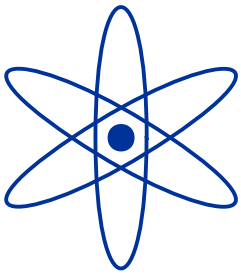

PHYSIK-DEPARTMENT

MAX-PLANCK-GESELLSCHAFT

Ultrasoft Renormalization of the Potentials in vNRQCD

Dissertation

von

Maximilian Stahlhofen

2008

TECHNISCHE
UNIVERSITÄT
MÜNCHEN

TECHNISCHE UNIVERSITÄT MÜNCHEN

Max-Planck-Institut für Physik
(Werner-Heisenberg-Institut)

Ultrasoft Renormalization of the Potentials in vNRQCD

Maximilian Horst Stahlhofen

Vollständiger Abdruck der von der Fakultät für Physik
der Technischen Universität München
zur Erlangung des akademischen Grades eines
Doktors der Naturwissenschaften (Dr. rer. nat.)
genehmigten Dissertation.

Vorsitzender:		Univ.-Prof. Dr. L. Oberauer
Prüfer der Dissertation:	1.	Priv.-Doz. Dr. A. H. I. Hoang
	2.	Univ.-Prof. Dr. A. J. Buras

Die Dissertation wurde am 30.12.2008
bei der Technischen Universität München eingereicht und
durch die Fakultät für Physik am 18.02.2009 angenommen.

Abstract

The effective field theory vNRQCD allows to describe among others the production of top-antitop pairs in electron-positron collisions at threshold, i.e. with very small relative velocity $v \ll 1$ of the quarks. Potentially large logarithms $\propto \ln v$ are systematically summed up and lead to a scale dependence of the Wilson coefficients of the theory.
The missing contributions to the cross section $\sigma(e^+e^- \to t\,\bar{t})$ in the resonance region at NNLL level are the so-called mixing contributions to the NNLL anomalous dimension of the S-wave production/annihilation current of the topquark pair. To calculate these one has to know the NLL renormalization group running of so-called potentials (4-quark operators). The dominant contributions to the anomalous dimension of these potentials come from vNRQCD diagrams with ultrasoft gluon loops.
The aim of this thesis is to derive the complete ultrasoft NLL running of the relevant potentials. For that purpose the UV divergent parts of about 10^4 two-loop diagrams are determined. Technical and conceptional issues are discussed. Some open questions related to the calculation of the non-Abelian two-loop diagrams arise. Preliminary results are analysed with regard to the consequences for the mentioned cross section and its theoretical uncertainty.

Zusammenfassung

Mit der effektiven Feldtheorie vNRQCD lässt sich u.a. die Produktion von Top-Antitop-Paaren in Elektron-Positron-Kollisionen an der Schwelle, d.h. mit sehr niedriger Relativgeschwindigkeit $v \ll 1$ der Quarks, beschreiben. Potentiell große Logarithmen $\propto \ln v$ werden dabei systematisch aufsummiert und führen zur Skalenabhängigkeit der Wilson-Koeffizienten der Theorie.
Die fehlenden Beiträge zum Wirkungsquerschnitt $\sigma(e^+e^- \to t\,\bar{t})$ im Resonanzbereich auf NNLL Niveau sind die sog. mixing Beiträge zur NNLL anomalen Dimension des S-Wellen-Produktions-/Vernichtungsstroms des Topquark-Paars. Um diese zu berechnen, muss man das NLL Renormierungsgruppenlaufen von sog. Potentialen (4-Quark-Operatoren) kennen. Die dominanten Beiträge zur anomalen Dimension dieser Potentiale stammen von vNRQCD Diagrammen mit ultrasoften Gluon-Schleifen.
Ziel dieser Arbeit ist, es das vollständige ultrasofte NLL Laufen der relevanten Potentiale herzuleiten. Dazu werden die UV divergenten Anteile von ca. 10^4 Zwei-Schleifen-Diagrammen bestimmt. Technische und konzeptionelle Schwierigkeiten werden diskutiert. Im Zusammenhang mit der Berechnung der nicht-abelschen Zwei-Schleifen-Diagramme ergeben sich einige noch offene Fragen. Vorläufige Ergebnisse werden im Hinblick auf die Konsequenzen für den angesprochenen Wirkungsquerschnitt und dessen theoretische Unsicherheit analysiert.

Contents

Chapter 1

Introduction

Among the particles within the Standard Model of elementary particle physics the top quark takes an exposed position due to its very large mass of 172.4 ± 1.2 GeV [1]. That is about 35 times the mass of the bottom quark, the next-to-heaviest fundamental matter particle. Along with the large mass comes a very large decay width $\Gamma_t \sim 1.5$ GeV of the top and correspondingly an extremely short lifetime $\tau_t = \frac{1}{\Gamma_t} \sim 10^{-24} s$. The by far predominant decay mode is $t \to bW^+$.
Both of these (related) properties have interesting consequences. The top mass enters many theoretical predictions of physical precision observables as e.g. the W boson mass through sizable quantum corrections ($\delta m_W \propto m_t^2$). Since there are also contributions from the Higgs mass m_h to δm_W a precise measurement of the W mass yields a good prediction for m_h provided the theoretical uncertainty of m_t is small enough. A high accuracy of the top mass may also help to discriminate between various, in particular supersymmetric, extensions of the standard model. In any case it will play a crucial role in exploring and testing the mechanism of electroweak symmetry breaking.
On the other hand it is the large decay width Γ_t, which only makes sufficiently precise m_t measurements possible, e.g. via a scan over the $t\bar{t}$ production threshold ($\sqrt{s} \sim 2m_t$) at a future e^+e^- collider [2]. It prohibits the formation of physical bound (toponium) states and gives rise to a smooth line-shape of the cross section for top pair production without sharp peaks in the resonance region. Loosely speaking the top quarks decay before they can hadronize [3]. Thus a meaningful perturbative approach to the analysis of the process $e^+e^- \to t\bar{t}$ at threshold using effective field theories becomes feasible, see section 2.2.
Apart from the top mass, which is determined from the value of the center of mass energy $\sqrt{s}$, where the total $t\bar{t}$ production cross section starts to rise, and represents the most prominent quantity to be measured, one can also extract the top Yukawa coupling[1], the strong coupling constant α_s, and of course the top width Γ_t from height and shape of the resonance [6–9]. The latter is particularly

[1]For an alternative measurement of the top Yukawa coupling via Higgs associated top pair production rates see Refs. [4, 5].

interesting for an accurate determination of the CKM matrix elements $|V_{tq}|$ from the respective branching ratios [10] and up to date no sensible method to directly measure Γ_t at hadron colliders like the Tevatron or the LHC is known [11].
Therefore the measurement of the resonance line-shape of the total cross section $\sigma_{\text{tot}}(e^+e^- \to t\bar{t})$ is a major aim of the proposed International Linear Collider (ILC) project [12]. It is expected that at this machine the top "threshold mass"[2] can be determined experimentally with an statistical uncertainty of about 40 MeV and the top width with an accuracy of about 2% [12].
These prospects put high demands on the precision of the theoretical prediction for position and shape of the $t\bar{t}$ resonance in e^+e^- collisions.

The appropriate theoretical tool to perform the corresponding calculations are non-relativistic effective field theories of QCD.
In this thesis we are mainly concerned with the improvement of the theory prediction for the normalization of $\sigma_{\text{tot}}(e^+e^- \to t\bar{t})$ at threshold, which does not affect the top mass measurement, but is crucial for the extraction of precise values for the other quantities mentioned above [9]. It turns out that to achieve a small theory error $\frac{\delta\sigma_{\text{tot}}}{\sigma_{\text{tot}}}$ a renormalization group improved (RGI) calculation summing large logarithmic terms $\propto (\alpha_s \ln v)^n$, where $v \ll 1$ is the velocity of the produced tops in the center of mass (c.m.) frame, is compulsory.
At present QCD fixed order results up to next-to-next-to-leading-order (NNLO), see Refs. [16, 17] for a detailed discussion, and parts of the next-to-next-to-next-to-leading-order (N^3LO) results are available [18–22]. They have been shown to allow for a determination of the top threshold mass with an total uncertainty substantially below 100 MeV, but suffer from a large error $\frac{\delta\sigma_{\text{tot}}}{\sigma_{\text{tot}}} \sim 20\%$ of the cross section normalization (at NNLO) [16].
In contrast the full QCD RGI next-to-leading-logarithmic (NLL) and partly known next-to-next-to-leading-logarithmic (NNLL) predictions [23–25] of $\sigma_{\text{tot}}(e^+e^- \to t\bar{t})$ raise the hope that the normalization uncertainty can be reduced to a value $\frac{\delta\sigma_{\text{tot}}}{\sigma_{\text{tot}}} \lesssim 3\%$, that matches the experimental error. There is however an anomalously large contribution to the NNLL result from the (ultrasoft) renormalization of the production and annihilation current of the top pair at three-loop level [26], which currently leads to $\frac{\delta\sigma_{\text{tot}}}{\sigma_{\text{tot}}} \sim 6\%$, if it is included in the analysis [27].
The missing ingredient for a complete NNLL order QCD prediction is the contribution to the production/annihilation current, that arises from two-loop graphs in the effective field theory and NLL renormalization group (RG) running of the involved four-quark operators, the so called "potentials". It is the aim of this thesis to derive the dominant (ultrasoft) contribution to the NLL running of these potentials. To this end we have to calculate the ultraviolet

[2] The translation of the threshold mass to the theoretically more useful $\overline{\text{MS}}$ mass implies a theoretical uncertainty computed in Ref. [13], see also Refs. [14–16].

(UV) divergences of the two-loop diagrams, which renormalize the potentials. There is a good chance that the results compensate for the large three-loop contribution in the RG evolution of the current and therefore decrease the theoretical uncertainty of the $t\bar{t}$ resonance line-shape to the desired value [28]. Electroweak effects in $\sigma_{\text{tot}}(e^+e^- \to t\bar{t})$, especially from the top decay, up to NNLL order have been studied in Refs. [29, 30]. They mainly affect the position of the resonance peak and thus the measurement of the top mass.

The outline of this work is as follows. In the second chapter the general concept of effective field theories is explained. As an particular representative we review the non-relativistic theory vNRQCD [31], in which quantitative calculations for heavy quark pair production close to threshold can be carried out. We sketch the construction of the effective Lagrangian including "potential", "soft" and "ultrasoft" degrees of freedom and point out the important characteristics of the effective theory.
The third chapter focuses on renormalization issues in vNRQCD. Besides some general subjects we discuss, in section 3.5, operators, which are required for a consistent renormalization and therefore have to be added to the vNRQCD Lagrangian. We argue in particular that operators consisting of six quark fields are necessary to guarantee a straightforward (ultrasoft) renormalization procedure at the multi-loop level. They are introduced in this context for the first time and are shown to be compatible with an earlier method using so called sum operators [32]. The six-quark operators generate an "effective" potential contributing notably to the NNLL anomalous dimension of the current, if two of their fields are contracted. They will therefore play a central role in this work.
In chapter 4 we show in detail how the running of the potentials affects the production/annihilation current of the top pair and therefore the theoretical prediction for $\sigma_{\text{tot}}(e^+e^- \to t\bar{t})$. We recall why NLL results of their coefficients are needed for a sufficient accuracy.
Chapter 5 comprises the full (already known) ultrasoft one-loop (LL) calculation for the relevant potentials in Feynman gauge and sets the stage for the two-loop (NLL) calculation in chapter 6. Specific soft (mixing) contributions are taken into account to obtain a factorized form for the solution of the respective renormalization group equations.
In chapter 6 we derive the new NLL results for the anomalous dimensions of the potentials from diagrams with two ultrasoft gluon loops. This represents the major part of this work. In the course of the calculations we discovered (most likely technical) problems, concerning part of the non-Abelian contributions, which are discussed in detail but are not resolved yet.
We present preliminary results for the NLL running of the potentials and finally analyse them numerically in chapter 7. We also show their impact on the evolution of the production/annihilation current at NNLL level and point up the effects of the problematic terms.

The outcome is very promising, but we refrain from a final conclusion until the issues encountered in chapter 6 are solved.

Part of this work has already been published in Ref. [33].

Chapter 2

The Effective Field Theory vNRQCD

2.1 Basic Concepts of Effective Field Theories

In modern particle physics effective field theories (EFT's) are an essential tool to describe physics in certain kinematic regions, where the corresponding full quantum field theory (QFT) fails to provide efficient techniques for quantitative calculations.
The aim of an EFT is to isolate the physical phenomena in a specific range of parameter space in order to provide an adequate description for them without caring or even knowing about the physics at other scales [34]. This is basically achieved by taking all scales that are below the parameter range of interest to zero and the ones above to infinity. The fact that this procedure, in particular the realization of the latter limit, works - if certain rules are respected, e.g. symmetries are preserved - is owing to the fundamental nature of quantum field theory [35–37].
In elementary particle physics the key parameter is the distance or equivalently the energy/momentum scale at which interactions take place. In particular one is often interested in low energy (large distance) limits of the standard model, where the production of heavy particles is kinematically not allowed and heavy intermediate modes cannot resonate.
Those heavy - or more generally non-resonant - degrees of freedom, correspond to short distance fluctuation modes in the path integral and can be "integrated out" [38, 39], which effectively is nothing else than to remove them from the theory. The formerly non-local interactions among the remaining particles, that were originally mediated by the non-resonant modes, are then reproduced by local operators in an effective Lagrangian. In the simplest setup the operators are organized in a power series within the EFT Lagrangian with the inverse heavy mass scale ($\frac{1}{M}$) as expansion parameter.

Thus to reach a given precision at low energies only a finite number of operators has to be taken into account. Subleading operators in this expansion however have mass dimension greater than four. The EFT is therefore non-renormalizable in the conventional sense [38]. Nevertheless it can be rendered finite to any precision by renormalizing the (Wilson) coefficients of the EFT operators up to the respective order in $(\frac{1}{M})$, provided that the underlying full QFT is renormalizable. Hence the perturbation theory approximation for physical observables remains still predictive. This is what is meant by renormalizability in the "modern" sense [40, 41].

Once the form of the relevant (possible) EFT operators is identified, effective and full theory have to be "matched" to obtain values for the couplings and Wilson coefficients, the so called "matching conditions". In practice the coefficients of the EFT are fixed by demanding that both theories produce the same results at the high scale ($\sim M$) up to the required order in $\frac{1}{M}$. For that purpose the renormalization scale μ in both theories is chosen to be $\sim M$. In order to avoid large logarithms and thus to provide sensible matching conditions, it is important to establish the connection between full and effective theory at a scale ($\sim M$), where the perturbative expansion of the full theory is under control. In cases where the matching calculation cannot be performed, either due to non-perturbative effects even at the high scale or because the underlying theory is simply not known, the values for the coefficients at a specific scale have to be extracted from experiments.

To actually apply the EFT constructed in this way, one has to run down all the coefficients (couplings) to the energy/momentum scale E ($\ll M$) of the process one is interested in by means of renormalization group equations (RGE's), which are derived in the EFT. Since interaction generated by a $(k+4)$ dimensional operator is of the order $(\frac{E}{M})^k$ (compared to the leading order kinetic terms), the accuracy of the predictions made by the EFT, that contains a finite number of such operators, increases by lowering E. At least as long as non-perturbative effects like confinement in QCD are negligible. Since the low energy EFT is supposed to correctly reproduce the dynamics of the full theory in the infrared (IR) it is clear that an essential feature of a proper EFT is to produce the same IR singularities.

The advantages of the EFT approach to QFT problems are numerous.
First of all the particle content of an EFT is typically less than in the underlying theory, usually simplifying actual calculations enormously. One speaks of "decoupling" of heavy particles [42].
Secondly the number of symmetries in the EFT is often increased: approximate symmetries of the full theory can be systematically made manifest in the EFT up to a certain order in the perturbative $(\frac{1}{M})$ expansion. A greater amount of symmetry generally produces additional powerful theoretical tools and can save one a lot of work in deriving theory predictions.
Last but not least a third advantage, which is crucial for this work, is the possi-

bility to resum potentially large "non-renormalization-group" logarithms of the full QFT, which might spoil the perturbation series, by actually transforming them into renormalization group logarithms in the EFT.

Famous and very successful examples for EFT's are e.g. Chiral Perturbation Theory (ChPT), "Fermi Theory" of weak interactions and "Heavy Quark Effective Theory" (HQET) [43], that has been designed for mesons consisting of a heavy and a light quark. In this thesis we will work with a version of "Non-Relativistic Quantum Chromodynamics" (NRQCD). It describes the physics of heavy quarkonia, in particular $t\bar{t}$-systems.

The basic principles of construction and application of EFT's are best explained using an explicit example. We will therefore shortly demonstrate them, focussing in particular on the above mentioned summation of large logarithms, by sketching a short calculation in a simplified version of Fermi theory [37].
Consider the standard model diagram for the electroweak decay of a bottom quark in Fig. 2.1 *a*) and the one-loop QCD correction in Fig. 2.1 *b*). We will neglect here any other decay channels as well as non-perturbative effects - in fact we regard the b quark as an unconfined particle - and set the light quark masses $m_u = m_d = 0$ for the sake of simplicity.

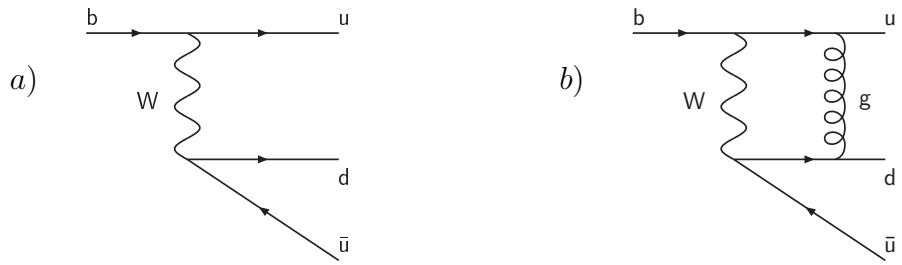

Figure 2.1: Tree level *a*) and one-loop *b*) standard model diagrams for b quark decay.

We find that the loop in Fig. 2.1 *b*) is finite and

$$\frac{\text{Fig. 2.1 } b)}{\text{Fig. 2.1 } a)} \;\sim\; \alpha_s\Big(\,\#\,+\,\ln\Big(\frac{m_b^2}{m_W^2}\Big)\Big) \;\sim\; \mathcal{O}(1)\,, \tag{2.1}$$

where # represents some number of $\mathcal{O}(1)$. Due to the large disparity of the scales m_W and m_b the logarithm in Eq. (2.1) is sizable (~ 6) and compensates for the α_s (~ 0.2) suppression of the one-loop corrections. Moreover we expect that adding further gluon loops to the one-loop graph produces large logarithms of this kind at all orders in the (α_s) perturbation series. This will obviously spoil the theoretical prediction for the process unless we find a way to resum all logarithmic terms $\sim \left[\alpha_s \ln\left(\frac{m_b^2}{m_W^2}\right)\right]^n$.

The trick is to integrate out the heavy W-boson and work in an EFT framework. In fact we are going to consider the limit, where $m_W \to \infty$ turning the logarithm in Eq. (2.1) into an UV logarithm.

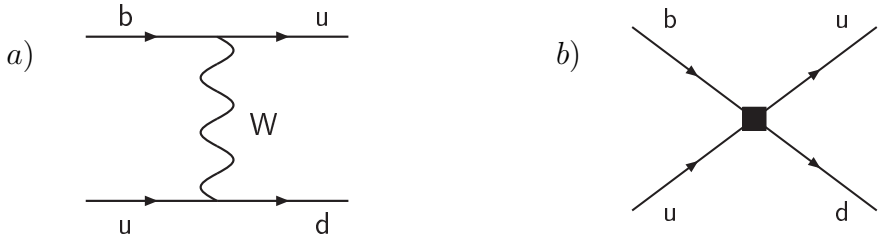

Figure 2.2: Four quark interaction mediated by a W-boson in the full theory a) and corresponding EFT interaction vertex b), where the W-boson has been integrated out.

To set up an suitable effective Lagrangian we take the full theory amplitude of the non-local interaction - the quark-W vertices are separated in spacetime when switching to position space - in Fig. 2.2 a) and expand in the inverse large mass ($\frac{1}{m_W}$):

$$\begin{aligned} \mathcal{A} &= \left(\frac{ig}{\sqrt{2}}\right)^2 V_{ub}V_{ud}^* \; (\bar{u}\,\gamma^\mu\,P_L\,b)\,(\bar{d}\,\gamma^\nu\,P_L\,u)\left(\frac{-ig_{\mu\nu}}{p^2-m_W^2}\right) = \\ &= \frac{i}{m_W^2}\left(\frac{ig}{\sqrt{2}}\right)^2 V_{ub}V_{ud}^* \; (\bar{u}\,\gamma^\mu\,P_L\,b)\,(\bar{d}\,\gamma_\mu\,P_L\,u) + \mathcal{O}\left(\frac{1}{m_W^4}\right). \end{aligned} \tag{2.2}$$

The leading order term of this expansion can also be generated by a local dimension 6 operator in the EFT:

$$O_1 = -\frac{4G_F}{\sqrt{2}}V_{ub}V_{ud}^* \; (\bar{u}\,\gamma^\mu\,P_L\,b)\,(\bar{d}\,\gamma_\mu\,P_L\,u)\,, \tag{2.3}$$

where $\frac{G_F}{\sqrt{2}} \equiv \frac{g^2}{8m_W^2}$. The associated Feynman graph is depicted in Fig. 2.2 b). To account for a possible renormalization scale dependence of O_1 beyond the one of its components (fields and couplings) we assign a Wilson coefficient C_1 to it. Thus the (renormalized) EFT Lagrangian contains a piece

$$\delta\mathcal{L} = C_1(\mu)\,O_1(\mu) \tag{2.4}$$

besides the usual full theory kinetic terms for the quarks.
We can now redo the one-loop calculation for the b decay up to $\mathcal{O}(\frac{1}{m_W^2})$ in the EFT using dimensional regularization and the $\overline{\text{MS}}$ renormalization scheme. As

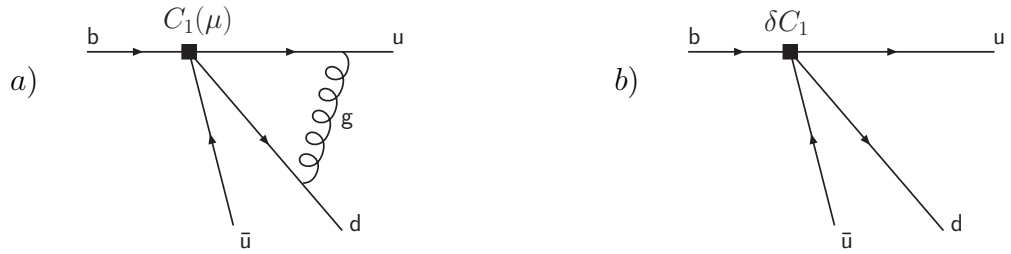

Figure 2.3: *a*) One-loop EFT diagram for b quark decay. The UV divergence from the loop in *a*) is absorbed by the counterterm in *b*).

expected the EFT one-loop diagram in Fig. 2.3 *a*) is (logarithmically) UV divergent:

$$\text{Fig. 2.3 } a) \quad \sim \quad \alpha_s \, C_1(\mu) \, \Big(\frac{1}{\epsilon} \, + \, \ln\Big(\frac{m_b^2}{\mu^2}\Big) \, + \, \# \Big) \, . \tag{2.5}$$

This UV divergence must be cancelled by the counterdiagram in Fig. 2.3 *b*) and we can set up a RGE of the form

$$\frac{d}{d\ln\mu^2} C_1(\mu) \, \sim \, \alpha_s(\mu) \, C_1(\mu) \, , \tag{2.6}$$

the analytic solution of which gives rise to an infinite sum of (LL) logarithms, when expanded in α_s:

$$C_1(\mu) \, = \, C_1(\mu_0) + \sum_{n=1}^{\infty} c_n \Big[\alpha_s \ln\Big(\frac{\mu^2}{\mu_0^2}\Big) \Big]^n \, , \tag{2.7}$$

where the c_n are coefficients of $\mathcal{O}(1)$.
Knowing the RG running of $C_1(\mu)$ we have to fix a starting value $C_1(\mu_0)$. As pointed out above, this is done by matching to the full theory at the high scale, in this case m_W. The (tree-level) matching calculation is sketched in Eq. (2.8), where $p^2 = \mu^2 = m_W^2$ is chosen in order to avoid large logarithms in full theory loop diagrams like Fig. 2.1 *b*), where we had $p^2 \sim m_b^2$.

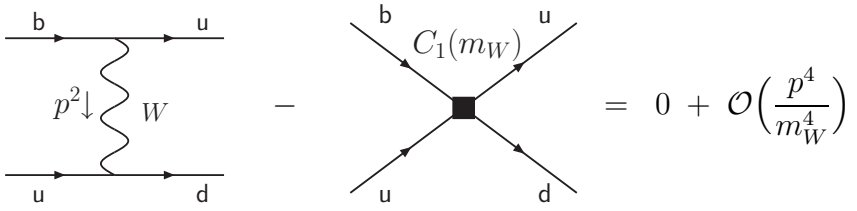

$$= \; 0 \; + \; \mathcal{O}\Big(\frac{p^4}{m_W^4}\Big) \tag{2.8}$$

At tree-level the result is trivially $C_1(m_W) = 1$ due to our construction of O_1 by expanding the full theory amplitude in Eq. (2.2). It will normally be more

complicated, if NLL running of $C_1(\mu)$ and correspondingly one-loop matching is considered [44]. To determine $C_1(\mu_0)$ in Eq. (2.7) we choose $\mu_0 = m_W$ and obtain $C_1(\mu_0 = m_W) = 1$.

The final result for the b decay in the EFT up to $\mathcal{O}(\alpha_s)$ and $\mathcal{O}\big(\frac{m_b^2}{m_W^2}\big)$ is then given by

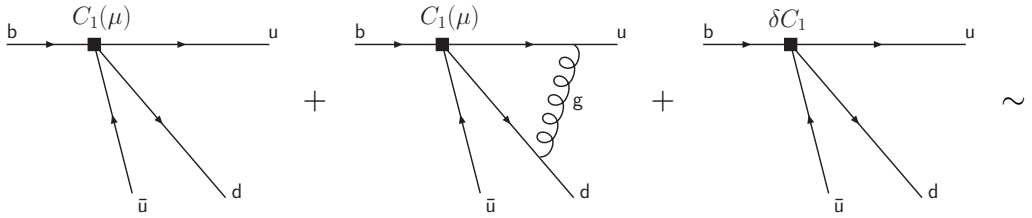

$$\sim \ \#\, G_F\, C_1(\mu) \ + \ G_F\, \alpha_s\, C_1(\mu)\, \Big(\, \# \ + \ \ln\Big(\frac{m_b^2}{\mu^2}\Big)\, \Big) \ . \tag{2.9}$$

To render the EFT logarithms $\ln\big(\frac{m_b^2}{\mu^2}\big)$ small at all orders of α_s we better choose now $\mu \sim m_b$. This choice sums at the same time all the full theory logarithms $\big[\alpha_s \ln\big(\frac{m_b^2}{m_W^2}\big)\big]^n$ in the analytic expression for the Wilson coefficient $C_1(\mu = m_b)$ as shown in Eq. (2.7).
Thus we finally found the desired result, which includes the problematic logarithms from all orders of the loop expansion, at the cost of loosing precision by omitting terms $\sim \frac{m_b^2}{m_W^2} < 1\%$ in Eq. (2.9). We could in principle increase the predictive power of the EFT up to any required precision by taking also dimension ≥ 8 operators in the effective Lagrangian, Eq. (2.4), into account. As for every perturbative QFT calculation this is however connected in practice to an exponentially growing amount of additional work.
The reason why the $\frac{1}{m_W}$ expansion implemented in the EFT framework also works for (UV divergent) loop diagrams, where we integrate over the whole momentum space, is that it only affects the UV structure of the theory and possible discrepancies to the full theory are corrected by the matching procedure or absorbed into (local) counterterms [45].

The EFT treatment of large logarithms $\sim \ln\big(\frac{m_b^2}{m_W^2}\big)$ presented here is, although much simpler, similar to the way we will sum up QCD logarithms of the form $\ln\frac{mv}{m}$, $\ln\frac{mv^2}{m}$ and $\ln\frac{mv^2}{mv}$ using vNRQCD in the course of this thesis.

To address the issue of renormalizability in the EFT consider UV divergent loops involving more than one higher dimensional operator (mass dimension > 4) like the one displayed in Fig. 2.4 *a*). At the first sight there is an infinite number of n-loop diagrams of this type with increasing number of legs. Therefore an infinite number of operators is required to absorb the divergences. Thus the EFT is regarded as non-renormalizable in the original sense [38].

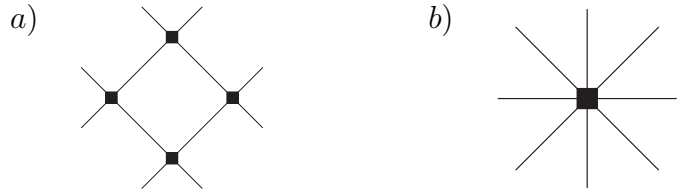

Figure 2.4: *a*) UV divergent EFT one-loop diagram including four operators of mass dimension > 4. *b*) Eight-field operator, whose RG running is affected by the divergence in *a*).

Looking at the $\frac{1}{m_W}$ power counting, we find however that the operator in Fig. 2.4 *b*), which is supposed to cancel the divergence in Fig. 2.4 *a*), is already at least of order $G_F^4 \sim \frac{1}{m_W^8}$ and therefore highly suppressed against the leading order interactions. This is a general feature of EFT's: at a given precision we only have to renormalize a finite set of operators and can safely ignore higher order divergences.
This kind of order by order renormalization only works, if the set of parameters needed to absorb the divergences from loop diagrams involving a fixed number of higher dimensional operators is finite. I.e. if the corresponding full theory is renormalizable in the conventional sense.

As a final remark we would like to emphasize, that interpreting the standard model itself as (the leading order terms of) an EFT motivates the construction of additional operators of higher mass dimension (> 4) that could describe new physics. By comparing the predictions from such extended models to experiments, information about the underlying theory can be gained.

2.2 Top Quark Threshold Physics

In the threshold region of quark-antiquark pair production, e.g. in $e^+e^- \to t\,\bar{t}$, where the kinetic energy of the quarks and their (relative) velocity v in the center-of-mass (c.m.) frame is small ($v \ll 1$), physics is generally governed by three different energy/momentum scales: the quark mass m, the quark three-momentum $\mathbf{p} \sim mv$ and the kinetic energy of the quarks $E \sim mv^2$. These are referred to as the "hard", the "soft" and the "ultrasoft" scales. For strong interacting systems in addition the hadronization scale Λ_{QCD} can be relevant.
The large separation of scales at low velocities ($v \sim 0.1$) gives rise to two main conceptual problems, when using conventional perturbation theory in standard model calculations that aim to describe the production process close to threshold. The first one originates from so called "Coulomb singularities". These are terms

$\sim \left[\frac{\alpha_s}{v}\right]^n$ that appear in the non-relativistic expansion of production diagrams at all orders of perturbation theory. Every further insertion of an intermediate gluon between the non-relativistic quark lines in Fig. 2.5 comes along with an additional factor of $\frac{1}{v}$ at leading order.

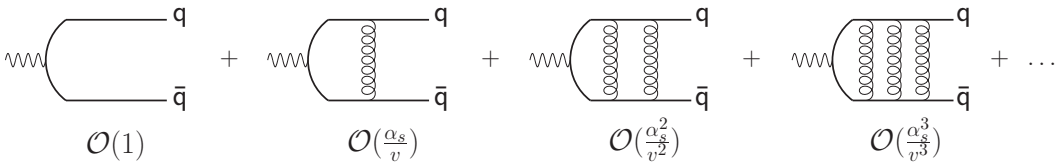

Figure 2.5: Coulomb singularities from "potential" gluons.

For approximate Coulomb systems in the final state the Virial Theorem tells us that $\alpha_s(mv) \simeq v$. In case the $q\,\bar{q}$ system is not Coulombic due to non-perturbative interactions, we even expect $\alpha_s(mv) > v$. Therefore the perturbation series in Fig. 2.5 breaks down. This breakdown comes as no surprise. The formation of bound states, for which kinetic and potential energy is of the same order of magnitude, does of course not arise from (small) perturbations around free particle states.
The second problem is that similar to the example in the previous section we will find large logarithms of the form

$$\ln\left(\frac{\mathbf{p}^2}{m^2}\right) \sim \ln(v^2)\,, \quad \ln\left(\frac{E^2}{m^2}\right) \sim \ln(v^4)\,, \quad \ln\left(\frac{E^2}{\mathbf{p}^2}\right) \sim \ln(v^2) \tag{2.10}$$

from loop diagrams at all orders in α_s causing fixed-order perturbation theory to become unreliable.

For QED bound states, e.g. positronium, an EFT framework (NRQED), that provides a solution to both problems was developed by Caswell and Lepage [46]. Thanks to the very large decay width $\Gamma_t \sim 1.5\,\text{GeV} \gg \Lambda_{QCD}$ and the large mass $m_t \sim 172$ GeV of the top quark a comparable approach to toponium dynamics is possible. The corresponding EFT framework proposed by Bodwin, Braaten and Lepage goes by the name of non-relativistic QCD (NRQCD) [47].
It has been shown by Fadin and Khoze [48] that the replacement

$$v \equiv \sqrt{\frac{\sqrt{s} - 2m_t}{m_t}} \;\to\; \sqrt{\frac{\sqrt{s} - 2m_t + i\Gamma_t}{m_t}} \tag{2.11}$$

of the physical velocity by an "effective" velocity is sufficient to account for the leading order effects from the top decay in NRQCD[1]. Thus Γ_t can be considered

[1] m_t is the pole or on-shell mass parameter in this context.

as an infrared cutoff and leads to the hierarchy $m_t \gg m_t v \gg m_t v^2 \sim \Gamma_t \gg \Lambda_{QCD}$ among the physical scales in the non-relativistic limit. Hence non-perturbative effects in the interaction between the top quarks as well as the interaction of the system with the non-perturbative QCD vacuum [49–51] are suppressed [3, 48]. As a consequence the top antitop system is Coulombic in the first approximation and we can estimate a typical (physical) velocity in the resonance region by [31]

$$v \approx \alpha_s(m_t v)^{\overline{\rm MS},{\rm LL}} = \frac{4\pi}{\beta_0 \ln(m_t^2 v^2/\Lambda_{QCD}^2)} \quad \Rightarrow \quad v \approx \alpha_s \approx 0.14\,, \qquad (2.12)$$

where $\beta_0 = 11 - \frac{2}{3}n_f$, the number of light quarks $n_f = 5$ and $\Lambda_{QCD} \simeq 300$ MeV. For other quarkonia like bottonium and charmonium the situation is more like $\Lambda_{QCD} \sim mv^2$ and $\Lambda_{QCD} \sim mv$ respectively and non-perturbative effects cannot be neglected.

In the NRQCD (NRQED) framework "potential" gluons (photons) like the ones in Fig. 2.5 are integrated out leaving four-quark operators named "potentials" in the effective Lagrangian in analogy to Fermi theory, cf. Fig. 2.2. The leading order four-quark operator can be translated to the Coulomb potential in a Schrödinger equation [52] for the Green function, which describes production and annihilation of the quark-antiquark system and can be solved analytically. The solution for this Green function is related to the sum of the Coulomb singularities of the production diagrams in Fig. 2.5 by the optical theorem [24, 25], see chapter 4. Higher order potentials in the EFT are treated as perturbations.

An adequate solution of the problem due to the large logarithms in Eq. (2.10) ($\alpha_s(m)\,\ln(\frac{m^2}{E^2}) \sim 0.8$) has been worked out by Luke, Manohar and Rothstein in Ref. [31], where a modified version of NRQCD called "velocity" NRQCD (vNRQCD) is introduced. The vNRQCD Lagrangian embodies a systematic expansion in the velocity v instead of $\frac{1}{m}$. To ensure that both, kinetic terms as well as the Coulomb potential, are leading order $\alpha_s \sim v$ is implied in the power counting. The hard scale m has been removed from dynamics and appears only as a parameter in the EFT, whereas the soft and the ultrasoft scale exist at the same time as required by the propagation of a non-relativistic heavy quark, see section 2.4. Obviously logarithms of E and $\mathbf{p}$ cannot be rendered small by a single choice for the renormalization scale μ. I.e. it is not possible to resum all large logarithms simultaneously via a RGE with only one renormalization scale. Introducing a second independent renormalization scale would however cause ill-defined RGE's. Thus the only way to avoid large logarithms when scaling the theory down from the hard scale to the soft and the ultrasoft scale respectively, is to establish a correlation between two renormalization scale parameters, referred to as μ_S and μ_U. It is uniquely fixed by requiring consistency of the effective theory and is in accordance with the heavy quark equations of motion [17, 26]:

$$\mu_U = \frac{\mu_S^2}{m}\,. \qquad (2.13)$$

Equivalently one can also express the RG dependence of couplings and Wilson coefficients in vNRQCD in terms of a "subtraction velocity" ν, where

$$\mu_S = m\nu \quad \text{and} \quad \mu_U = m\nu^2 \,. \tag{2.14}$$

The corresponding renormalization group is called "velocity renormalization group" (VRG) [31]. Eventually all potentially large logarithms in a vNRQCD calculation are summed into the coefficients by choosing $\nu = v$.

The R-ratio for $t\bar{t}$ production near threshold computed in vNRQCD thus takes the schematic form [24, 25]

$$\begin{aligned} R &= \frac{\sigma_{t\bar{t}}}{\sigma_{\mu^+\mu^-}} = v \sum_k \left(\frac{\alpha_s}{v}\right)^k \sum_i (\alpha_s \ln v)^i \\ &\quad \times \Big\{ 1\,(\text{LL});\ \alpha_s, v\,(\text{NLL});\ \alpha_s^2,\ \alpha_s v,\ v^2\,(\text{NNLL});\ \ldots \Big\}. \end{aligned} \tag{2.15}$$

The indicated terms are of leading logarithmic (LL), next-to-leading logarithmic (NLL) and next-to-next-to-leading logarithmic (NNLL) order.

An alternative approach to the physics of heavy quarkonia, where the dynamical scales are integrated out step by step, has been proposed by Soto and Pineda [53]. After eliminating the hard modes to obtain the NRQCD Lagrangian the theory is run down to the soft scale mv and matched to another EFT called "potential" NRQCD (pNRQCD), in which only the ultrasoft degrees of freedom (and fluctuations of $\mathcal{O}(\Lambda_{QCD})$) remain. Correspondingly a two-stage running of the coefficients is implemented. Details are described in Ref. [54]. Ref. [55] compares a less sophisticated two-stage setting to the one-stage method of vNRQCD.
An advantage of the pNRQCD framework is that it is also applicable in the physical situation, where $mv > \Lambda_{QCD} \gtrsim mv^2$, allowing studies of charmonium or higher bottonium excitations, which are not accessible by vNRQCD [56]. In the context of $t\bar{t}$ production at threshold (and $b\bar{b}$ sum rules) however vNRQCD results partly reach a more advanced level, i.e. up to NNLL, at present [26], see chapter 4.
Throughout this thesis we will only work in the framework of vNRQCD.

2.3 Threshold Expansion and the Method of Regions

We already stated in the previous section, that in the kinematic region of our interest the relative velocity ($\sim v$) of the top quarks scales like the strong coupling constant α_s and both are small (~ 0.1).

As pointed out in section 2.1 the determination of the matching conditions imposed by the full theory, in this case QCD, is a crucial step in the construction of an EFT. For this purpose we have to expand full theory diagrams including loop graphs in v in order to allow for a power counting scheme w.r.t. v to be established among the operators in the effective theory.
It is often too difficult to calculate the QCD loops analytically and expand the result afterwards, so we need a reliable method allowing us to expand the integrand before performing integrations. This should also work if the corresponding loop is divergent. And above all we do not want to do without the advantages of dimensional regularization [57,58] especially in multi-loop calculations. All those demands are satisfied by the so-called threshold expansion.

The threshold expansion is a prescription to obtain the expansion of loop diagrams w.r.t. a specified parameter using dimensional regularization. It was developed by Beneke and Smirnov [59] and is based on the more general method of regions. To apply it to a d-dimensional loop integral one has to proceed as follows:

1. Identify all relevant regions (scales) of the loop (four-)momentum (k), i.e. find out where the integrand gives sizable contributions to the whole integral. This is e.g. where the integrand has poles (from the propagators). The scale of k in the different regimes has to be expressed in powers of the expansion parameter (e.g. v).

2. Divide the integration into different parts according to each relevant region. The result is a number of separate (d-dim.) integrals that initially do not differ from each other in dimensional regularization.

3. Expand the integrand of each of these integrals strictly respecting the scaling of the loop momentum in terms of the expansion parameter as it was assigned to the corresponding region in the first step.

4. Carry out every integration over the entire (d-dim.) loop momentum space despite having assigned a certain scale to the integration variable before.

5. Add up all the contributions coming from the different integrals (and take the limit $d \to 4$). This is the final result.

To gain the correct result it is crucial to really carry out the expansion in a strict way: every term has to contribute only to a single power of the expansion parameter. One can also check the outcome by observing whether that is true. This can be done even before the integrations. One just has to consider the scaling of k as well as the scaling of the integration measure $d^{(d=4)}k$ in the different regimes.
To see how and why this method works properly, (although a rigorous mathematical proof for arbitrary Feynman graphs with external on-shell lines is still missing) one can for comparison use cutoffs to separate the different regions in

(four-)momentum space instead of dimensional regularization and calculate the integrals, one for each relevant momentum region, within finite ranges. Adding up all contributions afterwards, one realizes that all "intermediate" cutoffs disappear. Since in the presence of cutoffs, integration and expansion commute, it is obvious that the procedure gives the correct result. This is demonstrated e.g. in [17].

In the case of non-relativistic dynamics of a heavy $q\bar{q}$ pair with quark mass m the natural expansion parameter is the relative velocity v. Accordingly the relevant energy-momentum regions in the respective (QCD) diagrams imposed by their propagator structure are the following [59]:

$$\begin{array}{lcl} \text{hard} & : & (k^0, \mathbf{k}) \sim (m, m), \\ \text{soft} & : & (k^0, \mathbf{k}) \sim (mv, mv), \\ \text{potential} & : & (k^0, \mathbf{k}) \sim (mv^2, mv), \\ \text{ultrasoft} & : & (k^0, \mathbf{k}) \sim (mv^2, mv^2). \end{array} \tag{2.16}$$

Their configuration is most obvious if the heavy quark pair is in the c. m. frame.

By performing the threshold expansion of QCD loop diagrams for small v one gets an idea which are the relevant degrees of freedom in vNRQCD. They are defined in a way that every diagram of the EFT contributes to a single power in v and is associated with a certain term in the expansion of a full theory diagram. As we will see below vNRQCD distinguishes e.g. between "soft" and "ultrasoft" gluon modes whereas the heavy quark fields only carry energy and momentum according to the "potential" region.

2.4 The Effective Lagrangian

The Field Content

The vNRQCD Lagrangian [31] contains quark, gluon and ghost fields, that propagate in different momentum regions of Eq. (2.16) and can become on-shell in their domain. So there are potential heavy (anti)quark fields as well as soft and ultrasoft gluons. Besides that, light quarks (in topquark threshold physics all quarks except for the top), which are treated as massless, and ghosts exist as soft and ultrasoft degrees of freedom (dof's). They are often not mentioned explicitly but together with the respective gluons referred to as soft or ultrasoft fields. Any other particle modes like heavy quarks living in the soft regime can never be resonant in non-relativistic dynamics ($v \ll 1$) and are therefore "integrated" out, which in fact means nothing else than that they are eliminated from the non-relativistic EFT in analogy to the heavy vector bosons in Fermi's theory of weak interactions [34]. One speaks of partially integrating out the (Fourier) modes of particle fields in reference to the path integral (Wilsonian) approach to effective field theories, see e.g. Ref. [38].

The vNRQCD Label Formalism

In order to organize the Lagrangian as a power series in v, a kind of multipole expansion is applied to the fields [35, 52, 60]. This is achieved by the technique described in the following.
The original heavy quark four momentum in the (preferred) c.m. frame is split into three separate parts:

$$p^\mu = (m, 0) + (0, \mathbf{p}) + (k^0, \vec{k}\,) \,. \tag{2.17}$$

The first part is just a constant and is not treated as a dynamical variable. The second part is the soft component of the quark three-momentum ($\sim mv$) and the third part is the ultrasoft three-momentum ($\sim mv^2$) accompanied by the kinetic energy ($k^0 \equiv E \sim mv^2$) of the quark. Two-spinors of the non-relativistic heavy quark field in position space are rewritten in the following way:

$$\psi(x) \;=\; e^{-imt} \sum_{\mathbf{p}} e^{i\mathbf{p}\cdot\mathbf{x}}\, \psi_{\mathbf{p}}(x) \,, \tag{2.18}$$

where $\mathbf{p}$ is corresponding to the soft momentum and becomes a discrete label as illustrated in Fig. 2.6. The full momentum space ($\sim mv$) is considered to

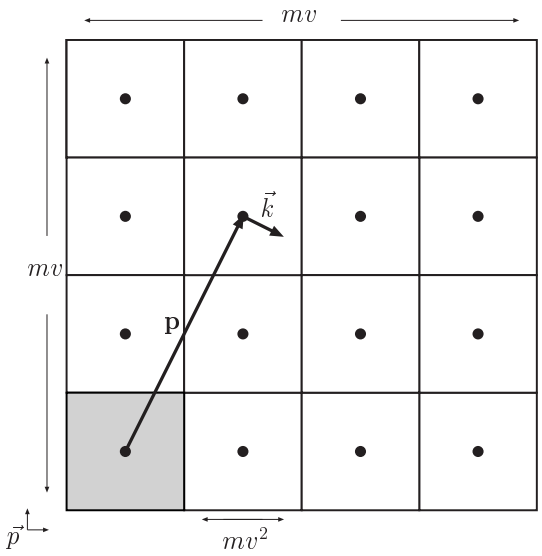

Figure 2.6: The momentum space of order mv is divided into boxes of size mv^2. An arbitrary momentum space vector is composed of a discrete soft label vector $\mathbf{p}$ and a ultrasoft vector $\vec{k}$ of length $\sim mv^2$.

be decomposed into boxes of side length mv^2 [31] and the soft label vectors are pointing to the center of these boxes. Only the ultrasoft four-momenta remain continuous variables. Thus the position space representation of the quantum mechanical ultrasoft three-momentum operator $\vec{k}$ is $-i\nabla$.

An analogous redefinition is performed for the heavy antiquark $\chi_{\mathbf{p}}(x)$ and the soft gluons $A_p^\mu(x)$ (as well as for all other soft fields).
The ultrasoft gluon field $A^\mu(x)$ represents only the ultrasoft modes ($k^\mu \sim mv^2$) of the full theory gluon and is therefore not labeled by a soft momentum. (The same applies to ultrasoft quarks and ghosts). Soft gluons have in contrast, besides the three-momentum, also energy of order mv. Their soft labels therefore have a zero-component.
Eq. (2.18) suggests to associate the $\mathbf{x}$ in the exponent with short distance effects ($\sim \frac{1}{mv}$) and the actual argument of the field $\psi_{\mathbf{p}}(x)$ with large length scales ($\sim \frac{1}{mv^2}$).

The Lagrange density of vNRQCD should be considered as a function only of the large scale variable x, the integration over small distances $\mathbf{x}$ actually has already been performed yielding (approximate) "delta-functions" of the soft momenta (coming from the exponential factors in Eq. 2.18) that constitute soft three-momentum conservation. These delta-functions are not explicitly written in the Lagrangian, but the corresponding conditions for the soft momenta are incorporated in the expressions for the operators.
The label formalism introduced above enables us loosely speaking to take a viewpoint on the spacetime grid from far away, so that we cannot resolve small distances and the operators in our Lagrangian appear to be local in x. This is a fundamental feature of low-energy EFT's [34].
Technically the labeling according to Eq. 2.18 provides a clear separation of soft and ultrasoft scales, which is necessary to set up a consistent v power counting in vNRQCD, see section 3.1. A similar label formalism was first used by Georgi to construct Heavy Quark Effective Theory (HQET) [43].

Particle/Antiparticle Convention

Another important issue is the particle/antiparticle convention in vNRQCD. In the Dirac representation, which is convenient for relativistic calculations, there are particle spinors with positive energy and antiparticle spinors with (formally) negative energy. Both types of spinors are in the same representation of the Poincaré group and of the gauge groups as well.
In non-relativistic theories like vNRQCD one often uses a different convention adapted to the non-relativistic nature of the (heavy quark) fields. Here we have two particle-type (positive energy) spinors, but one lives in the respective anti-representation.
The relation between the two-spinors in vNRQCD and the full theory four-

component spinors is thus defined as:

$$\psi^{\text{full}}(x) \;=\; \int d^3p \sum_s \left(e^{-ipx}\, u_s(\mathbf{p})\, a_s(\mathbf{p}) \;+\; e^{ipx}\, w_s^c(\mathbf{p})\, b_s^\dagger(\mathbf{p}) \right), \tag{2.19}$$

$$\text{where } u(\mathbf{p}) \;=\; \frac{\not{p} + m}{\sqrt{2p_0(p_0+m)}} \begin{pmatrix} \psi_{\mathbf{p}} \\ 0 \end{pmatrix}, \quad w(\mathbf{p}) \;=\; \frac{\not{p} + m}{\sqrt{2p_0(p_0+m)}} \begin{pmatrix} \chi_{\mathbf{p}} \\ 0 \end{pmatrix}$$

$$\text{and } w^c(\mathbf{p}) \;:=\; -i\gamma_2 w^*(\mathbf{p}) \;=\; \frac{-\not{p} + m}{\sqrt{2p_0(p_0+m)}} \begin{pmatrix} 0 \\ i\sigma_2\, \chi_{\mathbf{p}}^* \end{pmatrix}. \tag{2.20}$$

The actual creation and annihilation operators $(a, a^\dagger, b, b^\dagger)$ in Eq. (2.19) are not affected by the change of notation. In the following they are absorbed into the EFT two-spinors, so $\psi_{\mathbf{p}}^\dagger/\psi_{\mathbf{p}}$ denotes the heavy quark creator/annihilator and $\chi_{\mathbf{p}}^\dagger/\chi_{\mathbf{p}}$ is the vNRQCD heavy antiquark creator/annihilator.
The color structure of an interaction vertex of a quark with an ultrasoft gluon in the non-relativistic convention reads similar to the full theory

$$-\, i\, g\, \psi_{\mathbf{p}}^\dagger\, T^A\, \psi_{\mathbf{p}}\ ,$$

whereas the corresponding antiquark vertex takes the form

$$-\, i\, g\, \chi_{\mathbf{p}}^\dagger\, \bar{T}^A\, \chi_{\mathbf{p}}\ .$$

The $\bar{T}^A = -(T^A)^*$, $A = 1, ..., 8$, are the color matrices (SU(3) generators) in the anti-representation ($\bar{\mathbf{3}}$).
Since the heavy quark and antiquark fields are now manifestly of the same type and only differ in their interactions with gluons, the fermion flow of antiparticle lines has changed. As a consequence all the arrows of heavy quark lines in Feynman diagrams (if ever displayed explicitly) point in positive time direction.

Matching

In principle matching vNRQCD to full QCD means to proceed as follows [40].

- Write down the most general effective Lagrangian composed of the fields introduced above, so that every term contributes to a single power in v and α_s up to the required degree of precision (respecting $v \sim \alpha_s$).

- Use the equations of motions to drop all redundant terms [61].

- Expand a sufficient number of renormalized full QCD Feynman amplitudes to determine all the coefficients of the EFT interaction operators by demanding that vNRQCD yields the same result for these amplitudes. For

loop diagrams use the threshold expansion explained in section 2.3. To ensure that no large logarithms spoil the (perturbative) matching calculation, that fixes the Wilson coefficients, this is usually done at the "hard" (renormalization) scale. That is $\mu = m$ in the full and $\nu = 1$ in the effective theory respectively.

In practice however, one rather does it the other way round. After expanding a characteristic set of full theory amplitudes for a heavy quark-antiquark pair, we first identify the non-relativistic propagators in the leading terms and then construct an appropriate operator for every other component of the different terms in the expansion. Symmetries like gauge invariance or reparametrization invariance in vNRQCD, which is explained below, will furthermore fix the matching conditions for many other operators automatically. If renormalization requires operators (with zero matching coefficient) beyond that, we just introduce them by need, see section 3.5.

We are going to demonstrate this procedure here for the non-relativistic heavy (anti)quark propagator:
We take the inverse of the full theory tree-level quark two-point function in momentum space and expand it in v. The quark four-momentum p is decomposed as follows: $p = \binom{m+k_0}{\mathbf{p}+\mathbf{k}}$, where in the potential regime $\mathbf{p} \sim mv;\ k_0, \mathbf{k} \sim mv^2$. We find:

$$\bar{u}(p)\,(\not{p} - m)\,u(p) \;=\; \big(\psi^\dagger_{\mathbf{p}}\,,\,0\big)(\not{p}+m)\frac{\not{p}-m}{2p_0(p_0+m)}(\not{p}+m)\begin{pmatrix}\psi_{\mathbf{p}}\\ 0\end{pmatrix} =$$

$$= \psi^\dagger_{\mathbf{p}}\big(\,k_0 - \frac{\mathbf{p}^2}{2m}\,\big)\psi_{\mathbf{p}} + \psi^\dagger_{\mathbf{p}}\big(\,-\frac{\mathbf{kp}}{m} - \frac{\mathbf{k}^2}{2m} + \frac{k_0\mathbf{p}^2}{2m^2} - \frac{k_0^2}{2m} + \mathcal{O}(v^5)\big)\,\psi_{\mathbf{p}}\,. \qquad (2.21)$$

The first term is of leading order in v and is associated with the non-relativistic propagator, whereas the higher order terms are treated as perturbations (vertex insertions) in the EFT. Since vertices are by convention matched with on-shell external lines[2], we can substitute $k_0 \to \frac{\mathbf{p}^2}{2m} + \mathcal{O}(v^4)$. Diagrams with these kind of vertex insertions on the internal heavy quark lines are regarded as subleading terms of the multipole expansion.
The corresponding part of the effective Lagrangian is obtained by Fourier transforming the ultrasoft energies/momenta to position space and summing over the soft momentum label $\mathbf{p}$:

$$\delta\mathcal{L} = \sum_{\mathbf{p}} \psi^\dagger_{\mathbf{p}}(x)\,\big(\,i\partial_0 - \frac{(\mathbf{p}-i\nabla)^2}{2m} + \frac{\mathbf{p}^4}{8m^3}\,\big)\,\psi_{\mathbf{p}}(x)\,. \qquad (2.22)$$

For the antiquarks we derive an analogous result with ψ replaced by χ.
Note that the $\psi_{\mathbf{p}}/\chi_{\mathbf{p}}$ in Eq. (2.21) and Eq. (2.19) is not the same as $\psi_{\mathbf{p}}(x)/\chi_{\mathbf{p}}(x)$

[2]It makes no difference for the resulting observables whether one does this or not [62].

in Eq. (2.22) and Eq. (2.18). The difference is the x dependence, which comes from the partial Fourier transformation. We will however not care about this distinction in our notation any longer.
The actual expression for the heavy quark/antiquark propagator in momentum space is then given by

$$\frac{i}{k_0 - \frac{\mathbf{p}^2}{2m} + i\epsilon} \,. \tag{2.23}$$

To manifestly restore part of the SU(3) gauge invariance, namely the ultrasoft part, i.e. gauge invariance within every little box of Fig. 2.6, we replace the partial derivatives in Eq. (2.22) by the covariant derivatives $D^0 = \partial^0 + igA^0(x)$ and $\mathbf{D} = \nabla - ig\mathbf{A}(x)$.[3] These ultrasoft covariant derivatives only involve the ultrasoft gauge field which consistently scales like mv^2, see section 3.1. We would have obtained the same result by matching quark gluon interaction diagrams of the two theories.
Thus the "ultrasoft" part of the vNRQCD Lagrangian [17, 31, 32, 63] reads

$$\begin{aligned} \mathcal{L}_u &= \sum_{\mathbf{p}} \left\{ \psi^\dagger_{\mathbf{p}} \left[iD^0 - \frac{(\mathbf{p} - i\mathbf{D})^2}{2m} + \frac{\mathbf{p}^4}{8m^3} + \dots \right] \psi_{\mathbf{p}} + (\psi \to \chi,\, T \to \bar{T}) \right\} \\ &\quad -\frac{1}{4} G^{\mu\nu} G_{\mu\nu} + \dots \,. \end{aligned} \tag{2.24}$$

Here we added the kinetic term of the ultrasoft gluons, which has the same form as the one for gluons in full QCD. $G^{\mu\nu}$ is the ultrasoft field strength tensor.

Gauge and Reparametrization Invariance

As we have seen ultrasoft gauge symmetry is explicitly visible in the vNRQCD Lagrangian. This is not the case for soft gauge invariance, associated with short distance phase redefinitions of the fermion fields, because there are no soft heavy quarks in the theory, to which a single soft gluon could couple to. Higher order effects related to full theory quarks with energy and momentum $\sim mv$, are included in the Wilson coefficients that are determined by matching to full QCD in a fixed gauge, usually Feynman gauge [63].
Nevertheless there is strong evidence, that full gauge invariance is restored with the help of an additional symmetry present in the EFT. It is called "reparametrization invariance" [31].
Remember the decomposition of momenta into soft and ultrasoft pieces to set up the EFT in Eq. (2.17). It is of course not unique, we can rather shift the soft components by an ultrasoft amount ($\mathbf{q} \sim mv^2$),

$$\mathbf{p} \to \mathbf{p} - \mathbf{q}, \quad \mathbf{k} \to \mathbf{k} + \mathbf{q},$$

[3] Note that we are working in the convention, where $D^\mu = (D^0, -\mathbf{D})$.

and should obtain precisely the same effective Lagrangian describing the non-relativistic dynamics. Demanding invariance of the theory under this redefinition can simplify the construction of the vNRQCD Lagrangian a lot, because it states that every time a soft momentum appears, it has to go along with an ultrasoft one, namely $i\mathbf{D}$, as e.g. in Eq. (2.24). Incorporating this information can avoid some extensive, but unnecessary, matching calculations. Furthermore it fixes even the renormalization scale dependence of certain coefficients as we will see at an explicit example below.
A similar kind of symmetry with the same name also exists in HQET [43, 64].

Potentials in vNRQCD

A major part of the vNRQCD Lagrangian consists of four-quark operators, which are together with the appropriate Wilson coefficients referred to as potentials. At $\mathcal{O}(\alpha_s)$ these can be considered as QCD diagrams, where the interaction originally mediated by a potential gluon shrinks to a point. The relevant tree-level diagrams are depicted in Fig. 2.7.

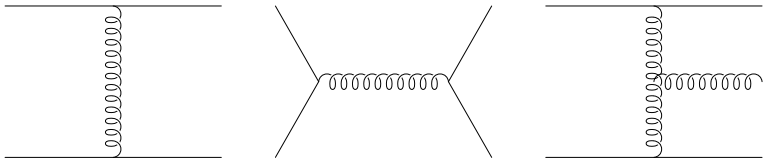

Figure 2.7: QCD diagrams for tree level matching of the potentials.

They differ significantly in the allowed color configuration for the heavy quark pair. Diagram b) contributes only to the color octet channel, whereas a) and c) contribute to both, the color singlet and the octet channel. The different channels refer to the SU(3) multiplet, to which the incoming and outgoing quark pair state belongs to. Since gluons live in the adjoint representation of SU(3) ($\mathbf{8}$), the single gluon in Fig 2.7 b) cannot transport a color singlet configuration.
For our main purpose, $t\,\bar{t}$ - production in e^+e^- - collisions, evidently only the color singlet channel is relevant.
Nonetheless the vNRQCD Lagrangian is usually written in a different (non-orthogonal, but complete) basis of operators in color space, namely the Casimir operators $1 \otimes \bar{1}$ and $T^A \otimes \bar{T}^A$, which commute with all the SU(3)-generators in the $\mathbf{3} \otimes \bar{\mathbf{3}}$ - representation ($T^B \otimes \bar{1} + 1 \otimes \bar{T}^B$, $B = 1, .., 8$) and therefore provide global color symmetry of the Lagrangian.
From an arbitrary color structure of the form $V_{1\otimes 1}\, 1 \otimes \bar{1} + V_{T\otimes T}\, T^A \otimes \bar{T}^A$ we can

project out singlet and octet components by means of the projection operators

$$\begin{aligned} P_{\text{singlet}} &= \left(1 - 2\frac{C_F}{C_A}\right) 1 \otimes \bar{1} \; - \; \frac{2}{C_A}\, T^A \otimes \bar{T}^A \quad \text{and} \\ P_{\text{octet}} &= 2\frac{C_F}{C_A}\, 1 \otimes \bar{1} \; + \; \frac{2}{C_A}\, T^A \otimes \bar{T}^A \,. \end{aligned} \tag{2.25}$$

$C_A = N_c$ and $C_F = \frac{N_c^2-1}{2N_c}$ are the SU(N_c) color constants.
Thus the above color structure can be rewritten in terms of the singlet/octet operators as $V_{\text{singlet}}\, P_{\text{singlet}} + V_{\text{octet}}\, P_{\text{octet}}$ and the coefficients are related by

$$\left[\begin{array}{c} V_{\text{singlet}} \\ V_{\text{octet}} \end{array} \right] = \left[\begin{array}{cc} 1 & -C_F \\ 1 & \frac{1}{2}C_A - C_F \end{array} \right] \left[\begin{array}{c} V_{1\otimes 1} \\ V_{T\otimes T} \end{array} \right] . \tag{2.26}$$

By definition the "potential" part of the Lagrangian is made up of four fermion fields and describes interactions between heavy quark and antiquark [17,31,32,63]:

$$\mathcal{L}_p \;=\; -\sum_{\mathbf{p},\mathbf{p}'} V_{\alpha\beta\lambda\tau}\,(\mathbf{p},\mathbf{p}')\;\; \psi^\dagger_{\mathbf{p}'\alpha}\, \psi_{\mathbf{p}\,\beta}\, \chi^\dagger_{-\mathbf{p}'\lambda}\, \chi_{-\mathbf{p}\,\tau} \;. \tag{2.27}$$

The different potentials are given as terms in an expansion series. We display them here up to v^2 or $\alpha_s v$ suppressed terms:

$$\begin{aligned} V(\mathbf{p},\mathbf{p}') \;=\; & (T^A \otimes \bar{T}^A)\left[\frac{\mathcal{V}_c^{(T)}}{\mathbf{k}^2} + \frac{\mathcal{V}_k^{(T)}\pi^2}{m|\mathbf{k}|} + \frac{\mathcal{V}_r^{(T)}(\mathbf{p}^2+\mathbf{p}'^2)}{2m^2\mathbf{k}^2} + \frac{\mathcal{V}_2^{(T)}}{m^2}\right. \\ & \left. + \frac{\mathcal{V}_s^{(T)}}{m^2}\mathbf{S}^2 + \frac{\mathcal{V}_\Lambda^{(T)}}{m^2}\Lambda(\mathbf{p}',\mathbf{p}) + \frac{\mathcal{V}_t^{(T)}}{m^2}\, T(\mathbf{k}) + \ldots \right] \\ & + (1 \otimes \bar{1})\left[\frac{\mathcal{V}_c^{(1)}}{\mathbf{k}^2} + \frac{\mathcal{V}_k^{(1)}\pi^2}{m|\mathbf{k}|} + \frac{\mathcal{V}_2^{(1)}}{m^2} + \frac{\mathcal{V}_s^{(1)}}{m^2}\mathbf{S}^2 + \ldots\right], \end{aligned} \tag{2.28}$$

where ($\mathbf{k} = \mathbf{p}' - \mathbf{p}$) and

$$\mathbf{S} = \frac{\boldsymbol{\sigma}_1 + \boldsymbol{\sigma}_2}{2}\,,\; \Lambda(\mathbf{p}',\mathbf{p}) = -i\frac{\mathbf{S}\cdot(\mathbf{p}'\times\mathbf{p})}{\mathbf{k}^2}\,,\; T(\mathbf{k}) = \boldsymbol{\sigma}_1\cdot\boldsymbol{\sigma}_2 - \frac{3\,\mathbf{k}\cdot\boldsymbol{\sigma}_1\,\mathbf{k}\cdot\boldsymbol{\sigma}_2}{\mathbf{k}^2}\,.$$

$\frac{\boldsymbol{\sigma}_1}{2}$ and $\frac{\boldsymbol{\sigma}_2}{2}$ are the spin operators acting on the heavy quark and antiquark respectively. The leading order potential is the well-known Coulomb potential V_c as expected from our knowledge about non-relativistic QED systems as e.g. positronium.
$\mathcal{L}_p$ in Eq. (2.27) is however obviously not reparametrization invariant. In order to allow for this symmetry, we have to add another piece to the Lagrangian. It

is derived in Ref. [62] to $\mathcal{O}(v^2, \alpha_s v)$ precision by demanding the implementation of the reparametrization invariant form of the Coulomb potential and reads

$$\begin{aligned}\mathcal{L}_{pu} &= \frac{2i\,\mathcal{V}_c^{(T)}\,f^{ABC}}{\mathbf{k}^4}\mu_S^{2\epsilon}\mu_U^{\epsilon}\,\mathbf{k}\cdot(g\mathbf{A}^C)\,\psi^\dagger_{\mathbf{p}'}\,T^A\psi_{\mathbf{p}}\,\chi^\dagger_{-\mathbf{p}'}\,\bar{T}^B\chi_{-\mathbf{p}} + \\ &+ \mathcal{V}_c^{(T)}\mu_S^{2\epsilon}\,\psi^\dagger_{\mathbf{p}'}\left[\frac{i\mathbf{k}\cdot\overleftrightarrow{\nabla}}{\mathbf{k}^4} - \frac{\overleftrightarrow{\nabla}^2}{2\mathbf{k}^4} + 2\frac{(\mathbf{k}\cdot\overleftrightarrow{\nabla})^2}{\mathbf{k}^6}\right]T^A\psi_{\mathbf{p}}\,\chi^\dagger_{-\mathbf{p}'}\,\bar{T}^A\chi_{-\mathbf{p}} + \\ &+ \mathcal{V}_c^{(T)}\mu_S^{2\epsilon}\,\psi^\dagger_{\mathbf{p}'}\,T^A\psi_{\mathbf{p}}\,\chi^\dagger_{-\mathbf{p}'}\left[\frac{-i\mathbf{k}\cdot\overleftrightarrow{\nabla}}{\mathbf{k}^4} - \frac{\overleftrightarrow{\nabla}^2}{2\mathbf{k}^4} + 2\frac{(\mathbf{k}\cdot\overleftrightarrow{\nabla})^2}{\mathbf{k}^6}\right]\bar{T}^A\chi_{-\mathbf{p}}\,. \end{aligned} \tag{2.29}$$

$\overleftrightarrow{\nabla} = \overrightarrow{\nabla} + \overleftarrow{\nabla}$ is the sum of nabla operators acting on the fermion fields to the left and to the right.
The first term describes the coupling of an ultrasoft gluon to the Coulomb potential and matches onto the graph in Fig. 2.7 *c*). The other terms are referred to as higher order terms of the multipole expanded Coulomb potential. Corresponding Feynman rules are given in Appendix A.
Reparametrization and ultrasoft gauge invariance require that the Wilson coefficient of the operators in Eq. 2.29 remains the same as for the Coulomb potential, i.e. $\mathcal{V}_c^{(T)}(\nu)$, for all ν at all orders in perturbation theory.

By matching to the tree-level diagrams in Fig 2.7 *a*) and *b*) the potential Wilson coefficients at $\nu = 1$ are determined [63, 65]:

$$\begin{aligned}&\mathcal{V}_c^{(T)} = 4\pi\alpha_s(m)\,, \quad \mathcal{V}_r^{(T)} = 4\pi\alpha_s(m)\,, \quad \mathcal{V}_s^{(T)} = -\frac{4\pi\alpha_s(m)}{3} + \frac{1}{N_c}\,\pi\,\alpha_s(m)\,, \\ &\mathcal{V}_\Lambda^{(T)} = -6\pi\alpha_s(m)\,, \quad \mathcal{V}_t^{(T)} = -\frac{\pi\alpha_s(m)}{3}\,, \quad \mathcal{V}_s^{(1)} = \frac{(N_c^2-1)}{2N_c^2}\,\pi\,\alpha_s(m)\,, \\ &\mathcal{V}_c^{(1)} = 0\,, \quad \mathcal{V}_2^{(T)} = 0\,, \quad \mathcal{V}_2^{(1)} = 0\,. \end{aligned} \tag{2.30}$$

Although the $\mathcal{V}_2$'s are zero at $\nu = 1$, their operators are listed in Eq. (2.27), because they have non-trivial one-loop anomalous dimensions in vNRQCD and therefore do not vanish for $\nu < 1$, as we will see later.
The coefficients $\mathcal{V}_k$ are zero so far and do not run at one-loop level, but receive a non-zero value when matching to full theory one loop diagrams [65]:

$$\mathcal{V}_k^{(T)} = \alpha_s^2(m)\Big(\frac{7C_A}{8} - \frac{C_d}{8}\Big)\,, \quad \mathcal{V}_k^{(1)} = \alpha_s^2(m)\frac{C_1}{2}\,, \tag{2.31}$$

with $C_d = 8C_F - 3C_A$ and $C_1 = C_F(\frac{1}{2}C_A - C_F)$.
For this reason the "$\frac{1}{m|\mathbf{k}|}$"-potentials ($\sim \frac{\alpha_s^2}{v}$) formally contribute to the same order as the "$\frac{1}{m^2}$"-potentials V_r, V_2, V_s, V_Λ and V_t ($\sim \alpha_s$).

At this point we should already remark, that actually a "true" four-quark operator $\propto \frac{1}{m|\mathbf{k}|}$ does not exist in vNRQCD. Rather an "effective" potential interaction of this form, denoted $V_{k,\text{eff}}$, is generated by six-quark or sum operators introduced in subsection 3.5.2 and Refs. [32] and [26] respectively. This subtlety is important for a consistent renormalization procedure and a major issue of this thesis. It will be discussed in detail in subsection 3.5.2.
In this work we are mainly concerned with the spin-independent potentials V_r, V_2 and $V_{k,\text{eff}}$ because they are, up to the required precision, the only ones that are directly renormalized by ultrasoft gluon loops, as will become clear later on.

Soft Gluon Interactions

Although the energy ($\sim mv^2$) of non-relativistic heavy quark systems is to small to allow the production of free soft gluons, they do occur in loops and play an important role in renormalization of vNRQCD. They are for instance responsible for the LL running of the Coulomb potential $\left(\mathcal{V}_c^{(T)}\right)$ [31, 66] and must not be neglected.
Because of energy conservation at least two soft gluons must take part in interactions with the heavy quarks in vNRQCD. They do not interact with ultrasoft gluons.
The reason is, that the EFT is local in the long distance variable x. Short distance modes like soft gluons are not affected by ultrasoft gauge transformations, weakly varying over long distances. To them, such a transformation appears to be global. Sloppily speaking, an intermediate soft gluon exchanged by two quarks, very close to each other, cannot resolve the relative phase shift of the quark fields induced by an ultrasoft gauge transformation. It only realizes an equal change of the two absolute phases.
For $v \ll 1$ soft and ultrasoft gluons are effectively gauge fields of two independent SU(3) gauge groups and do therefore not couple to one another. In vNRQCD a soft gauge symmetry actually does not even exist, but is implemented indirectly via reparametrization invariance, as mentioned above.
Including soft light quarks φ_q and ghosts c_q, the "soft" Lagrangian has terms

$$\begin{aligned}
\mathcal{L}_s \;=\; & \sum_q \left\{ |q^\mu A_q^\nu - q^\nu A_q^\mu|^2 + \bar{\varphi}_q \not{q} \varphi_q + \bar{c}_q \, q^2 c_q \right\} \\
& - g^2 \sum_{\mathbf{p},\mathbf{p}',q,q'} \left\{ \frac{1}{2} \psi^\dagger_{\mathbf{p}'} \, [A^\mu_{q'}, A^\nu_q] U^{(\sigma)}_{\mu\nu} \, \psi_{\mathbf{p}} + \frac{1}{2} \psi^\dagger_{\mathbf{p}'} \, \{A^\mu_{q'}, A^\nu_q\} W^{(\sigma)}_{\mu\nu} \, \psi_{\mathbf{p}} \right. \\
& \left. + \psi^\dagger_{\mathbf{p}'} \, [\bar{c}_{q'}, c_q] Y^{(\sigma)} \, \psi_{\mathbf{p}} + (\psi^\dagger_{\mathbf{p}'} \, T^B Z^{(\sigma)}_\mu \, \psi_{\mathbf{p}}) \, (\bar{\varphi}_{q'} \gamma^\mu T^B \varphi_q) \right\} \\
& + (\psi \to \chi, \, T \to \bar{T}) + \dots \, ,
\end{aligned} \tag{2.32}$$

where q and q' are soft four momentum labels. $U^{(\sigma)}_{\mu\nu}$, $W^{(\sigma)}_{\mu\nu}$, $Y^{(\sigma)}$, and $Z^{(\sigma)}_\mu$ are functions of ($\mathbf{p}$, $\mathbf{p}'$, q, q') and matrices in spin. σ ($= k-4$) denotes the order

in v, to which the corresponding soft vertex contributes in the power counting formula Eq. (3.4), introduced in section 3.1. They are fixed at $\nu = 1$ by tree-level matching to the diagrams in Fig. 2.8 *a*), *b*) and *c*). Intermediate off-shell quarks in Fig. 2.8 *a*) and *b*) and gluons in Fig. 2.8 *c*) have been integrated out.
The explicit expressions for $U_{\mu\nu}^{(\sigma)}$, $W_{\mu\nu}^{(\sigma)}$, $Y^{(\sigma)}$, and $Z_{\mu}^{(\sigma)}$ can be found in Ref [63]. The resulting effective vertex associated with the soft interaction operators in Eq. (2.32) is depicted in Fig. 2.8 *d*).

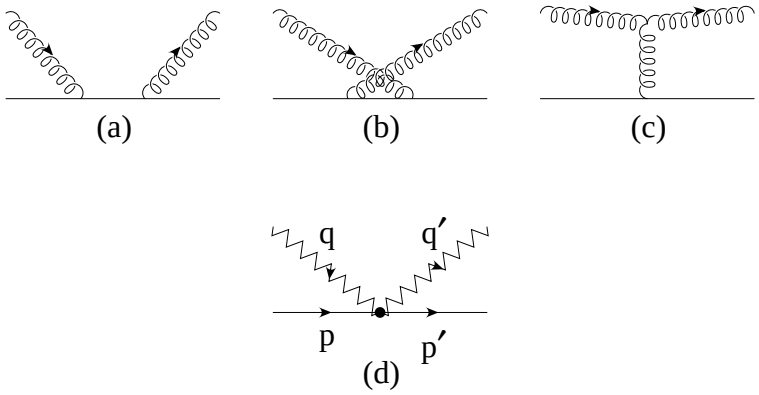

Figure 2.8: The gluon Compton scattering graphs *a*), *b*), *c*) in QCD generate a vNRQCD operator *d*) local in x. Analogous diagrams with external massless quarks or ghosts match on similar effective operators, see Eq. (2.32). Soft modes are represented by zigzag lines.

Altogether the Lagrangian of vNRQCD (in the c.m. frame) basically consists of four different parts (Eqs. 2.24, 2.27, 2.29 and 2.32):

$$\mathcal{L}_{\text{vNRQCD}} \;=\; \mathcal{L}_u \;+\; \mathcal{L}_p \;+\; \mathcal{L}_{pu} \;+\; \mathcal{L}_s \,. \tag{2.33}$$

The vNRQCD Feynman rules relevant for this work are presented in Appendix A.

Currents

To describe production and annihilation processes of the heavy quark pair in vNRQCD, we need to introduce currents composed of one quark and one antiquark field, which couple to external vector boson (γ, Z) fields. They are determined by expanding the full theory vector ($\bar{q}\gamma^{\mu}q$) and axial vector ($\bar{q}\gamma^{\mu}\gamma^{5}q$) currents in the c.m. frame.
Up to $\mathcal{O}(v^2)$ one finds the effective operators [25]

$$\begin{aligned}
\boldsymbol{O}_{\mathbf{p},1} &= \psi_{\mathbf{p}}{}^{\dagger}\,\boldsymbol{\sigma}(i\sigma_2)\,\chi^{*}_{-\mathbf{p}}\,, \qquad (2.34)\\
\boldsymbol{O}_{\mathbf{p},2} &= \frac{1}{m^2}\,\psi_{\mathbf{p}}{}^{\dagger}\,\mathbf{p}^2\boldsymbol{\sigma}(i\sigma_2)\,\chi^{*}_{-\mathbf{p}}\,,\\
\boldsymbol{O}_{\mathbf{p},3} &= \frac{-i}{2m}\,\psi_{\mathbf{p}}{}^{\dagger}\,[\,\boldsymbol{\sigma},\boldsymbol{\sigma}\cdot\mathbf{p}\,]\,(i\sigma_2)\,\chi^{*}_{-\mathbf{p}}\,.
\end{aligned}$$

Figure 2.9: Full theory *a*) and effective *b*) quark-antiquark production diagrams at tree level. The particle coupling to the current in *a*) can be a photon or a Z boson.

$\boldsymbol{O}_{\mathbf{p},1}$ and $\boldsymbol{O}_{\mathbf{p},2}$ produce quark-antiquark pairs in the ${}^3S_1$ state. $\boldsymbol{O}_{\mathbf{p},3}$ produces a ${}^3P_1$ state. There is also a D-Wave current $\boldsymbol{O}_{\mathbf{p},4}$ at $\mathcal{O}(v^2)$. The corresponding production annihilation correlator is however suppressed by v^4 and will therefore not play a role in this thesis, see chapter 4.
Thus the relevant effective vector and axial vector production currents read

$$\begin{aligned} \mathbf{J}^v_{\mathbf{p}} &= c_1(\nu)\boldsymbol{O}_{\mathbf{p},1} + c_2(\nu)\boldsymbol{O}_{\mathbf{p},2}\,, \\ \mathbf{J}^a_{\mathbf{p}} &= c_3(\nu)\boldsymbol{O}_{\mathbf{p},3}\,. \end{aligned} \tag{2.35}$$

The c_i are the associated Wilson coefficients. The zero component of the currents vanishes as they are defined in the c.m. frame of the heavy quark-antiquark system.
Tree level matching to the full theory diagram in Fig. 2.9 *a*) results in the condition $c_1(\nu = 1) = 1$ [31]:

$$\bar{u}(\mathbf{p})\,\gamma^i\,w^c(-\mathbf{p}) \;=\; \psi^\dagger_{\mathbf{p}}\,\sigma^i(i\sigma_2)\,\chi^*_{-\mathbf{p}} \;+\; \ldots\;. \tag{2.36}$$

From the next-to-leading $\mathcal{O}(v^2)$ terms we find $c_2(\nu = 1) = -\frac{1}{6}$ and from expanding the full theory axial vector current $c_3(\nu = 1) = 1$ [25].
For the NNLL prediction of the $t\,\bar{t}$ threshold cross section the full matching result for c_1 up to two-loop precision is needed, see chapter 4. It has been derived in Refs. [24, 25, 67, 68].
The respective annihilation currents $\boldsymbol{O}^\dagger_{\mathbf{p},i}$ are obtained by complex conjugation. Fig. 2.9 *b*) shows an effective production current vertex as we depict it in this thesis.

Chapter 3

Renormalization in vNRQCD

In this chapter we discuss some general aspects of renormalization in vNRQCD. We are thereby concentrating on the treatment of UV divergences generated by ultrasoft loops. The most economic framework to make use of the renormalization group formalism in perturbative QCD (see e.g. [58]) is the $\overline{\rm MS}$ renormalization scheme [69] in combination with dimensional regularization [57]. For effective field theories like vNRQCD this approach has the additional advantage of preserving the power counting [37] as elucidated among other things in the following sections.

3.1 Power counting

We have already argued that the use of dimensional regularization (cf. section 2.3) and setting up ($\overline{\rm MS}$) RGE's to resum potentially large logarithms requires a consistent velocity power counting in the EFT. We claimed that the vNRQCD Lagrangian, introduced in 2.4, allows for this condition. Here we show that this is true and present a power counting formula which allows us to determine systematically to which order in the v expansion a given vNRQCD Feynman diagram contributes.
First we have to identify the v scaling of the fields. For the lowest order action $S^{(0)}$ of the theory, which necessarily comprises the kinetic terms of the fields, we require the v scaling to be zero in accordance with the v scaling of the canonical commutation relations:

$$\begin{aligned} S^{(0)} &= \int d^4x\, \mathcal{L}_{\rm kin}(x) + \ldots = \int d^4x \left(\sum_{\mathbf{p}} \psi^\dagger_{\mathbf{p}} \left(iD^0 - \frac{\mathbf{p}^2}{2m} \right) \psi_{\mathbf{p}} \right. \\ &\quad \left. -\frac{1}{4} G^{\mu\nu} G_{\mu\nu} + \sum_q |q^\mu A^\nu_q - q^\nu A^\mu_q|^2 \right) + \ldots \sim v^0 \,. \end{aligned} \tag{3.1}$$

The normalization of the fields is now chosen to match this condition. Since $\partial^\mu \sim v^2$ the integration measure scales like $d^4x \sim v^{-8}$ and we immediately conclude that $A^\mu \sim v^2$ from the ultrasoft kinetic terms in Eq. (3.1).

Sums over soft momenta have to be treated carefully. Remember where they originate from: to manifestly separate ultrasoft and soft momenta, the vNRQCD Lagrangian is formulated in ultrasoft position space representation and simultaneously in soft momentum space representation. Switching for a moment back to full position space representation, where the summation over short distances x_s in the action has not been carried out yet, we find:

$$\begin{aligned} \int d^4x \sum_{\mathbf{p}} \;&\to\; \int d^0x \int d^3x_s \;\sim\; v^{-2}v^{-3} \quad \text{and} \\ \int d^4x \sum_{q} \;&\to\; \int d^4x_s \;\sim\; v^{-4}\,. \end{aligned} \tag{3.2}$$

The scaling we obtain in this way will be consistently used for the left hand side expressions in Eq. (3.2) as they appear in the original vNRQCD action.
Now it is straightforward to derive also the scaling behavior of the soft gluon and the heavy quark fields (in $d = 4$ dimensions). We end up with

quantity:	$\mathbf{p}$	$\psi_{\mathbf{p}},\ \chi_{\mathbf{p}}$	A_p^μ	D^0	$\mathbf{D}$	A^μ
scaling:	v	$v^{3/2}$	v	v^2	v^2	v^2

. (3.3)

The scaling with respect to the heavy quark mass m corresponds to the mass dimension of the fields which is the same as in the full theory.
Knowing the v counting of every operator, we can now determine it for any (arbitrary) vNRQCD amplitude. In Ref. [31] a power counting formula is derived which automatizes this procedure. Input parameters are N_s, the number of soft subgraphs which are disconnected when all potential lines are erased, and $V_k^{(i)}$, the number of operator insertions with scaling v^k. The index i specifies whether a vertex involves only ultrasoft fields ($i = u$), at least one heavy quark and no soft fields ($i = p$), or one or more soft fields ($i = s$).
A general Feynman diagram is then of order v^δ, where

$$\delta = 5 + \sum_k \Big[(k-8)V_k^{(u)} + (k-5)V_k^{(p)} + (k-4)V_k^{(s)} \Big] - N_s\,. \tag{3.4}$$

In many cases it is more convenient to refer to the order in v of a diagram or an operator as

$$\delta' = \delta - 5\,, \tag{3.5}$$

because one can simply add up this quantity for separate parts of a Feynman diagram to get the over all δ'.
As an example, consider the Coulomb potential. It has $\delta' = -1$ but its coefficient contains a factor of α_s. Every further Coulomb interaction adds a factor $\frac{\alpha_s}{v}$, i.e. it subtracts 1 from δ'. The natural field of application of the (v)NRQCD framework is exactly the situation where $\alpha_s \sim v$ ($\ll 1$). As we mentioned in section 2.2 we

also formally have to account for this relation and are forced to resum all terms containing such Coulomb singularities, since they scale like $(\frac{\alpha_s}{v})^n \sim 1$ in the total counting.
Inserting ultrasoft and soft vertices never decreases the order in v, since for all those operators $k \geq 8$ and $\sigma = k - 4 \geq 0$ respectively [31]. Even if a soft subdiagram is attached, it comes along with at least one compensating factor of α_s.
Most of the time in this work we refer to the relative order of an operator compared to the leading order operator of the same type. The $\frac{1}{m^2}$ - potentials are e.g. sometimes called $\mathcal{O}(v^2)$ potentials. Unless explicitly stated it will be clear from the context whether the relative or the absolute order in v is indicated.

3.2 Loops

Having specified a power counting, we are able to continue the Lagrangian unambiguously to $d = 4 - 2\epsilon$ dimensions leaving the couplings dimensionless, the relation $D^\mu \sim mv^2$ fixed and retaining the power counting of the action, i.e. $S^{(n)} \sim v^n$. To achieve this we have to multiply every coupling constant with one of the two scale parameters $\mu_U = m\nu^2$ and $\mu_S = m\nu$ to the right power in terms of ϵ. Here $\nu \sim v$ is understood[1]. The d-dimensional version of the Lagrangian then reads

$$\begin{aligned}
\mathcal{L} &= \sum_{\mathbf{p}} \psi^\dagger_{\mathbf{p}}(x) \left(i(\partial_0 + i\mu_U^\epsilon\, gA^0) + \ldots + \mu_U^\epsilon\, g\, \frac{\mathbf{p}\,\mathbf{A}}{m} + \ldots \right) \psi_{\mathbf{p}}(x) + \ldots \\
&- \mu_S^{2\epsilon} \sum_{\mathbf{p},\mathbf{p}'} V\, \psi^\dagger_{\mathbf{p}'} \psi_{\mathbf{p}} \chi^\dagger_{-\mathbf{p}'} \chi_{-\mathbf{p}} + \mu_S^{2\epsilon} \sum_{\mathbf{p},\mathbf{p}'} F_j^{ABC}\, g\mu_U^\epsilon\, \mathbf{A}_j^C \psi^\dagger_{\mathbf{p}'} T^A \psi_{\mathbf{p}} \chi^\dagger_{-\mathbf{p}'} \bar{T}^B \chi_{-\mathbf{p}} \\
&+ -g^2 \mu_S^{2\epsilon} \sum_{\mathbf{p},\mathbf{p}',q,q'} \frac{1}{2}\, \psi^\dagger_{\mathbf{p}'}\, [A^\mu_{q'}, A^\nu_q] U^{(\sigma)}_{\mu\nu}\, \psi_{\mathbf{p}} + \ldots\,, \qquad (3.6)
\end{aligned}$$

where $A^\mu \sim (mv^2)^{1-\epsilon}$, $A^\mu_q \sim (mv)^{1-\epsilon}$ and $\psi_{\mathbf{p}} \sim \chi_{\mathbf{p}} \sim (mv)^{\frac{3}{2}-\epsilon}$. Eq. (3.6) suggests that there are actually two kinds of the strong coupling constant g (α_s), one "soft" coupling constant accompanied by a factor of $\mu_S^{(2)\epsilon}$ and one "ultrasoft" coupling constant accompanied by a factor of $\mu_U^{(2)\epsilon}$. They differ in their respective RG running as we will see later. This statement is confirmed by the fact that full SU(3) gauge symmetry is broken in vNRQCD. Only at the hard scale $\nu = 1$, where vNRQCD is matched to full QCD, both couplings have the same value. Nevertheless they are correlated as μ_U and μ_S are.
Assigning the correct powers to the $\mu_{U/S}$'s in order to match the above requirements it is at the same time ensured that every $\mu_{U/S}$ takes the right place to

[1] If we were to use a cutoff regularization scheme instead of dimensional regularization to handle UV divergences in the EFT, we would accordingly need two kinds of cutoffs one soft ($m > \Lambda_S > mv$) and one ultrasoft ($mv > \Lambda_U > mv^2$).

avoid large logarithms in loop calculations by choosing $\nu \sim v$.
This can be understood from the fact that the action S in d dimensions retains its scaling as a series of integer powers of v. Therefore n-point functions always scale like the product of their n external fields at lowest order and loops only add integer powers of v to the scaling of the higher order terms in the α_s expansion. Thus every loop automatically receives the proper renormalization scale according to the scale of its loop three-momentum, which due to a consistent multipole expansion is by construction identical to the scale of the external three-momentum flowing through it. In this way we will only obtain logarithms of the ratio of an external momentum and the appropriate renormalization scale when performing loop calculations in vNRQCD. All these logarithms are obviously rendered small by choosing $\nu \sim v$.
In vNRQCD there are depending on the dominant momentum region three different types of loops. In Fig 3.1 typical representatives are shown.

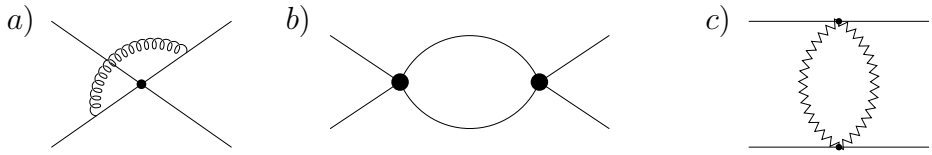

Figure 3.1: Typical vNRQCD loops, ultrasoft (a), potential (b) and soft (c).

The loop integrations have to be carried out over the full momentum space, i.e. for every component of the loop momentum from $-\infty$ to $+\infty$. This is the case even for ultrasoft loops, where the loop momentum is considered to be of order $mv^2 \ll mv$. The reason is that vNRQCD is constructed to be local in the large distance variable x^μ, which implies that an ultrasoft gluon is formally able to mediate short distance interactions associated with large momentum transport. Physically this is obviously not true, but the mistake we make affects only the UV divergences of the EFT and is corrected within the renormalization procedure and by matching to full QCD.
The renormalization scale dependence of the couplings/Wilson coefficients remains the same, even if we used an UV cutoff Λ_U with $mv > \Lambda_U > mv^2$ to regulate ultrasoft loops. In local QFT's the running of the couplings and coefficients is induced by logarithms of the dynamical scales, which are generated by loop graphs.
For ultrasoft loops the argument of the logarithms would consequently be some ultrasoft momentum. Each of these logarithms goes along with a logarithmic divergence, which is used in the renormalization group formalism to infer the running of the coefficients caused by the associated logarithms. The initial conditions to solve the corresponding RGE's are then obtained by matching vNRQCD to full QCD. Non-logarithmic (power) UV divergences are simply subtracted by

appropriate counterterms in the renormalization procedure and do not have any physical impact [41]. Using dimensional regularization they are even neglected automatically by default.
Apart from the physically important logarithms the result of a loop diagram also comprises other finite terms, which by construction scale like the loop itself using the v counting of the last section. This was achieved by the multipole expansion of the Lagrangian. The (one and only) relevant momentum region of a loop integration in vNRQCD is either soft, e.g. in Fig 3.1 (c), ultrasoft (a) or potential (b). It is determined by the pole structure of the integrand. In a (hypothetical) cutoff scheme there could in addition arise terms depending on the cutoffs separating the different momentum regions (hard, soft, ultrasoft). These terms obviously break the power counting introduced in the last section and either cancel each other[2] or are subtracted by the matching procedure.
Thus the physically relevant contributions from a loop diagram are only the finite terms including the logarithms responsible for the running of couplings and coefficients and are independent of whatever cutoff is used for the loop integrals. Therefore we can safely take all cutoffs to infinity or zero respectively as done in dimensional regularization.
The advantage of a scaleless regulator like in dimensional regularization is that it preserves gauge invariance and allows (v) power counting according to Eq. (3.4), which formally would be broken in a cutoff scheme [37]. Namely these features make it in combination with the $\overline{\text{MS}}$ renormalization scheme the most convenient and powerful method to systematically derive the evolution of the coefficients in vNRQCD.
That is why in practice all loop integrations are carried out over the whole momentum space regardless of the scale, which was originally assigned to the loop momentum (soft/ultrasoft), and by which the respective loop diagram is actually governed. Translated to position space this means that the formulation of vNRQCD including operators, which are local in the ultrasoft position variable is a consistent way to describe physics in the associated range of application.
A similar situation also arises in the Standard Model which is a local QFT as well. There we integrate over the full momentum space, without knowing about physics at very short distances. Instead of matching, SM couplings are fixed at a certain scale by measurements.
Related to the (soft) label formalism implemented to provide a manifest distinction between the momenta of the different scales in vNRQCD there are some technical issues regarding loop integrals to be discussed in the following.
An ultrasoft loop integration has the form

$$\mu_U^{4-d} \int \frac{d^d k}{(2\pi)^d} \,. \tag{3.7}$$

[2] after the zero-bin subtraction, see section 3.7 and Ref. [70]

The factor $\mu_U^{2\epsilon}$ provides an integer v scaling of the integral and the elimination of possibly large logarithms if $\nu \sim v$ is chosen.
For potential loops an additional summation over soft three-momenta has to be performed:

$$\mu_S^{4-d} \sum_{\mathbf{q}}^{d\,\mathrm{dim.}} \int \frac{d^d k}{(2\pi)^d} \,. \tag{3.8}$$

To handle the summation, it is convenient to recombine the decomposed three-momentum space of Fig 2.6 and convert the combination of the sum and the ultrasoft integral to a d-dimensional integral over continuous soft three-momenta q^μ. The integration over the time component of the loop momentum $dk^0 \to dq^0$ remains ultrasoft, but is again carried out over the full energy range. Hence we can rewrite the potential loop integration as

$$\mu_S^{4-d} \int \frac{d^d q}{(2\pi)^d} \,. \tag{3.9}$$

Note, that μ_S, which is suggested by the above Lagrangian, is indeed the right choice of renormalization scale, since it is the integration over the soft three-momentum, which determines the scale here. By means of the $i\epsilon$ prescription of the propagators in the loop it is ensured that the q^0 integration alone will not be divergent. Just as in any other QFT it can always be performed using the residue theorem giving a finite result, which typically depends on the spacelike components of the loop momentum. Thus it is also clear that logarithms, that are associated with logarithmic divergences generated by a potential loop, can only depend on the (external) soft scales involved in the loop.
Soft loops are treated similarly:

$$\mu_S^{4-d} \sum_{q}^{d\,\mathrm{dim.}} \int \frac{d^d k}{(2\pi)^d} \;\to\; \mu_S^{4-d} \int \frac{d^d q}{(2\pi)^d} \,. \tag{3.10}$$

Here the summation/integration over the energy is consistently affected by the replacement, too.
So in any case, even for multi-loop diagrams, we can simply perform ordinary d-dimensional loop momentum integrations. The theory actually knows by itself how to deal with the different scales.

3.3 Running of α_s

In the last section we claimed that there are actually two kinds of the strong coupling constant in vNRQCD, the soft $\alpha_s(\mu_S)$ and the ultrasoft $\alpha_s(\mu_U)$, that differ in their renormalization scale dependence. In an arbitrary QFT they could

in fact be totally independent although they have the same value at the hard scale:

$$\alpha_s(\mu_S = m) \;=\; \alpha_s(\mu_U = m)\,. \tag{3.11}$$

In this case however full QCD as the underlying theory (and the notation used above) suggests of course that the two couplings have the same functional dependence and are only evaluated at different but correlated scales $\mu_{U/S}$.
Indeed it turns out that the two couplings are subject to the same RGE with respect to the corresponding μ:

$$\frac{d}{d\ln\mu_{U/S}^2}\,\alpha_s(\mu_{U/S}) = \beta(\mu_{U/S})\;. \tag{3.12}$$

Viewed as functions of the fundamental renormalization parameter in vNRQCD ν they are different though:

$$\alpha_s(\mu_S) = \alpha_s(m\nu) \quad \text{and} \quad \alpha_s(\mu_U) = \alpha_s(m\nu^2)\;. \tag{3.13}$$

The function $\beta(\mu)$ is found to be the exactly the same as for full QCD with $n_f = 5$ light (massless) quarks, if the heavy quark is identified with the top.
This becomes clear when looking at the vNRQCD Lagrangian. Apart from the soft label formalism applied to the soft sector, which is however just a matter of notation, the soft as well as the ultrasoft sector for the light particles (gluons, ghosts, light quarks) take the form of ordinary QCD. The non-relativistic character of the theory is only visible in the kinetic terms of the heavy quarks and in their interactions among each other or with the light degrees of freedom. Moreover the soft and ultrasoft sectors of light particles are naturally decoupled. I.e. there is no direct interaction between soft and ultrasoft fields. This has been pointed out for the case of the gluons already in section 2.4 and analogously applies also to light quarks and ghosts.
The heavy quarks are not involved in the renormalization of the strong coupling constants, since their hard (and soft) modes have been integrated out in the derivation of vNRQCD and are not part of the effective theory. Therefore there is no operator in vNRQCD, which would describe the production/annihilation of a heavy quark-antiquark pair from/to light particles. Only currents, that couple to external fields, can do this job (cf. section 4.1). Consequently there is no heavy quark loop contributing to the self-energy of the (ultra)soft gluon, which could affect the anomalous dimension of the respective coupling.
Thus for the case of the top quark being the heavy particle we have effectively two decoupled copies of QCD with $n_f = 5$ flavors and different renormalization scales μ_S and μ_U in which the evolution of the respective coupling constant is independently computed.
The well known results for the RGE's in $d = 4 - 2\epsilon$ dimensions read

$$\frac{d\alpha_s}{d\ln\mu_{U/S}^2} \;=\; -\epsilon\,\alpha_s \;-\; \frac{\alpha_s^2}{4\pi}\,\beta_0 \;-\; \frac{\alpha_s^3}{(4\pi)^2}\,\beta_1 \;-\; \ldots\,, \tag{3.14}$$

where $\beta_0 = \frac{11}{3}C_A - \frac{4}{3}Tn_f$, $\beta_1 = \frac{34}{3}C_A^2 - 4C_FTn_f - \frac{20}{3}C_ATn_f$ and $T = \frac{1}{2}$, $n_f = 5$. For convenience we define the abbreviations

$$\alpha_S := \alpha_s(\mu_S)\,, \quad \alpha_U := \alpha_s(\mu_U)\,, \quad \alpha_h := \alpha_s(m)\ . \tag{3.15}$$

At one-loop (LL) level for $d = 4$ we only have to take into account the β_0 term of Eq. (3.14) and its solution takes the analytic form:

$$\alpha_s^{\rm LL}(\mu_{U/S}) = \frac{4\pi}{\beta_0 \ln(\frac{\mu_{U/S}^2}{\Lambda_{QCD}^2})}\ . \tag{3.16}$$

We can use this result to express the LL vNRQCD couplings $\alpha_S^{\rm LL}$ and $\alpha_U^{\rm LL}$ in terms of each other:

$$\alpha_U^{\rm LL} = \frac{\alpha_h\,\alpha_S^{\rm LL}}{2\alpha_h - \alpha_s^{\rm LL}} \quad \text{or} \quad \alpha_S^{\rm LL} = \frac{2\alpha_h\,\alpha_U^{\rm LL}}{\alpha_U^{\rm LL} + \alpha_h}\ . \tag{3.17}$$

The solution of Eq. (3.14) for β_0, $\beta_1 \neq 0$ and $\beta_{i>1} = 0$ still contains contributions of all logarithmic orders, LL, NLL, NNLL, etc. as can be checked easily. For later use we would like to extract only the complete LL and NLL contributions. Therefore we consequently have to expand in $\alpha = \alpha_{U/S}$ consistently assuming $\alpha^2 \ln\nu \ll \alpha \ln\nu \sim 1$ and drop all terms of higher than NLL order:

$$\begin{aligned} d\alpha &= (-b_0\alpha^2 - b_1\alpha^3)\, d\ln\nu \\ \frac{d\alpha}{b_0\alpha^2}\,(1 - \frac{b_1}{b_0}\alpha) &= -d\ln\nu \end{aligned} \tag{3.18}$$

$$\begin{aligned} \Rightarrow \quad \int_\alpha^{\alpha_h} \frac{d\alpha}{b_0\alpha^2}\,(1 - \frac{b_1}{b_0}\alpha) &= \ln\nu \\ \frac{1}{b_0\alpha} - \frac{b_1}{b_0^2}\,\ln\frac{\alpha_h}{\alpha} - \frac{1}{b_0\alpha_h} &= \ln\nu \\ 1 - \frac{b_1}{b_0}\,\alpha\,\ln\frac{\alpha_h}{\alpha} - \frac{\alpha}{\alpha_h} &= b_0\,\alpha\,\ln\nu \\ \alpha\left(\frac{1}{\alpha_h} + b_0\,\ln\nu\right) &= 1 + \frac{b_1}{b_0}\,\alpha\,\ln\frac{\alpha}{\alpha_h} \\ \Rightarrow \qquad \alpha &= \frac{\alpha_h}{1 + b_0\,\alpha_h\,\ln\nu}\left(1 + \frac{b_1}{b_0}\,\alpha\,\ln\frac{\alpha}{\alpha_h}\right) \end{aligned} \tag{3.19}$$

Eq. (3.19) is now solved to NLL precision by one iteration, yielding

$$\alpha^{\rm NLL} = \alpha^{\rm LL}\left(1 + \frac{b_1}{b_0}\alpha^{\rm LL}\,\ln\frac{\alpha^{\rm LL}}{\alpha_h}\right), \tag{3.20}$$

where we have inserted the LL result

$$\alpha^{\mathrm{LL}}(\nu) = \frac{\alpha_h}{1 + b_0\, \alpha_h \ln \nu} \,, \tag{3.21}$$

which is equivalent to Eq. (3.16). The constants are $b_0 = \frac{\beta_0}{\pi}$, $b_1 = \frac{\beta_1}{4\pi^2}$ for the ultrasoft coupling $\alpha = \alpha_U$ and $b_0 = \frac{\beta_0}{2\pi}$, $b_1 = \frac{\beta_1}{8\pi^2}$ for the soft coupling $\alpha = \alpha_S$. Furthermore we will use

$$d \ln \nu = -\frac{d\alpha^{\mathrm{LL}}}{b_0 (\alpha^{\mathrm{LL}})^2} \tag{3.22}$$

in later computations.

3.4 Mixing

When renormalizing an EFT, there will generally be mixing between the higher dimensional operators of different orders in the additional expansion parameter, which in vNRQCD is the velocity parameter v. This means e.g. that the counterterm of an operator absorbs an UV divergence from a loop involving an operator of the same type w.r.t. the fields it is composed of, but contributing to a different order regarding the power counting. As we will see in section 3.5 operators can also mix into the renormalization of operators with a smaller number of external legs by generating a tadpole graph.
Consider for example the vNRQCD potentials listed in Eq. (2.28). We will use the following convention for the renormalized (V) and bare quantities (V^0):

$$\left[\begin{array}{c} V^0_{1\otimes 1} \\ V^0_{T\otimes T} \end{array} \right] = \mu_S^{2\epsilon} \left[\begin{array}{c} V_{1\otimes 1} + \delta V_{1\otimes 1} \\ V_{T\otimes T} + \delta V_{T\otimes T} \end{array} \right] =: \mu_S^{2\epsilon} \left(\vec{V} + \delta\vec{V}\right) = \vec{V}^0 \,. \tag{3.23}$$

To cancel divergences generated e.g. by ultrasoft gluons at one loop like in Fig. 3.1(a) we add a generic counterterm

$$\delta\vec{V} = A\,\vec{V} + \vec{C} \tag{3.24}$$

to the potential $\vec{V}$, where A is a 2×2 matrix and $\vec{C}$, $\vec{V}$ and $\delta\vec{V}$ are vectors in the $(1\otimes\bar{1},\, T^A\otimes\bar{T}^A)$ color space. $\vec{C}$ is parametrizing here divergent terms e.g. from soft matrix elements (see section 5.4) without any potential interaction.
From the independence of the unrenormalized quantity $\vec{V}^0$ on the renormalization scale $\nu = \mu_S/m$, we can now derive a generic form for the RGE's of the potentials

in $d = 4 - 2\epsilon$ dimensions:

$$\begin{aligned}
\nu\frac{d}{d\nu}\,\vec{V}^0 &= 0 \\
\Rightarrow \qquad \nu\frac{d}{d\nu}\vec{V} &= -2\epsilon\,(\vec{V}+\delta\vec{V}) - \nu\frac{d}{d\nu}\,\delta\vec{V} \qquad (3.25)\\
\nu\frac{d}{d\nu}\vec{V} &= -2\epsilon\,(\,(1+A)\vec{V}+\vec{C}\,) - \nu\frac{d}{d\nu}\,(A\,\vec{V}+\vec{C}) \\
(1+A)\,\nu\frac{d}{d\nu}\,\vec{V} &= -2\epsilon\,(\,(1+A)\vec{V}+\vec{C}\,) - (\nu\frac{d}{d\nu}\,A)\,\vec{V} - \nu\frac{d}{d\nu}\,\vec{C} \\
\Rightarrow \qquad \nu\frac{d}{d\nu}\vec{V} &= -2\epsilon\,\vec{V} \,-\, (1+A)^{-1}\Big[2\epsilon\,\vec{C} \,-\, \nu\frac{d}{d\nu}\,\vec{C} - \,(\nu\frac{d}{d\nu}A)\,\vec{V}\Big]\,. \qquad (3.26)
\end{aligned}$$

Ultrasoft one-loop renormalization in section 5.2 for instance, yields a matrix A of order v^2, so (the Wilson coefficients of) potentials that differ by an order of v^2 are mixed, e.g.

$$\begin{aligned}
\delta\mathcal{V}_2^{(1)} &= -\frac{\alpha_U}{3\pi m^2\epsilon}\,C_1\,\mathcal{V}_c^{(T)} \,+\, \ldots\,, \\
\Rightarrow \quad \nu\frac{d}{d\nu}\,\mathcal{V}_2^{(1)}(\nu) &= -\frac{4}{3\pi}\,C_1\,\alpha_U\,\mathcal{V}_c^{(T)}(\nu) \,+\, \ldots\,. \qquad (3.27)
\end{aligned}$$

We find that due to mixing at LL the evolution of the $\mathcal{O}(v^2)$ potential coefficient $\mathcal{V}_2^{(1)}(\nu)$ is governed by the evolution of the $\mathcal{O}(v^0)$ potential $\mathcal{V}_c^{(T)}(\nu)$ and $\alpha_U(\nu)$. The running of the leading order Coulomb potential $\mathcal{V}_c^{(T)}$ in contrast is generated only by soft matrix element corrections. A one-loop diagram with the topology in Fig 3.1(c) gives e.g. the LL contribution [63].

3.5 Operators Induced by Renormalization

In this section operators are presented that have zero matching coefficient at the hard scale $\nu = 1$ but receive non-trivial counterterms to absorb UV divergences from ultrasoft loops. Running the scale down to $\nu < 1$ their coefficients will change to non-zero values. These operators finally contribute via mixing to the running of the potentials and the production/annihilation currents.

3.5.1 Four-Quark Operators With Two Soft Fields

The first type of operators describes soft Compton scattering off a heavy quark antiquark pair. In the ultrasoft renormalization procedure they are needed to cancel the divergences generated by the diagrams in Fig 3.2 and the analogous

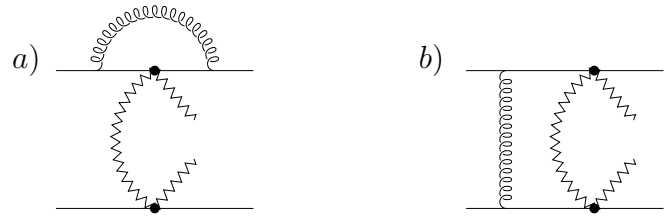

Figure 3.2: Diagrams contributing to the counterterms of the operators $\mathcal{O}_{2i}$. Spiral lines denote ultrasoft gluons, zigzag lines denote soft gluons, light quarks or ghosts.

diagrams, where the ultrasoft gluon is attached to the four heavy quark lines in all other possible ways.
It is worth mentioning here that the divergence produced by the diagram in Fig. 3.2(a) is not cancelled by a counterdiagram subtracting the subdivergences of the upper soft vertex. An appropriate counterterm would be inevitably gauge dependent and spoil the gauge invariance of the renormalized soft Lagrangian $\mathcal{L}_s$, as pointed out in Ref. [32]. It does therefore not exist in vNRQCD.
Another reason is more demonstrative: the vNRQCD Lagrangian is meant to describe the physics of a heavy quark-antiquark system. For convenience it is formulated in the rest frame of the $q\,\bar{q}$ pair, but it could in principle be written in a boosted frame just as well. Though it is not manifestly Lorentz invariant, all observables calculated from it actually are, since they are all related to the relative dynamics of the heavy quark, e.g. the invariant mass of the system. If one thinks of only one single heavy quark interacting with gluons, the relative velocity v obviously looses its meaning. Moreover, in the rest frame of the quark only one scale, the quark mass, is left making a distinction between soft and ultrasoft dof's impossible. For this reason the soft single quark sector $\mathcal{L}_s$ is renormalized only by soft gluons (light quarks, ghosts) [62, 63].
Thus divergent diagrams like in Fig 3.3 and the corresponding counterterms are actually not part of the theory.

Figure 3.3: Examples of imaginable mixed soft-ultrasoft loop diagrams involving one heavy quark. They do not contribute to the renormalization of vNRQCD.

The six-field operators $\mathcal{O}_{2i}$ that are constructed to absorb the UV divergences of one-loop diagrams involving both heavy quarks such as in Fig. 3.2 are graphically represented by Fig. 3.4. With the two external soft fields being light quarks φ_q,

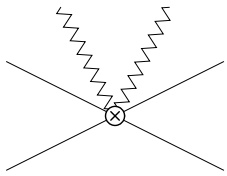

Figure 3.4: Six-field vertex corresponding to the renormalization induced operators $\mathcal{O}_{2i}$.

gluons A_q^μ and ghosts c_q respectively they have the following structure

$$\begin{aligned}
\mathcal{O}_{2\varphi}^{(\sigma)} &= \alpha_S^2\,\mu_S^{4\epsilon}\ (\psi_{\mathbf{p}'}^\dagger\,\Gamma_{\varphi,\psi}^{(\sigma)}\,\psi_{\mathbf{p}})\,(\chi_{-\mathbf{p}'}^\dagger\,\Gamma_{\varphi,\chi}^{(\sigma)}\,\chi_{-\mathbf{p}})\ (\overline{\varphi}_{-q}\,\Gamma_{\varphi}^{(\sigma)}\,\varphi_q)\,,\\
\mathcal{O}_{2A}^{(\sigma)} &= \alpha_S^2\,\mu_S^{4\epsilon}\ (\psi_{\mathbf{p}'}^\dagger\,\Gamma_{A,\psi}^{(\sigma)}\,\psi_{\mathbf{p}})\,(\chi_{-\mathbf{p}'}^\dagger\,\Gamma_{A,\chi}^{(\sigma)}\,\chi_{-\mathbf{p}})\ (A_{-q}^\mu\,\Gamma_{A,\mu\nu}^{(\sigma)}\,A_q^\nu)\,,\\
\mathcal{O}_{2c}^{(\sigma)} &= \alpha_S^2\,\mu_S^{4\epsilon}\ (\psi_{\mathbf{p}'}^\dagger\,\Gamma_{c,\psi}^{(\sigma)}\,\psi_{\mathbf{p}})\,(\chi_{-\mathbf{p}'}^\dagger\,\Gamma_{c,\chi}^{(\sigma)}\,\chi_{-\mathbf{p}})\ (\bar{c}_{-q}\,\Gamma_{c}^{(\sigma)}\,c_q)\,.
\end{aligned} \tag{3.28}$$

and appear in the Lagrangian together with their Wilson coefficients $C_{2i}^{(\sigma)}$:

$$\delta\mathcal{L}^{(\sigma)} = \sum_i C_{2i}^{(\sigma)} \sum_{\mathbf{p},\mathbf{p}',q} \mathcal{O}_{2i}^{(\sigma)}\,. \tag{3.29}$$

The index σ refers as usual to the (relative) power counting of the operators. The Γ_i's represent matrices in spin and color and are functions of $\mathbf{p}$, $\mathbf{p}'$ and q^μ. For $\sigma = 0$ they are given in the Appendix of Ref [32]. Some of them contain the soft vertex functions $U_{\mu\nu}^{(\sigma)}$, $W_{\mu\nu}^{(\sigma)}$, $Y^{(\sigma)}$, $Z_\mu^{(\sigma)}$ listed in Ref. [63].
Remarkably, the soft coupling constant α_S has been included explicitly in the operator structure and is not absorbed in the Wilson coefficients C_{2i} as e.g. for the case of the potentials in Eq. (2.28) (cf. e.g. Eq. (3.27), where $\mathcal{V}_c = 4\pi\alpha_S$). In doing so we actually anticipate a factorization of the contributions to the running of the $\mathcal{O}_{2i}$ operators, which is similar to the factorization of soft and ultrasoft terms in the running of the potentials described in section 5.5.
Having understood how the factorized form of the potential coefficients comes about, you can moreover imagine that anticipating an analogous form for the operators $\mathcal{O}_{2i}$, which are themselves involved in generating the factorization in section 5.5, is the only way to avoid performing a formally infinite number of iterations in the renormalization procedure: each iteration step would provide the factorized form of the coefficient of the operator needed in the previous step and would involve more and more soft fields.
Thus the counterterm associated to α_S in Eqs. (3.28) automatically cancels a whole class of divergent contributions from soft loops involving a factor of $C_{2i}^{(\sigma)}$, which we therefore do not have to take into account by hand. At one-loop only ultrasoft loop diagrams like in Fig. 3.2 contributing to $\delta C_{2i}^{(\sigma)}$ have to be considered, see section 5.4.

Matching at tree level, which will be sufficient for this work, yields $C_{2i}(\nu = 1) = 0$. This is because any possible full theory amplitude is already exactly reproduced in the EFT by the time ordered product of two pre-existing soft four-field operators, that have been matched to the QCD single quark interaction diagrams in Fig. 2.8. An example for such a matching calculation is sketched in Fig. 3.5.

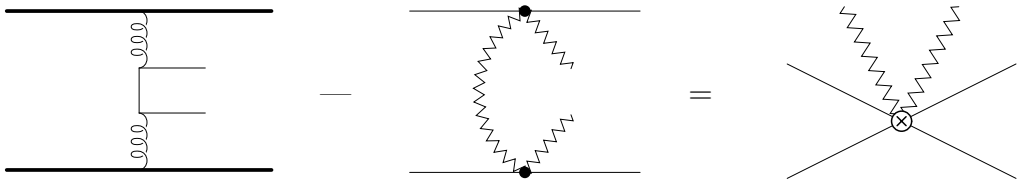

Figure 3.5: Example of the matching calculation for $\mathcal{O}_{2\varphi}^{(\sigma)}$. Here the zig-zag lines denote soft massless fermions. At the high scale ($\nu = 1$) the graphs on the left exactly cancel, so the coefficient of the operator on the right is zero. This has been taken from Ref. [32].

For completeness we should also mention that there is a similar class of operators with six heavy quark and two soft fields called $\mathcal{O}_{(6+2)i}$. They will be discussed and used for the derivation of the factorized form of the $\frac{1}{m\mathbf{k}}$ - potentials in subsection 5.4.2. Their construction and renormalization goes very much along the lines of the $\mathcal{O}_{2i}$ operators, so it is not necessary to present the details here.

3.5.2 Six-Quark vs. Sum Operators

In the ultrasoft renormalization of the $\frac{1}{m\mathbf{k}}$ - potentials another type of zero matching operators plays a central role. They are composed of six heavy (anti)quark fields and describe the scattering of a (anti)quark off a quark-antiquark potential. The soft momentum of the scattered (anti)quark before and after the scattering remains the same. In many respects this resembles soft particle scattering off a heavy quark-antiquark pair associated with the six-field operators $\mathcal{O}_{2i}$ discussed in the previous subsection. The six-quark operators are denoted by $\mathcal{O}_{6i}$ or $\mathcal{O}_{\bar{6}i}$, if the scattered particle is a quark or antiquark respectively.
As will be shown below one can equivalently use so called sum operators $\mathcal{O}_{ki}$ for the purpose of renormalizing the $\frac{1}{m\mathbf{k}}$ - potentials instead of the $\mathcal{O}_{6i}$'s. This approach has been applied at one-loop level in Ref. [32]. Nevertheless using six-quark operators is at least in my point of view more intuitive and easier to handle although we have to consider a lot more diagram topologies in this case. More importantly it ensures that the renormalization procedure is free of technical ambiguities at multi-loop level, which is not true for the sum operators. However it turns out that the ambiguities in the latter case can be removed by assigning a certain prescription to the evaluation of the diagrams generating the counterterms of the $\mathcal{O}_{ki}$ operators as we will see in the following.

Common to both approaches is that in fact no four-quark operator with the momentum structure $\frac{1}{m\mathbf{k}}$ exists in the Lagrangian that could absorb UV divergences from ultrasoft loops in a consistent way. This means that concerning ultrasoft effects the $\frac{1}{m\mathbf{k}}$ - potentials ($\mathcal{V}_k$) in Eq. (2.28) are not renormalization scale dependent.

To understand this let us first consider the diagrams, which would naively contribute to the ultrasoft renormalization of $\frac{1}{m\mathbf{k}}$ - potentials in Eq. (2.28). For reasons that will be explained later (see section 3.6) every UV divergent ultrasoft loop will increase the v scaling of a diagram at least by two. Therefore diagrams with a topology like the one shown in Fig 3.1 *a*) do not renormalize V_k even if V_c is inserted in the loop. In order to obtain the right scaling $\propto \frac{1}{v}$ we have to add a potential loop by attaching another Coulomb potential to this structure. In section 3.1 we learned that such a loop scales like $\frac{\alpha_S}{v}$ and therefore adds a power of the coupling constant α_S but subtracts at the same time a power of v. Note that a potential loop like this is UV finite.
Thus the lowest order diagrams that would contribute to a direct ultrasoft renormalization of V_k are based on two-loop topologies with one ultrasoft gluon as e.g. shown in Fig. 3.6 *a*) and *b*).

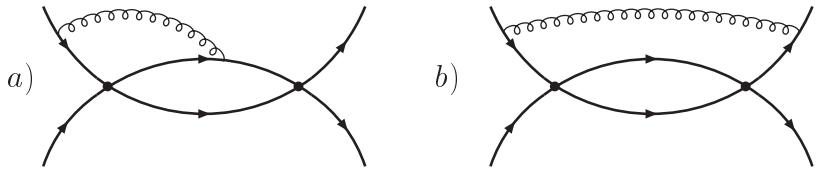

Figure 3.6: Examples of two-loop graphs that would affect the ultrasoft running of V_k at lowest order.

For one ultrasoft loop everything seems to be fine [62]. The problems arise for more than one ultrasoft loop so actually at three loop level [32]. Consider for example graphs like in Fig. 3.7 *a*) with an additional ultrasoft light quark loop. After subtraction of the subdivergence from the light quark bubble by adding the counterdiagram in Fig 3.7 *b*) we are left with an overall UV divergent term of the form

$$\frac{1}{|\mathbf{k}|}\Big(\frac{\mu_S^2}{\mathbf{k}^2}\Big)^{\epsilon}\Big[\frac{1}{2\epsilon^2}\Big(\frac{\mu_U^2}{E^2}\Big)^{2\epsilon}-\frac{1}{\epsilon^2}\Big(\frac{\mu_U^2}{E^2}\Big)^{\epsilon}\Big]=\frac{1}{|\mathbf{k}|}\Big[-\frac{1}{2\epsilon^2}-\frac{1}{2\epsilon}\ln\Big(\frac{\mu_S^2}{\mathbf{k}^2}\Big)+\dots\Big], \qquad (3.30)$$

where as usual $\mathbf{k}$ is the difference of the soft momenta of the incoming quarks and E is their kinetic energy. The factor in front of the square brackets on the left hand side comes from the potential loop integration and is obviously finite. Inside these square brackets the first term is associated with the three loop graph Fig. 3.7 *a*) and the second with the two-loop counterdiagram Fig. 3.7 *b*). The problematic term in Eq. (3.30) is the second term inside the brackets on

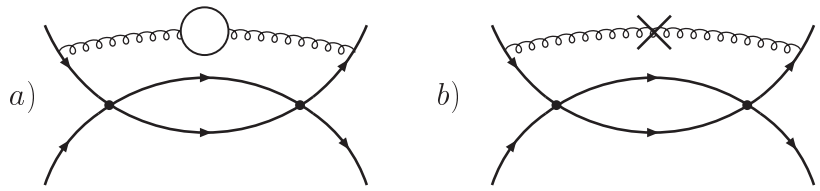

Figure 3.7: *a*) Example for three loop diagram with one potential and two ultrasoft loops. *b*) Counterdiagram to subtract the subdivergence from the ultrasoft light quark loop in *a*). The $\times$ denotes the counterterm insertion associated with the fermion bubble divergence.

the right hand side. It can neither be absorbed by a counterterm $\delta\mathcal{V}_k$ of the $\frac{1}{m\mathbf{k}}$ - potentials, since a $\ln(\mu_S^2)/\epsilon$ term would render the anomalous dimension of $\mathcal{V}_k$ infinite and moreover $\ln(\mathbf{k}^2)$ would spoil (non-manifest) Lorentz invariance of the Lagrangian, nor by a counterterm of a new non-analytic operator for the same reasons. Thus we must have made a mistake in the renormalization procedure described above. Otherwise vNRQCD would be inconsistent and therefore useless.
Fortunately the former is the case. The inconsistency occurs because we started renormalizing the $\frac{1}{m\mathbf{k}}$ - potentials at lowest order by two-loop diagrams. Although the potential loop is finite, the factor $(\frac{\mu_S^2}{\mathbf{k}^2})^\epsilon$ it adds to Eq. (3.30), is actually the source of the problem.

Six-Quark Operator Approach

Thus it is better to cut the potential loop and first consider diagrams with six external legs consequently renormalizing six-quark operators and close the potential loop afterwards. As a matter of fact ultrasoft loops do not renormalize the four-quark operator V_k directly in this procedure. Instead we only obtain an "effective" $\frac{1}{m\mathbf{k}}$ - potential generated by a six-quark operator, where two (predefined) heavy quark lines are closed to a tadpole.
The six-quark operators to be renormalized by diagrams like in Fig. 3.8 take the following form, after kinematic constraints have been imposed:

$$\begin{aligned}
\mathcal{O}_{6i} &= \frac{\mu_S^{4\epsilon}}{m}\,[\,\mathsf{cs}\,]_i \sum_{\mathbf{p},\mathbf{p}',\mathbf{q}} f_i(\mathbf{p},\mathbf{p}',\mathbf{q})\,\left[\psi^\dagger_{\mathbf{p}'}\,\psi_{\mathbf{p}}\,\chi^\dagger_{-\mathbf{p}'}\,\chi_{-\mathbf{p}}\,\psi^\dagger_{\mathbf{q}}\,\psi_{\mathbf{q}}\right], \\
&\quad \text{and} \qquad (3.31)\\
\mathcal{O}_{\bar{6}i} &= \frac{\mu_S^{4\epsilon}}{m}\,[\,\overline{\mathsf{cs}}\,]_i \sum_{\mathbf{p},\mathbf{p}',\mathbf{q}} f_i(\mathbf{p},\mathbf{p}',\mathbf{q})\,\left[\psi^\dagger_{\mathbf{p}'}\,\psi_{\mathbf{p}}\,\chi^\dagger_{-\mathbf{p}'}\,\chi_{-\mathbf{p}}\,\chi^\dagger_{-\mathbf{q}}\,\chi_{-\mathbf{q}}\right],
\end{aligned}$$

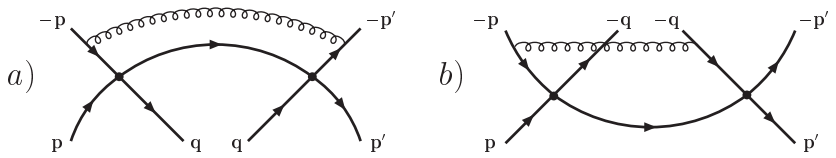

Figure 3.8: Examples for six (quark) leg diagrams obtained by cutting the potential loop in Fig. 3.6. Of course there are at least two possibilities to cut the potential loop for each two-loop topology of the Fig. 3.6 type. If not stated otherwise in all depicted graphs the heavy quark lines in the lower half represent quarks and the ones in the upper half antiquarks. The soft momentum labels displayed here refer to the soft three-momentum in the direction of the fermion flow (indicated by the little arrows) of the respective heavy (anti)quarks.

depending on whether the additional particle scattered off the potential-like quark-antiquark structure is a quark (potential loop is cut at the bottom as e.g. in Fig. 3.8 *a*)) or an antiquark (potential loop is cut at the top as e.g. in Fig. 3.8 *b*)). The f_i's are functions of the external soft three-momenta $\mathbf{p}$, $\mathbf{p}'$ and $\mathbf{q}$ and $[\,\mathsf{cs}\,]_i$ and $[\,\overline{\mathsf{cs}}\,]_i$ represent the color structure of the respective operators.
For the generation of an effective $\frac{1}{m\mathbf{k}}$ - potential by closing the heavy quark lines associated with the scattered (anti)quark to form a tadpole (Fig. 3.9), obviously only a subset of all possible color configurations of the $\mathcal{O}_{6i}$ operators is relevant. Due to color symmetry the associated Wilson coefficients $\mathcal{C}_{6i}$ and their counterterms are universal for all color configurations of the external fields. For our purpose we can therefore just as well define six-quark operators, that are closed in color space. I.e. we take the diagonal sum with respect to the color indices of the two (anti)quark fields with momentum $(-)\mathbf{q}$. Since closed color structures are usually more compact and can always be written in the $1\otimes\bar{1}$, $T^A\otimes\bar{T}^A$ basis we introduce the following versions of six-quark operators (together with their counterparts with four antiquark and two quark fields) for practical use:

$$\mathcal{O}_{6i}^{(1)} = \frac{\mu_S^{4\epsilon}}{m}\,1\otimes\bar{1}\sum_{\mathbf{p},\mathbf{p}',\mathbf{q}} f_i(\mathbf{p},\mathbf{p}',\mathbf{q})\left[\psi^\dagger_{\mathbf{p}'}\,\psi_{\mathbf{p}}\,\chi^\dagger_{-\mathbf{p}'}\,\chi_{-\mathbf{p}}\,\psi^\dagger_{\mathbf{q}}\,\psi_{\mathbf{q}}\right], \tag{3.32}$$

$$\mathcal{O}_{6i}^{(T)} = \frac{\mu_S^{4\epsilon}}{m}\,T^A\otimes\bar{T}^A\sum_{\mathbf{p},\mathbf{p}',\mathbf{q}} f_i(\mathbf{p},\mathbf{p}',\mathbf{q})\left[\psi^\dagger_{\mathbf{p}'}\,\psi_{\mathbf{p}}\,\chi^\dagger_{-\mathbf{p}'}\,\chi_{-\mathbf{p}}\,\psi^\dagger_{\mathbf{q}}\,\psi_{\mathbf{q}}\right].$$

Their Wilson coefficients $\mathcal{C}_{6i}^{(1,T)}$ ($\mathcal{C}_{\bar{6}i}^{(1,T)}$) will finally induce the ultrasoft running of the effective $\frac{1}{m\mathbf{k}}$ - potential.
Having defined the relevant operators we are now going to sketch the renormalization program using the six-quark operator approach step by step.
First we calculate the divergent terms of all six-quark leg diagrams with ultrasoft loops matching the power counting requirement specified above and close the po-

tential loop in color space. Note that in addition to the kind of topologies shown in Fig. 3.8 there are also graphs involving the $\psi\psi^\dagger\chi\chi^\dagger\mathbf{A}$ vertex of Eq. (2.29) (see section 5.3). From the counterterms $\delta\mathcal{C}_{6i}^{(1,T)}$ which are supposed to cancel these divergences we can then derive the running of $\mathcal{C}_{6i}^{(1,T)}(\nu)$ by means of the renormalization group formalism.

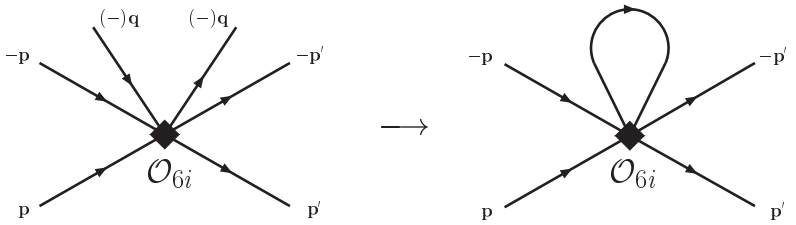

Figure 3.9: Closing the potential (anti)quark tadpole generated by the $\mathcal{O}_{6i}^{(1,T)}$ ($\mathcal{O}_{\bar{6}i}^{(1,T)}$) operators.

To close the two (anti)quark lines of the renormalized $\mathcal{O}_{6i}^{(1,T)}$ operators with momentum $(-)\mathbf{q}$ as illustrated in Fig. 3.9 we have to add the heavy quark propagator

$$\frac{i}{q_0 - \frac{\mathbf{q}^2}{2m} + i\epsilon} \tag{3.33}$$

to the momentum structure encoded in the $f_i(\mathbf{p}, \mathbf{p}', \mathbf{q})$'s and perform the integration over the potential loop momentum q. Since the only dependence on q_0 comes from the above propagator, we always find

$$\int \frac{dq_0}{2\pi} \frac{i}{q_0 - \frac{\mathbf{q}^2}{2m} + i\epsilon} \;=\; \frac{i}{2\pi}(-i\pi) \;=\; \frac{1}{2} \tag{3.34}$$

for the q_0 integral of the tadpole. The $\mathbf{q}$ integration over the $f_i(\mathbf{p}, \mathbf{p}', \mathbf{q})$'s then yields a $\frac{1}{|\mathbf{k}|}$ structure resembling a potential V_k, cf. Eq. (5.16).
The tadpole graph constructed in this way acts in all respects, e.g. in the renormalization of the effective currents (section 4.2), like the corresponding four-quark operator and is therefore referred to as an effective $\frac{1}{m\mathbf{k}}$ - potential $V_{k,\text{eff}}$.
A detailed calculation of the RG evolution of $V_{k,\text{eff}}$ at LL and NLL level along the lines sketched above is presented in sections 5.3 and 6.3.

Sum Operator Approach

An alternative way to deal with the UV divergences in diagrams like Fig. 3.6 *a*) and *b*) is the so-called sum operator approach, which will be shown to be equivalent to the method using six-quark operators, when describing the dynamics of a heavy quark-antiquark pair in vNRQCD. It was first introduced in Ref. [32].

Similar to the six-quark operator approach the integration over the potential loop three-momentum $\mathbf{q}$ will be carried out only after the UV divergences from the ultrasoft loops have been absorbed avoiding the problems explained in the beginning of this section. The integration over the zero component (q_0) of the potential loop momentum in contrast has been performed already in the first place.
To subtract the UV singularities obtained using this prescription we obviously need to add special four-quark operators to the Lagrangian, that explicitly contain a sum over the soft momentum label $\mathbf{q}$, which is understood to be replaced by the corresponding integral like

$$\sum_{\mathbf{q}} \to \int \frac{d^{d-1}q}{(2\pi)^{d-1}}\,, \tag{3.35}$$

when the operator is inserted in a matrix element. These so-called sum operators $\mathcal{O}_{ki}$ come along with the Wilson coefficients $\mathcal{V}_{ki}$ and read e.g. at LL level (see section 5.3)

$$\begin{aligned}
\mathcal{O}_{k1}^{(1)} &= \frac{\mu_S^{4\epsilon}}{m}\, 1\otimes\bar{1} \sum_{\mathbf{p},\mathbf{p}',\mathbf{q}} (f_0+f_1+2f_2)\, \left[\psi^\dagger_{\mathbf{p}'}\,\psi_{\mathbf{p}}\,\chi^\dagger_{-\mathbf{p}'}\,\chi_{-\mathbf{p}}\right], \\
\mathcal{O}_{k2}^{(T)} &= \frac{\mu_S^{4\epsilon}}{m}\, T^A\otimes\bar{T}^A \sum_{\mathbf{p}',\mathbf{p}',\mathbf{q}} (f_1+f_2)\, \left[\psi^\dagger_{\mathbf{p}'}\,\psi_{\mathbf{p}}\,\chi^\dagger_{-\mathbf{p}'}\,\chi_{-\mathbf{p}}\right].
\end{aligned} \tag{3.36}$$

Note that unlike the sums over the labels on the fields $\mathbf{p}$ and $\mathbf{p}'$ the "free" sum over $\mathbf{q}$ itself (i.e. without an accompanying ultrasoft spacetime integral like in Eq. (3.2)) scales like $v^{-2\epsilon}$ and therefore requires an additional compensating factor $\mu_S^{2\epsilon}$ in the renormalized four-quark operators in Eq. (3.36). This is because the $\mathbf{q}$ sum actually represents the integral in Eq. (3.35) and is only used in the Lagrangian to somehow be consistent with the notation adopted to implement the multipole expansion in vNRQCD.
As already mentioned the $\mathcal{O}_{ki}$ operators are renormalized at leading order by diagrams like in Fig. 3.6 after the q_0 and before the $\mathbf{q}$ integration is performed, whereas the $\mathcal{O}_{6i}$ operators are renormalized by six-leg diagrams as shown in Fig. 3.8 before closing the potential loop and performing any potential loop integration at all.
Obviously the number of (closed) diagrams contributing to the running of the $\mathcal{V}_{ki}$ is much smaller than the number of corresponding six-leg diagrams. On the other hand performing the q_0 integration before the ultrasoft loop momentum (k) integration using the residue theorem has a very similar effect as cutting the potential loop in the way it is done to obtain the six-leg diagrams of the Fig. 3.8 type.
To be more precise let us consider the graph in Fig. 3.6 *a*) and the respective six-leg diagrams shown in Fig. 3.10 as an example.

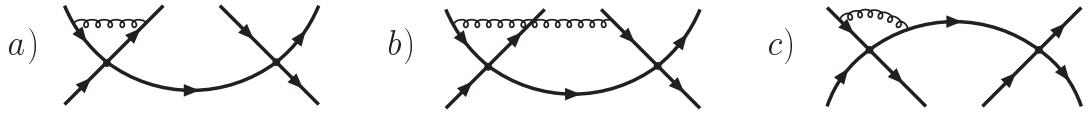

Figure 3.10: six-leg topologies obtained by cutting the potential loop in Fig. 3.6 *a*) in all possible ways.

The heavy quark loop in Fig, 3.6 *a*) has the propagator structure

$$\frac{i}{-q_0 + A_+} \cdot \frac{i}{q_0 + k_0 + A_+} \cdot \frac{i}{q_0 + A_+} \ , \tag{3.37}$$

where $A_+ := E - \frac{\mathbf{q}^2}{2m} + i\epsilon$. Each of these propagators represents a pole in the complex q_0 plane. The associated residues are given by

$$\mathsf{Res}[q_0 = -A_+] = \frac{i^3}{2A_+\, k_0} \ , \qquad \mathsf{Res}[q_0 = -k0 - A_+] = \frac{-i^3}{k_0(k_0 + 2A_+)} \tag{3.38}$$

in the lower half of the complex plane and

$$\mathsf{Res}[q_0 = A_+] = \frac{-i^3}{2A_+(k_0 + 2A_+)} \tag{3.39}$$

in the upper half. We observe now that each of the residues is in one-to-one correspondence with one of the (cut) diagrams displayed in Fig. 3.10: the residues in the lower half of the complex q_0 plane $\mathsf{Res}[q_0 = -A_+]$ and $\mathsf{Res}[q_0 = -k0 - A_+]$ correspond to the graphs Fig. 3.10 *a*) and *b*) respectively and the residue in the upper half $\mathsf{Res}[q_0 = A_+]$ to Fig. 3.10 *c*). Only the sign of $\mathsf{Res}[q_0 = A_+]$ seems to be not correct and there is an additional factor of i from the additional propagator in Fig. 3.6, whereas the missing $i\epsilon$ in the $\frac{1}{k_0}$ propagators in Eq. (3.38) does not matter. The difference between choosing $+i\epsilon$ or $-i\epsilon$ as prescription to perform the k_0 integral always amounts to a scaleless integral and vanishes in dimensional regularization. This can be checked easily applying the residue theorem to the k_0 integration. Remember that we have omitted a propagator with an artificial off-shellness a (see chapter 5) of the form

$$\frac{i}{k_0 + a + i\epsilon} \tag{3.40}$$

from the upper left external leg of each diagram in this discussion.
Now that we have assigned a six-leg diagram corresponding to the different possible cuts on the potential loop of the original two-loop diagram in Fig. 3.6 *a*) to every term that arises in the q_0 integration of the potential loop, we go on to show complete agreement of the two methods.

Due to the residue theorem we can either close the q_0 integration contour in the lower half or in the upper half of the complex plane. In the former case the result is the sum of the residues in Eq. (3.38) times a factor $\frac{(-2\pi i)}{2\pi}$ in the latter it is the residue in Eq. (3.39) times $\frac{(2\pi i)}{2\pi}$. The 2π in the denominator comes from the usual convention for the Fourier transformation to momentum space. Together with the i from the additional heavy quark propagator and the minus sign we encountered in Eq. (3.39) (as a consequence of the sign of q_0 in the first propagator of Eq. (3.37)) the contributions from the residue terms in the evaluation of the q_0 integral of diagram Fig. 3.6 *a*) exactly match the amplitudes of the corresponding diagrams in Fig. 3.10.
In the six-quark operator approach the divergent terms of such amplitudes are absorbed by the counterterms of the $\mathcal{O}_{6i}$. Then the running of $\mathcal{C}_{6i}$ is determined and finally $V_{k,\text{eff}}$ is generated by closing the potential tadpole (Fig. 3.9), where a factor of $\frac{1}{2}$ is added by the q_0 integration (Eq. (3.34)).
In the sum operator approach the (same) divergent terms are absorbed by the counterterms of the $\mathcal{O}_{ki}$. The running of $\mathcal{V}_{ki}$ is computed and $V_{k,\text{eff}}$ is generated only by performing the $\mathbf{q}$ integration without the factor $\frac{1}{2}$. But of course not all of the residues contribute to the q_0 integral of the potential loop. As mentioned above either the residues in the lower half of the complex plane (Eq. 3.38) or the residues in the upper half (Eq. 3.39) occur in the result. Alternatively we can just as well take all of them into account, but then we have to weight them by a factor of $\frac{1}{2}$. Therefore we obtain exactly the same $V_{k,\text{eff}}$ as in the six-quark operator approach.
This is also required by consistence insofar that the tadpole diagrams generated by the counterterms of the $\mathcal{O}_{6i}$ operators are supposed to cancel the divergences of all the fully evaluated two-loop diagrams like Fig. 3.6 *a*) or *b*), which of course are still part of the theory.

There is one subtlety in the above argument concerning the case that self-energy subdiagrams of the heavy quarks are involved. Consider for instance the diagrams displayed in Fig. 3.11.
The six-leg graphs Fig. 3.11 *a*) and *b*) can be associated with two of the four possible cuts on the potential loop in Fig. 3.11 *d*). The contributions from the residue corresponding to the two cuts on the lines to the left and to the right of the self-energy vanish as scaleless integrals in dimensional regularization. In the six-quark operator approach the divergences from self-energies on the respective external legs are canceled exactly by counterterm insertions. Thus the one-to-one correspondence statement we formulated above still holds.
The interesting point concerns the counterdiagrams in Fig. 3.11 *c*) and *e*). In Fig. 3.11 *e*) we can graphically cut the potential loop in three ways to obtain different diagrams. Two of the six-leg diagrams generated like this (by cutting on the left and right of the counterterm insertion) have already been used to

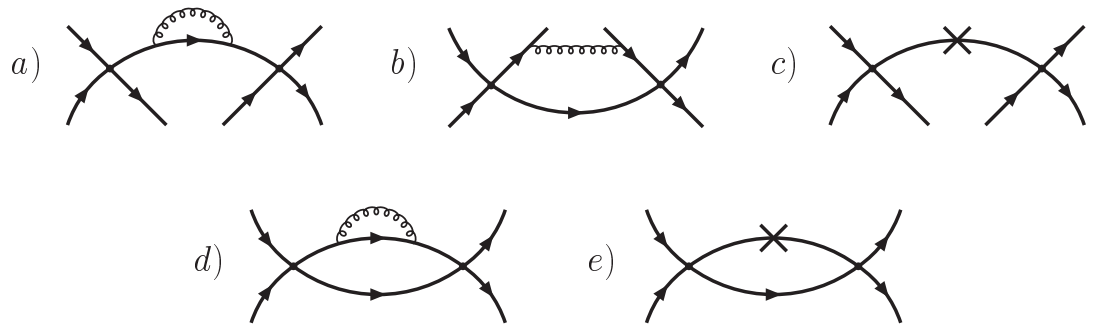

Figure 3.11: *d*) Two-loop diagram with potential loop and heavy quark self-energy subdiagram. *e*) Counterdiagram to subtract the subdivergence in *d*). *a*) - *c*) Six-leg graphs corresponding to the non-vanishing cuts on the potential loop in *d*) and *e*).

cancel the divergences of the six-leg loop diagrams which are not displayed. The third cut yields diagram Fig. 3.11 *c*) and cancels the divergence of Fig. 3.11 *a*). However, using the sum operator approach we only find two poles in the complex q_0 plane of the loop in Fig. 3.11 *e*), because the self-energy counterterm insertion together with the additional propagator just adds a correction factor to the pre-existing propagator. One of the residues obviously corresponds directly to the cut on the lower propagator (Fig. 3.11 *c*)).
But what about the other residue? The answer is rather tricky: it subtracts a divergence in one residue of graph Fig. 3.11 *d*) which reproduces the same amplitude as diagram Fig. 3.11 *b*). This diagram is actually UV finite because of the additional propagators in the loop and is neglected in the renormalization of the six-quark operators. Nevertheless a divergence exists in the six-quark operator approach which is interpreted as infrared singularity. In the calculation of the closed potential loop however the divergence occurs at an intermediate step and formally must be taken into account. It is exactly canceled by the residue of Fig. 3.11 *e*), which has not been identified with an ordinary six-leg diagram.
Therefore the relation between the graphical cuts to obtain the six-leg diagrams and the residues in the sum operator approach is not always straightforward, but still exists also for the case of two-loop diagrams with heavy quark self-energies. The final result is the same for both methods: the diagrams containing a self-energy subdivergence (as the only ultrasoft loop) are exactly cancelled by the appropriate counterdiagrams and do not contribute to the anomalous dimensions of the $\mathcal{O}_{6i}$ or the $\mathcal{O}_{ki}$ operators.
We have shown that the six-quark operator approach is not just another way of organizing the terms we obtain in the sum operator approach, but is a stand-alone method, where e.g. infrared singularities consequently must not be taken into account in the renormalization process. One does not need any information

about the "original" potential loop diagram. Actually it will turn out below that it is rather the other way around: the renormalization of the $\mathcal{O}_{ki}$ operators is inspired by the evaluation of the corresponding six-leg diagrams.

So far we have neglected higher order terms of the multipole expansion of our example graphs in the discussion. They arise e.g. from insertions of the kinetic $\frac{\mathbf{p}\cdot\nabla}{m}$ or $\frac{\nabla^2}{2m}$ operators on the heavy quark lines or from the replacement of a Coulomb potential by one of its higher order relatives (Eq. (2.29)) inside the ultrasoft loop and come along with powers of the ultrasoft momentum k in the numerator of Eq. 3.37. To obtain these higher order contributions in a systematic way we can add the ultrasoft three-momentum $\vec{k}$ (not to be confused with the soft $\mathbf{k} = \mathbf{p}' - \mathbf{p}$) to the soft $\mathbf{q}$ in the loop as if they would be of the same order and expand in $\vec{k}$ up to the given order afterwards. In this way we automatically find all the higher order terms in the multipole expansion for the respective loop diagram. The propagator in the middle of Eq. 3.37 for example is replaced in this procedure in the following way.

$$\frac{i}{q_0 + k_0 + A_+} = \frac{i}{q_0 + k_0 + E - \frac{\mathbf{q}^2}{2m} + i\epsilon} \rightarrow \frac{i}{q_0 + k_0 + E - \frac{(\mathbf{q}+\vec{k})^2}{2m} + i\epsilon} \tag{3.41}$$

For each two-loop diagram of the Fig. 3.6 type, except for diagrams with disconnected self-energies on the external legs, there are two possibilities to route the ultrasoft momentum k. Given an arbitrary routing we always find another one through the propagators of the potential loop which are not part of the former routing. Mathematically the different routings can be transformed into each other by shifting the potential loop momentum $q^\mu = (q_0, \mathbf{q})$ by $\pm\, k^\mu$. But before performing both integrals over k and q (including $\mathbf{q}$!) they are in general not equivalent.

This causes an ambiguity in the sum operator approach, which at LL level does not affect the final running of $V_{k,\mathrm{eff}}$, but makes a consistent renormalization of the operators at the multi-loop level cumbersome. The reason is that according to the routing we have chosen for the n-loop diagrams with closed potential loop we have to introduce sum operators $\mathcal{O}_{ki}$ with different soft momentum, i.e. f_i functions, to absorb the divergences. Therefore we will generally find a different operator basis to be renormalized at $(n+1)$-loop level if we do not assign a unique and consistent prescription how to route the ultrasoft momenta. For an operator basis changing from loop level to loop level it is not possible to derive well-defined anomalous dimensions of the respective Wilson coefficients.

Interestingly in the LL renormalization of the $\mathcal{O}_{ki}$ operators using Coulomb gauge [32] the form of the $\mathcal{O}_{ki}$, that receive a non-vanishing counterterm, is unambiguous (Eq. (3.36)), because only a few diagrams [62] without kinetic operator insertions, i.e. of leading order in the multipole expansion, have to be evaluated here. In Feynman gauge however at the same order also diagrams of higher order in the multipole expansion contribute [62]. Thus $\vec{k}$ appears in the

integrands, and we are consequently confronted with different results for the $\mathcal{O}_{ki}$ (with non-trivial running) depending on the routing of the ultrasoft momentum. Obviously we do not have such ambiguity problems in the six-quark operator approach, since there is a unique routing for all six-leg diagrams contributing in the renormalization procedure. Fortunately this fact guides us towards a prescription for how to evaluate the diagrams with potential loop (e.g. Fig. 3.6), which provides a consistent renormalization in the sum operator approach as well:

1.) Determine all residues according to the poles of the propagator structure of the potential loop in the complex q_0 plane for arbitrary routing of the ultrasoft momentum k.

2.) Shift the soft three-momentum $\mathbf{q}$ by $\pm\vec{k}$ for each residue in such a way, that in the original potential loop there would have been no ultrasoft $\vec{k}$ flow through the propagator line(s), that vanishes (is set on-shell) in the respective residue. Graphically this means: never cut through the routing of $\vec{k}$.

3.) Perform the ultrasoft loop momentum integration over k.

4.) Sum all the residues together with the above mentioned factor of i and the correct sign and divide by two.

The operator basis to absorb the divergences found in this way at LL in Feynman gauge agrees with Eq. (3.36), which is also obtained in Coulomb gauge.

All arguments given in this subsection for the example with one ultrasoft loop can be straightforwardly generalized to the case with two and more ultrasoft loops.
So the final outcome of the above discussion is basically that the derivation of the running of $V_{k,\text{eff}}$ can be done by renormalizing six-quark operators $\mathcal{O}_{6i}$ or sum operators $\mathcal{O}_{ki}$. Both approaches are equivalent in this respect provided we follow the above prescription for the renormalization of the sum operators. The difference regarding the respective Wilson coefficients of corresponding operators in both approaches is only a factor of $\frac{1}{2}$:

$$\mathcal{V}_{ki} \,=\, \frac{1}{2}\,(\mathcal{C}_{6i} + \mathcal{C}_{\bar{6}i})\;. \tag{3.42}$$

Most of the time we were referring to the $\mathcal{O}_{6i}$ so far, we also understood the (charge conjugated) $\mathcal{O}_{\bar{6}i}$ operators and we will continue to do so unless explicitly stated otherwise.
For illustration and to point out the details of the LL and NLL calculations in sections 5.3 and 6.3 we will mainly use the six-quark operator approach. Nevertheless we will usually present the final results for $\delta\mathcal{V}_{ki}$ and $\mathcal{V}_{ki}$, since the factor of $\frac{1}{2}$ from closing the tadpole (Fig. 3.9) is already included and to compare our (LL) results to previous literature, such as Ref. [32].

3.6 Wilson Lines and Field Redefinition

In this section we will prove a general statement concerning ultrasoft renormalization in vNRQCD, that is mainly used in this work to perform important cross checks of the calculations in chapters 5 and 6. It says that quantum corrections to physical observables, such as couplings and Wilson coefficients, generated by ultrasoft gluon loops attached to a heavy quark-antiquark pair will at least contribute a factor of v^2 to the power counting of the calculated quantity.
As an example consider the Coulomb potential and an ultrasoft gluon loop attached to it in all possible ways like in Fig. 5.1. The UV divergent parts of these diagrams will generally contribute to the renormalization of the potential four-quark operators in Eq. (2.27).
From the part of the vNRQCD Lagrangian describing the interaction of ultrasoft gluons with heavy (anti)quarks

$$\mathcal{L}_u \;=\; \sum_{\mathbf{p}} \psi^\dagger_{\mathbf{p}} \Big[iD^0 \,+\, i\,\frac{\mathbf{p}\cdot\mathbf{D}}{m} \,+\, \frac{\mathbf{D}^2}{2m} \,+\, \ldots \Big] \psi_{\mathbf{p}} \,+\, \ldots \,, \tag{3.43}$$

where $D^0 = \partial^0 + igA^0$ and $\mathbf{D} = \nabla - ig\mathbf{A}$, we know that there are different kinds of interaction terms for $\mathbf{A}$ gluons at different orders in v. The A^0 gluon however only couples at leading order ($\sim v^0$).
The claim is now that due to the above statement the ultrasoft contribution to the counterterm of the Coulomb potential $\delta\mathcal{V}_c$ ($\sim v^0$) must vanish. It is induced by the lowest order diagrams of the Fig. 5.1 type, i.e. only A^0 gluons are involved and there are no kinetic operator insertions placed on the heavy quark lines. Indeed taking into account also the lowest order wavefunction counterterms associated with the external legs (cf. Eqs. 5.10 and 5.11) the overall divergence to be absorbed by $\delta\mathcal{V}_c$ adds up to zero [31]. Thus ultrasoft radiative corrections do not renormalize the leading order quark-antiquark potential in vNRQCD but they do e.g. cause mixing between the $\mathcal{O}(v^2)$ potentials and the Coulomb potential of the form of Eq. (3.27) as we will see in detail in section 5.2.
Of course one can check all this by explicitly calculating the Feynman diagrams, but there is also a very general argument why the above statement is true for any observable in vNRQCD affected by ultrasoft renormalization.

The idea is to perform a field redefinition in such a way that the interaction of the A^0 gluon at $\mathcal{O}(v^0)$ vanishes in the redefined Lagrangian and we are left with ultrasoft gluon interaction terms of order $\geq v^2$. It is inspired by similar concepts that have been used in the effective field theories HQET and "Soft Collinear Effective Theory" (SCET) to decouple soft gluons from heavy quarks and ultrasoft gluons from collinear fields in the respective leading order Lagrangians [36, 71].
The field redefinition involves a so called (ultrasoft) Wilson line given by

$$W(x) = \mathcal{P} \exp\left(ig \int_{-\infty}^{x_0} ds\, A^0(s,\vec{x}) \right) \,, \tag{3.44}$$

where $\mathcal{P}$ denotes the path ordering operator, which orders the gauge fields from left to right in the order of decreasing s values. It obeys the (defining) property that the zero component of the ultrasoft covariant derivative acting on it vanishes:

$$D^0\, W(x) \,=\, 0\,, \tag{3.45}$$

and the unitary condition

$$W^\dagger(x)\, W(x) \,=\, 1\,. \tag{3.46}$$

Combining these equations we find

$$W^\dagger D^0 W\, \psi \,=\, \partial^0\, \psi \tag{3.47}$$

for an arbitrary test function $\psi(x)$. The $SU(3)$ gauge transformation law for $W(x)$ reads (see e.g. [38])

$$W(x) \,\to\, U(x) W(x) U^{-1}(-\infty, \vec{x})\,, \tag{3.48}$$

where $U(x) = \exp[i\alpha^A(x) T^A]$ is the $SU(3)$ gauge transformation matrix in the fundamental representation.
Defining a new heavy quark field $\Phi_{\mathbf{p}}(x)$ by

$$\psi_{\mathbf{p}}(x) \,=\, W(x) \Phi_{\mathbf{p}}(x) \tag{3.49}$$

will therefore preserve the gauge invariance of $\mathcal{L}_u$, if $\Phi_{\mathbf{p}}(x)$ transforms like $\Phi_{\mathbf{p}}(x) \to U(-\infty, \vec{x}) \Phi_{\mathbf{p}}(x)$. For the argument below we can just as well adopt the convention $U(-\infty, \vec{x}) \equiv 1$ and consider $\Phi_{\mathbf{p}}(x)$ as gauge invariant. So $\Phi_{\mathbf{p}}(x)$ and $\psi_{\mathbf{p}}(x)$ are related by an unitarity transformation and both fields are equal in the limit of vanishing interaction with the gluon field:

$$\Phi_{\mathbf{p}}(x) \,\xrightarrow{g \to 0}\, \psi_{\mathbf{p}}(x) \tag{3.50}$$

i.e. they are subject to the same free field equations of motion.
We conclude that for the calculation of physical S-matrix elements using the LSZ formula [72] the field redefinition in Eq. (3.49) actually only amounts to an ordinary change of variables in the path integral (see e.g. [39]) and physical observables remain unchanged no matter if $\Phi_{\mathbf{p}}(x)$ or $\psi_{\mathbf{p}}(x)$ is used as fundamental heavy quark field. Sometimes this goes under the name of "Haag's Theorem" [73].

In terms of the redefined field $\Phi_{\mathbf{p}}(x)$ the Lagrangian Eq. (3.43) reads

$$\mathcal{L}_u = \sum_{\mathbf{p}} \Phi^\dagger_{\mathbf{p}} \left[i\partial^0 \,+\, W^\dagger i\, \frac{\mathbf{p}\cdot\mathbf{D}}{m} W \,+\, W^\dagger \frac{\mathbf{D}^2}{2m} W \,+\, \ldots \right] \Phi_{\mathbf{p}} + \ldots\,, \tag{3.51}$$

where Eq. (3.47) was applied to turn the zero component of the ultrasoft covariant derivative D^0 into a partial derivative.
We immediately observe that in the new theory defined by Eq. (3.51) there is

no interaction whatsoever of the heavy quark with ultrasoft gluons at leading order ($\sim v^0$). All effects of A^0 gluons are now encoded in the W's appearing first at order $v \sim \frac{\mathbf{p}}{m}$ and it is obvious that there is no ultrasoft contribution to the running of the Coulomb potential. Since the original and the redefined theory are physically equivalent results like that must hold in both frameworks as was shown above for the example of the Coulomb potential.
Extracting the leading order (w.r.t. g and v) A^0 interaction term hidden in the second term of Eq. (3.51) we find

$$\begin{aligned}
\Phi_{\mathbf{p}}^\dagger\, W^\dagger i\,\frac{\mathbf{p}\cdot\mathbf{D}}{m} W\,\Phi_{\mathbf{p}} &= \Phi_{\mathbf{p}}^\dagger\,(1-ig\int ds\,A^0)\,i\frac{\mathbf{p}\nabla}{m}\,(1+ig\int ds\,A^0)\,\Phi_{\mathbf{p}} + \dots \\
&= \Phi_{\mathbf{p}}^\dagger\Big[(-ig\int ds\,A^0)\,i\frac{\mathbf{p}\nabla}{m} + i\frac{\mathbf{p}\nabla}{m}\,(ig\int ds\,A^0)\Big]\Phi_{\mathbf{p}} + \dots \\
&= -g\,\Phi_{\mathbf{p}}^\dagger\left(\frac{\mathbf{p}\nabla}{m}\int_{-\infty}^{x_0} ds\,A^0(s,\vec{x})\right)\Phi_{\mathbf{p}} + \dots\,. \qquad (3.52)
\end{aligned}$$

It can be rewritten using

$$\begin{aligned}
\int_{-\infty}^{x_0} ds\,A^0(s,\vec{x}) &= \int_{-\infty}^{\infty} ds\;\theta(x_0-s)\int\frac{d^4k}{(2\pi)^4}\,\hat{A}^0(k)\,e^{-i(k_0 s-\vec{k}\vec{x})} \\
&= \int_{-\infty}^{\infty} ds\int\frac{d\omega}{2\pi}\,\frac{i\,e^{-i\omega(x_0-s)}}{\omega+i\epsilon}\int\frac{d^4k}{(2\pi)^4}\,\hat{A}^0(k)\,e^{-i(k_0 s-\vec{k}\vec{x})} \\
&= \int\frac{d^4k}{(2\pi)^4}\,\hat{A}^0(k)\int d\omega\,\frac{i\,e^{-i(\omega x_0-\vec{k}\vec{x})}}{\omega+i\epsilon}\,\delta(\omega-k_0) \\
&= \int\frac{d^4k}{(2\pi)^4}\,\hat{A}^0(k)\,\frac{i}{k_0+i\epsilon}\,e^{-ik\cdot x} \qquad (3.53)
\end{aligned}$$

in terms of the ultrasoft momentum space Fourier transform $\hat{A}^0(k)$ of the gluon field as

$$-g\,\Phi_{\mathbf{p}}^\dagger\left(\frac{\mathbf{p}\nabla}{m}\int\frac{d^4k}{(2\pi)^4}\,\frac{i}{k_0+i\epsilon}\,\hat{A}^0(k)\,e^{-ik\cdot x}\right)\Phi_{\mathbf{p}}\,. \qquad (3.54)$$

Since ∇ in Eq. (3.54) essentially yields a factor of $\vec{k}$, the momentum space Feynman rules for the leading order A^0 and $\mathbf{A}$ interaction with heavy quarks in the redefined theory indeed scale like $\frac{\mathbf{p}}{m}$. To generate ultrasoft quantum corrections to a heavy quark-antiquark system of course at least two of these vertices are needed and contribute at least a factor of v^2 to the scaling according to the power counting formula Eq. (3.4). This is exactly what has been stated in the beginning. Eq. (3.54) moreover allows us to more or less directly keep track of how the different terms in the calculations of chapter 5 and 6 would arise in the redefined theory.

3.7 Zero-Bin Subtraction and the Pull-Up Mechanism

In low energy effective field theories, that contain distinct fields for different momentum regions of the same physical particle like vNRQCD or SCET [71], typically important subtleties regarding infrared singularities exist in the context of renormalization. They occur in particular when the operators involving the respective degrees of freedom are all matched onto the underlying full theory at the same (high) scale. We will address these issues in this section using a simple example at one-loop level. For a general and more detailed discussion we refer to Ref. [70].

For the construction of vNRQCD the (physical) gluon field as it appears in QCD was split into different modes w.r.t. the scale of the energy (E) and the three-momentum (p) they carry, e.g. soft ($E \sim p \sim mv^2$), potential ($E \sim mv^2, p \sim mv$), ultrasoft ($E \sim p \sim mv^2$) etc.. The non-resonant degrees of freedom, e.g. the potential gluon, were integrated out, but the soft and the ultrasoft gluon survive this process and represent fundamental fields in the effective Lagrangian.
In section 3.1 we have derived a different power counting according to the assigned momentum regime of the two gluons in vNRQCD. Furthermore we have found in section 3.3 that the strong coupling constants associated with soft and ultrasoft gluons differ from each other as well, when they are run down from the hard matching scale $\mu_S = \mu_U = m$ to the soft $\mu_S = mv$ and ultrasoft scale $\mu_U = mv^2$ respectively in order to resum potentially large logarithms within the RGI effective theory framework.
The resummation of large logarithms resulting amongst others in two different strong coupling constants α_S and α_U is the big advantage and the essential difference of the effective field theory approach compared to a non-relativistic fixed order calculation. The latter basically amounts to expanding loop integrals in full QCD using the method of regions explained in section 2.3.
To point out the subtleties in the renormalization of vNRQCD mentioned above it is sometimes helpful to study to which extent both approaches resemble each other.

Consider for example the full QCD box diagram shown Fig. 3.12.

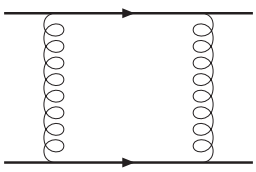

Figure 3.12: Box diagram in full QCD.

Performing the threshold expansion there will be contributions from the loop momentum regions defined in Eq. (2.16) at different orders in v. Among them there is one corresponding to the soft EFT diagram in Fig. 3.13 a)[3].

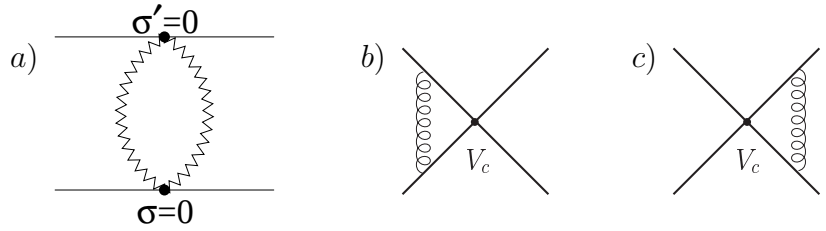

Figure 3.13: vNRQCD loop diagrams: a) soft (gluon) loop. b), c) Coulomb potential dressed with ultrasoft gluons.

When carrying out the soft loop integration in vNRQCD according to Eq.(3.10) we find this diagram to be infrared divergent. In the threshold expanded QCD box this divergence is exactly canceled by an UV divergence from a contribution in the ultrasoft regime that corresponds to the sum of the vNRQCD diagrams in Figs. 3.13 b) and c) with ultrasoft (A^0) gluon loops. This is because the correctly expanded QCD diagram can of course not depend on the cutoffs separating the different momentum regions.
In the EFT though, this cancellation does not take place, since due to the resummation of logarithms of different dynamical scales the coupling of the soft gluons in Fig. 3.13 a) and the ultrasoft gluons in Figs. 3.13 b), c) do not coincide for $\nu < 1$: $\frac{\alpha_S}{\epsilon_{IR}} - \frac{\alpha_U}{\epsilon_{UV}} \neq 0$. Soft infrared singularities of the above kind however turn out to be unphysical, because they can not be removed from physical observables like bound state energies or scattering processes e.g. by taking into account the complete set of real corrections, i.e. Bremsstrahlung.
That is why, in the earlier literature, a so called pull-up mechanism was implemented in the EFT calculations by hand [66] in order to convert these divergences into UV ones, $\frac{\alpha_S}{\epsilon_{IR}} \to \frac{\alpha_S}{\epsilon_{UV}}$. These were then absorbed by appropriate counterterms and contributed correctly to the anomalous dimensions of the vNRQCD Wilson coefficients [25, 62].

The occurrence of IR singularities in soft EFT diagrams like Fig. 3.13 a), which are actually supposed to describe short distance effects, as well as the existence of UV divergences in the ultrasoft diagrams Figs. 3.13 b), c) associated with large distance physics, indicates that there is formally a double counting w.r.t. the covered momentum region among these amplitudes. Whereas there is no problem with the ultrasoft UV divergences and a double counting in the

[3]The graph in Fig. 3.13 a) actually includes contributions associated with the crossed QCD box graph as well, but those are neglected in the following argument for simplicity. For details see Ref. [70].

UV region is automatically corrected for by the renormalization and matching procedure, as argued in section 3.2, the IR region has to be treated more carefully in the EFT.

The reason for the double counting in the infrared is our sloppy treatment of the sums over the soft labels of the soft (gluon, ghost, light quark) fields in the vNRQCD Lagrangian. Actually these sums should be carried out over the full range of discrete values for the soft label q on a grid corresponding to Fig. 2.6 except for $q = 0$, i.e. $\sum_q \to \sum_{q\neq 0}$. That is because the zero-bin (grey area in Fig. 2.6) is already reserved for the ultrasoft fields.
As a consequence the replacement according to Eq. (3.10) for soft loops is not completely correct. More precisely the regions, where one of the soft propagators involved in the loop only carries ultrasoft momentum, i.e. the zero-bins, should be removed from the soft loop integral. Since the replacement Eq. (3.10) in practice simplifies calculations a lot by allowing the use of dimensional regularization also for soft loops, we would like to keep it and only subtract the zero-bins, one for each soft propagator, after the total integration. A consistent prescription of how to perform this zero-bin subtraction has been first set up and investigated in Ref. [70].

It turns out that the zero-bin subtraction not only avoids the IR double counting as described above, but also automatically effects a conversion of unphysical soft IR singularities into UV divergences as by the pull-up mechanism.
To determine the different zero-bin contributions, which have to be subtracted from a soft loop, we have to fix the soft loop momentum label in the original integrand to the zero-bin values of each soft propagator and integrate the terms obtained in this way over the residual ultrasoft momenta. In dimensional regularization the limits of the ultrasoft integration in the zero-bin regions are again formally taken to infinity.
To distinguish the zero-bins from soft integrals we therefore have to expand consistently in the residual ultrasoft loop momentum in analogy to the method of regions as described in section 2.3. The expansion must be done up to high enough order that the difference between the original and the zero-bin integrand vanishes when the soft loop momentum approaches the respective zero-bin value and the residual ultrasoft momentum is set to zero as well. I.e. the (infrared) poles of both integrands agree.

Thus the zero-bin contributions for an arbitrary soft vNRQCD loop basically arise from the integrand of the corresponding full QCD diagram, as e.g. Fig. 3.12, by a twofold expansion. In the first the loop momentum is assumed to be of $\mathcal{O}(mv)$ and in the second it is assumed to be of $\mathcal{O}(mv^2)$. Therefore the total subtraction term generally consists of a number of scaleless integrals that vanish in dimensional regularization. However some of these integrals might have the divergent structure $\frac{1}{\epsilon_{IR}} - \frac{1}{\epsilon_{UV}}$.

Since a possible $\frac{1}{\epsilon_{IR}}$ term of the soft integral exactly matches the total $\frac{1}{\epsilon_{IR}}$ term of the zero-bin contributions by construction, the subtraction results in a reinterpretation of the infrared divergences of soft loops according to the pull-up mechanism.

In fact the only effect of the zero-bin subtraction procedure is to reveal that the logarithms of soft external scales associated with logarithmic infrared singularities from soft gluon (ghost, light quark) loops do not cancel in the calculation of measurable quantities and have to be resumed in a renormalization group improved EFT in the same way as their UV counterparts.
As an aside note that a corresponding pull-up mechanism does not exist for heavy quark potential loops, because there is only one heavy quark field in the EFT in contrast to two light quark fields (soft and ultrasoft), and therefore no need to subtract zero-bins in order to avoid a double counting. This means that soft IR singularities from potential loops must cancel otherwise [31].

Let us return now to our example diagram in Fig. 3.13 *a*), where the three-momentum exchange of the two heavy quarks is $\mathbf{k} = \mathbf{p}' - \mathbf{p}$. The routing of the soft loop momentum q^μ is chosen w.l.o.g. such that the soft gluon propagator on the left hand side is proportional to $\frac{1}{q_0^2 - \mathbf{q}^2 + i\epsilon}$ and the one on the right hand side to $\frac{1}{q_0^2 - (\mathbf{k}-\mathbf{q})^2 + i\epsilon}$.
The two zero-bins therefore have the soft momentum labels $q_1^\mu = 0$ and $q_2^\mu = (0, \mathbf{k})$ respectively. Replacing q in the soft loop integrand by $q_{1,2} + l$, where l is the residual ultrasoft momentum in the zero-bins, gives terms proportional to $\frac{1}{(l^2+i\epsilon)(l_0^2 - (\mathbf{k}-\vec{l})^2 + i\epsilon)}$ and $\frac{1}{(l_0^2 - (\mathbf{k}+\vec{l})^2 + i\epsilon)(l^2+i\epsilon)}$. In this case it is sufficient to keep only the leading order of the expansion in l and we find that the integrand of both subtraction terms comprises the structure $\frac{-1}{(l^2+i\epsilon)\,\mathbf{k}^2}$. So one of the original soft gluons is replaced by an ultrasoft gluon and the other one by a Coulomb potential ($\frac{1}{\mathbf{k}^2}$) just as in Figs. 3.13 *b*) and *c*).

A more careful analysis [70] shows that also the missing heavy quark propagators in the ultrasoft loops are correctly reproduced in the zero-bin subtraction terms when the full structure of the soft vertices is taken into account. An important difference to the depicted Feynman graphs in Figs. 3.13 *b*) and *c*) is however that the external quark lines must be set on-shell in the zero-bin contributions, since otherwise they would not be scaleless. All strong coupling constants remain of course soft (α_S).
After the subtraction of this kind of scaleless amplitudes the spurious $\frac{1}{\epsilon_{IR}}$ divergence of the soft loop Fig. 3.13 *a*) is turned into the $\frac{1}{\epsilon_{UV}}$ divergence given in Eq. (5.29)[3].

From the relation between soft and ultrasoft loops in vNRQCD, which was pointed out above using the example graphs in Fig. 3.13, we can furthermore conclude that every UV divergent ultrasoft loop goes along with an IR divergence from a soft loop of the same form but with opposite sign and α_U replaced by α_S.

The latter is pulled up to the UV after the zero-bin subtraction. In a fixed order calculation these divergences would even cancel as required by the method of regions.

Since the zero-bin subtraction has to be done for each soft propagator in a vNRQCD Feynman diagram irrespective of the number of loops the findings of this section basically hold at all orders in the loop expansion [70].
As far as this work is concerned we actually only make use of the last statement. According to it we will postulate the existence of a soft pendant for the ultrasoft UV divergences we find in chapters 5 and 6. These additional terms, that only differ in sign and the type of the coupling constant, are called "pull-up terms" [66].

Chapter 4

Phenomenological Impact of the Running of the Potentials

As already mentioned in the introduction the main motivation for this work is to decrease the theoretical uncertainty in the normalization of the resonance cross section for top pair production in $e^+ e^-$ collisions. At present the error in the RGI prediction of this quantity, estimated by variation of the renormalization scale (ν) and the convergence behavior of higher order corrections, amounts to 6% [27].

In this chapter we reveal the effects of the running of the vNRQCD potentials on the total cross section for $t\bar{t}$ production in the threshold region. We point out why in particular the ultrasoft running at NLL level is important to reach the aim of a theoretical uncertainty $\frac{\delta\sigma_{\rm tot}}{\sigma_{\rm tot}}$ below 3%. Such a small theory error is needed to match the statistical uncertainties of future experimental data from a linear collider [9] in order to extract precise values for Γ_t, α_s and the top Yukawa coupling y_t as explained in the introduction.
We outline the strategy to calculate $\sigma_{\rm tot}(e^+e^- \to t\bar{t}\,)$ within the vNRQCD framework in section 4.1. The NNLL running of the Wilson coefficient $c_1(\nu)$ of the effective production (annihilation) current for a non-relativistic $t\bar{t}$ pair in a ${}^3S_1$ state is identified to be the source of the relatively large error in the current (incomplete) NNLL result.
In section 4.2 the different contributions to the anomalous dimension of $c_1(\nu)$ are specified and further investigated. We argue why it is worth determining the ultrasoft part of the missing NNLL 'mixing' contribution. This is actually where the NLL RG running of the potentials up to $\mathcal{O}(v^2)$ enters, whose derivation is the main purpose of this thesis.

Another field of application for the NLL results of the vNRQCD potentials is the bottom mass determination from Υ sum rules, i.e. from large-n ($4 \lesssim n \lesssim 10$) moments of the total cross section for the Υ meson (bottonium in ${}^3S_1$ state) production in $e^+ e^-$ collisions [17, 74]. We will however not address it in the current thesis and refer to future publications on this subject.

4.1 The Cross Section $\sigma_{\rm tot}(e^+e^- \to t\,\bar{t}\,)$

The total cross section $\sigma_{\rm tot}(e^+e^- \to \gamma^*, Z^* \to q\,\bar{q})$ for $q\,\bar{q}$ production from $e^+\,e^-$ annihilation via a virtual photon or Z boson in full QCD can be cast into the generic form

$$\sigma_{\rm tot}^{\gamma,Z}(s) = \sigma_{\rm pt}\Big[\, F^v(s)\, R^v(s) + F^a(s) R^a(s)\Big]\,, \tag{4.1}$$

where $\sqrt{s}$ is the c.m. energy and $\sigma_{\rm pt} = 4\pi\alpha^2/(3s)$ is the LO total production cross section for massless particles. The usual method used to determine the vector and axial-vector R-ratios of $q\,\bar{q}$ production is based on the optical theorem (see e.g. [38]) and yields

$$\begin{aligned} R^v(s) &= \frac{4\pi}{s}\,{\rm Im}\left[-i\int d^4x\, e^{iq\cdot x}\left\langle\, 0\,\middle|\, T\, j^v_\mu(x)\, j^{v\mu}(0)\,\middle|\, 0\,\right\rangle\right]\,, \\ R^a(s) &= \frac{4\pi}{s}\,{\rm Im}\left[-i\int d^4x\, e^{iq\cdot x}\left\langle\, 0\,\middle|\, T\, j^a_\mu(x)\, j^{a\mu}(0)\,\middle|\, 0\,\right\rangle\right]\,. \end{aligned} \tag{4.2}$$

In Eq. (4.2) j^v_μ, j^a_μ refer to the vector and axial-vector currents, that produce (annihilate) a quark-antiquark pair in the full theory respectively and $q = (\sqrt{s}, 0)$. The prefactors $F^v(s)$, $F^a(s)$ contain the effects from the γ and Z exchange and are given in Ref. [25].
Switching to vNRQCD the R-ratios adopt the parametric structure of Eq. (2.15). At NNLL level the currents have to be replaced by their non-relativistic counterparts $\mathbf{J}^{v,a}_{\mathbf{p}}$ in Eq. (2.35) and we obtain

$$\begin{aligned} R^v(s) &= \frac{4\pi}{s}\,{\rm Im}\Big[\, c_1^2(\nu)\, \mathcal{A}_1(v,m,\nu) + 2\, c_1(\nu)\, c_2(\nu)\, \mathcal{A}_2(v,m,\nu)\,\Big]\,, \\ R^a(s) &= \frac{4\pi}{s}\,{\rm Im}\Big[\, c_3^2(\nu)\, \mathcal{A}_3(v,m,\nu)\,\Big]\,, \end{aligned} \tag{4.3}$$

where the $\mathcal{A}_i$ are effective current correlators scaling as $\mathcal{A}_1 \sim v^0$ and $\mathcal{A}_{2,3} \sim v^2$. The dominant one is associated with leading order S-wave production of a heavy quark antiquark pair and is given by

$$\mathcal{A}_1(v,m,\nu) = i\sum_{\boldsymbol{p},\boldsymbol{p}'}\int d^4x\, e^{i\hat{q}\cdot x}\left\langle\, 0\,\middle|\, T\, \boldsymbol{O}_{\mathbf{p},1}(x)\boldsymbol{O}^\dagger_{\boldsymbol{p}',1}(0)\middle|\, 0\,\right\rangle, \tag{4.4}$$

where now $\hat{q} = (\sqrt{s} - 2m, 0)$ and $\boldsymbol{O}_{\mathbf{p},1}$ is taken from Eq. (2.34).
By choosing $\nu \sim v$ all logarithmic terms of the form $(\alpha_s \ln v)^n$ (LL), $\alpha_s(\alpha_s \ln v)^n$ (NLL) and $\alpha_s^2(\alpha_s \ln v)^n$ (NNLL) appearing in the contributing matrix elements at all orders in α_s are resummed into the Wilson coefficients in Eq. (4.3) as emphasized in section 2.2. As far as this thesis is concerned, we are only interested in the $c_1^2(\nu)$ term of Eq. (4.3), since the other terms first enter at NNLL order and are already fully known [25].

The non-relativistic character of (v)NRQCD, in particular the existence of static potentials like the Coulomb potential V_c allows us to express the current correlators $\mathcal{A}_i$ in terms of Green functions of a time-independent two-body Schrödinger equation (see e.g. [75]). The LL order contribution to $\mathcal{A}_1$ e.g. reads

$$\mathcal{A}_1(v,m,\nu) \;=\; 6\,N_c\,G^0(a,v,m,\nu) \,+\, \ldots\,, \tag{4.5}$$

where $a = -\mathcal{V}_c^{(s)}(\nu)/(4\pi)$ for QCD color singlets.
$G^0(a,v,m,\nu)$ is the well known Green function of the time-independent Schrödinger operator for a Coulombic potential ($\propto \frac{1}{r}$) in position space at zero-distances [76–78][1]. The latter means that we have to evaluate the Green function for the $q\,\bar{q}$ pair being produced and annihilated at a single point in spacetime in accordance with the locality of the quark production (annihilation) currents in Eq. (4.2).

In Refs. [25, 32] the derivation of the $\mathcal{A}_i$ is discussed in detail and complete results are presented up to NNLL. A corrected NNLL result for $\mathcal{A}_1$ allowing for subtleties concerning the sum operator approach of subsection 3.5.2 is given in Ref. [26]. The higher order terms in the perturbative expansion involve the $\mathcal{O}(\alpha_S)$ and $\mathcal{O}(\alpha_S^2)$ (soft matrix element) corrections to the Coulomb potential, the kinetic operator $\frac{\mathbf{p}^4}{8m^3}$ and the potentials $V_{k,\rm eff}$ ($\sim v\alpha_s$), V_s, V_2 and V_r ($\sim v^2$) contributing in the Schrödinger equation. Quantum corrections from matrix elements with ultrasoft gluons do not contribute directly at NNLL precision, since they scale at least like $\alpha_U\,v^2$ according to the statement in section 3.6. However they cause (ultrasoft) running of the potentials $V_{k,\rm eff}$, V_2 and V_r and therefore affect the renormalization scale dependence of the correlators $\mathcal{A}_i(v,m,\nu)$ and the Wilson coefficients $c_i(\nu)$ associated with the nonrelativistic currents in Eq. (4.3), as we will see in the remainder of this work.

By using the expression for the effective velocity parameter v including the top width Γ_t in Eq. (2.11) in the Green functions, leading order effects of the short lifetime of the top quarks are taken into account according to the optical theorem [29, 48, 79]. Thus, the poles of the Green functions, which correspond to possible bound states of the $t\,\bar{t}$ system, are shifted (far) away from the real axis. This results in a smooth line shape of $\sigma_{\rm tot}$ at threshold, rather than in sharp resonance peaks as in the case of more stable particles, cf. Fig. 4.1.

Whereas c_2 and c_3 only appear in terms, which are already of NNLL order as $\mathcal{A}_2$ and $\mathcal{A}_3$ are and therefore only their LL running is needed in Eq. (4.3), the LL term in Eq. (4.5) comes along with a factor c_1^2. Thus a complete NNLL prediction of $\sigma_{\rm tot}(e^+e^- \to t\,\bar{t}\,)$ at threshold requires results for c_1 up to the same order.

[1] The UV divergence in the real part of G^0 only becomes relevant when electroweak corrections and related top quark instability effects are taken into account, see Ref. [29].

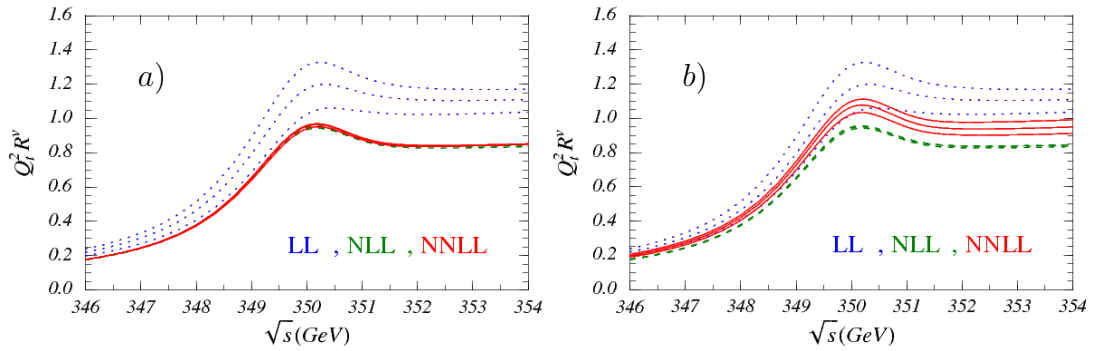

Figure 4.1: vNRQCD results for $Q_t^2 R^v$ ($Q_t = \frac{2}{3}$) including leading order effects from the top width as described in the text. For the NNLL prediction (solid lines) shown in panel *a*) (like in Refs. [25,32]) only NLL running of the Wilson coefficient c_1 was used. In panel *b*) (taken from Ref. [27]) in addition the NNLL non-mixing contribution to c_1 from Ref. [26] is included. The LL (dotted lines) and NLL results (dashed lines) in both pictures are complete and the input parameters are $M^{1S} = 175$ GeV and $\Gamma_t = 1.43$ GeV. In these plots the 1S (threshold) mass definition according to Refs. [15, 80] is used and for each order three curves are plotted with $\nu = 0.15$, 0.2 and 0.3.

4.2 Current Renormalization

Let us take a closer look at the Wilson coefficient $c_1(\nu)$. For NNLL precision we need to know the matching condition $c_1(\nu = 1)$ up to two loops. It is given e.g. in Refs. [26, 81][2]. The RG evolution of $c_1(\nu)$ is obtained by solving the RGE

$$\nu \frac{\partial}{\partial \nu} \ln[c_1(\nu)] \;=\; \gamma_{c_1}^{\rm NLL}(\nu) + \gamma_{c_1}^{\rm NNLL}(\nu) + \dots \,. \tag{4.6}$$

The LL anomalous dimension of $c_1(\nu)$ is zero because the only divergent one loop graphs at $\mathcal{O}(\alpha_s v^0)$ are generated by A^0 gluons and the statement of section 3.6 applies.

At NLL order the anomalous dimension has been calculated in Refs. [31, 32] from the loop diagrams shown in Fig. 4.2.
It reads

$$\begin{aligned} \gamma_{c_1}^{\rm NLL}(\nu) \;=\; & -\frac{\mathcal{V}_c^{(s)}(\nu)}{16\pi^2}\left[\frac{\mathcal{V}_c^{(s)}(\nu)}{4} + \mathcal{V}_2^{(s)}(\nu) + \mathcal{V}_r^{(s)}(\nu) + \mathbf{S}^2\,\mathcal{V}_s^{(s)}(\nu)\right] \\ & + \frac{1}{2}\mathcal{V}_{k,\rm eff}^{(s)}(\nu)\,, \end{aligned} \tag{4.7}$$

where $\mathbf{S}^2 = 2$ is the squared total quark spin for the spin-triplet configuration and LL running of the color singlet coefficients $\mathcal{V}_i^{(s)}(\nu)$ and $\mathcal{V}_{k,\rm eff}^{(s)}(\nu)$ is understood.

[2] See also the references cited at the end of section 2.4.

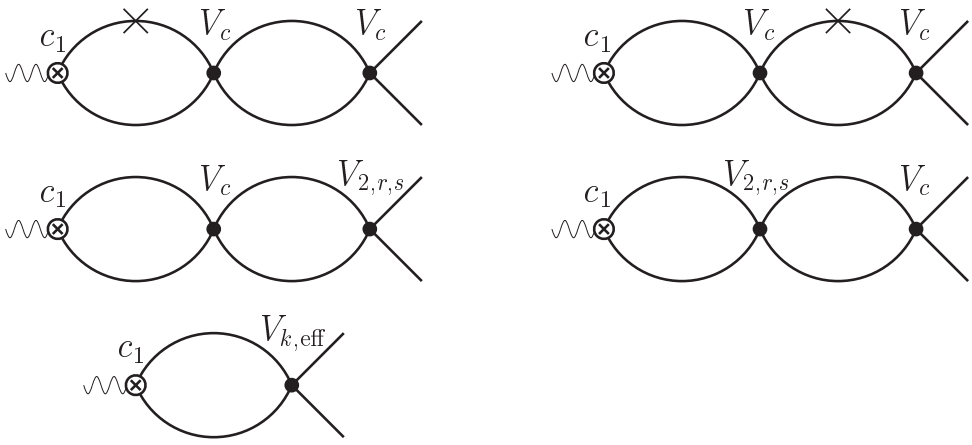

Figure 4.2: $\mathcal{O}(\alpha_s^2 v^0)$ loop graphs contributing to the NLL running of $c_1(\nu)$. The $\times$ denotes a kinetic $\frac{\mathbf{p}^4}{8m^3}$ operator insertion according to Eq. (2.24) and can be attached to the lower propagators of the potential loops as well. In the six-quark operator approach described in subsection 3.5.2 the vertex denoted by $V_{k,\mathrm{eff}}$ actually represents a tadpole of the type in Fig. 3.9.

The correct effective V_k potential is generated by two types of sum operators (six-quark operators). One of them are the $\mathcal{O}_{ki}$ defined in subsection 3.5.2. Another one is introduced in Ref. [26] instead of "real" V_k potentials to absorb the UV divergences from $\mathcal{O}(\alpha_S^3)$ graphs with a divergent soft loop [62]. This is done for similar consistency reasons as described in subsection 3.5.2 in the context of ultrasoft renormalization. The coefficient $\mathcal{V}_{k,\mathrm{eff}}^{(s)}$ then takes the form[3]

$$\mathcal{V}_{k,\mathrm{eff}}^{(s)}(\nu) \;=\; \alpha_S^2\big[\frac{C_F}{2}(C_F-2C_A)\big] \,+\, \big(\mathcal{V}_{k,\mathrm{eff}}^{(s)}(\nu)\big)_{us}\,. \tag{4.8}$$

The first term arises from LL soft renormalization [26] and the second term represents the ultrasoft contributions, which will be calculated in this thesis, and is a linear combination of the coefficients $\mathcal{V}_{ki}$ of the sum operators $\mathcal{O}_{ki}$. In Eq. (5.49) the already known LL result [32] for $\big(\mathcal{V}_{k,\mathrm{eff}}^{(1,T)}(\nu)\big)_{us}$ is given.

The NNLL anomalous dimension of $c_1(\nu)$ is split into two parts

$$\gamma_{c_1}^{\mathrm{NNLL}}(\nu) \;=\; \gamma_{c_1,nm}^{\mathrm{NNLL}}(\nu) \,+\, \gamma_{c_1,m}^{\mathrm{NNLL}}(\nu)\,, \tag{4.9}$$

to which we will refer to as "mixing" (m) and "non-mixing" (nm) contributions. The latter is induced by pure three-loop graphs. A typical example is shown in Fig. 4.3.

Besides diagrams with an ultrasoft gluon exchange of the kind displayed in Fig. 4.3

[3]There is a misprint in Ref. [26]: a factor $\frac{1}{2}$ is missing in the soft contributions. The correct result, though obtained with a "real" potential V_k, can be found in Ref. [32].

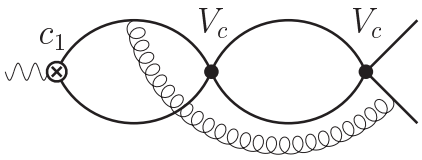

Figure 4.3: Example of a three-loop diagram with ultrasoft gluon contributing to $\gamma^{\rm NNLL}_{c_1,nm}(\nu)$.

also three-loop diagrams that come from insertions of subleading soft matrix element corrections to the potentials contribute to $\gamma^{\rm NNLL}_{c_1,nm}(\nu)$. Similar to $\gamma^{\rm NLL}_{c_1}$ it depends on the Wilson coefficients $\mathcal{V}_i^{(s)}(\nu)$ and $\mathcal{V}_{ki}^{(s)}(\nu)$ for which the LL approximation is used. The full analytic result is derived in Ref. [26].

What remains is the mixing part of the NNLL running of $c_1(\nu)$. Apart from higher order electroweak corrections [29, 30, 82] it is the only missing piece in the NNLL vNRQCD prediction for the total top pair production cross section at threshold, Eq. (4.1).
$\gamma^{\rm NNLL}_{c_1,m}$ is the NLL correction to the two-loop anomalous dimension and has therefore exactly the same form as $\gamma^{\rm NLL}_{c_1}$, but the LL potential coefficients are substituted by their NLL corrections. Terms of higher than NNLL order are dropped. One can think of $\gamma^{\rm NNLL}_{c_1,m}$ as being generated by the two-loop graphs of Fig. 4.2, each with one potential replaced by its NLL order correction term, and all possible permutations. (In this context we refer to the six-quark operators $\mathcal{O}_{6i}$ and sum operators $\mathcal{O}_{ki}$ respectively as "potentials" as well.) Thus we can write the solution of Eq.(4.6) as

$$\ln\left[\frac{c_1(\nu)}{c_1(1)}\right] \;=\; \xi^{\rm NLL}(\nu) \,+\, \big(\xi^{\rm NNLL}_{\rm m}(\nu) \,+\, \xi^{\rm NNLL}_{\rm nm}(\nu)\big) \,+\, \ldots\,, \qquad (4.10)$$

where $\xi^{\rm NLL}$ is the integral of $\gamma^{\rm NLL}_{c_1}$, $\xi^{\rm NNLL}_{\rm m}$ of $\gamma^{\rm NNLL}_{c_1,m}$ and $\xi^{\rm NNLL}_{\rm nm}$ of $\gamma^{\rm NNLL}_{c_1,nm}$.

All we need to know to calculate the missing part of the NNLL running $\xi^{\rm NNLL}_{\rm m}$ are the NLL corrections to the potential coefficients in vNRQCD. Except for the coefficient of the Coulomb potential $\mathcal{V}_c^{(s)}$ [32, 54, 83] and for the spin-dependent potential $\mathcal{V}_s^{(s)}$ [84] no complete determination for the subleading evolution exists at present. The aim of this work is to determine the ultrasoft contributions $\propto \alpha_S\alpha_U(\alpha_U \ln v)^n$ to the NLL running of $\mathcal{V}_i$ and $\mathcal{V}_{ki}$ since they are considered to be dominant as will be discussed in the following.

The analysis of the three-loop (non-mixing) terms $\xi^{\rm NNLL}_{\rm nm}$ in Ref. [26] revealed that the contributions involving the exchange of ultrasoft gluons are more than one order of magnitude larger than those arising from soft matrix element insertions and are as large as the known NLL contributions $\xi^{\rm NLL}$. The reason is related to the larger size of the ultrasoft coupling α_U and to a rather large coefficient

multiplying the ultrasoft terms. These large ultrasoft contributions are responsible for the uncertainty in the normalization of the most up-to-date threshold cross section prediction of at best 6% [27], which is quite far from the required precision as mentioned in the beginning of this section. (See also Ref. [85] for an alternative analysis without NNLL non-mixing effects.) The corresponding effects of the soft matrix element corrections are only at the level of several per mil.

In Fig. 4.1 the size of the (ultrasoft) NNLL non-mixing contributions is illustrated by two plots of the R-ratio R^v vs. the c.m. energy $\sqrt{s}$: one prediction neglects them (a) whereas the other one includes them (b). The shift of about 10% as well as the larger renormalization group dependence of the NNLL results in Fig. 4.1 b) compared to Fig. 4.1 a) is a consequence of the large gap in the resonance region ($v \sim 0.15$) between the two curves for $\frac{c_1(\nu)}{c_1(1)}$ plotted in Fig. 4.4.

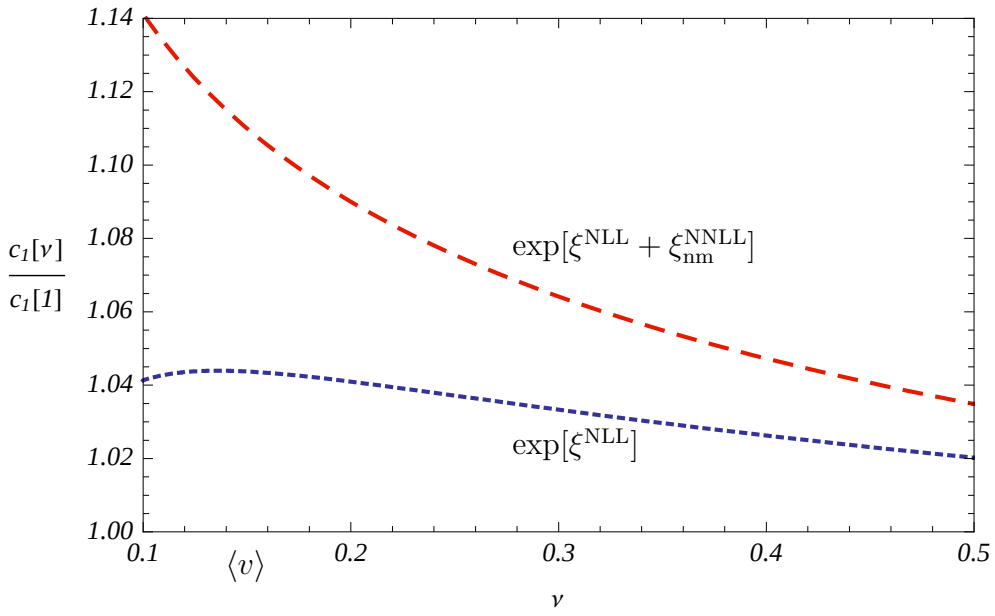

Figure 4.4: NLL (dotted line) and three-loop induced NNLL (dashed line) running of $c_1(\nu)$. $\langle v \rangle$ denotes a typical value for v in the threshold region.

As already stated we observe that mainly the $\xi^{\rm NNLL}_{\rm nm}$ contributions from graphs with an ultrasoft loop as the one in Fig. 4.3 produce this gap. They therefore give rise to the relatively large uncertainty in the prediction of the $t\bar{t}$ production cross section at threshold.

From the above analysis it is reasonable to assume that the ultrasoft effects, which form a gauge-invariant subset, also dominate the mixing contributions. This assumption is consistent with the results for the NLL evolution of the coefficient $\mathcal{V}_s^{(s)}$ [84], which is dominated by soft effects and was found to have a very small numerical effect [86]. From the parametric point of view this can be

understood from the fact that ultrasoft effects can affect the coefficients of the spin-dependent potentials only indirectly through mixing via potential loop divergences, since at this order the coupling of ultrasoft gluons to heavy quarks are spin-independent. For the coefficient of spin-dependent potentials this leads to ultrasoft NLL terms $\propto \alpha_S^2(\alpha_U \ln v)^n$, where α_S and α_U are the strong coupling at the soft and ultrasoft scales, respectively, i.e. $\alpha_U > \alpha_S$. These terms are parametrically suppressed compared to ultrasoft NLL terms $\propto \alpha_S \alpha_U(\alpha_U \ln v)^n$ that can affect the spin-independent potential coefficients through diagrams with two ultrasoft loops (see chapter 6).
We therefore expect that ultrasoft effects are dominating the higher order evolution of the spin-independent potentials V_2, V_r, $V_{k,\text{eff}}$.

The motivation to perform the corresponding calculations is of course the hope that the ultrasoft mixing contribution to the NNLL anomalous dimension of $c_1(\nu)$ will compensate for the large non-mixing contributions and substantially reduce the gap in Fig. 4.4. This would directly result in the desired improvement of the theoretical prediction for the $t\bar{t}$ threshold production at a future linear collider experiment.

Chapter 5

LL Ultrasoft Running of the Potentials

In the last chapter we have given the motivation for the ultrasoft renormalization of the $\mathcal{O}(\frac{1}{m^2})$ and $\mathcal{O}(\frac{1}{m\mathbf{k}})$ vNRQCD potentials up to NLL order. In this chapter we will carry out, as the first step, the actual calculation at one-loop (LL) level. This calculation has already been performed for the $\frac{1}{m^2}$ - potentials in Ref. [63] using Feynman gauge and for the $\frac{1}{m\mathbf{k}}$ - potentials in Ref. [62] using Coulomb gauge.

At two-loop (NLL) level Coulomb gauge turns out to be a very awkward choice. E.g. already the full analytic one-loop expression of the gluon self-energy, which is needed as subdiagram in many two-loop diagrams, is very cumbersome to determine due to its noncovariant nature and not known by now [87].
The complete results for V_2, V_r and $V_{k,\text{eff}}$ computed in the references cited above are gauge invariant as they are physical observables. Nevertheless all of the one-loop diagrams also appear as subdiagrams in two-loop graphs and we would like to monitor the cancellation of subdivergences diagram by diagram, when the corresponding counterdiagrams are added. That is why we will redo here the whole one-loop calculation in Feynman gauge, which is the preferred gauge at two-loop level.
All vNRQCD Feynman rules in Feynman gauge needed for this work can be found in Appendix A.

We will apply dimensional regularization ($d = 4 - 2\epsilon$) and carry out the renormalization program in the $\overline{\text{MS}}$ scheme. The advantages of this choice have already been explained in chapter 3. One disadvantage of this approach is that UV and IR divergences are not distinguishable a priori. Since the RG running of couplings and Wilson coefficients is associated only with the UV divergences, we therefore have to find a way to make sure that we do not absorb IR divergences in the counterterms.
To avoid all possible IR divergences in our diagrams right from the start we simply set all the external heavy quarks off-shell. That means we choose the energy of external quarks in a way that $E - \frac{\mathbf{p}^2}{2m} \equiv a$ holds, where E and $\mathbf{p}$ are

the corresponding energy and 3-momentum of the quark respectively and a is a universal "off-shellness".
From the technical point of view this simple trick allows us to shift the IR poles of the loop integrals away from the real axis into the complex plane by formally assigning an imaginary part to the off-shell parameter a with the same sign as the $i\epsilon$ in the corresponding propagator. The leading UV divergence of a diagram is obviously not affected by introducing off-shellnesses on the external legs. The UV finite parts of the standard one-loop integrals in Appendix B exhibit the typical logarithmic dependence on the off-shell parameters as a manifestation of (logarithmic) IR singularities.
After having determined the UV singularity of a one-loop diagram, we have to set a to zero, because we are going to perform on-shell renormalization by convention.

At two-loop level this procedure is more involved, since the subleading $\frac{1}{\epsilon}$ poles of two-loop diagrams can depend logarithmically on the off-shellness. But these logarithms will cancel naturally after the subtraction of all subdivergences. The overall divergence absorbed by an adequate counterterm must of course not depend on the parameter a.

5.1 Wavefunction Renormalization

As parts of the "potential" term in the renormalized Lagrangian Eq. (2.27) and in order to subtract subdivergences from heavy quark self-energies at two-loop level (see chapter 6) it is clear that we will need the wavefunction counterterms of the heavy quark fields when determining the potential counterterms. Computing them at one-loop up to $\mathcal{O}(v^2)$ is what we will start with.
At $\mathcal{O}(v^0)$ there is only one diagram contributing to the renormalization of the heavy quark fields:

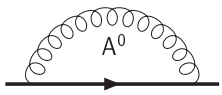

$$\begin{aligned} &= \int \frac{d^dk}{(2\pi)^d}(-i\mu_U^\epsilon g_U\, T^B)\,\frac{i}{k_0+a}\,\frac{(-i)\,\delta^{AB}}{k^2}\,(-i\mu_U^\epsilon g_U\, T^A) \\ &= -4\pi\alpha_U C_F\,\mu_U^{2\epsilon}\int\frac{d^dk}{(2\pi)^d}\left[(k_0+a)\,k^2\,\right]^{-1} \\ &= -i\,a\,\frac{\alpha_U C_F}{2\pi\epsilon}\,+\,\mathcal{O}(\epsilon^0) \quad . \end{aligned} \tag{5.1}$$

Here and in the following (if not stated otherwise), the heavy quark propagators are understood to come along with a (causal) "$i\epsilon$" in the denominator which has the same sign as the off-shellness a. Equivalently one could think of the off-shellness to have an infinitesimal positive imaginary part. Similarly the gluon propagator receives an "$i\epsilon$" with the same sign as the square of the gluon four-momentum. It is usually not displayed as well.

So in the above case we actually have to make the following replacements

$$\frac{i}{k_0+a} \to \frac{i}{k_0+a+i\epsilon} \qquad \text{and} \qquad \frac{(-i)\,\delta^{AB}}{k^2} \to \frac{(-i)\,\delta^{AB}}{k^2+i\epsilon}$$

before we integrate over the loop momentum k.
The integration in the second step of Eq. (5.1) then can be performed using the standard integral (B.7) in Appendix B.

The next to leading contribution to the heavy quark self-energy w.r.t. the v counting at one loop comes from the following two diagrams:

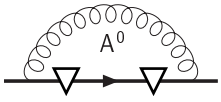

$$\begin{aligned} &= (-4\pi\alpha_U C_F)\,(-\frac{p^i p^j}{m^2})\,\mu_U^{2\epsilon}\!\int\!\frac{d^dk}{(2\pi)^d}\,\frac{-k^ik^j}{(k_0+a)^3k^2} \\ &= (-4\pi\alpha_U C_F)\,\frac{\mathbf{p}^2}{m^2}\,\frac{1}{d-1}\,\mu_U^{2\epsilon}\!\int\!\frac{d^dk}{(2\pi)^d}\,\frac{k_0^2-k^2}{(k_0+a)^3k^2} \\ &= -i\,a\,\frac{\alpha_U C_F}{2\pi\epsilon}\,\frac{\mathbf{p}^2}{m^2} + \mathcal{O}(\epsilon^0) \end{aligned} \tag{5.2}$$

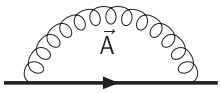

$$= +i\,a\,\frac{\alpha_U C_F}{2\pi\epsilon}\,\frac{\mathbf{p}^2}{m^2} + \mathcal{O}(\epsilon^0) \tag{5.3}$$

For the first diagram we used the integral formula (B.1) in addition to the already known standard integral (B.7), which is used for the second graph.
In (5.2) we also encounter a scaleless integral when canceling the k^2 in the numerator, but since it contains no logarithmic UV divergences it can safely be set to zero.

From these results we can now determine the wavefunction counterterm as follows. The relation between the bare ($\psi^0_{\mathbf{p}}$) and the renormalized quark field ($\psi_{\mathbf{p}}$) is defined to be

$$\psi^0_{\mathbf{p}} = Z^{\frac{1}{2}}_{\psi,\mathbf{p}}\,\psi_{\mathbf{p}}\,; \quad Z_{\psi,\mathbf{p}} = 1 + \delta Z_{\psi,\mathbf{p}}\,. \tag{5.4}$$

The counterterm $\delta Z_{\psi,\mathbf{p}}$ carries a soft momentum label just like the wavefunction itself, since a priori there can be different counterterms for different wavefunctions depending on the label $\mathbf{p}$. We will show below why this $\mathbf{p}$ dependence vanishes in Feynman gauge.
The kinetic term of the heavy quarks in the renormalized Lagrangian then reads

$$\mathcal{L} = \sum_{\mathbf{p}} \left[\psi^\dagger_{\mathbf{p}}\,(i\partial^0 - \frac{\mathbf{p}^2}{2m})\,\psi_{\mathbf{p}} + \delta Z_{\psi,\mathbf{p}}\,\psi^\dagger_{\mathbf{p}}\,(i\partial^0 - \frac{\mathbf{p}^2}{2m})\,\psi_{\mathbf{p}}\right] + \ldots \tag{5.5}$$

and the heavy quark wavefunction counterterm insertion corresponding to the second term is

$$= \; i\,\delta Z_{\psi,\mathbf{p}}\,(E - \frac{\mathbf{p}^2}{2m}) \; = \; i\,a\,\delta Z_{\psi,\mathbf{p}}\;. \tag{5.6}$$

To absorb the above ultrasoft self-energy divergences, we demand

$$+ \quad (5.1) + (5.2) + (5.3) \quad = \quad \mathcal{O}(\epsilon^0)$$

or

$$\begin{aligned} \delta Z_{\psi,\mathbf{p}} &= \delta Z_{\psi}^{(1,0)} + \mathcal{O}(\alpha_U^2)\;, \\ \delta Z_{\psi}^{(1,0)} &= \frac{\alpha_U C_F}{2\pi\epsilon}\;. \end{aligned} \tag{5.7}$$

Here and in the following the upper index $(1,0) = (\mathcal{O}(\alpha_U)\,,\,\mathcal{O}(v))$ indicates the respective order in α_U and v.

Obviously the contributions at $\mathcal{O}(v^2)$ from diagrams (5.2) and (5.3) add up to zero. This is also true for higher orders in v. The reason is Lorentz invariance, which is, although not manifestly visible in the Lagrangian, still respected by the effective theory up to an arbitrary order in v. A $\mathbf{p}$-dependent δZ_ψ would obviously break this symmetry. In Coulomb gauge however such a counterterm is allowed and indeed exists [28], because Lorentz invariance is broken explicitly by the gauge condition and only restored for physical quantities in a rather intricate way as a consequence of gauge invariance.
Moreover it is interesting that there is a contribution to the wavefunction renormalization already at $\mathcal{O}(v^0)$ despite the field redefinition argument of section 3.6. However this is no contradiction, since the wavefunction counterterm and the corresponding μ dependence of the fields respectively are not physical but cancel in physical S-matrix elements due to the LSZ formula.

There are also other self-energy diagrams with the right power counting:

a) 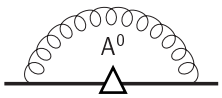

b) 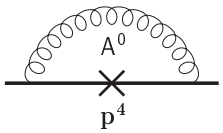

But they are not contributing here for the following reasons.
Diagram a) is proportional to the square of the off-shellness a. Its contribution to the heavy quark wavefunction counterterm will therefore vanish after setting a to zero.
Diagram b) does not yield anything new, the result is actually fixed by consistency. Since the $\frac{\mathbf{p}^4}{8m^3}$ term in the Lagrangian is of order v^2 compared to the leading order kinetic terms one should view diagram b) as a correction to the

corresponding two-quark vertex rather than as a self-energy of the heavy quark. But the divergence turns out to be already absorbed completely by $\delta Z_\psi^{(1,0)}$ which is part of the respective counterdiagram, so that the $\frac{\mathbf{p}^4}{8m^3}$ term itself is not renormalized and does not get a nontrivial Wilson coefficient. This is consistent with the requirement be that the expansion of $\sqrt{p^2-m^2}$ as it appears in the vNRQCD Lagrangian is protected from quantum corrections due to (approximate) Lorentz and reparametrization invariance. I.e. all terms in the expansion must have exactly the same renormalization scale dependence, which is carried by the heavy quark fields.

For the same reason also the mass m is not renormalized in vNRQCD. It is just a parameter constructed to have the value of the pole mass (obtained from on-shell matching) and cannot be scale dependent because the terms in the above mentioned expansion come along with different powers of m.
All these statements are valid up to arbitrary order in the v expansion and serve as important cross checks at higher loop level. Due to charge conjugation symmetry it is clear that the wavefunction counterterm for the antiquark field χ is the same as for ψ, so we have

$$\delta Z_\psi = \delta Z_\chi \, .$$

5.2 $\frac{1}{m^2}$ - Potentials

Unlike the wavefunctions the vNRQCD potentials and the scale dependence of their Wilson coefficients are physical observables. That is why here the argument of section 3.6, which uses ultrasoft Wilson lines for a field redefinition, holds. Therefore we can immediately state that there is no ultrasoft contribution to the renormalization of the Coulomb potential as it is the leading order four-quark operator in the v expansion. Technically this means that at one-loop level all diagrams of a Coulomb potential with an ultrasoft A^0 gluon loop attached in all possible ways add up such, that the sum is exactly canceled by the product of the Coulomb potential itself and the wavefunction counterterms $\delta Z_\psi^{(1,0)}$ from the four external legs, leaving no divergence to be absorbed by $\delta \mathcal{V}_c$.

At two-loop level we will use this statement as a cross check but at one loop we will not show the cancellation here explicitly.
Since for diagrams where a Coulomb potential is "dressed" with an ultrasoft gluon loop there are always two couplings of the gluon with a heavy quark, the lowest order potentials, which are renormalized to cancel the corresponding one-loop UV singularities, are the so-called $\frac{1}{m^2}$ - potentials ($\mathcal{O}(v^2)$).

Dressing the Coulomb Potential

Dressing the Coulomb potential with an ultrasoft gluon we arrive at the topologies in Fig. 5.1.

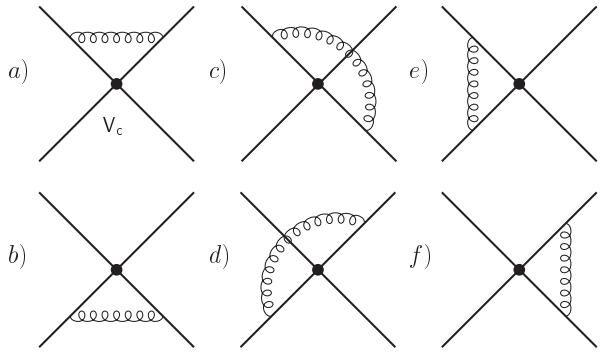

Figure 5.1: One-Loop topologies from "dressing" a Coulomb potential with an ultrasoft gluon

Based on these topologies there are two classes of diagrams contributing to the renormalization of the potentials at $\mathcal{O}(v^2)$. Similar to the renormalization of the heavy quark wavefunction the ultrasoft gluon can either be a $\mathbf{A}$ gluon or a A^0 gluon. The latter is accompanied by two insertions of the $\frac{\mathbf{p}\cdot\nabla}{m}$ operator on the heavy quark lines in the loop.
With only one insertion of $\frac{\mathbf{p}\cdot\nabla}{m}$ the integrand is antisymmetric in the spatial components of the loop momentum and the diagram vanishes. That is why the diagrams of Fig. 5.1 do not contribute to the running of the $\frac{1}{m\mathbf{k}}$ - potentials.
Diagrams with a $\frac{\nabla^2}{2m}$ insertion are proportional to the off-shellness a $(= E - \frac{\mathbf{p}^2}{2m} = E - \frac{\mathbf{p}'^2}{2m})$ and are therefore not taken into account in on-shell renormalization. Diagrams with a $\frac{\mathbf{p}^4}{8m^3}$ insertion are UV finite.

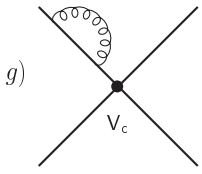

Figure 5.2: Ultrasoft gluon loop attached to an external leg.

Of course there is also the possibility that the gluon loop is attached to only one heavy quark leg, as in Fig. 5.2 and its up-down and left-right mirror graphs, but the diagrams corresponding to the two classes described above add up to zero just like the self-energy diagrams in 5.1.
Moreover graphs with one $\mathbf{A}$ gluon attached directly to the potential using the

vNRQCD vertex (A.6) such as

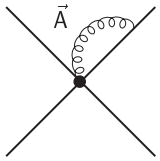

$$\propto \frac{\alpha_U}{\epsilon}\left(E - \frac{\mathbf{p}^2}{2m}\right) + \ldots \tag{5.8}$$

have the right power counting, but are again proportional to the off-shellness a, because there is only one heavy quark propagator in the loop (as for the heavy quark self-energies) and will not affect on-shell counterterms.

The results for the UV divergent parts of the graphs in Fig. 5.1 and Fig. 5.2 contributing to the running of the $\frac{1}{m^2}$ - potentials are taken from Ref. [63] and displayed in table 5.1.

Topology	Color Factor	**A** gluon	A^0 gluon, $2 \times \frac{\mathbf{p}\cdot\nabla}{m}$
a)	$T^B X^A T^B \otimes \bar{X}^A$	$\mathbf{p}\cdot\mathbf{p}'$	$-\frac{1}{3}(\mathbf{p}^2 + \mathbf{p}'^2 + \mathbf{p}\cdot\mathbf{p}')$
b)	$X^A \otimes \bar{T}^B \bar{X}^A \bar{T}^B$	$\mathbf{p}\cdot\mathbf{p}'$	$-\frac{1}{3}(\mathbf{p}^2 + \mathbf{p}'^2 + \mathbf{p}\cdot\mathbf{p}')$
c)	$X^A T^B \otimes \bar{T}^B \bar{X}^A$	$-\mathbf{p}\cdot\mathbf{p}'$	$-\frac{1}{3}(\mathbf{p}^2 + \mathbf{p}'^2 - \mathbf{p}\cdot\mathbf{p}')$
d)	$T^B X^A \otimes \bar{X}^A \bar{T}^B$	$-\mathbf{p}\cdot\mathbf{p}'$	$-\frac{1}{3}(\mathbf{p}^2 + \mathbf{p}'^2 - \mathbf{p}\cdot\mathbf{p}')$
e)	$X^A T^B \otimes \bar{X}^A \bar{T}^B$	$\mathbf{p}^2$	$\frac{1}{3}\mathbf{p}^2$
f)	$T^B X^A \otimes \bar{T}^B \bar{X}^A$	$\mathbf{p}'^2$	$\frac{1}{3}\mathbf{p}'^2$
g)	$C_F X^A \otimes \bar{X}^A$	$-(\mathbf{p}^2 + \mathbf{p}'^2)$	$\mathbf{p}^2 + \mathbf{p}'^2$

Table 5.1: Results for the divergent parts of the diagrams contributing to the renormalization of the $\frac{1}{m^2}$ - potentials [63]. To obtain the expression for a diagram with either one **A** gluon and no kinetic operator insertion or one A^0 gluon and two $\frac{\mathbf{p}\cdot\nabla}{m}$ insertions one has to build the product of the color factor, the momentum factor in the respective column and $-iV_c^{(X)}(\mathbf{p},\mathbf{p}')\,\alpha_U/(2\pi\epsilon\, m^2)$. For topology g) also mirror graphs are understood.

To illustrate the calculation we pick out topology e) as an example and calculate the diagrams for the case of an A^0 gluon being attached to an arbitrary potential $V_{X\otimes X}$ with color structure $X^A \otimes \bar{X}^A$, where two insertions of $\frac{\mathbf{p}\cdot\nabla}{m}$ are

placed on the internal quark lines in all three possible ways:

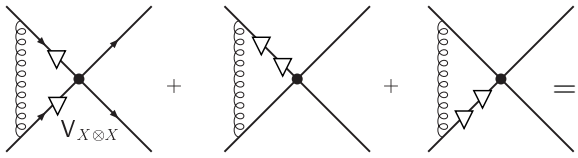

$$= (X^A T^B \otimes \bar{X}^A \bar{T}^B)\, \frac{-4\pi\alpha_U V_{X\otimes X}}{(d-1)\, m^2}$$

$$\cdot \mu_U^{2\epsilon} \int \frac{d^d k}{(2\pi)^d} \frac{k_0^2 - k^2}{k^2} \left[\frac{(-1)(-1)\mathbf{p}^2}{(k_0+a)^2(-k_0+a)^2} + \frac{2\mathbf{p}^2}{(k_0+a)^3(-k_0+a)} \right] =$$

$$= (X^A T^B \otimes \bar{X}^A \bar{T}^B)\, \frac{-4\pi\alpha_U V_{X\otimes X}}{3\, m^2}\, (-\mathbf{p}^2) \left[\frac{-i}{8\pi^2\epsilon} \right] + \mathcal{O}(\epsilon^0) \quad . \tag{5.9}$$

The two factors of (-1) in the first term in the second line of Eq. (5.9) come from the different sign of the soft 3-momentum $\mathbf{p}$ for the two incoming quark lines and from the fact that the ultrasoft momentum k is running through the two $\frac{\mathbf{p}\cdot\nabla}{m}$ insertions in opposite ways. In the second step we used the standard one-loop integral (B.10) given in Appendix B. One can find the result also in table 5.1, if one replaces V by the Coulomb potential V_c.
The ultrasoft gluon does obviously not affect the soft (momentum) structure of the potentials, therefore all the results of table 5.1 are also valid for arbitrary potentials in the loop.

The color factors expressed in the $1\otimes\bar{1}$, $T^A\otimes\bar{T}^A$ basis depending on the color structure $X^A\otimes\bar{X}^A$ of the potential which is being dressed are listed in table 5.2. They were determined by means of the relations in Appendix C.

Color Factor	$X = T$	$X = 1$
$T^B X^A T^B \otimes \bar{X}^A$	$(C_F - \frac{C_A}{2}) T^A \otimes \bar{T}^A$	$C_F 1 \otimes \bar{1}$
$X^A \otimes \bar{T}^B \bar{X}^A \bar{T}^B$	$(C_F - \frac{C_A}{2}) T^A \otimes \bar{T}^A$	$C_F 1 \otimes \bar{1}$
$X^A T^B \otimes \bar{T}^B \bar{X}^A$	$(C_A - 2C_F)(\frac{1}{2} C_F 1 \otimes \bar{1} + T^A \otimes \bar{T}^A)$	$T^A \otimes \bar{T}^A$
$T^B X^A \otimes \bar{X}^A \bar{T}^B$	$(C_A - 2C_F)(\frac{1}{2} C_F 1 \otimes \bar{1} + T^A \otimes \bar{T}^A)$	$T^A \otimes \bar{T}^A$
$X^A T^B \otimes \bar{X}^A \bar{T}^B$	$\frac{1}{2} C_F (C_A - 2C_F) 1 \otimes \bar{1} + \frac{1}{2}(C_A - 4C_F) T^A \otimes \bar{T}^A$	$T^A \otimes \bar{T}^A$
$T^B X^A \otimes \bar{T}^B \bar{X}^A$	$\frac{1}{2} C_F (C_A - 2C_F) 1 \otimes \bar{1} + \frac{1}{2}(C_A - 4C_F) T^A \otimes \bar{T}^A$	$T^A \otimes \bar{T}^A$

Table 5.2: One-loop color structures in the $1\otimes\bar{1}$, $T^A\otimes\bar{T}^A$ basis.

Using the renormalization convention in Eq. (3.23) and Eq. (5.4) we can derive the expression for the potential counterdiagram at order α_U in terms of δV and

δZ from the renormalized Lagrangian as follows:

$$= -i\mu_s^{2\epsilon}\Big[\delta V_{1\otimes 1}\, 1\otimes\bar{1} + \delta V_{T\otimes T}\, T^A\otimes\bar{T}^A + \\ + (\delta Z_{\psi,\mathbf{p}} + \delta Z_{\psi,\mathbf{p}'})(V_{1\otimes 1}\, 1\otimes\bar{1} + V_{T\otimes T}\, T^A\otimes\bar{T}^A)\Big]. \quad (5.10)$$

In order to render the theory UV finite we demand that all one-loop UV divergences with potential structure are absorbed by this counterdiagram at all orders in v. Schematically we have:

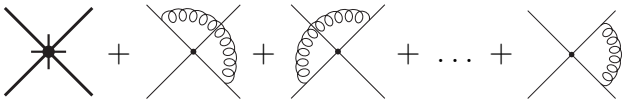

$$= \mathcal{O}(\epsilon^0)\,. \quad (5.11)$$

By this condition the contributions to the counterterms $\delta V_{X\otimes X}$ from the one-loop diagrams in table 5.1 are fixed and we can write

$$\delta\vec{V} \;=\; \begin{bmatrix}\delta V_{1\otimes 1}\\ \delta V_{T\otimes T}\end{bmatrix} \;=\; A\;\begin{bmatrix} V_{1\otimes 1}\\ V_{T\otimes T}\end{bmatrix} \;=\; A\,\vec{V} \quad (5.12)$$

for arbitrary potentials $V_{X\otimes X}$ in a compact vector form, where

$$A^{(1,2)} = \frac{\alpha_U}{3\pi m^2\epsilon}\begin{bmatrix} C_F\,\mathbf{k}^2 & -\frac{1}{2}C_F(C_A-2C_F)\,\mathbf{k}^2 \\ -\mathbf{k}^2 & -\frac{3}{2}(C_A-2C_F)\mathbf{k}^2 + C_A(\mathbf{p}^2+\mathbf{p}'^2)\end{bmatrix}\,, \quad (5.13)$$

and $\mathbf{k} = \mathbf{p}' - \mathbf{p}$.
The index $(1,2)$ of A in Eq. 5.13 again denotes the corresponding order in α_U and v.
In the beginning of this section we already found that $A^{(1,0)} = 0$.

To determine the contribution to the one-loop counterterms of the $\frac{1}{m^2}$-potentials $\mathcal{V}_r$ and $\mathcal{V}_2$ one just has to set

$$\vec{V} = \begin{bmatrix} 0 \\ \frac{\mathcal{V}_c(\nu)}{\mathbf{k}^2}\end{bmatrix} \quad (5.14)$$

on the right hand side of Eq. (5.12) and identify the coefficients of the corresponding soft momentum structures $\frac{\mathbf{p}^2+\mathbf{p}'^2}{2m^2\mathbf{k}^2}$ for $\mathcal{V}_r$ and $\frac{1}{m^2}$ for $\mathcal{V}_2$ when using $A = A^{(1,2)}$. The results are shown in section 5.5.

5.3 $\frac{1}{m|\mathbf{k}|}$ - Potentials

Whereas the ultrasoft renormalization of the $\frac{1}{m^2}$ - potentials basically amounts to dressing the Coulomb potential with ultrasoft gluons the ultrasoft renormalization of the $\frac{1}{m\mathbf{k}}$ - potentials is somewhat more complicated, as already mentioned in section 3.5. There we argued that we actually have to renormalize six-quark operators $\mathcal{O}_{6i}$ (or sum operators $\mathcal{O}_{ki}$) in order to be consistent at higher loop level and to derive well-defined RGE's. By contracting two of the six-quark fields of such an operator a nonzero tadpole diagram (Fig. 3.9) is induced which then acts as an effective $\frac{1}{m\mathbf{k}}$ - potential.
It is more or less straightforward to perform this procedure at one-loop level as we will demonstrate here.

In Fig. 5.3 and Fig. 5.4 we present the one-loop topologies up to mirror graphs with two external quark and four external antiquark lines (potential loop is cut at the top), which possibly play a role in the renormalization of the six-quark operators.

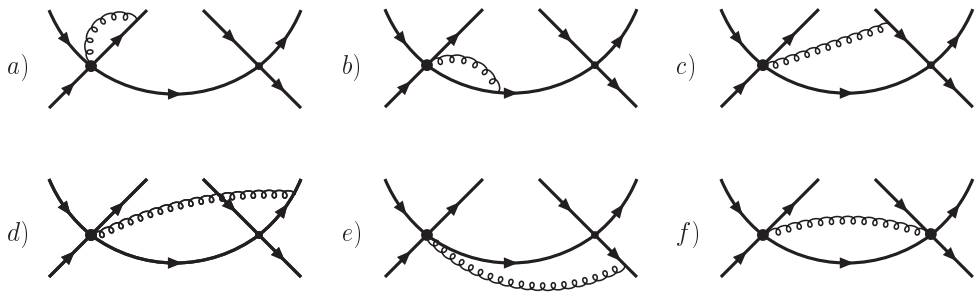

Figure 5.3: One-Loop topologies contributing to the running of the six-quark operators $\mathcal{O}_{6i}$ (and $\mathcal{O}_{\bar{6}i}$), where the ultrasoft gluon is directly connected to at least one potential. Diagram a) stands for all three diagrams with the gluon attached to one of the external legs on the left. Left-right and up-down mirror graphs are not shown.

The direct coupling of an ultrasoft gluon to a heavy quark potential structure as it appears in Fig. 5.3 refers to a $\psi\psi^\dagger\chi\chi^\dagger\mathbf{A}$ vertex. A $\psi\psi^\dagger\chi\chi^\dagger A^0$ vertex cannot exist, since gauge invariance would additionally require a Lorentz violating $\psi\psi^\dagger\chi\chi^\dagger\partial^0$ term in the vNRQCD Lagrangian[1].

Again there are several classes of diagrams matching the power counting requirement that the corresponding graph with closed potential loop should be of $\mathcal{O}(v)$ compared to the leading order Coulomb potential. The effective $\frac{1}{m\mathbf{k}}$ - potentials, which are finally generated by the six-quark operators, then scale

[1] An operator of the (schematic) form $\psi\psi^\dagger\chi\chi^\dagger(\partial^0 - \frac{\mathbf{p}^2}{2m})$ is allowed, but vanishes by the heavy quark equations of motion [61, 62].

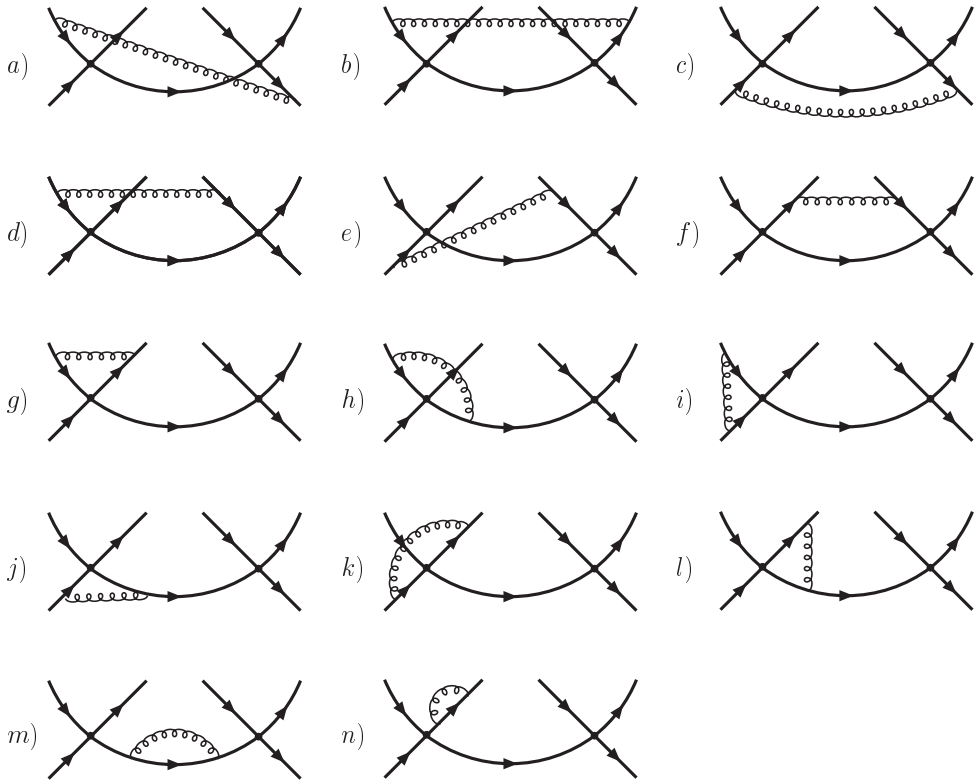

Figure 5.4: One-Loop topologies contributing to the renormalization of the $\mathcal{O}_{6i}$ (and $\mathcal{O}_{\bar{6}i}$) operators with a gluon coupling only to heavy quark legs. Mirror graphs are not displayed. Diagram n) represents all possible self-energy attachments at the external legs.

at leading order like $\alpha_U \alpha_S^2 v^{-1}$. The different diagrammatic contributions at LL depending on the class and the type of topology are specified in table 5.3. In addition there are also diagrams with two Coulomb potentials and an ultrasoft tadpole generated by the 'seagull' $\mathbf{A}^2$ operator which is attached to one of the heavy quark lines. But they do not exhibit logarithmic UV divergences and therefore do not contribute to any anomalous dimension.
Having identified all diagrams responsible for the ultrasoft renormalization of the $\mathcal{O}_{6i}$ operators we now proceed to point out the important issues of their calculation.

New in the renormalization procedure of the six-quark operators in contrast to the $\frac{1}{m^2}$ - potentials is that we have to take into account subdivergences (others than self-energies) already at one-loop level.
More precisely topologies g) - l) in Fig. 5.4 are obviously one point reducible and one part already contributed to the running of the $\frac{1}{m^2}$ - potentials for the case of a Coulomb potential in the loop. These contributions are subtracted from

Class \ Topologies	Fig. 5.3	Fig. 5.4
A gluon, no ins.	I	0 (diagrams finite or canceled by subdivergences)
A^0 gluon, $2\times$ 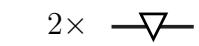	no contribution since $\psi\psi^\dagger\chi\chi^\dagger A^0$ - vertex does not exist.	0 (diagrams finite or canceled by subdivergences)
A^0 gluon, $1\times$ 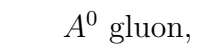		II
A^0 gluon, $2\times$ 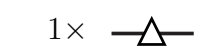		III
A^0 gluon, $1\times$ 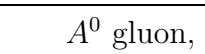 , $1\times$		IV
A^0 gluon, $1\times$ 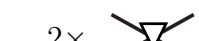		V

Table 5.3: Contributions (I-V) to the running of the $\mathcal{O}_{6i}$ operators at one loop classified by the type of the ultrasoft gluon ($\mathbf{A}/A^0$), the number and type of the kinetic insertions on the internal heavy quark lines and by number and type of the higher order relatives of the Coulomb potential, used as four-quark vertices in the diagram. The expressions for the latter as well as for the leading order $\psi\psi^\dagger\chi\chi^\dagger\mathbf{A}$ vertex used in I can be found in Appendix A. For the interactions of single gluons coupling to the heavy quark lines the lowest order standard $\psi\psi^\dagger A^0$ and $\psi\psi^\dagger\mathbf{A}$ vertices are understood.

the overall divergence, which is to be absorbed by six-quark counterterms, by adding a diagram with the corresponding $\frac{1}{m^2}$ - potential counterterm as displayed in Fig. 5.5 *a*). The same applies for the graphs 5.4 *m*) and *n*) which include self-energy subdivergences canceled by the counterdiagrams in Fig. 5.5 *b*) and *c*). This and the fact that for the respective classes diagrams with three heavy quark propagators are UV finite, is the reason why the first two entries in the right column of table 5.3 are zero.

Similarly one can explain on a diagrammatic level that the field redefinition argument of section 3.6 also holds for the renormalization of the six-quark operators: the sum of all UV divergences from diagrams based on the topologies of Fig. 5.4 with a A^0 gluon and two leading order Coulomb potentials but without any ki-

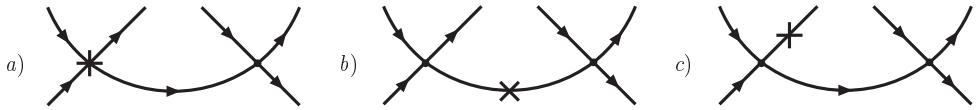

Figure 5.5: Counterdiagrams to subtract the subdivergences of diagrams with potential (a) or self-energy subgraphs (b,c) in Fig. 5.4.

netic insertions vanishes after subtraction of subdivergences.
Therefore the $\mathcal{O}_{6i}$ operators renormalized by contributions I-V in table 5.3 are the leading order (zero matching) six-quark operators induced by ultrasoft renormalization.

Although divergent parts of diagrams and counterdiagrams exactly cancel in the first two classes in the right column of table 5.3 there are still contributions to the anomalous dimension of the $\mathcal{O}_{6i}$ operators even from the topologies g) - l) in Fig. 5.4. This is the case for the configurations II, IV and V in table 5.3. Counterdiagrams for the subdivergences in these cases do not exist when performing on-shell renormalization. The reason is that the corresponding four leg subdiagrams are proportional to positive powers of the off-shellness. As part of a six-leg diagram in Fig. 5.4 however, one of the four legs, namely the propagator connecting the two potential vertices, carries a physical off-shellness ($2E-\mathbf{q}^2/m$), which is not set to zero.
Besides that, in one particle reducible six-leg topologies one power of the physical off-shellness is anyway canceled by the heavy quark propagators outside the loop. Therefore the six-leg diagram as a whole does take part in the ultrasoft renormalization procedure.
The calculation of the different diagram types in table 5.3 goes along the lines of the previously shown $\frac{1}{m^2}$ - diagrams and Eq. (5.9) and uses the same standard one-loop integrals (Appendix B).

The only point to mention explicitly is that a consistent application of the multipole expansion introduced in section 2.4 requires that kinetic insertions ($\frac{\mathbf{p}\cdot\nabla}{m}$, $\frac{\nabla^2}{2m}$) and the higher order Coulomb potentials from Eq. 2.29 are to be placed exclusively inside an ultrasoft loop. Outside the ultrasoft loops in Figs. 5.3, 5.4 there is formally no ultrasoft momentum flow. All graphs with insertions of operators with (ultrasoft) ∇'s together then build up the sub-leading terms in the multipole expansion.
Of course in addition to the topologies in Figs. 5.3, 5.4 also the respective up-down mirror graphs, where the two potentials are connected by an antiquark line (at the top) and the lower quark line is cut in two pieces, exist. These graphs analogously contribute in the renormalization of the six-quark operators $\mathcal{O}_{\bar{6}i}$ consisting of four quark and two antiquark fields. Due to quark-antiquark (charge conjugation) symmetry however, the Wilson coefficients of both types of

six-quark operators as well as their contribution to the effective $\frac{1}{m|\mathbf{k}|}$ - potential after closing the potential quark/antiquark tadpole are the same: $\delta\mathcal{C}_{6i} = \delta\mathcal{C}_{\bar{6}i}$.

In table 5.4 the results for the contributions I-V are listed. This is done not for every single topology, but for groups of topologies related by the residue theorem. Each of the topologies in one group corresponds to a different cut on an internal heavy quark line of the same two-loop topology with one ultrasoft and one closed potential loop (see section 3.5). To see this one also has to consider the mirror graphs of each diagram, which are understood to be also members of the respective group, and the mirror graphs of the original two-loop diagram.
Owing to compactness of the expressions we present here the results for the various divergences, to be absorbed by $\delta\mathcal{C}_{6i}^{(1,T)}$, with the color structure of the closed tadpole (two-loop) diagram, before performing the potential loop integral. This renders the color structure more simple and since we are only interested in the running of the effective $\frac{1}{m|\mathbf{k}|}$ - potential rather than in $(3 \to 3)$ scattering amplitudes, we do not loose valuable information in doing so.
Moreover we do not distinguish in table 5.4 between contributions to $\delta\mathcal{C}_{6i}^{(1,T)}$ and $\delta\mathcal{C}_{\bar{6}i}^{(1,T)}$, but give the sum of both instead: to the result of each diagram also the result of its up-down (and all other) mirror diagrams is added.

So far we have tacitly assumed that the amplitude of a diagram does not change if we draw it left-right reversed, without changing the fermion flow, or turn it upside down. In other words the mirror diagrams give the same result as the original Feynman graph. This is indeed true for the quark-antiquark interaction diagrams considered here and it is worthwhile to point out the origin of these symmetries.
The up-down mirror graph is generated obviously by exchanging quarks and antiquarks in the amplitude and their associated momenta, whereas for the left-right mirror diagram only the momenta of the external (anti)quarks are interchanged from left to right. We already know that merely replacing quark fields by antiquark fields and vice versa without changing their momenta leaves the amplitudes invariant due to QCD/vNRQCD charge conjugation symmetry.
Moreover (non-manifest) Lorentz invariance restricts the amplitudes to depend exclusively on the absolute value of the relative momentum of the quark-antiquark system ($|\mathbf{k}| = |\mathbf{p}' - \mathbf{p}|$) and its c.m. energy ($E \propto \mathbf{p}^2 + \mathbf{p}'^2$; $\mathbf{p}^2 = \mathbf{p}'^2$), if the two legs from the cut potential loop are set on-shell and the sum over $\mathbf{q}$ is taken or the potential loop is closed, respectively. Therefore its obvious that interchanging the soft momentum labels ($\mathbf{p} \leftrightarrow \mathbf{p}'$; $\mathbf{p} \leftrightarrow -\mathbf{p}$, $\mathbf{p}' \leftrightarrow -\mathbf{p}'$) as described above does not change the result of our diagrams.
To obtain the left-right mirror amplitude, we additionally have to invert the fermion flow, which only affects the color structure of the matrix element, since the ultrasoft diagrams considered here are not spin dependent. From global $SU(3)$ and charge conjugation invariance we know that the closed color structure must be a linear combination of $1 \otimes \bar{1}$ and $T^A \otimes \bar{T}^A$ with real coefficients and

is therefore hermitian. Thus we can conclude that inverting the fermion flow, which results in reversing the order of the color matrices in the amplitude, i.e. taking the hermitian conjugate of the color structure, again leaves the total matrix element unchanged.
For the diagrams with a $\psi\psi^\dagger\chi\chi^\dagger\mathbf{A}$ vertex, which contributes a if^{ABC} factor to the color structure the above statement is valid just as well. To see this consider the equivalent color structure of the corresponding full QCD diagram.

The soft three momentum structure of the different contributions in table 5.4 is encoded in the functions $f_i(\mathbf{q},\mathbf{p},\mathbf{p}')$:

$$\begin{aligned} f_0 &= \frac{\mathbf{p}'\cdot(\mathbf{q}-\mathbf{p})}{(\mathbf{q}-\mathbf{p})^4\,(\mathbf{q}-\mathbf{p}')^2} + (\mathbf{p}\leftrightarrow\mathbf{p}')\,, \\ f_1 &= \frac{\mathbf{q}\cdot(\mathbf{q}-\mathbf{p})}{(\mathbf{q}-\mathbf{p})^4\,(\mathbf{q}-\mathbf{p}')^2} + (\mathbf{p}\leftrightarrow\mathbf{p}')\,, \\ f_2 &= \frac{(\mathbf{q}-\mathbf{p}')\cdot(\mathbf{q}-\mathbf{p})}{(\mathbf{q}-\mathbf{p})^4\,(\mathbf{q}-\mathbf{p}')^4}\,(\mathbf{q}^2-\frac{\mathbf{p}'^2}{2}-\frac{\mathbf{p}^2}{2})\,. \end{aligned} \tag{5.15}$$

As expected performing the $\mathbf{q}$ integral (in three dimensions) over these functions, when closing the potential loop, yields the $\frac{1}{|\mathbf{k}|}$ structure of $V_{k,\mathrm{eff}}$:

$$\int\frac{d^3q}{(2\pi)^3}\,f_0=\frac{1}{16|\mathbf{k}|}\,,\quad \int\frac{d^3q}{(2\pi)^3}\,f_1=\frac{3}{16|\mathbf{k}|}\,,\quad \int\frac{d^3q}{(2\pi)^3}\,f_2=\frac{1}{16|\mathbf{k}|}\,. \tag{5.16}$$

The explicit expressions for the color structures cs1 and cs2 in the $1\otimes\bar{1}$, $T^A\otimes\bar{T}^A$ basis are given in Eq. (5.17).

By multiplying the results of table 5.4 with a factor $\frac{1}{2}$, which amounts to performing the integral over the zero component of the potential loop momentum (Eq. (3.34)), we arrive at the contributions to the counterterms of the sum operators $\mathcal{O}_{ki}$, which were determined in Coulomb gauge in Ref. [32]. As argued in section 3.5 it makes no difference for the value of $\mathcal{V}_{k,\mathrm{eff}}(\nu)$ if we use six-quark operators ($\mathcal{O}_{6i}$) or four-quark sum operators ($\mathcal{O}_{ki}$) to subtract the divergences encountered in the above diagrams. Both approaches are equivalent in this respect.
Since we have chosen to present the results for closed color structure, they are, to be precise, used to determine the running of the $\mathcal{O}_{6i}^{(1,T)}/\mathcal{O}_{ki}^{(1,T)}$ operators introduced in Eq. (3.32)/(3.36).

Group of topologies incl. all mirror graphs	Contribution defined in table 5.3	Result $\cdot \left(\frac{\alpha_U \mathcal{V}_c^2}{m\,\pi\,\epsilon}\right)^{-1}$
Fig. 5.3 $a)+b)+c)$	I	$-4if_1 \cdot \mathsf{cs1}[a]$
Fig. 5.3 $d)+e)$	I	$4if_0 \cdot \mathsf{cs1}[d]$
Fig. 5.3 $f)$	I	$4if_2 \cdot \mathsf{cs1}[f]$
Fig. 5.4 $a)$	II + III + IV + V	$-\frac{i}{6}(f_0 - 7f_1)\ \mathsf{cs2}[a]$
Fig. 5.4 $b)+c)$	II + III + IV + V	$\frac{i}{6}(7f_0 + 7f_1 + 8f_2)\ \mathsf{cs2}[b]$
Fig. 5.4 $d)+g)+j)$	II + III + IV + V	$-\frac{4i}{3}(f_0 + 2f_1 + 2f_2)\ \mathsf{cs2}[d]$
Fig. 5.4 $e)+h)+k)$	II + III + IV + V	$-\frac{4i}{3}f_1 \cdot \mathsf{cs2}[e]$
Fig. 5.4 $i)$	II + IV + V	0 (vanishes on-shell)
Fig. 5.4 $l)$	II + IV + V	$\frac{i}{6}(f_0 + f_1)\ \mathsf{cs2}[l]$
Fig. 5.4 $f)+m)+n)$	II + III + IV + V	$\frac{i}{6}(f_0 + 9f_1 + 8f_2)\ \mathsf{cs2}[f]$

Table 5.4: Results for the overall divergence of diagram groups renormalizing the six-quark operators $\mathcal{O}_{6i}$ in Feynman gauge. The f_i are functions of the soft momentum labels $\mathbf{q}$, $\mathbf{p}$ and $\mathbf{p}'$ and are defined in Ref. [32] and in Eq. (5.15). The color structures $\mathsf{cs1}$ and $\mathsf{cs2}$ are the color structures of the associated closed two-loop diagram and are therefore common to all diagrams within a group. Explicit expressions can be found in Eq. (5.17).

$$
\begin{aligned}
\mathsf{cs1}[a] &= if^{CDA}T^BT^C\otimes\bar{T}^B\bar{T}^A\bar{T}^D = \\
&= \frac{1}{4}\left[C_AC_F(C_A-2C_F)\,1\otimes\bar{1} + C_A(C_A-4C_F)\,T^A\otimes\bar{T}^A\right] \\
\mathsf{cs1}[d] &= if^{DCA}T^BT^D\otimes\bar{T}^A\bar{T}^B\bar{T}^C \\
&= -\frac{1}{4}C_AC_F(C_A-2C_F)\,1\otimes\bar{1} \\
\mathsf{cs1}[f] &= i^2f^{ABC}f^{DGC}T^AT^D\otimes\bar{T}^B\bar{T}^G = \\
&= -\frac{1}{2}C_AC_F(C_A-2C_F)\,1\otimes\bar{1} - \frac{1}{4}C_A(C_A-4C_F)\,T^A\otimes\bar{T}^A \\
\mathsf{cs2}[a] &= T^CT^AT^B\otimes\bar{T}^A\bar{T}^B\bar{T}^C = \\
&= \frac{1}{4}(C_A-2C_F)\left[C_F(C_A-4C_F)\,1\otimes\bar{1} + 2(C_A-3C_F)\,T^A\otimes\bar{T}^A\right] \\
\mathsf{cs2}[b] &= T^AT^B\otimes\bar{T}^C\bar{T}^A\bar{T}^B\bar{T}^C = \\
&= \frac{1}{4}(C_A-2C_F)\left[2C_F^2\,1\otimes\bar{1} - (C_A-4C_F)\,T^A\otimes\bar{T}^A\right] \\
\mathsf{cs2}[d] &= T^AT^B\otimes\bar{T}^A\bar{T}^C\bar{T}^B\bar{T}^C = \\
&= -\frac{1}{4}(C_A-2C_F)\left[C_F(C_A-2C_F)\,1\otimes\bar{1} + (C_A-4C_F)\,T^A\otimes\bar{T}^A\right] \\
\mathsf{cs2}[e] &= T^AT^BT^C\otimes\bar{T}^A\bar{T}^C\bar{T}^B = \\
&= \frac{1}{2}(C_A-2C_F)\left[C_F(C_A-2C_F)\,1\otimes\bar{1} + (C_A-3C_F)\,T^A\otimes\bar{T}^A\right] \\
\mathsf{cs2}[l] &= T^AT^BT^C\otimes\bar{T}^A\bar{T}^B\bar{T}^C = \\
&= \frac{1}{4}\left[C_F(C_A-2C_F)(C_A-4C_F)1\otimes\bar{1} + (C_A^2-6C_AC_F+12C_F^2)T^A\otimes\bar{T}^A\right] \\
\mathsf{cs2}[f] &= T^AT^B\otimes\bar{T}^A\bar{T}^C\bar{T}^C\bar{T}^B = \\
&= \frac{1}{2}C_F\left[C_F(C_A-2C_F)\,1\otimes\bar{1} + (C_A-4C_F)\,T^A\otimes\bar{T}^A\right] \qquad (5.17)
\end{aligned}
$$

Summing the contributions in the right column of table 5.4 yields

$$
\begin{aligned}
-2iC_A\frac{\alpha_U\mathcal{V}_c^2}{3m\pi\epsilon}\Big[\, & C_F(C_A-2C_F)(f_0+f_1+2f_2)1\otimes\bar{1} + \\
& (C_A-4C_F)(f_1+f_2)T^A\otimes\bar{T}^A\,\Big]\,. \qquad (5.18)
\end{aligned}
$$

This result finally fixes the soft momentum structure of the $\mathcal{O}_{6i}^{(1,T)}$ operators induced by the ultrasoft renormalization procedure. It is the same as for the

corresponding $\mathcal{O}_{ki}$ operators defined in Eq. (3.36).
Dividing by two one can now read off the known ultrasoft one-loop counterterms of the sum operators $\mathcal{O}_{ki}$ first determined in Ref. [32] using Coulomb gauge:

$$\begin{aligned} \delta\mathcal{V}_{k1}^{(1)} &= -C_A C_F (C_A - 2C_F)\,\frac{\alpha_U}{3\pi\epsilon}(-\mathcal{V}_c^2) \\ \delta\mathcal{V}_{k2}^{(T)} &= -C_A (C_A - 4C_F)\,\frac{\alpha_U}{3\pi\epsilon}(-\mathcal{V}_c^2) \end{aligned} \tag{5.19}$$

These are used in section 5.5 to calculate the anomalous dimension of the $\mathcal{O}_{ki}^{(1,T)}/\mathcal{O}_{6i}^{(1,T)}$ and finally the running of $V_{k,\text{eff}}$. The six-quark operator Wilson coefficients $\mathcal{C}_{6i}^{(1,T)}$ and their counterterms $\delta\mathcal{C}_{6i}^{(1,T)}$ are according to Eq. (3.42) given by:

$$(\delta)\mathcal{C}_{6i}^{(1,T)} = (\delta)\mathcal{C}_{\bar{6}i}^{(1,T)} = (\delta)\mathcal{V}_{ki}^{(1,T)}\,. \tag{5.20}$$

We will often not distinguish between quantities associated with operators related by charge conjugation symmetry as e.g. $\mathcal{O}_{6i}^{(1,T)}$ and $\mathcal{O}_{\bar{6}i}^{(1,T)}$ in the following. Instead we will refer only to the symbols without bar and imply that a given statement correspondingly holds for the charge conjugated counterpart as well, unless stated otherwise.

5.4 Soft Mixing Contributions

As the title already indicates the contributions to the running of the vNRQCD potentials discussed in this section are not purely ultrasoft. Using the counting of section 4 they are parametrically suppressed by a factor $\frac{\alpha_S}{\alpha_U}$ compared to the direct ultrasoft contributions, which arise from the counterterms determined in the last two sections, and their numerical suppression turns out to be even larger. So they could be neglected just like the purely soft running of the potentials or the soft-ultrasoft mixing contributions to the evolution of the spin dependent potential V_s at NLL (see section 4).
Nevertheless we include the soft mixing terms in our calculation and later in the analysis of the results for $\mathcal{V}_2$, $\mathcal{V}_r$ and $\mathcal{V}_{k,\text{eff}}$ basically for three reasons:

- They lead to a rather simple form of the total results for the $\mathcal{V}$'s, where soft and ultrasoft contributions factorize.
- They illustrate the size of the contributions neglected in this work.
- They can be computed with very few effort, since we can simply recycle the results of the last two sections.

5.4.1 Soft Mixing Contributions to the $\frac{1}{m^2}$ - Potentials

In section 3.5 the six-field operators $\mathcal{O}_{2i}^{(\sigma)}$ (Eq. (3.28), Fig. 3.4) have been introduced. They are describing soft Compton scattering off a non-relativistic quark-antiquark pair. Connecting the soft lines as shown in Fig. 5.6, a divergence is generated by the tadpole graph, which has to be canceled by the counterterms of appropriate vNRQCD potentials.

Figure 5.6: Closing the respective soft (gluon, light quark, ghost) lines of an operator $\mathcal{O}_{2i}$.

To calculate this divergence and the corresponding counterterms, we first need to know the Wilson coefficients $C_{2i}^{(\sigma)}(\nu)$ of the operators $\mathcal{O}_{2i}^{(\sigma)}$. As argued in section 3.5 they vanish at the hard scale ($C_{2i}^{(\sigma)}(1) = 0$).
In particular, we need to determine the coefficients $C_{2i}^{(2)}(\nu)$. At the required precision higher order ($\sigma > 2$) operators do not contribute in the renormalization of potentials.
As sketched in section 3.5 (Fig. 3.2) the $\mathcal{O}_{2i}^{(\sigma)}$ are renormalized by ultrasoft gluons. Therefore we can immediately conclude $C_{2i}^{(0)}(\nu) = 0$ from power counting, since the ultrasoft gluon loop scales like v^2 taking into account the leading order terms of the multipole expansion.
Similar to the six-quark operators of the previous section it is sufficient for the purpose of renormalizing the potentials to consider only operators and respective matrix elements, where the soft lines are closed in color space. We can also define operators $\mathcal{O}_{2i}^{(\sigma)(1,T)}$ in the $1\otimes\bar{1}$, $T^A\otimes\bar{T}^A$ basis with this convention.
Of course ultrasoft gluons attached to soft diagrams like in Fig. 3.2 do not change the soft structure of the matrix elements.

Thus we make an ansatz for the soft Compton scattering matrix elements $\langle i\mathcal{O}_{2i}^{(2)}\rangle_{4Q2i}$ using a specific set of operators that have the form

$$\begin{aligned}
\mathcal{O}_{2p}^{(2),(1)} &= \frac{\mathbf{p}^2+\mathbf{p}'^2}{2m^2}\sum_i \mathcal{O}_{2i}^{(0),(1)}, \quad \mathcal{O}_{2p}^{(2),(T)} = \frac{\mathbf{p}^2+\mathbf{p}'^2}{2m^2}\sum_i \mathcal{O}_{2i}^{(0),(T)}, \\
\mathcal{O}_{2k}^{(2),(1)} &= \frac{\mathbf{k}^2}{m^2}\sum_i \mathcal{O}_{2i}^{(0),(1)}, \quad \mathcal{O}_{2k}^{(2),(T)} = \frac{\mathbf{k}^2}{m^2}\sum_i \mathcal{O}_{2i}^{(0),(T)}
\end{aligned} \tag{5.21}$$

and the corresponding Wilson coefficients $C_{2p}^{(1,T)}$ and $C_{2k}^{(1,T)}$. It reads

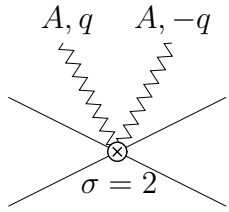

$$= \sum_i C_{2i}^{(2)} \langle i\mathcal{O}_{2i}^{(2)} \rangle_{4Q2i} \;\; =$$

$$= \Big(C_{2k}^{(1)} \frac{\mathbf{k}^2}{m^2} + C_{2p}^{(1)} \frac{\mathbf{p}^2+\mathbf{p}'^2}{2m^2} \Big) \sum_i \langle i\mathcal{O}_{2i}^{(0),(1)} \rangle_{4Q2i} \; +$$

$$+ \Big(C_{2k}^{(T)} \frac{\mathbf{k}^2}{m^2} + C_{2p}^{(T)} \frac{\mathbf{p}^2+\mathbf{p}'^2}{2m^2} \Big) \sum_i \langle i\mathcal{O}_{2i}^{(0),(T)} \rangle_{4Q2i} \; =$$

$$= \Big\{ \Big(C_{2k}^{(1)} \frac{\mathbf{k}^2}{m^2} + C_{2p}^{(1)} \frac{\mathbf{p}^2+\mathbf{p}'^2}{2m^2} \Big) 1 \otimes \bar{1} + \Big(C_{2k}^{(T)} \frac{\mathbf{k}^2}{m^2} + C_{2p}^{(T)} \frac{\mathbf{p}^2+\mathbf{p}'^2}{2m^2} \Big) T^A \otimes \bar{T}^A \Big\} \cdot$$

$$\cdot \Big[\sum_{A,\varphi,c} \text{soft struc.} \Big] \;\; , \tag{5.22}$$

where the summation over the soft gluon color index A is understood and A, φ, c below the last sum refer to the three possible types of external soft particles: gluons, light quarks and ghosts. $\langle i\mathcal{O}_{2i}^{(\sigma)} \rangle_{xy}$ denotes here a matrix element with closed color structure and with external fields indicated by xy. It is generated only by the operator $\mathcal{O}_{2i}^{(\sigma)}$ itself without its Wilson coefficient.
The soft structure in this ansatz is the same as for the leading $\sigma = 0$ operators $\mathcal{O}_{2i}^{(0)}$ and can be inferred from the $\Gamma_i^{(0)}$'s given in the Appendix of Ref. [32]. In terms of matrix elements one finds

$$\sum_i \langle i\mathcal{O}_{2i}^{(0)} \rangle_{4Q2i} \;=\; T^A \otimes \bar{T}^A \Big[\sum_{A,\varphi,c} \text{soft struc.} \Big] \;=$$

$$= \quad$$

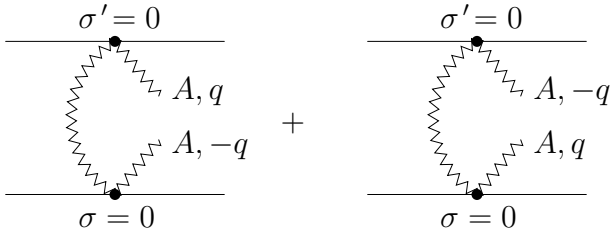

$$, \tag{5.23}$$

where the A's indicate again, that the sum over the soft gluon index has to be taken and all external fields have to obey the respective on-shell conditions (e.g. $q^2 = 0$, $\not{q}\,\varphi_q = 0$) as usual.

Using this setup, it is no longer difficult to determine the counterterms $\delta C_{2p}^{(1,T)}$

and $\delta C_{2k}^{(1,T)}$ by making use of the analogy to the calculation in section 5.2:

$$\Big(\delta C_{2k}^{(1)}\frac{\mathbf{k}^2}{m^2}+\delta C_{2p}^{(1)}\frac{\mathbf{p}^2+\mathbf{p}'^2}{2m^2}\Big)1\otimes\bar{1}+\Big(\delta C_{2k}^{(T)}\frac{\mathbf{k}^2}{m^2}+\delta C_{2p}^{(T)}\frac{\mathbf{p}^2+\mathbf{p}'^2}{2m^2}\Big)T^A\otimes\bar{T}^A \;=$$

$$= -\Bigg(\quad + \quad + \ldots + (q\leftrightarrow -q)\Bigg)\cdot\Big[\sum_{A,\varphi,c}\text{soft struc.}\Big]^{-1}$$

$$-\left(\delta Z_{\psi,\mathbf{p}}+\delta Z_{\psi,\mathbf{p}'}\right)T^A\otimes\bar{T}^A \;=$$

$$= -\Bigg(\quad + \quad + \ldots \Bigg)\cdot\Big[-i\,V_{T\otimes T}\Big]^{-1}$$

$$-\left(\delta Z_{\psi,\mathbf{p}}+\delta Z_{\psi,\mathbf{p}'}\right)T^A\otimes\bar{T}^A \;=\; \begin{bmatrix} 1\otimes\bar{1} \\ T^A\otimes\bar{T}^A\end{bmatrix} A^{(1,2)}\begin{bmatrix}0\\1\end{bmatrix} \;=$$

$$= \frac{\alpha_U}{3\pi m^2\epsilon}\Big[-\frac{1}{2}C_F(C_A-2C_F)\,\mathbf{k}^2\,1\otimes\bar{1}\;+$$

$$+\Big(-\frac{3}{2}(C_A-2C_F)\,\mathbf{k}^2\;+\;C_A\,(\mathbf{p}^2+\mathbf{p}'^2)\Big)\,T^A\otimes\bar{T}^A\Big]\,. \tag{5.24}$$

From Eq. (5.24) we can now read off

$$\delta C_{2k}^{(1,T)} \;=\; A_{\mathbf{k}}^{(1,T)}\,\frac{\alpha_U}{\epsilon}\,,\quad \delta C_{2p}^{(1,T)} \;=\; A_{\mathbf{p}}^{(1,T)}\,\frac{\alpha_U}{\epsilon}\,, \tag{5.25}$$

where the constants $A_{\mathbf{k},\mathbf{p}}^{(1,T)}$ are defined as[2]

$$\begin{aligned} A_{\mathbf{k}}^{(1)} \;&=\; -\frac{C_F(C_A-2C_F)}{6\pi}\,,\quad A_{\mathbf{k}}^{(T)} \;=\; -\frac{C_A-2C_F}{2\pi}\,,\\ A_{\mathbf{p}}^{(1)} \;&=\; 0\,,\quad A_{\mathbf{p}}^{(T)} \;=\; \frac{2C_A}{3\pi}\,. \end{aligned} \tag{5.26}$$

Owing to the independence of the unrenormalized Wilson coefficient C_{2i}^0 ($C_{2i}=C_{2k,p}^{(1,T)}$) on the renormalization scale ν we can set up the RGE's:

$$\begin{aligned} \nu\frac{d}{d\nu}C_{2i}^0 \;&=0\;=\;\nu\frac{d}{d\nu}(C_{2i}(\nu)+\delta C_{2i}(\nu))\,,\\ \Rightarrow\quad \nu\frac{d}{d\nu}C_{2i}(\nu) \;&=\; -\nu\frac{d}{d\nu}\,\delta C_{2i}(\nu)\,. \end{aligned} \tag{5.27}$$

[2]Note that the constants with index $\mathbf{p}$ differ from the ones given in Ref. [33] by a factor of two due to a different convention in the definition of the operators $\mathcal{O}_{2p}^{(2)}$.

The solutions to Eqs. (5.27) are determined in section 5.5.
We continue with the calculation of the closed soft loop on the right hand side of Fig. 5.6.

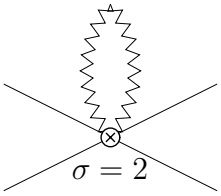

$$
\begin{aligned}
&= \sum_i C_{2i}^{(2)} \langle i\mathcal{O}_{2i}^{(2)} \rangle_{4Q} \; = \\
&= \Big[\Big(C_{2k}^{(1)} \frac{\mathbf{k}^2}{m^2} + C_{2p}^{(1)} \frac{\mathbf{p}^2+\mathbf{p}'^2}{2m^2} \Big) 1 \otimes \bar{1} \; + \\
&\quad + \Big(C_{2k}^{(T)} \frac{\mathbf{k}^2}{m^2} + C_{2p}^{(T)} \frac{\mathbf{p}^2+\mathbf{p}'^2}{2m^2} \Big) T^A \otimes \bar{T}^A \Big] \Big[\sum_{A,\varphi,c} \text{soft loop} \Big]
\end{aligned} \tag{5.28}
$$

As was shown in Ref [32] closing the two respective soft lines of the $\sigma = 0$ operators, one obtains a structure for the one-loop four-quark matrix elements that is identical to the one-loop soft matrix element corrections of the Coulomb potential, given by

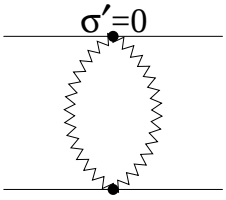

$$
\begin{aligned}
&= \sum_i \langle i\mathcal{O}_{2i}^{(0)} \rangle_{4Q} \; = \\
&= T^A \otimes \bar{T}^A \Big[\sum_{A,\varphi,c} \text{soft loop} \Big] \; = \\
&= T^A \otimes \bar{T}^A \Big(\, - \, i \, \frac{\alpha_S^2 \, \beta_0}{\mathbf{k}^2 \epsilon} \, + \, \mathcal{O}(\epsilon^0) \Big) \, .
\end{aligned} \tag{5.29}
$$

Having in mind the diagrammatic definition of the soft structure of the $\sigma = 0$ operators one might naively think that a factor of two, from closing the two diagrams in Eq. (5.23) is missing in Eq. (5.29). But this is not true, since when closing the soft structure in Eq. (5.23) the soft propagators connecting the heavy quark lines on the left have to be evaluated for on-shell loop momentum q. This means we have to set $q^2 = 0$ and $\not{q}\,\varphi_q = 0$ here respectively, whereas the soft propagator on the right retains its general form. This modification yields a compensating factor $\frac{1}{2}$, which can be understood best using the residue theorem for the q_0 integration, and we obtain the same result as for the ordinary soft loop depicted in Eq. (5.29).
Thus the divergent term arising from the soft tadpole in Eq. (5.28) reads

$$
\begin{aligned}
&-i \, \frac{\alpha_S^2 \, \beta_0}{\mathbf{k}^2 \epsilon} \cdot \Big[\Big(C_{2k}^{(1)}(\nu) \frac{\mathbf{k}^2}{m^2} + C_{2p}^{(1)}(\nu) \frac{\mathbf{p}^2+\mathbf{p}'^2}{2m^2} \Big) 1 \otimes \bar{1} \; + \\
&\qquad \Big(C_{2k}^{(T)}(\nu) \frac{\mathbf{k}^2}{m^2} + C_{2p}^{(T)}(\nu) \frac{\mathbf{p}^2+\mathbf{p}'^2}{2m^2} \Big) T^A \otimes \bar{T}^A \Big] \, .
\end{aligned} \tag{5.30}
$$

Because of its color and momentum structure this divergence has obviously to be canceled by contributions to the counterterms $\delta V_2^{(1,T)}$ and $\delta V_r^{(1,T)}$. Adding these contributions to Eq. (5.12) we end up with

$$\delta\vec{V} \;=\; A\,\vec{V} \,+\, \vec{C}\,, \tag{5.31}$$

where

$$\vec{C} \;=\; -\frac{\alpha_S^2\,\beta_0}{\mathbf{k}^2\epsilon}\left[\begin{array}{c} C_{2\mathbf{k}}^{(1)}\,\frac{\mathbf{k}^2}{m^2} \,+\, C_{2\mathbf{p}}^{(1)}\,\frac{\mathbf{p}^2+\mathbf{p}'^2}{2m^2} \\ C_{2\mathbf{k}}^{(T)}\,\frac{\mathbf{k}^2}{m^2} \,+\, C_{2\mathbf{p}}^{(T)}\,\frac{\mathbf{p}^2+\mathbf{p}'^2}{2m^2} \end{array}\right]\,. \tag{5.32}$$

In this way the divergence from the soft tadpole in Eq. (5.28) mixes into the respective anomalous dimensions of the $\frac{1}{m^2}$ - potentials.

5.4.2 Soft Mixing Contributions to the $\frac{1}{m|\mathbf{k}|}$ - Potentials

The outcome of the last subsection suggests that there are similar soft mixing contributions also to the running of $V_{k,\mathrm{eff}}$. Indeed it is rather simple to construct diagrams with two external soft particles (gluons, light quarks, ghosts) and an ultrasoft gluon loop that renormalize eight-field operators $\mathcal{O}_{(6+2)i}$ (six heavy quark and two soft fields) or the respective sum operators (four heavy quark and two soft fields) in analogy to the $\mathcal{O}_{2i}$ operators of the previous subsection.
Replacing one Coulomb potential with the soft structure of Eq. (5.23) in the graphs of Fig. 5.3 and 5.4 for example results in new eight leg diagrams which cause the ultrasoft running of eight-field (zero matching) operators, whose two soft lines can be connected to a divergent tadpole as demonstrated in Fig. 5.6 for the $\mathcal{O}_{2i}$'s.
The soft tadpole graph then mixes in the anomalous dimensions of the six-quark (sum) operators $\mathcal{O}_{6i}$ ($\mathcal{O}_{ki}$), which generate the effective $\frac{1}{m\mathbf{k}}$ - potential $V_{k,\mathrm{eff}}$, and affects its evolution in a similar way as the $\frac{1}{m^2}$ - potentials V_2 and V_r are affected by the tadpoles in Fig. 5.6.

To find the complete set of eight leg diagrams contributing, not only the Coulomb potential but also its higher order relatives (the first two subleading terms in the multipole expansion in Eq. (2.29)) and the leading order $\psi\psi^\dagger\chi\chi^\dagger\mathbf{A}$ vertex, all related by reparametrization invariance, have to be replaced by corresponding soft structures with two external soft lines. We do not show these matrix elements here explicitly, but it is clear that they exist as a consequence of reparametrization invariance. Their closed versions cause the soft running of the different members of the "Coulomb potential family", which is manifest in the renormalization scale dependent coefficient $\mathcal{V}_c(\nu)$, as noted in section 3.4.
The different contributions to the running of the eight-field operators can be classified in the same way as it was done in table 5.4 and also the cancellation of subdivergences, which are subtracted by the counterterms of the $\mathcal{O}_{2i}$ operators,

follows the lines of the $\mathcal{O}_{6i}$ renormalization. Therefore we can immediately infer that the ultrasoft counterterms of the $\mathcal{O}_{(6+2)i}$ operators equal the ones of the $\mathcal{O}_{6i}$'s (Eq. (5.20)) up to the factor $(-\mathcal{V}_c^2)$, where again all operators are defined with fully closed color structure by convention:

$$\begin{aligned} \delta C^{(1)}_{(6+2)1} &= A_1^{(1)}\,\frac{\alpha_U}{\epsilon}\,, & \delta C^{(T)}_{(6+2)2} &= A_2^{(T)}\,\frac{\alpha_U}{\epsilon}\,, \\ A_1^{(1)} &= -\frac{C_A C_F (C_A - 2C_F)}{3\pi}\,, & A_2^{(T)} &= -\frac{C_A (C_A - 4C_F)}{3\pi}\,. \end{aligned} \tag{5.33}$$

From Eqs. (5.33) one can now setup RGE's for the Wilson coefficients $C^{(1,T)}_{(6+2)i}$ as described for C_{2i} in Eq. (5.27) and determine their evolution taking into account the zero matching conditions. This is done in the next section.

The main difference to the previous subsection is that here we have two possibilities for each topology in Figs. 5.3 and 5.4 to replace a potential interaction by a corresponding (open) soft structure. This yields a factor of two when closing the soft tadpole generated by the $\mathcal{O}_{(6+2)i}$'s. Thus adding the soft mixing contributions from this tadpole to Eqs. (5.19) in analogy to Eq. (5.31) we obtain

$$\delta\mathcal{V}^{(1,T)}_{ki} = (-\mathcal{V}_c^2)\,\delta C^{(1,T)}_{(6+2)i} - 2\left[-i\frac{\alpha_S^2\beta_0}{\epsilon}\right](-i\mathcal{V}_c)\,C^{(1,T)}_{(6+2)i}\,. \tag{5.34}$$

The first term is the pure ultrasoft contribution from Eqs. (5.19) expressed in terms of $\delta C^{(1,T)}_{(6+2)i}$ for reasons that will become clear later. The second term comprises the new soft mixing contribution including the just mentioned factor of two, the soft tadpole divergence and the coefficient of the remaining potential interaction.

Eqs. (5.31) and (5.34) already contain the complete information about all the soft mixing terms that we will consider in this work. Also at two-loop level they will retain their form. Only the Wilson coefficients $C^{(1,T)}_{(6+2)i}$ and $C^{(1,T)}_{2i}$ and their respective counterterms (the matrix A can be deduced from the $\delta C^{(1,T)}_{2i}$ and vice versa), which are directly affected by UV divergences from ultrasoft loops will change.

5.5 RGE's and Running

In the beginning of the previous section we claimed that the inclusion of the soft mixing terms in the anomalous dimension of the vNRQCD potentials, although numerically suppressed, has the advantage that the integrated result for the Wilson coefficients will take an elegant factorized form. Moreover it turns out that even the process of integrating, i.e. solving the RGE's becomes much easier.
In the following we will reveal the origin of the factorization of soft and ultrasoft

contributions in the results for the $\mathcal{V}$'s, when taking into account the soft mixing terms derived above.

We start with the general expression for the counterterms of the $\frac{1}{m^2}$ - potentials as vectors in color space:

$$\delta\vec{V} \;=\; A\,\vec{V}_c \,+\, \vec{C}\;, \quad \text{where we set } \; \vec{V}_c = \begin{bmatrix} 0 \\ \frac{\mathcal{V}_c(\nu)}{\mathbf{k}^2} \end{bmatrix} \; \text{ on the r.h.s..} \tag{5.35}$$

From Eq. (5.24) we know that

$$\delta\vec{C}_{2i} \;:=\; \begin{bmatrix} \delta C^{(1)}_{2\mathbf{k}}\,\frac{\mathbf{k}^2}{m^2} \,+\, \delta C^{(1)}_{2\mathbf{p}}\,\frac{\mathbf{p}^2+\mathbf{p}'^2}{2m^2} \\ \delta C^{(T)}_{2\mathbf{k}}\,\frac{\mathbf{k}^2}{m^2} \,+\, \delta C^{(T)}_{2\mathbf{p}}\,\frac{\mathbf{p}^2+\mathbf{p}'^2}{2m^2} \end{bmatrix} = A \begin{bmatrix} 0 \\ 1 \end{bmatrix}\;, \tag{5.36}$$

so we can equivalently write

$$\delta\vec{V} \;=\; V_c(\nu)\,\delta\vec{C}_{2i} \;-\; \frac{\alpha_S^2\,\beta_0}{\mathbf{k}^2\epsilon}\,\vec{C}_{2i}(\nu)\;, \tag{5.37}$$

where $\vec{C}_{2i}$ is defined in agreement with Eq. (5.36) and $V_c(\nu) = \frac{\mathcal{V}_c(\nu)}{\mathbf{k}^2} = \frac{4\pi\alpha_S(\nu)}{\mathbf{k}^2}$. According to Eq. (3.25) the RGE for $\vec{V}$ is given by

$$\nu\frac{d}{d\nu}\vec{V} \;=\; -2\epsilon\,(\vec{V}+\delta\vec{V}) - \nu\frac{d}{d\nu}\,\delta\vec{V}\;. \tag{5.38}$$

Inserting Eq. (5.37), dropping higher order terms ($\sim\alpha_{S/U}^3$) as well as terms that vanish in $d=4$ dimensions and using $\nu\frac{d}{d\nu}V_c = -2\epsilon V_c - 2\frac{\alpha_S^2\beta_0}{\mathbf{k}^2} + \ldots$ we obtain

$$\begin{aligned}
\nu\frac{d}{d\nu}\vec{V} \;&=\; -2\epsilon\,V_c\,\delta\vec{C}_{2i} \;+\; 2\frac{\alpha_S^2\,\beta_0}{\mathbf{k}^2}\,\vec{C}_{2i} - \nu\frac{d}{d\nu}\,\delta\vec{V} \\
&=\; -2\epsilon\,V_c\,\delta\vec{C}_{2i} - \Big(\nu\frac{d}{d\nu}V_c\Big)\,\vec{C}_{2i} - \Big(\nu\frac{d}{d\nu}V_c\Big)\,\delta\vec{C}_{2i} - V_c\,\Big(\nu\frac{d}{d\nu}\delta\vec{C}_{2i}\Big) + \\
&\quad +\Big(\nu\frac{d}{d\nu}\frac{\alpha_S^2\,\beta_0}{\mathbf{k}^2\epsilon}\Big)\,\vec{C}_{2i} + \frac{\alpha_S^2\,\beta_0}{\mathbf{k}^2\epsilon}\Big(\nu\frac{d}{d\nu}\vec{C}_{2i}\Big)\,.
\end{aligned} \tag{5.39}$$

From the one-loop results for δC_{2i} ($\sim\alpha_U$) we derive the LL result for C_{2i} (~ 1) by solving $\nu\frac{d}{d\nu}\vec{C}_{2i} = -\nu\frac{d}{d\nu}\delta\vec{C}_{2i} \sim \alpha_U$ (Eq. (5.27)). Thus we can neglect the last term and further simplify the above LL anomalous dimension:

$$\begin{aligned}
\nu\frac{d}{d\nu}\vec{V} \;&=\; -2\epsilon\,V_c\,\delta\vec{C}_{2i} - \Big(\nu\frac{d}{d\nu}V_c\Big)\,\vec{C}_{2i} + 2\epsilon\,V_c\,\delta\vec{C}_{2i} + V_c\,\Big(\nu\frac{d}{d\nu}\vec{C}_{2i}\Big) + \\
&\quad -4\Big(\frac{\alpha_S^2\,\beta_0}{\mathbf{k}^2}\Big)\,\vec{C}_{2i} \\
&=\; \Big(\nu\frac{d}{d\nu}V_c\Big)\,\vec{C}_{2i} + V_c\,\Big(\nu\frac{d}{d\nu}\vec{C}_{2i}\Big) \\
&=\; \nu\frac{d}{d\nu}\big(V_c\,\vec{C}_{2i}\big)\,.
\end{aligned} \tag{5.40}$$

Similarly we find for the coefficients of the $\mathcal{O}_{ki}$ sum operators as a result of Eq. (5.34)

$$\begin{aligned}
\nu\frac{d}{d\nu}\mathcal{V}_{ki} &= -4\epsilon\,\delta\mathcal{V}_{ki} - \nu\frac{d}{d\nu}\delta\mathcal{V}_{ki} \\
&= 4\epsilon\,\mathcal{V}_c^2\,\delta C_{(6+2)i} - 8\alpha_S^2\beta_0\,\mathcal{V}_c\,C_{(6+2)i} + \Big(\nu\frac{d}{d\nu}\mathcal{V}_c^2\Big)\delta C_{(6+2)i} \\
&\quad +\mathcal{V}_c^2\Big(\nu\frac{d}{d\nu}\delta C_{(6+2)i}\Big) - 2\Big(\nu\frac{d}{d\nu}\frac{\alpha_S^2\,\beta_0}{\epsilon}\mathcal{V}_c\Big)C_{(6+2)i} \\
&= -\mathcal{V}_c^2\Big(\nu\frac{d}{d\nu}C_{(6+2)i}\Big) - 2\frac{\alpha_S^2\,\beta_0}{\epsilon}\Big(\nu\frac{d}{d\nu}\mathcal{V}_c\Big)C_{(6+2)i} \\
&= -\mathcal{V}_c^2\Big(\nu\frac{d}{d\nu}C_{(6+2)i}\Big) - \Big(\nu\frac{d}{d\nu}\mathcal{V}_c^2\Big)C_{(6+2)i} \\
&= \nu\frac{d}{d\nu}\Big(-\mathcal{V}_c^2\,C_{(6+2)i}\Big)\,, \qquad (5.41)
\end{aligned}$$

where the factor 4ϵ in the first line comes from the exponent of $\mu_S = m\nu$ in the expression for the unrenormalized Wilson coefficient $\mathcal{V}_{ki}^0 = \mu_S^{4\epsilon}(\mathcal{V}_{ki} + \delta\mathcal{V}_{ki})$.

The anomalous dimensions in Eqs. (5.40) and (5.41) obviously show a factorization of terms subject to pure soft running ($\mathcal{V}_c$) and pure ultrasoft running (C_{2i}, $C_{(6+2)i}$) at LL. Therefore the integrated result is basically the product of a series summing the leading ultrasoft logarithms and a sum over the leading soft logarithms. This structure is actually not surprising, since soft and ultrasoft loops in the diagrams relevant for the described renormalization procedure do not interact with each other as already mentioned. So one could as well resum the respective logarithms independently and in two successive steps as it would be done systematically in pNRQCD [53, 56].

What remains to be computed now is the evolution of the coefficients C_{2i} and $C_{(6+2)i}$. At LL level their RGE's take the generic form

$$\nu\frac{d}{d\nu}C_i \;=\; 2A_i\,(2\alpha_U - \alpha_S)\,, \qquad (5.42)$$

if the formally soft contribution induced by the pull-up mechanism according to section 3.7 and Ref. [70] respectively is added by substituting $\frac{\alpha_U}{\epsilon} \to \frac{\alpha_U}{\epsilon} - \frac{\alpha_S}{\epsilon}$ in the original ultrasoft one-loop counterterm which is parametrized here as $\delta C_i = A_i\frac{\alpha_U}{\epsilon}$. The different factors in front of the soft and ultrasoft coupling are due to their different dependence on the subtraction velocity ν:

$$\nu\,\frac{d\alpha_U}{d\nu} = -\,4\,\epsilon\,\alpha_U - \frac{\alpha_U^2}{\pi}\beta_0 + \mathcal{O}(\alpha_U^3), \quad \nu\,\frac{d\alpha_S}{d\nu} = -\,2\,\epsilon\,\alpha_S - \frac{\alpha_S^2}{2\pi}\beta_0 + \mathcal{O}(\alpha_S^3)\,. \quad (5.43)$$

Eq. (5.42) can also be rewritten as

$$\begin{aligned} dC_i &= 2A_i\,(2\,\alpha_U\,d\ln\nu\,-\,\alpha_S\,d\ln\nu) \\ &= 2A_i\,(2\,\alpha_U\Big(-\frac{\pi d\alpha_U}{\beta_0\alpha_U^2}\Big)\,-\,\alpha_S\Big(-\frac{2\pi d\alpha_S}{\beta_0\alpha_S^2}\Big)) \\ &= -\frac{4\,\pi}{\beta_0}\,A_i\,\Big(\frac{d\alpha_U}{\alpha_U}\,-\,\frac{d\alpha_S}{\alpha_S}\Big)\,, \end{aligned} \tag{5.44}$$

where we consistently assumed LL running of $\alpha_{U,S}$ and used Eq. (3.22) in the second step. This equation can now be integrated easily and we find

$$\begin{aligned} C_i(\nu) &= -\frac{4\,\pi}{\beta_0}\,A_i\,\big(\ln\frac{\alpha_U}{\alpha_h}-\ln\frac{\alpha_S}{\alpha_h}\big)\,+\,C_i(1) \\ &= -\frac{4\,\pi}{\beta_0}\,A_i\,\ln\frac{\alpha_U}{\alpha_S}\,. \end{aligned} \tag{5.45}$$

Finally we set $C_i(1) = 0$, which is the appropriate matching condition for all operators ($\mathcal{O}_{2i}$, $\mathcal{O}_{(6+2)i}$) considered here. Obviously for this kind of LL results the effect of the pull-up term amounts to a change from α_h to α_S in the argument of the logarithm.

The respective parameters A_i ($= A^{(1,T)}_{\mathbf{k},\mathbf{p}}$, $A^{(1,T)}_{1,2}$) are given in Eqs. (5.26) and (5.33). With these results the integrated Eqs. (5.40) and (5.41) read

$$\big(\mathcal{V}_2^{(1,T)}(\nu)\big)_{us} = -\frac{16\pi^2}{\beta_0}A^{(1,T)}_{\mathbf{k}}\,\alpha_s(m\nu)\,\ln\frac{\alpha_s(m\nu^2)}{\alpha_s(m\nu)}\,, \tag{5.46}$$

$$\big(\mathcal{V}_r^{(1,T)}(\nu)\big)_{us} = -\frac{16\pi^2}{\beta_0}A^{(1,T)}_{\mathbf{p}}\,\alpha_s(m\nu)\,\ln\frac{\alpha_s(m\nu^2)}{\alpha_s(m\nu)}\,, \tag{5.47}$$

$$\big(\mathcal{V}_{k1,2}^{(1,T)}(\nu)\big)_{us} = \frac{64\pi^3}{\beta_0}A^{(1,T)}_{1,2}\,\alpha_s(m\nu)^2\,\ln\frac{\alpha_s(m\nu^2)}{\alpha_s(m\nu)}\,. \tag{5.48}$$

They respect the 'ultrasoft' matching conditions $(\mathcal{V}^{(1,T)}_{2,r}(1))_{us} = (\mathcal{V}^{(1,T)}_{k1,2}(1))_{us} = 0$. The total matching conditions like $\mathcal{V}^{(T)}_r(1) = 4\pi\alpha_h$ have already been implemented in the pure soft LL contributions, which have been computed in Ref. [63] and must be added to $(\mathcal{V}^{(1,T)}_2)_{us}$ and $(\mathcal{V}^{(1,T)}_r)_{us}$ to obtain the full renormalization group dependence.

As well, although not affected by ultrasoft renormalization, there is another set of sum operators similar to the $\mathcal{O}_{ki}$. They were first introduced in Ref. [26] and receive their running at LL from divergent soft and potential loop diagrams [62].

Using Eqs. (3.36), (5.16) and Eq. (5.48) we can compute the RG evolution of the effective Wilson coefficients $(\mathcal{V}_{k,\mathrm{eff}}^{(1/T)})_{us}$. They have to be added to the soft coefficients $(\mathcal{V}_{k,\mathrm{eff}}^{(1/T)})_{soft}$ derived in Refs. [26, 62] to incorporate all effects from the tadpole graphs generated by the six-quark operators $\mathcal{O}_{6i}^{(1/T)}$ (Fig. 3.9) or the matrix elements generated by the sum operators $\mathcal{O}_{ki}^{(1/T)}$, respectively. The outcome is[3]

$$\begin{aligned}
\left(\mathcal{V}_{k,\mathrm{eff}}^{(1)}(\nu)\right)_{us} &= -\frac{3}{8\pi^2}\mathcal{V}_{k1}^{(1)}(\nu) \;=\; 6\,\alpha_s(m\nu)^2\,C_{(6+2)1}^{(1)}(\nu)\,, \\
\left(\mathcal{V}_{k,\mathrm{eff}}^{(T)}(\nu)\right)_{us} &= -\frac{1}{4\pi^2}\mathcal{V}_{k2}^{(T)}(\nu) \;=\; 4\,\alpha_s(m\nu)^2\,C_{(6+2)2}^{(T)}(\nu)\,. \qquad (5.49)
\end{aligned}$$

Eqs. (5.46)-(5.49) represent the final results for the ultrasoft LL running of the potentials up to $\mathcal{O}(v^2)$ including soft mixing and pull-up contributions.
They have also been determined in Ref. [32] using Coulomb gauge and a different convention, where the $\mathcal{V}_{ki}$ do not include the factor $(-\mathcal{V}_c^2)$ and equal the $C_{(6+2)i}$ in our convention.

[3]Mind the factor π^2 in the definition of V_k.

Chapter 6

NLL Ultrasoft Running of the Potentials

The current chapter contains the complete two-loop equivalent of the calculation carried out in chapter 5 at one loop. It yields the corresponding NLL results for the running of the leading potentials V_2, V_r and $V_{k,\mathrm{eff}}$ affected by ultrasoft renormalization. The expressions for the various contributions to the counterterms derived in chapter 5 will be needed to subtract one-loop subdivergences in the two-loop renormalization procedure.
Some of the (qualitative) results found in chapter 5 like the factorization of soft and ultrasoft contributions in the evolution of the $\mathcal{V}$'s also hold at NLL level and will not be completely rederived here. The arguments will only be extended if necessary to apply to the two-loop case as well. Furthermore the pull-up mechanism works according to Ref. [70] at higher loop level in the same way as at one loop and we will again include the respective terms in our calculation.

The results of sections 6.1 and 6.2 have already been published in Ref. [33]. Here we will present the most important details of how they are obtained. The calculation in section 6.3 in contrast is completely new, by far more extensive and unpublished to date. Including soft mixing contributions and pull-up terms as mentioned we arrive in section 6.4 at the final ultrasoft NLL results for the Wilson coefficients $\mathcal{V}_2$, $\mathcal{V}_r$ and $\mathcal{V}_{k,\mathrm{eff}}$ which will be used in the analysis of chapter 7.

6.1 Wave function Renormalization

The ultrasoft two-loop topologies depicted in Fig. 6.1 contribute to the heavy quark self-energy in Feynman gauge.
Figs. 6.1 *c*) and *d*) already indicate that we have to deal in general with two new types of topologies at two-loop level: one-loop diagrams with gluon self-energy insertions and so called "non-Abelian" diagrams, which involve the three-gluon self-interaction vertex.

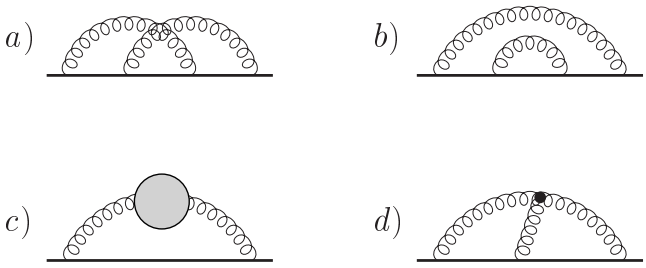

Figure 6.1: Topologies with two ultrasoft loops contributing to the heavy quark wave function renormalization. The bubble in c) represents the ultrasoft gluon self-energy including gluon, ghost and light quark loops.

The expression for the gluon self-energy insertion is determined by evaluating the following ultrasoft gluon ghost and light quark bubble diagrams (in $d = 4 - 2\epsilon$ dimensions) and reads (see e.g. Ref. [38])

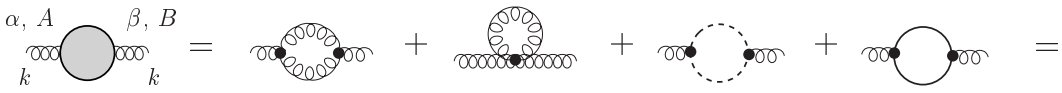

$$= \; i\, 4^{2-d} \pi^{\frac{3-d}{2}} \mu_U^{2\epsilon}\, \alpha_U\, (C_A \frac{3d-2}{d-2} - 4 n_f T)\, \frac{\Gamma(2-\frac{d}{2})\Gamma(\frac{d}{2})}{\Gamma(\frac{d+1}{2})}\, \cdot$$
$$\cdot\, \delta^{AB}\, [\, g^{\alpha\beta} k^2 - k^\alpha k^\beta\,](-k^2)^{\frac{d-4}{2}}\, . \qquad (6.1)$$

In contrast to $g^{\alpha\beta}$ the second term of the ultrasoft momentum structure in Eq. (6.1) $\propto k^\alpha k^\beta$ has, viewed as a matrix, also non-vanishing off-diagonal entries. Therefore not only equal pairs of $A^0/\mathbf{A}$ gluons but also one A^0 and one $\mathbf{A}$ gluon can couple to the self-energy bubble at the same time.
In addition to the diagrams based on the two-loop topologies in Fig. 6.1 we also need to take into account one-loop graphs including $\mathcal{O}(\alpha_U)$ counterterms of the type shown in Fig. 6.2.

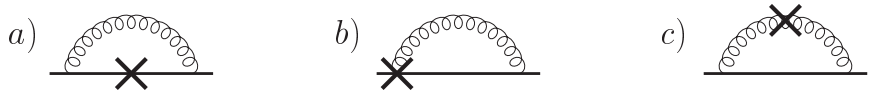

Figure 6.2: One-loop $\mathcal{O}(\alpha_U^2)$ topologies with counterterm insertions contributing to the heavy quark wave function renormalization. The mirror graph of b) is understood.

The Feynman rules for the respective one-loop counterterm insertions/vertices

are given by

$$= i\,\delta Z_\psi^{(1,0)}\,(E - \frac{\mathbf{p}^2}{2m})\,, \tag{6.2}$$

$$= i\,\delta Z_A^{(1)}\,\delta^{AB}\,[\,-g^{\alpha\beta}k^2 + k^\alpha k^\beta\,]\,, \tag{6.3}$$

$$= (\delta Z_\psi^{(1,0)} + \delta Z_g^{(1)} + \frac{1}{2}\delta Z_A^{(1)}) \times$$

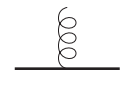

. (6.4)

Eq. (6.4) is valid for A^0 as well as for $\mathbf{A}$ gluons coupling to the heavy quark. δZ_A and δZ_g are defined in the usual way by

$$\begin{aligned} (A^\mu)^0 &= Z_A^{1/2} A^\mu\,, \qquad Z_A = 1 + \delta Z_A\,, \\ g_U^0 &= \mu_U^\epsilon Z_g\, g_U\,, \qquad Z_g = 1 + \delta Z_g\,, \end{aligned} \tag{6.5}$$

and are obtained at $\mathcal{O}(\alpha_U)$ by requiring that they cancel the divergences of Eq. (6.1) and the standard one-loop vertex correction diagram with a A^0 ($\mathbf{A}$) loop, respectively. For the same reason as δZ_ψ (see section 5.1) they cannot depend on the soft momentum label $\mathbf{p}$ in Feynman gauge and scale therefore as v^0. Consequently the contributions to the counterdiagram in Eq. (6.4) that go with a factor $\frac{\mathbf{p}^2}{m^2}$ add up to zero as they did for δZ_ψ. One finds

$$\delta Z_A^{(1)} = \Big(\frac{n_f T}{3\pi} - \frac{5C_A}{12\pi}\Big)\frac{\alpha_U}{\epsilon}\,, \tag{6.6}$$

$$\delta Z_g^{(1)} = -\,\beta_0\,\frac{\alpha_U}{8\pi\epsilon}\,, \tag{6.7}$$

where the index (1) indicates the order in α_U. Eq. (6.7) is consistent with the running of α_U determined by the general argument in section 3.3. This confirms that the coupling constant g_U is of course the same for the interaction of ultrasoft gluons with light quarks and with heavy quarks.
To take into account also higher orders (up to $\mathcal{O}(v^2)$) in the multipole expansion we have to insert additionally kinetic operators like $\frac{\mathbf{p}\cdot\nabla}{m}$ and $\frac{\nabla^2}{2m}$ on the heavy quark lines inside the ultrasoft loops in Figs. 6.1 and 6.2 as shown already in the previous chapter. These operator insertions come along with the counterterms of their two heavy quark fields, but are not renormalized as a whole due to the Lorentz invariance statement in section 5.1. Diagrammatically the associated counterterm insertions are therefore related to the original insertions by

$$= \delta Z_\psi^{(1,0)} \times$$

, (6.8)

$$= \delta Z_\psi^{(1,0)} \times$$

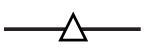

. (6.9)

The counterdiagrams on the left hand side exactly cancel the (sub)divergence of a heavy quark self-energy diagram with an A^0 loop and one insertion of the respective kinetic operator.

Knowing all Feynman rules for the counterterm insertions needed to subtract the corresponding subdivergences we are now in the position to identify all kinds of contributions to the heavy quark wavefunction renormalization from ultrasoft two-loop diagrams up to $\mathcal{O}(v^2)$. They are classified by number and type of vertices and insertions in the diagrams. Each class comprises all graphs generated by the possible combinations of these components. The v scaling is determined by the power counting formula Eq. 3.5. The total contributions to δZ_ψ after subtraction of subdivergences together with a representative example diagram for each class are presented in table 6.1.
Of course one can construct also other $\mathcal{O}(\alpha_U^2)$ diagrams, that have a scaling $\leq v^2$, with different topologies or are composed of different vertices and operator insertions, as e.g. $\frac{\nabla^2}{2m}$. But these are either not logarithmically divergent or vanish in the on-shell limit ($a \to 0$) or because of an antisymmetric integrand. In any case they do not affect the anomalous dimension of the heavy quark fields.
The two-loop integrals we had to perform in the course of the calculation are a special case of the type we find in the two-loop renormalization of the $\frac{1}{m^2}$-potentials and can all be completely reduced to the one-loop integrals listed in Appendix B by partial fraction decomposition. We will apply this method to an example integral in the next section. In case of the contributions from non-Abelian diagrams in table 6.1 the overall integrand itself vanishes already before integration.

Color charge conservation constrains the color structures of the topologies in Fig. 6.1 to be proportional to the unit matrix:

$$\mathsf{cs}[6.1\,a] = T^A T^B T^A T^B = C_F\big(C_F - \frac{C_A}{2}\big)1\,, \quad \mathsf{cs}[6.1\,b] = T^A T^B T^B T^A = C_F^2\,1\,,$$

$$\mathsf{cs}[6.1\,c] = T^A T^A = C_F\,1\,, \quad \mathsf{cs}[6.1\,d] \;=\; i f^{ABC} T^A T^B T^C = -\frac{1}{2} C_A C_F\,1\,.$$

For the non-Abelian topology d) the color structure changes sign depending on the ordering of the $\mathbf{A}$ and A^0 vertices on the heavy quark line.
As argued in section 5.1 the $\mathcal{O}(v^2)$ (Feynman gauge) contributions to δZ_ψ in table 6.1 must add up to zero just as for the one-loop case. This represents a nontrivial cross check of our calculation. In addition our total result

$$\delta Z_\psi^{(2,0)} \;=\; \frac{C_F(4C_F + 4n_f T - 9C_A)\alpha_U^2}{32\pi^2\epsilon^2} + \frac{C_F(19C_A - 8n_f T)\alpha_U^2}{48\pi^2\epsilon} \tag{6.10}$$

agrees with the $\mathcal{O}(\alpha_s^2 m^0)$ wave function renormalization constant in heavy quark effective theory (HQET), see e.g. Ref. [88]. There is agreement since the purely ultrasoft sector of (v)NRQCD is closely related to HQET [89].

Example Diagram	Contribution to δZ_ψ	Order
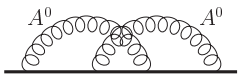	$\frac{C_F(C_F-C_A)\alpha_U^2}{8\pi^2\epsilon^2} + \frac{C_A C_F \alpha_U^2}{8\pi^2\epsilon}$	$\mathcal{O}(v^0)$
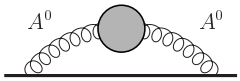	$-\frac{C_F(5C_A-4\,Tn_f)\alpha_U^2}{32\pi^2\epsilon^2} + \frac{C_F(13C_A-8\,Tn_f)\alpha_U^2}{48\pi^2\epsilon}$	$\mathcal{O}(v^0)$
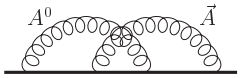	$-\frac{C_F(C_F-C_A)\mathbf{p}^2\alpha_U^2}{4\,m^2\pi^2\epsilon^2} - \frac{C_A C_F \mathbf{p}^2\alpha_U^2}{4\,m^2\pi^2\epsilon}$	$\mathcal{O}(v^2)$
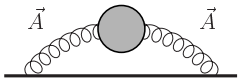	$\frac{C_F(15\,C_A-12\,Tn_f)\mathbf{p}^2\alpha_U^2}{288\,m^2\pi^2\epsilon^2} - \frac{C_F(46\,C_A-32\,Tn_f)\mathbf{p}^2\alpha_U^2}{288\,m^2\pi^2\epsilon}$	$\mathcal{O}(v^2)$
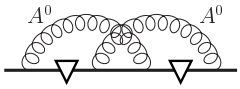	$\frac{C_F(C_F-C_A)\mathbf{p}^2\alpha_U^2}{4\,m^2\pi^2\epsilon^2} + \frac{C_A C_F \mathbf{p}^2\alpha_U^2}{4\,m^2\pi^2\epsilon}$	$\mathcal{O}(v^2)$
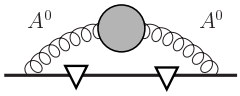	$-\frac{C_F(75\,C_A-60\,Tn_f)\mathbf{p}^2\alpha_U^2}{288\,m^2\pi^2\epsilon^2} + \frac{C_F(110\,C_A-64\,Tn_f)\mathbf{p}^2\alpha_U^2}{288\,m^2\pi^2\epsilon}$	$\mathcal{O}(v^2)$
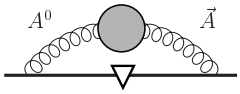	$\frac{C_F(15\,C_A-12\,Tn_f)\mathbf{p}^2\alpha_U^2}{72\,m^2\pi^2\epsilon^2} - \frac{C_F(16\,C_A-8\,Tn_f)\mathbf{p}^2\alpha_U^2}{72\,m^2\pi^2\epsilon}$	$\mathcal{O}(v^2)$
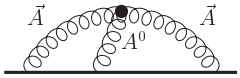	0	$\mathcal{O}(v^2)$
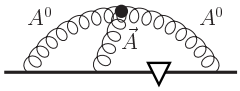	0	$\mathcal{O}(v^2)$

Table 6.1: Contributions to δZ_ψ at ultrasoft two-loop level. Subdivergences have been subtracted by appropriate counterdiagrams. Each row is associated with a different class of contributions including a representative example diagram. If the example diagram has the topology Fig. 6.1 *a*) the corresponding diagrams with topology Fig. 6.1 *b*) are understood to be part of the respective class as well.

In analogy to the one-loop renormalization of the $\frac{1}{m^2}$ - potentials we will need the above expression in the next section.

6.2 $\frac{1}{m^2}$ - Potentials

From the technical point of view the ultrasoft renormalization procedure for the $\frac{1}{m^2}$ - potentials at two-loop level is quite similar to the wave function renormal-

ization in the previous section. Although the number of topologies, shown in Fig. 6.3 is much larger and the color structures are more complicated, which of course makes the calculation more extensive, the classification of diagrams defined in table 6.2 is analogous to table 6.1.
In comparison to the two-loop heavy quark self-energy diagrams (Fig. 6.1) there is just one more heavy quark propagator in the integrands. The insertion of the (Coulomb) potential in the middle is not affected by the ultrasoft momenta and can be treated basically as a universal factor in front of the integrals. The main technical difference is actually that there are diagrams in Fig. 6.3 with heavy quark propagators for which the fermion and the ultrasoft momentum flow do not coincide like in the one-loop example Eq. (5.9).

Class	Topology	Insertions/Vertices	Order
1	Fig. 6.3 a	four gA^0 vertices	$\mathcal{O}(v^0)$
2	Fig. 6.3 b	one gluon self-energy insertion and two gA^0 vertices	$\mathcal{O}(v^0)$
3	Fig. 6.3 a	two gA^0 and two $g\frac{\mathbf{p}\cdot\mathbf{A}}{m}$ vertices	$\mathcal{O}(v^2)$
4	Fig. 6.3 b	one gluon self-energy insertion and two $g\frac{\mathbf{p}\cdot\mathbf{A}}{m}$ vertices	$\mathcal{O}(v^2)$
5	Fig. 6.3 a	two gA^0 vertices and two insertions of the $\frac{\mathbf{p}\cdot\nabla}{m}$ operator on the internal quark lines	$\mathcal{O}(v^2)$
6	Fig. 6.3 b	one gluon self-energy insertion, two gA^0 vertices and two insertions of the $\frac{\mathbf{p}\cdot\nabla}{m}$ operator on the internal quark lines	$\mathcal{O}(v^2)$
7	Fig. 6.3 b	one gluon self-energy insertion, one gA^0, one $g\frac{\mathbf{p}\cdot\mathbf{A}}{m}$ vertex and one insertion of the $\frac{\mathbf{p}\cdot\nabla}{m}$ operator on the internal quark lines	$\mathcal{O}(v^2)$
8	Fig. 6.3 c	one triple gluon interaction, one gA^0 and two $g\frac{\mathbf{p}\cdot\mathbf{A}}{m}$ vertices	$\mathcal{O}(v^2)$
9	Fig. 6.3 c	one triple gluon interaction, two gA^0, one $g\frac{\mathbf{p}\cdot\mathbf{A}}{m}$ vertex and one insertion of the $\frac{\mathbf{p}\cdot\nabla}{m}$ operator on the internal quark lines	$\mathcal{O}(v^2)$

Table 6.2: Classification of divergent diagrams contributing to the potential counterterms at two-loop level.

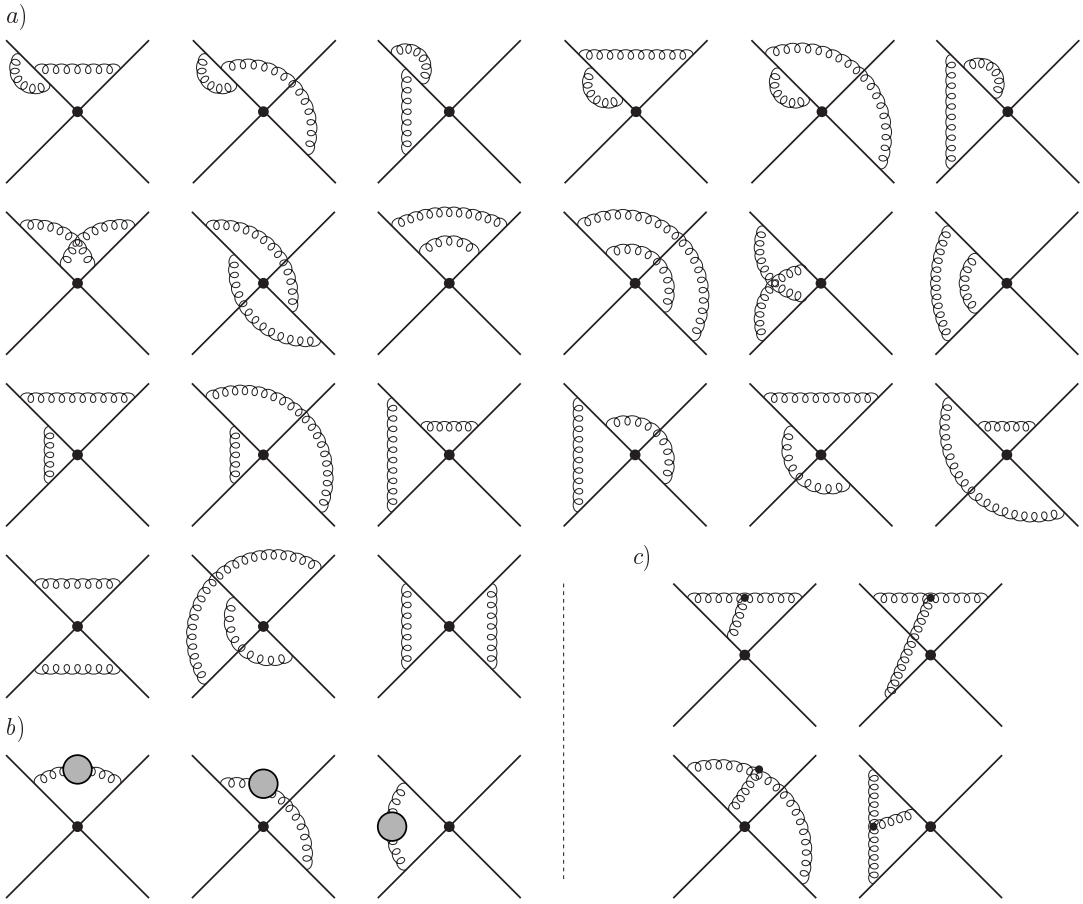

Figure 6.3: Topologies obtained by dressing a potential with two ultrasoft gluon loops: a) "Abelian", b) with gluon self-energy, c) "Non-Abelian". Left-right and up-down mirror graphs are not displayed.

Diagrams with the potential vertices from the higher order terms of the multipole expansion of the Coulomb potential (Eq. (2.29)) in the center of the Fig. 6.3 graphs vanish in the on shell limit. This can be verified easily by counting powers only of the ultrasoft scale, since the only scale of this kind occurring in the calculation of the ultrasoft loops is the artificial off-shellness a, which has been introduced to regulate IR singularities (see beginning of chapter 5). Diagrams with a $\frac{\nabla^2}{2m}$ insertion and diagrams where one $\mathbf{A}$ gluon couples directly to a central $\psi^2\chi^2\mathbf{A}$ vertex (Eq. (2.29)) do not contribute for the same reason.

The two-loop integrals for the diagrams with Abelian topology (Fig. 6.3 *a*)) can all be solved analytically. We use partial fraction decomposition w.r.t. the zero components of the ultrasoft loop momenta (k, l) to split the integrands into terms that comprise powers of at most three different heavy quark propagators. After that we carry out the integration over the momentum which appears only in one of the propagators of each term using the standard one-loop formula (B.7). In some cases we have to reverse the sign of the loop momentum first to match (B.7). The result depends of course only on the second loop momentum and the off-shellness a and takes again the form of a product of two propagators with different exponents. One of these exponents is non-integer and involves the dimension $d = 4 - 2\epsilon$. Together with the remaining gluon propagator these integrals have again the generic form of a basic one-loop integral given by (B.10).

The above procedure is demonstrated in Eq. (6.11) for a typical example of an Abelian two-loop diagram, which is a member of the fifth class in table 6.2. This particular diagram yields a pure two-loop contribution to the potential counterterm, since it contains no one-loop subdivergence: erasing the outer gluon propagator the inner loop itself would vanish due to an antisymmetric integrand. That is why the result is a single $\frac{1}{\epsilon}$ term and there are no (IR) logarithms of the off-shellness a left, which would have to be canceled by a corresponding one-loop counterdiagram.
The numerator of the two-loop integrand in this case comes from two $\frac{\mathbf{p}\cdot\nabla}{m}$ insertions on different heavy quark lines and reads (up to signs): $[\mathbf{p}\cdot(\vec{k}+\vec{l})][\mathbf{p}\cdot\vec{l}]$. Since the denominator of ultrasoft loop integrals only depends on k^0 and k^2, we can eliminate $\vec{k}$ in this term because of antisymmetry and transform the numerator using the formula in Eq. (B.1) w.r.t. the l integration into $\mathbf{p}^2\,\vec{l}^{\,2}$. Thus we are basically left with:

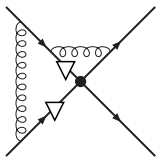

$$\propto \int\frac{d^dk}{(2\pi)^d}\int\frac{d^dl}{(2\pi)^d}\;\frac{l_0^2-l^2}{(l_0+a)(l_0+k_0+a)^2(-l_0+a)^2(k_0+a)\,l^2k^2}$$

$$= \iint\left[\frac{-l_0}{(l_0+a)(l_0+k_0+a)^2(-l_0+a)^2}+\frac{1}{(l_0+a)(-l_0+a)^2(k_0+a)}\right.$$
$$\left.-\frac{1}{(l_0+a)(l_0+k_0+a)(-l_0+a)^2}\right](l^2k^2)^{-1}$$

$$= \iint\left[-\frac{1}{(l_0+k_0+a)^2(-l_0+a)^2}+\frac{a}{(l_0+a)(l_0+k_0+a)^2(-l_0+a)^2}\right.$$
$$\left.+\frac{1}{(l_0+a)(-l_0+a)^2(k_0+a)}-\frac{1}{(l_0+a)(l_0+k_0+a)(-l_0+a)^2}\right](l^2k^2)^{-1}$$

$$
\begin{aligned}
&= \int \left[\frac{\gamma_1(d)}{(-l_0-a)^{4-d}(-l_0+a)^2} + \frac{\gamma_1(d)\; a}{(-l_0-a)^{5-d}(-l_0+a)^2} + \frac{\gamma_2(d)\; (-a)^{d-3}}{(l_0+a)(-l_0+a)^2} \right. \\
&\quad \left. + \frac{\gamma_2(d)}{(-l_0-a)^{4-d}(-l_0+a)^2} \right] (l^2)^{-1} \\
&= (-a)^{2(d-4)} \Big[\big(\gamma_1(d) + \gamma_2(d)\big)\, \tilde{\gamma}_1(d) + \gamma_1(d)\, \tilde{\gamma}_2(d) + \gamma_2(d)\, \gamma_3(d) \Big] \\
&= -\frac{1}{64\pi^4 \epsilon}\,. \qquad (6.11)
\end{aligned}
$$

The γ_i and $\tilde{\gamma}_i$ are functions of the dimension d and generate the UV divergent $\frac{1}{\epsilon}$ terms when expanded. They can be deduced easily from Eqs. (B.7) and Eq. (B.10), e.g.:

$$
\begin{aligned}
\tilde{\gamma}_1(d) \;=\; & i\, 2^{d-8} \pi^{-d/2} \Gamma(3-d) \Gamma\Big(\frac{d}{2}-1\Big) \Big(2\,(3d-10)\Gamma(4-d)\Gamma(6-d) + \\
& + \Gamma(8-2d)(d-5)\, {}_2F_1[3-d, d-4; 5-d; -1] - 2\, {}_2F_1[3-d, d-3; 6-d; -1] \Big) \\
& \cdot \Big(\Gamma(4-d)\Gamma(6-d) \Big)^{-1}. \qquad (6.12)
\end{aligned}
$$

The γ_i typically include a number of gamma functions and the $\tilde{\gamma}_i$ in addition hypergeometric functions of the type of the above example. We have expanded the latter in the dimensional $\epsilon = \frac{4-d}{2}$ analytically to extract the divergent parts of the two-loop diagrams using the `Mathematica` package `HypExp` [90] (and checked the expansions numerically).

The integrals associated with the graphs in Fig. 6.3 *b*), where the gluon self-energy subdivergence Eq. 6.1 has been inserted actually have already a (generalized) one-loop structure and can be computed without an extensive partial fraction decomposition as for the Abelian integrals. Consider for example the following class 7 diagram. Here one three momentum component k^i in the numerator comes from the $\frac{\mathbf{p}\cdot\nabla}{m}$ insertion and the other k^j together with k_0 and $(-k^2)^{\frac{d-4}{2}}$ from the self-energy Eq. 6.1:

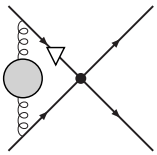

$$
\propto\; \mathbf{p}^i \mathbf{p}^j \int \frac{d^d k}{(2\pi)^d}\, \frac{k_0 k^i k^j (-k^2)^{\frac{d-4}{2}}}{(k_0+a)^2(-k_0+a)(k^2)^2} \;\propto
$$

$$
\begin{aligned}
\propto\; & \int \frac{k_0(k_0^2-k^2)}{(k_0+a)^2(-k_0+a)(-k^2)^{4-\frac{d}{2}}} = -\int \frac{(k_0+a)^2 - 2a(k_0+a) + a^2 - k^2}{(k_0+a)^2(-k^2)^{4-\frac{d}{2}}} + \\
& + a \int \frac{(k_0+a)^2 - 2a(k_0+a) + a^2 - k^2}{(k_0+a)^2(-k_0+a)(-k^2)^{4-\frac{d}{2}}} \;=\; \ldots\,. \qquad (6.13)
\end{aligned}
$$

The factor $(-k^2)^{4-\frac{d}{2}}$ in the denominators causes IR singularities at intermediate steps when there are no compensating factors of k_0 or k^2 in the numerator. But since we know from the original form of the integrand that they will cancel in the final result we just do not care about them and treat them as if they were UV divergences. Multiplying the result of Eq. (6.13) by the associated factor $\mu_U^{4\epsilon}$ and by $\Gamma(2-\frac{d}{2})$, which contains the self-energy divergence in Eq. 6.1 we obtain

$$-\frac{3\,i}{32\pi^2\epsilon^2}+\frac{i\,(12\ln(\frac{-a}{\mu_U})+3\ln(\pi)+18\ln(2)-1)}{32\pi^2\epsilon}\,, \tag{6.14}$$

where we replaced μ_U by its $\overline{\rm MS}$ version: $\mu_U \to \mu_U\, e^{\frac{1}{2}(\gamma-\ln(4\pi))}$. The $\ln(-a)$ term will be subtracted by the obvious counterdiagram with the counterterm insertion given in Eq. (6.3) instead of the self-energy bubble.

The non-Abelian integrals we have to deal with in classes 8 and 9 are due to the third gluon propagator a bit more involved. They can all be reduced by algebraic manipulations like in the above examples and by shifting the loop momenta to either of the following generic forms.

$$\begin{aligned} I_1(\alpha,\beta,\gamma,\delta,\eta,\varphi) \;&=\; \int\frac{d^dk}{(2\pi)^d}\int\frac{d^dl}{(2\pi)^d} \\ &\cdot\Big[(-k_0-a)^\alpha(k_0-a)^\beta(-l_0-a)^\gamma(-k^2)^\delta(-l^2)^\eta(-(k-l)^2)^\varphi\Big]^{-1} \end{aligned} \tag{6.15}$$

$$\begin{aligned} I_2(\alpha,\beta,\gamma,\delta,\eta,\varphi) \;&=\; \int\frac{d^dk}{(2\pi)^d}\int\frac{d^dl}{(2\pi)^d} \\ &\cdot\Big[(-k_0-a)^\alpha(-k_0-l_0-a)^\beta(-l_0-a)^\gamma(-k^2)^\delta(-l^2)^\eta(-(k+l)^2)^\varphi\Big]^{-1} \end{aligned} \tag{6.16}$$

We can further on always decompose $I_1(\alpha,\beta,\gamma,\delta,\eta,\varphi)$ into the integrals over the partial fractions $I_1(0,\beta,\gamma,\delta,\eta,\varphi)$ and $I_1(\alpha,0,\gamma,\delta,\eta,\varphi)$ for integer α, β.
Using the integration by parts (IBP) method [91] we find the recurrence relations

$$I_1(0,\beta,\gamma,\delta,\eta,\varphi) \;= \tag{6.17}$$

$$=\;\frac{-\beta\,\boldsymbol{\beta^+\gamma^-}+\delta\,\boldsymbol{\delta^+(\eta^--\varphi^-)}+2\varphi\,\boldsymbol{\varphi^+(\delta^--\eta^-)}}{d-\beta-3\delta}\;I_1(0,\beta,\gamma,\delta,\eta,\varphi)\,,$$

$$I_1(\alpha,0,\gamma,\delta,\eta,\varphi) \;= \tag{6.18}$$

$$=\;\frac{-\alpha\,\boldsymbol{\alpha^+\gamma^-}-\delta\,\boldsymbol{\delta^+(\eta^--\varphi^-)}}{d-\alpha-\delta-2\varphi}\;I_1(\alpha,0,\gamma,\delta,\eta,\varphi)\,,$$

$$I_2(\alpha,\beta,\gamma,\delta,\eta,\varphi) \;= \tag{6.19}$$

$$=\;\frac{-\alpha\,\boldsymbol{\alpha^+\gamma^-}+\beta\,\boldsymbol{\beta^+(\alpha^--\gamma^-)}+\delta\,\boldsymbol{\delta^+(\eta^--\varphi^-)}+2\varphi\,\boldsymbol{\varphi^+(\delta^--\eta^-)}}{d-\alpha-3\delta}\;I_2\,,$$

where the bold Greek letters $\boldsymbol{\alpha^{\pm}}$ etc. represent operators acting on the integrals $I_{1,2}$ as

$$\boldsymbol{\alpha^{\pm}}\, I_{1,2}(\alpha,\beta,\gamma,\delta,\eta,\varphi) \;=\; I_{1,2}(\alpha\pm 1,\beta,\gamma,\delta,\eta,\varphi) \quad \text{etc.}\,. \tag{6.20}$$

Together with the identities

$$I_2(0,\beta,\gamma,\delta,\eta,\varphi) \;=\; I_1(\beta,0,\gamma,\varphi,\eta,\delta)\,, \tag{6.21}$$
$$I_2(\alpha,\beta,0,\delta,\eta,\varphi) \;=\; I_1(\alpha,0,\beta,\delta,\varphi,\eta)\,, \tag{6.22}$$

we can now reduce every integral $I_{1,2}$ with integer values for α, β, ..., φ, by applying Eqs. (6.17)-(6.19) sufficiently many times, to a combination of integrals $I_{1,2}$, for which at least two parameters out of $\{\alpha, \beta, \gamma\}$ are zero or one out of $\{\delta, \eta, \varphi\}$ is zero. Shifting the integration variables the resulting integrals can then be expressed as (products of) Abelian integrals and solved similar to Eq. (6.11). In the course of this calculation an additional one-loop integral, Eq. (B.6), is required.
Since the total contribution from triangle graphs involving the non-Abelian triple gluon vertex to the counterterm Eq. (6.4) vanishes at $\mathcal{O}(v^0)$ and $\mathcal{O}(v^2)$ the subdivergences in the two-loop diagrams in classes 8 and 9 must cancel exactly to avoid terms $\propto \ln(\frac{-a}{\mu_U})$. Consequently the sum of all non-Abelian diagrams does not contain a $\frac{1}{\epsilon^2}$ divergent term and yields a pure two-loop contribution to the anomalous dimension of the potentials.

The simplest way to determine the color factors in terms of C_A and C_F for many of the Abelian topologies in Fig. 6.3 *a*) is to perform a Fierz transformation (Eq. (C.21)) on the color structures. Taking the third topology in the first column of Fig. 6.3 with a central $X^A\otimes\bar{X}^A$ potential as an example we have

$$\begin{aligned} X^B T^C \otimes \bar{T}^A \bar{X}^B \bar{T}^C \bar{T}^A \;&=\; X^B T^C \otimes \big(\bar{T}^A_{ij}\bar{X}^B_{jk}\bar{T}^C_{kl}\bar{T}^A_{lm}\big) \;= \\ &=\; X^B T^C \otimes \Big(\bar{X}^B_{jk}\bar{T}^C_{kl}\,\frac{1}{2}\big[\delta_{im}\delta_{lj} - (C_A{-}2C_F)\delta_{ij}\delta_{lm}\big]\Big) \;= \\ &=\; X^B T^C \otimes \frac{1}{2}\big(\,\mathrm{tr}[\bar{X}^B\bar{T}^C]\,\bar{1} - (C_A{-}2C_F)\bar{X}^B\bar{T}^C\big)\,. \end{aligned} \tag{6.23}$$

For $X = 1$ the above expression is simply proportional to $T^A\otimes\bar{T}^A$ (cf. Eq. (C.1)). For $X = T$ it reduces to a combination of $1\otimes\bar{1}$ and one of the one-loop color structures in table 5.2. In the cases, e.g. $T^A X^B T^C \otimes \bar{X}^B\bar{T}^A\bar{T}^C$, where the Fierz identity Eq. (C.21) cannot be used to simplify the color structures for arbitrary X like in Eq. (6.23), still a subsequent application of the table 5.2 results is sufficient to express them in the $1\otimes\bar{1}$, $T^A\otimes\bar{T}^A$ basis as soon as X is specified.
The color factors for the four non-Abelian topologies turn out to equal each other up to a sign depending on the positions of A^0 and $\mathbf{A}$ interaction vertices on the heavy quark lines. For $X = 1$ the basic structure is $-\frac{1}{2}C_A T^A\otimes\bar{T}^A$ as

a result of the formulae (C.19) and (C.20) in the Appendix. For $X = T$ it is $-\frac{1}{4}C_A C_F(C_A - 2C_F)\,1\otimes\bar{1}$ according to the second one-loop identity in Eq. 5.17 and its hermitian conjugate counterpart respectively.

In contrast to the one-loop calculation the Abelian diagrams contributing at two-loop level contain a number of (one-loop) subdivergences. As already mentioned in the context of the self-energy diagrams these are subtracted by adding the obligatory one-loop counterdiagrams. These equal the one-loop diagrams in table 5.1 in which either one wavefunction counterterm insertion Eq. (6.2) is placed on a heavy quark propagator or one of the quark gluon interactions, kinetic insertions or the potential is replaced by the corresponding countervertices, given in Eqs. (6.4), (6.8) and (5.10) respectively, in all possible ways. The potential counterdiagram in the latter equation is needed here at $\mathcal{O}(\alpha_U\, v^\sigma)$ for $\sigma = 0$ and $\sigma = 2$. In the first case it reduces to $-\,2\,i\mu_s^{2\epsilon}\delta Z_\psi^{(1,0)}(V_{1\otimes1}\,1\otimes\bar{1} + V_{T\otimes T}\,T^A\otimes\bar{T}^A)$ since $\delta V^{(1,0)} = 0$.
If all relevant counterterms have been taken into account correctly the logarithms of the off-shellness a cancel consistently.

The two-loop $\mathcal{O}(\alpha_U^2\, v^\sigma)$ equivalent to Eq. (5.10) for $\sigma \le 2$ reads

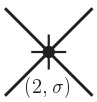

$$
\begin{aligned}
&= -i\mu_s^{2\epsilon}\Big[\delta V_{1\otimes1}^{(2,\sigma)}\,1\otimes\bar{1} + \delta V_{T\otimes T}^{(2,\sigma)}\,T^A\otimes\bar{T}^A + \\
&+ 2\,\delta Z_\psi^{(1,0)}(\delta V_{1\otimes1}^{(1,\sigma)}\,1\otimes\bar{1} + \delta V_{T\otimes T}^{(1,\sigma)}\,T^A\otimes\bar{T}^A) + \\
&+ \Big((\delta Z_\psi^{(1,0)}(\delta Z_{\psi,\mathbf{p}}^{(1,\sigma)} + \delta Z_{\psi,\mathbf{p}'}^{(1,\sigma)}) + \delta Z_{\psi,\mathbf{p}}^{(2,\sigma)} + \delta Z_{\psi,\mathbf{p}'}^{(2,\sigma)}\Big)\cdot \\
&\quad\cdot (V_{1\otimes1}\,1\otimes\bar{1} + V_{T\otimes T}\,T^A\otimes\bar{T}^A)\Big]\,. \qquad (6.24)
\end{aligned}
$$

Although we have already seen in the last section that the sum of all contributions to $\delta Z_{\psi,\mathbf{p}}^{(2,2)}$ as well as for $\delta Z_{\psi,\mathbf{p}}^{(1,2)}$ ($\delta Z_{\psi,\mathbf{p}}^{(1,0)} \equiv Z_\psi^{(1,0)}$) vanishes we still display the corresponding terms in Eq. (6.24), since we also want to show the partial results for $\delta V^{(2,2)}$ from each class in table 6.2.
Before we do this however we should have a look at the $\sigma = 0$ case, where only classes 1 and 2 contribute. According to section 3.6 we expect a vanishing potential counterterm at the leading order in v. Indeed we find

$$\delta V_{1\otimes1}^{(2,0)} \;=\; \delta V_{T\otimes T}^{(2,0)} \;=\; 0\,. \qquad (6.25)$$

This result represents of course an important and highly non-trivial cross-check of the methods used to calculate the diagrams in all classes. Besides the color structures (that only depend on the topology) in particular the techniques to solve two-loop integrals such as Eq. (6.11) are tested. Moreover the set of relevant topologies in Fig. 6.3 *a*) and *b*) is checked for completeness.

The ultrasoft two-loop contributions to the matrix A introduced in Eq. (5.12) are presented in table 6.3. For convenience we define two basic matrices M_{Ab}, M_{nonAb} compatible with the soft momentum structure generated by Abelian (3-7) and non-Abelian (8+9) classes, respectively.

$$M_{\mathsf{Ab}} = \begin{bmatrix} C_F\,\mathbf{k}^2 & -\frac{1}{2}C_F(C_A-2C_F)\,\mathbf{k}^2 \\ -\mathbf{k}^2 & -\frac{3}{2}(C_A-2C_F)\,\mathbf{k}^2 + C_A(\mathbf{p}^2+\mathbf{p}'^2) \end{bmatrix}, \tag{6.26}$$

$$M_{\mathsf{nonAb}} = \begin{bmatrix} 0 & \frac{1}{2}(C_A-2C_F)C_F\left(\mathbf{k}^2 - \frac{9}{4}(\mathbf{p}^2+\mathbf{p}'^2)\right) \\ -\frac{1}{4}(4\mathbf{k}^2+\mathbf{p}^2+\mathbf{p}'^2) & -\frac{5}{8}(C_A-4C_F)(\mathbf{p}^2+\mathbf{p}'^2) \end{bmatrix} + \\ + \left(\frac{1}{\pi^2}-\frac{1}{6}\right) M_{\mathsf{Ab}}\,. \tag{6.27}$$

Class	Contribution to $A^{(2,2)}$
3	$\left(-\frac{C_A\alpha_U^2}{8m^2\pi^2\epsilon^2} + \frac{C_A\alpha_U^2}{4m^2\pi^2\epsilon}\right) M_{\mathsf{Ab}}$
4	$\left(-\frac{(15C_A-12Tn_f)\alpha_U^2}{288m^2\pi^2\epsilon^2} + \frac{(46C_A-32Tn_f)\alpha_U^2}{288m^2\pi^2\epsilon}\right) M_{\mathsf{Ab}}$
5	$\left(\frac{C_A\alpha_U^2}{24m^2\pi^2\epsilon^2} - \frac{C_A\alpha_U^2}{8m^2\pi^2\epsilon}\right) M_{\mathsf{Ab}}$
6	$\left(\frac{(75C_A-60Tn_f)\alpha_U^2}{864m^2\pi^2\epsilon^2} - \frac{(110C_A-64Tn_f)\alpha_U^2}{864m^2\pi^2\epsilon}\right) M_{\mathsf{Ab}}$
7	$\left(-\frac{(15C_A-12Tn_f)\alpha_U^2}{144m^2\pi^2\epsilon^2} + \frac{(16C_A-8Tn_f)\alpha_U^2}{144m^2\pi^2\epsilon}\right) M_{\mathsf{Ab}}$
8+9	$\frac{C_A\alpha_U^2}{6m^2\epsilon} M_{\mathsf{NonAb}}$

Table 6.3: Two-loop $\mathcal{O}(\alpha_U^2\, v^2)$ contributions to the matrix A from the diagram classes defined in table 6.2.

As expected the non-Abelian contributions do not generate an overall $\frac{1}{\epsilon^2}$ divergence, because the one-loop subdivergences cancel as argued above. This is not true for the single results of classes 8 and 9 alone, which are not displayed here: both contain the same $\frac{1}{\epsilon^2}$ term differing only in the sign.
The total result has been published in Ref. [33] and reads

$$A^{(2,2)} \;=\; \frac{\alpha_U^2}{m^2}\left(-\frac{11C_A-4Tn_f}{72\,\pi^2\epsilon^2} + \frac{(-3\pi^2+47)C_A-10Tn_f}{108\,\pi^2\epsilon}\right) M_{\mathsf{Ab}} + \frac{\alpha_U^2}{m^2}\frac{C_A}{6\epsilon}\, M_{\mathsf{NonAb}}\,. \tag{6.28}$$

The fermionic terms ($\propto T n_f$) arise from light quark bubble insertions in the gluon lines of Fig. 5.1 and constitute therefore the total UV divergence of a gauge invariant subset of two-loop diagrams. As a final cross check we verified that these terms agree with the ones we have computed already in a previous work [28] using Coulomb gauge[1].

6.3 $\frac{1}{m|\mathbf{k}|}$ - Potentials

Already the sheer number of $\mathcal{O}(10^4)$ diagrams (including mirror graphs) we have to deal with in the renormalization of the (effective) $\frac{1}{m\mathbf{k}}$ - potentials at NLL level indicates that compared to the previous calculations with at most $\mathcal{O}(10^3)$ diagrams much more effort is necessary. To handle the great number of Feynman diagrams we developed `Mathematica` codes to automatize the generation and evaluation of the corresponding amplitudes. The main technical difficulty within this process is to to solve the two-loop integrals (or at least determine their UV divergent part), which involve more than one external scale/off-shellness: one artificial off-shellness (a) from the external quark legs and one physical off-shellness from the internal quark lines of the respective six-leg diagrams.
To tackle the problem systematically we split the calculation into different parts according to the different types of contributing topologies: diagrams with gluon self-energy insertions, Abelian diagrams and non-Abelian diagrams. The latter involve one triple gluon self-interaction vertex.

6.3.1 Diagrams with Gluon Self-Energy Insertions

The two-loop diagrams with a gluon self-energy are obviously the easiest kind of diagrams we are to compute. They are based on the one-loop six-leg topologies in Figs. 5.3 and 5.4, where the self-energy bubble of Eq. (6.1) is inserted in the ultrasoft gluon line.
In addition to the contributions I-V analogous to the ones in table 5.3 we can also have an $\mathbf{A}$ and an A^0 gluon, both coupling to the self-energy bubble as for the $\frac{1}{m^2}$ potentials. We classify the diagrams with this configuration as shown in table 6.4.
After some algebraic manipulation similar to Eq. (6.13) the loop integrals basically take the same form as the one-loop integrals in section 5.3. The only difference is that we now have non-integer exponents of $(-k^2)$ and therefore non-integer values for the γ parameter in the general formulae in Appendix B.

The color factors in the $1\otimes\bar{1}$, $T^A\otimes\bar{T}^A$ basis are obtained by multiplying the one-loop results in Eq. (5.17) by C_A for gluon and ghost bubbles and $n_f T$ for a light fermion loop in accordance with Eq. (6.1).

[1] We found perfect agreement after adding a missing contribution corresponding to class 6 in table 6.2 to the Coulomb gauge results in Ref. [28].

Topologies / Class	Fig. 5.3 + gluon self-energy ins.	Fig. 5.4 + gluon self-energy ins.
A and A^0 gluon, $1\times$ 	VI	0 (diagrams finite or canceled by subdivergences)
A and A^0 gluon, $1\times$ 	VII	VIII

Table 6.4: Contributions (VI-VIII) to the running of the six-quark operators $\mathcal{O}_{6i}$ from two-loop diagrams including a self-energy subdiagram on the ultrasoft gluon lines. This table should be viewed as an extension to table 5.3, that classifies the one-loop contributions (I-V) which of course have a two-loop analog where a gluon self-energy bubble is inserted.

In table 6.5 we give some partial results.

Contributions	Result $\cdot \left[\frac{i\mathcal{V}_c^2\alpha_U^2}{m\,\pi^2}\Big(C_F(C_A-2C_F)(f_0+f_1+2f_2)1\otimes\bar{1}+(C_A-4C_F)(f_1+f_2)\,T^A\otimes\bar{T}^A\Big)\right]^{-1}$
I	$\frac{C_A(5C_A-4Tn_f)}{96\epsilon^2} - \frac{C_A(23C_A-16Tn_f)}{144\epsilon}$
II+III+IV+V	$-\frac{5C_A(5C_A-4Tn_f)}{288\epsilon^2} + \frac{C_A(55C_A-32Tn_f)}{432\epsilon}$
VI+VII+VIII	$\frac{C_A(5C_A-4Tn_f)}{48\epsilon^2} - \frac{C_A(2C_A-Tn_f)}{18\epsilon}$

Table 6.5: Results for the ultrasoft two-loop contributions with gluon self-energy insertion specified in table 5.3 (I-V) and table 6.4 (VI-VIII). In contrast to the results in table 5.4 these are only the divergent parts of diagrams with two quark and four antiquark legs or vice versa (up-down symmetry). Alternatively they can be viewed as the UV divergences to be absorbed by the counterterms $\delta\mathcal{V}_{ki}$ (see subsection 3.5.2).

The expression for each diagram before integrating is basically the corresponding one-loop integrand times some factor involving the ultrasoft loop momentum (k) from the self-energy in Eq. (6.1), which only differs for the different gluon configurations $2\times A^0$ (I), $2\times\mathbf{A}$ (II+III+IV+V) or $A^0\,\&\,\mathbf{A}$ (VI+VII+VIII). In addition consistency requires, as we will see in section 6.4, that the $\frac{1}{\epsilon^2}$ term of

the total two-loop UV divergence

$$\mathrm{I}+\ldots+\mathrm{VIII} = \left[\frac{C_A(5C_A-4Tn_f)}{72\epsilon^2}-\frac{C_A(31C_A-20Tn_f)}{216\epsilon}\right]\frac{i\mathcal{V}_c^2\alpha_U^2}{m\,\pi^2}$$
$$\cdot\left[C_F(C_A-2C_F)(f_0+f_1+2f_2)1\otimes\bar{1}+(C_A-4C_F)(f_1+f_2)\,T^A\otimes\bar{T}^A\right] \quad (6.29)$$

is proportional to the same linear combination of f_i functions as at one-loop level, cf. Eq. (5.18). Hence it is not surprising that not only the contributions I and II+III+IV+V, which have obvious one-loop analogs, but also VI+VII+VIII have this structure.

6.3.2 Abelian Diagrams

The set of the so called Abelian diagrams comprises the largest number of diagrams taking part in the renormalization of the six-quark operators $\mathcal{O}_{6i}$.
There are 907 possible ways to connect two discrete ultrasoft gluon lines to the basic six-leg structure made up of two heavy quark potentials and one intermediate (either quark or antiquark) propagator. In this counting we only allowed for single gluon interaction with a heavy quark line/potential and did include the topologies associated with one or two-loop wavefunction renormalization of the external legs. 442 of these involve at least one interaction vertex of the $\psi\psi^\dagger\chi\chi^\dagger\mathbf{A}$ type in Eq. (2.29). Some typical representatives are shown in Figs. 6.4 and 6.5 respectively.

As in the one-loop case the corresponding diagrams with the potential loop cut at the bottom side is understood to participate in the renormalization of the six-quark operators. To be precise the diagrams of Fig. 6.4 and Fig. 6.5 type actually renormalize the operators $\mathcal{O}_{\bar{6}i}$ containing four quark and two antiquark fields. Nevertheless, as explained in subsection 3.5.2, the anomalous dimensions of the $\mathcal{O}_{\bar{6}i}$ and $\mathcal{O}_{6i}$ operators equal each other as a consequence of charge conjugation symmetry. Therefore it is enough to determine only one of them.
Again one can as well think of topologies that include the "seagull" $\psi\psi^\dagger\mathbf{A}^2$ operator and are not depicted here. But such diagrams either contain vanishing (not logarithmically divergent) scale less integrals from the tadpole graphs mentioned in section 5.3 or fail to match the power counting of the six-quark operators, which finally generate the effective $\frac{1}{m|\mathbf{k}|}$ - potential.
The latter is also true for graphs, where two gluons are connected to a potential interaction via a $\psi\psi^\dagger\chi\chi^\dagger\mathbf{A}^2$ as it occurs in the expansion in Eq. 2.29 at higher orders. Remember that even the lowest order $\psi\psi^\dagger\mathbf{A}$ vertex comes along with one power of v.
The configurations with respect to the type of the ultrasoft gluons (A^0, $\mathbf{A}$) and possible kinetic insertions ($\frac{\mathbf{p}\cdot\nabla}{m}$, $\frac{\nabla^2}{2m}$) on the internal heavy quark lines which yield the required v scaling are strongly related to the ones found for the one-loop diagrams in table 5.3. Actually the only difference is that we add an A^0 loop to the

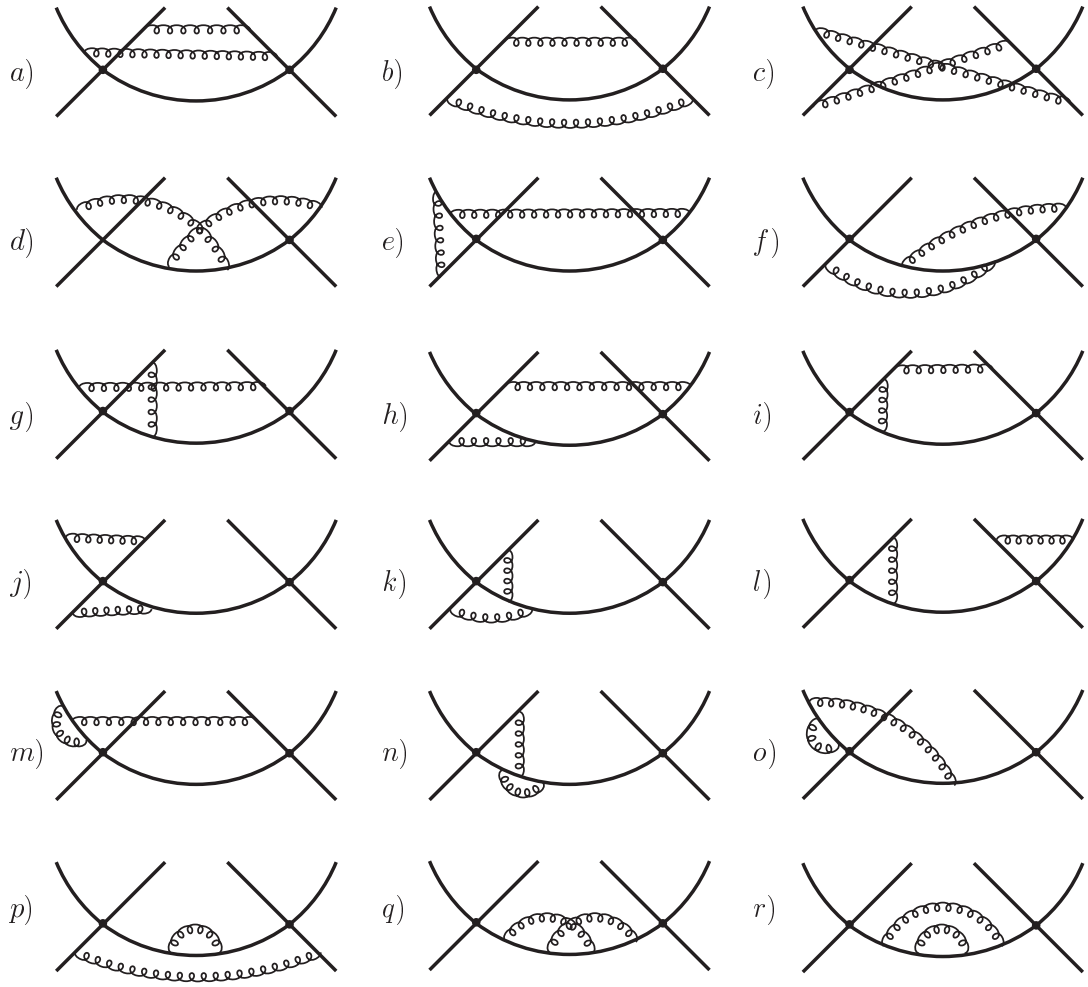

Figure 6.4: Some of the 465 Abelian ultrasoft two-loop topologies with six heavy quark (two quark, four antiquark) legs and exclusively single gluon interaction vertices on the heavy quark lines. They are relevant for the NLL renormalization of the six-quark operators $\mathcal{O}_{6i}$ in Feynman gauge.

one-loop diagrams in all possible ways. Of course this increases the number of internal quark lines and therefore the possibilities to position the kinetic operators $\frac{\mathbf{p}\cdot\nabla}{m}$ and $\frac{\nabla^2}{2m}$ in order to obtain the higher order terms of the multipole expansion, but the number and combinations of insertions and higher order Coulomb potentials remains unchanged as dictated by power counting.
Similar to the one-loop situation components like the $\psi\psi^\dagger\mathbf{A}\nabla$ interaction vertex or the $\mathcal{O}(v^4)$ kinetic insertion $\frac{\mathbf{p}^4}{8m^3}$ will not appear in the relevant diagrams, since in the former case the order in v is at least by one too high[2] and in the latter the

[2]Apart from this only one ∇ would give rise to antisymmetric integrands.

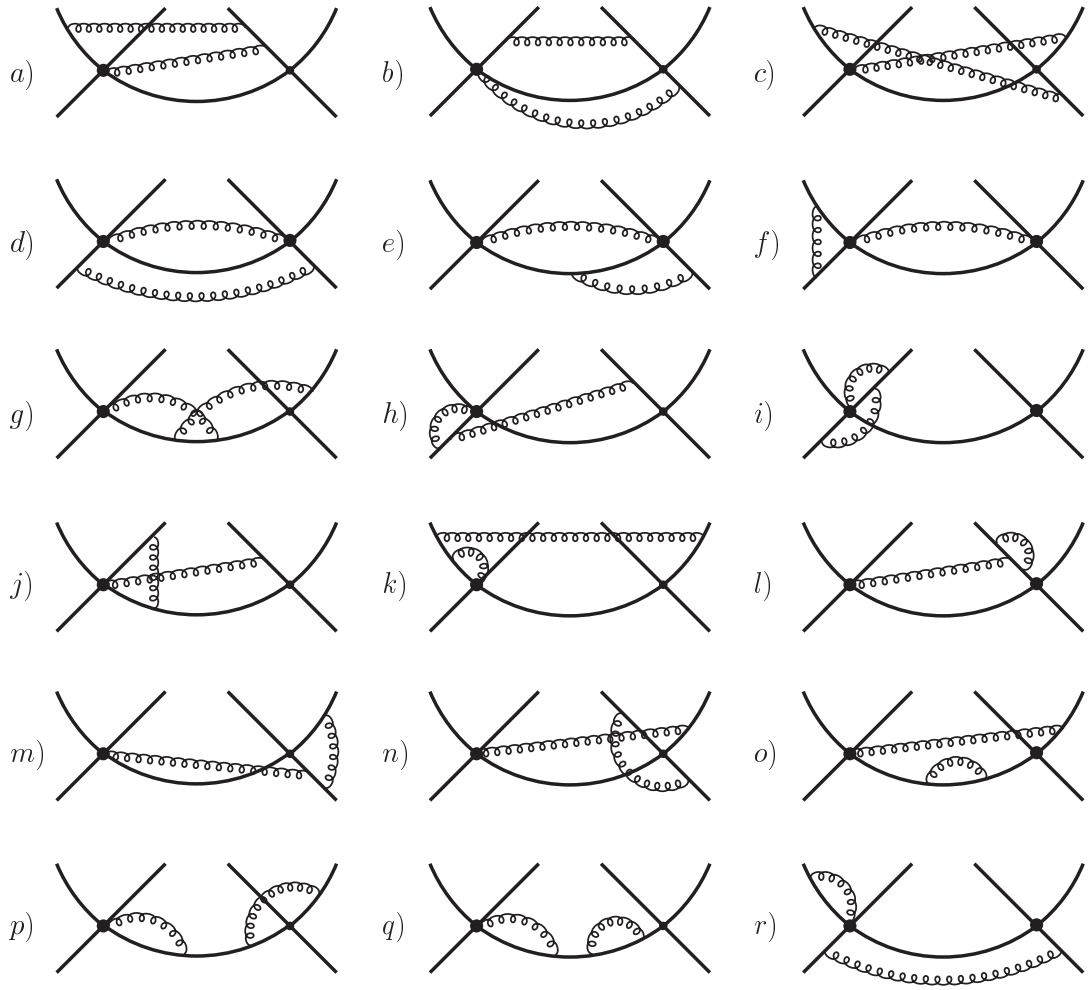

Figure 6.5: A selection of the 442 Abelian topologies with two ultrasoft gluon loops and six heavy quark (two quark, four antiquark) legs, which involve one or two $\psi\psi^\dagger\chi\chi^\dagger\mathbf{A}$ vertices apart from standard $\psi\psi^\dagger\mathbf{A}$ and $\psi\psi^\dagger A^0$ interactions. Diagrams with a topology of the type i) or r) are certainly proportional to the external off-shellness a, cf. Eq. (5.9), and will therefore not contribute in the on-shell renormalization procedure.

diagrams are UV finite as can be checked by counting heavy quark propagators. An analogous argument applies to the Feynman graphs with topologies as in Fig. 6.4 and one $\mathbf{A}$ and one A^0 loop at lowest order in the multipole expansion as well as to diagrams with two A^0 gluons and two $\frac{\mathbf{p}\cdot\nabla}{m}$ insertions, which are not canceled by the counterterms of the potential vertices anyway. That is why the corresponding contributions to $\delta\mathcal{V}_{ki}$ at NLL like at LL level vanish.
Therefore we are left with again five nonzero entries in table 6.6, which lists the contributing diagram classes and very much resembles table 5.3 as mentioned

already.

Class \ Topologies	Fig. 6.5	Fig. 6.4
gluons: $1\times A^0$, $1\times\mathbf{A}$ no ins.	I	0 (diagrams finite or canceled by subdivergences)
gluons: $2\times A^0$ $2\times$ 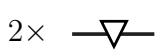	no contribution since $\psi\psi^\dagger\chi\chi^\dagger A^0$ vertex does not exist.	0 (diagrams finite or canceled by subdivergences)
gluons: $2\times A^0$, $1\times$ 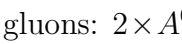		II
gluons: $2\times A^0$, $2\times$ 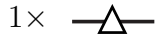		III
gluons: $2\times A^0$, $1\times$ 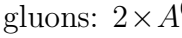 , $1\times$		IV
gluons: $2\times A^0$, $1\times$ 		V

Table 6.6: Abelian contributions (I-V) to the ultrasoft running of the $\mathcal{O}_{6i}$ operators at two-loop (NLL) level. For all vertices not specified explicitly the lowest order standard versions are understood as they have been already used in the one-loop diagrams, cf. table 5.3.

At two-loop level also the subtraction of subdivergences naturally becomes more involved compared to what we had to do in section 5.3. Now we have to distinguish between one- and two-loop subdivergences and the corresponding one-loop and tree-level counterdiagrams.
As for the $\frac{1}{m^2}$ - potentials the one-loop counterdiagrams are constructed by replacing one propagator, vertex or kinetic insertion in the original one-loop diagrams of table 5.3 by its one-loop counterterm in all possible ways[3]. In addition to the counterterms we already used in section 6.1 and 6.2 we have to include here the ones of the leading order $\psi\psi^\dagger\chi\chi^\dagger\mathbf{A}$, the $\psi\psi^\dagger\chi\chi^\dagger\nabla$ and the $\psi\psi^\dagger\chi\chi^\dagger\nabla^2$ operators. All of these operators have as required by reparametrization invariance the same Wilson coefficient $\mathcal{V}_c$ which is not affected by ultrasoft quantum

[3]The quark and gluon propagator counterterms are understood to be composed of the insertions in Eqs. (6.2) and (6.3) and the respective propagators to the left and right.

corrections ($(\delta\mathcal{V}_c)_{us} = 0$) as discussed in section 3.6. Nevertheless there are non-vanishing contributions to the corresponding countervertices from the quark and gluon wavefunction counterterms (δZ_ψ, δZ_A) as well as from δZ_g in analogy to Eqs. (6.4) and (5.10):

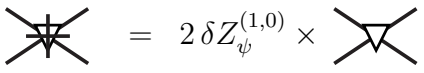

$$= \; 2\,\delta Z_\psi^{(1,0)} \times \quad , \tag{6.30}$$

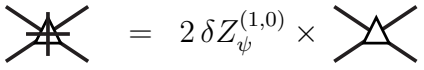

$$= \; 2\,\delta Z_\psi^{(1,0)} \times \quad , \tag{6.31}$$

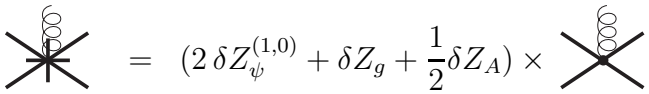

$$= \; (2\,\delta Z_\psi^{(1,0)} + \delta Z_g + \frac{1}{2}\delta Z_A) \times \quad . \tag{6.32}$$

Another type of one-loop counterdiagrams we have to take into account is obtained by dressing the $\mathcal{O}(\alpha_U\, v^2)$ counterterm of the six-quark operators $\mathcal{O}_{6i}$ determined in section 5.3 with a A^0 gluon loop that includes two quark propagators as shown in Fig. 6.6.

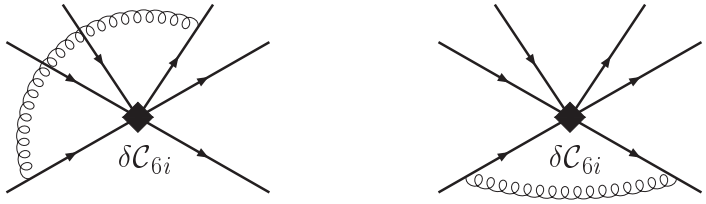

Figure 6.6: Examples for one-loop counterdiagrams with a $\mathcal{O}(\alpha_U\, v^2)$ six-quark countervertex $\propto \delta\mathcal{C}_{6i}$ and an ultrasoft A^0 gluon loop. Amongst others these diagrams e.g. subtract subdivergences in graphs that have topologies like Fig. 6.4 *b*), *c*), *p*) or Fig. 6.5 *d*).

Besides the one-loop counterdiagrams we also have to allow for tree-level counterdiagrams without gluons that contain either one $\mathcal{O}(\alpha_U^2\, v^2)$ or one $\mathcal{O}(\alpha_U\, v^2)$ and one $\mathcal{O}(\alpha_U\, v^0)$ counterterm. Examples are depicted in Fig. 6.7.

Having identified all diagrams contributing to the anomalous dimension of the Wilson coefficients $\mathcal{C}_{6i}$ we have to determine their divergent parts. For the special case of the Abelian diagrams considered here this process goes very much along the lines of the calculation of the Abelian diagrams in section 6.2.
The fact that we have now in addition to the artificial off-shellness a on the external legs an physical off-shellness $2A$ ($A = E - \frac{\mathbf{q}^2}{2m}$) on the internal heavy quark lines (cf. Eqs. (3.38) and (3.39)) does not make a fundamental difference in the procedure of solving the two-loop integrals. The integrand still consists of two gluon propagators, a number of heavy quark propagators and some powers of k_0

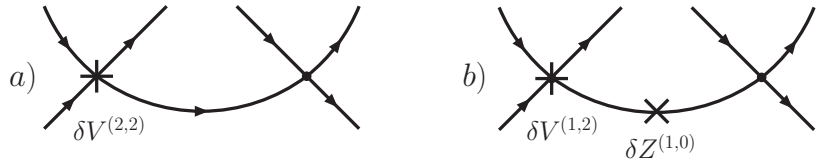

Figure 6.7: Non-vanishing tree-level six-leg counterdiagrams at $\mathcal{O}(\alpha_U^2\, v^2)$. Mirror graphs are understood. They are supposed to cancel (together with the appropriate one-loop counterdiagrams) e.g. subdivergences in diagrams with topologies of the form Fig. 6.4 j), k).

or l_0 in the numerator. By algebraic manipulations including partial fraction decomposition in analogy to Eq. (6.11) we can always reduce an arbitrary Abelian two-loop integral even with two different off-shellnesses to integrals where only one quark and one gluon propagator depends on the loop momentum k. This corresponds to line three in Eq. (6.11). The k integration can then be performed using the well known integral formula Eq. (B.7). After another partial fraction decomposition w.r.t. l_0 we arrive at a sum of generalized one-loop integrals that match either Eq. (B.11) or (B.12).
This procedure can be automatized and allows us to solve the relevant integrals completely analytically yielding expressions, that typically contain a number of Gamma and Hypergeometric functions depending on the dimension d like e.g. in Eq. (6.12). As already mentioned the expansion in $\epsilon = \frac{4-d}{2}$ can then be carried out using the `Mathematica` package `HypExp 1.1` [90].
So there is in principle no serious difficulty in the determination of the UV divergences in the Abelian two-loop integrals associated with the above diagrams, if formulae Eq. (B.11) and (B.12) are provided.

The color factors in the $1\otimes\bar{1}$, $T^A\otimes\bar{T}^A$ basis of the topologies in Figs. 6.4 and 6.5 are obtained by applying the same techniques and formulae, like e.g. the Fierz identities Eq. (C.21), as in the previous sections. Moreover in many cases the results of section 5.3 can be recycled to simplify substructures of the total color structures. To perform this task we developed another `Mathematica` routine that returns the color factors for all relevant two-loop topologies in terms of the fundamental constants C_A and C_F (see Appendix C) using a few functions related to $SU(N)$ algebra from the `FeynCalc 4.1.1.0` package [92].

The sum of contributions II-V in table 6.6 represents the next-to-leading order term of the multipole expansion of the most basic diagrams of the Fig. 6.4 type with only A^0 gluons. In contrast the contribution I is a leading order term for a completely different type of topologies. It therefore makes sense to distinguish

between the following partial results after subtraction of subdivergences.

$$\mathrm{I} \;=\; \left(\frac{C_A(C_A-6C_F)}{8\,\epsilon^2}-\frac{C_A^2}{4\,\epsilon}\right)\frac{i\mathcal{V}_c^2\alpha_U^2}{m\,\pi^2}$$
$$\cdot\left[C_F(C_A-2C_F)(f_0+f_1+2f_2)1\otimes\bar{1}\;+\;(C_A-4C_F)(f_1+f_2)\,T^A\otimes\bar{T}^A\right], \qquad (6.33)$$

$$\mathrm{II}+\mathrm{III}+\mathrm{IV}+\mathrm{V} \;=\; \left(-\frac{C_A(C_A-6C_F)}{24\,\epsilon^2}+\frac{C_A^2}{8\,\epsilon}\right)\frac{i\mathcal{V}_c^2\alpha_U^2}{m\,\pi^2}$$
$$\cdot\left[C_F(C_A-2C_F)(f_0+f_1+2f_2)1\otimes\bar{1}\;+\;(C_A-4C_F)(f_1+f_2)\,T^A\otimes\bar{T}^A\right]. \qquad (6.34)$$

These divergences are as the ones in table 6.5 understood to be canceled either by the counterterms of the $\mathcal{O}_{6i}/\mathcal{O}_{\bar{6}i}$ (according to Eq. (6.35)) or the counterterms of the $\mathcal{O}_{ki}$ operators, since we know from subsection 3.5.2 and Eq. (5.20) that $\delta\mathcal{V}_{ki}=\frac{1}{2}(\delta\mathcal{C}_{6i}+\delta\mathcal{C}_{\bar{6}i})$ and $\delta\mathcal{C}_{6i}=\delta\mathcal{C}_{\bar{6}i}$.
Interestingly the Abelian results in Eqs. (6.33) and (6.34) are both proportional to the one-loop soft momentum structure in Eq. (5.18). Whereas for the $\frac{1}{\epsilon^2}$ term it is required by consistency, see section 6.4, there is a priori no such reason for the $\frac{1}{\epsilon}$ term to have this form. However having a closer look at the topologies in Figs. 6.4 and 6.5 we observe that every two-loop diagram based on them always has a subdivergence and a $\frac{1}{\epsilon^2}$ term. Hence none of the diagrams yields a pure two-loop $\frac{1}{\epsilon}$ divergence and the soft structure of the $\frac{1}{\epsilon^2}$ terms is inherited by the associated $\frac{1}{\epsilon}$ terms as one can conclude from the form of the involved integrals.
The Non-Abelian diagrams in section 6.2 and in the next section obviously do not all have one-loop subdivergences. Therefore their total structure is not protected by the argument sketched above as we already observed in table 6.3.
We also performed the cross check inspired by the field redefinition argument of section 3.6 also for the Abelian diagrams with two A^0 gluons, two Coulomb potentials, no insertions and topologies as in Fig. 6.4. The overall divergence of these diagrams vanishes indeed.

Finally we derive the expression for the $\mathcal{O}(\alpha_U^2)$ countervertex of the $\mathcal{O}_{6i}$ operators including $\delta\mathcal{C}_{6i}$ at $\mathcal{O}(\alpha_U)$ and the $\mathcal{O}(\alpha_U)$ wavefunction counterterms from the renormalized vNRQCD Lagrangian:

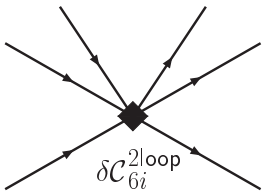

$$= -\frac{i\mathcal{V}_c^2}{m}\Big[\big(\delta\mathcal{C}_{61}^{(1),(2)}+\frac{6}{2}\delta Z_\psi^{(1,0)}\delta\mathcal{C}_{61}^{(1)(1)}\big)\,(f_0+f_1+2f_2)\,1\otimes\bar{1}$$
$$+\big(\delta\mathcal{C}_{62}^{(T),(2)}+\frac{6}{2}\,\delta Z_\psi^{(1,0)}\,\delta\mathcal{C}_{62}^{(T)(1)}\big)\,(f_1+f_2)\,T^A\otimes\bar{T}^A\Big]+\ldots\,. \qquad (6.35)$$

The second upper index of the $\delta\mathcal{C}_{6i}$ indicates the order in α_U. For $i = 1, 2$ the $\mathcal{O}_{6i}$ operators are defined here in accordance with Eq. (3.36). An analogous equation holds for the counterterms of the $\mathcal{O}_{\bar{6}i}$ operators.
Actually there are terms $\propto \frac{6}{2}\big((\delta Z_\psi^{(1,0)})^2 + \delta Z_\psi^{(2,0)}\big)\,\mathcal{C}_{6i}$ missing in Eq. 6.35. A corresponding term $\propto \frac{6}{2}\delta Z_\psi^{(1,0)}\mathcal{C}_{6i}$ already existed at one-loop level, but was tacitly neglected as well. The reason is that these terms cancel exactly with the diagrams, where the six-quark operator vertex $\propto \mathcal{C}_{6i}$ itself is dressed with one or two A^0 gluons similar to Fig. 6.6, according to the statement in section 3.6.
One might furthermore be worried about the terms $\propto \frac{6}{2}\delta Z_\psi^{(1,0)}\delta\mathcal{C}_{61}^{(1,T)(1)}$, since the factor $\frac{6}{2}$ differs from the factor $\frac{4}{2}$ of the corresponding terms in the sum operator approach. But in the same manner as the omitted terms mentioned above they cancel with the $\frac{1}{\epsilon^2}$ contributions from the diagrams depicted in Fig. 6.6 in the six-quark operator approach. In the sum operator approach there is a cancellation with corresponding four-leg diagrams.
Taking moreover into account that for diagrams with closed potential loop there are two internal heavy quark lines, which can be dressed with a one-loop self-energy, one can show that our observation that $\delta\mathcal{V}_{ki} = \delta\mathcal{C}_{6i} = \delta\mathcal{C}_{\bar{6}i}$ is explicitely confirmed at (ultrasoft) two-loop level.

6.3.3 Non-Abelian Diagrams

At first sight the calculation of the two-loop diagrams with non-Abelian topology, see Fig. 6.8 and 6.9, seems to be less involved than the one described in the previous chapter. This is because the number of Feynman graphs to be considered is much smaller and there are less subdivergences to be subtracted by appropriate counterdiagrams. Large parts of the `Mathematica` codes for the automatic generation of the graphs based on the 141 different non-Abelian two-loop topologies have been adapted from the routines we have developed for the Abelian case.
The more complicated non-Abelian integrals with two off-shellnesses (one artificial, one physical) can still be handled by partial fraction decomposition and integration by parts (IBP) similar to how we proceeded in section 6.2. We will come back to the details below.
Although everything seems to work out straightforwardly we find the results to be inconsistent as will be discussed in the following. After working hard to find possible errors in our codes and the calculation of the loop integrals we are pretty sure that the source of the problem is not an ordinary calculational mistake, although we can of course not one hundred percent exclude this, but of a systematic kind. Unfortunately we were not able to solve it up to now.
Some rough ideas of conceivable methods of resolution are discussed at the end of this section and have to be investigated further. However this was not possible within the scope of this PhD thesis due to a lack of time, but subsequent work

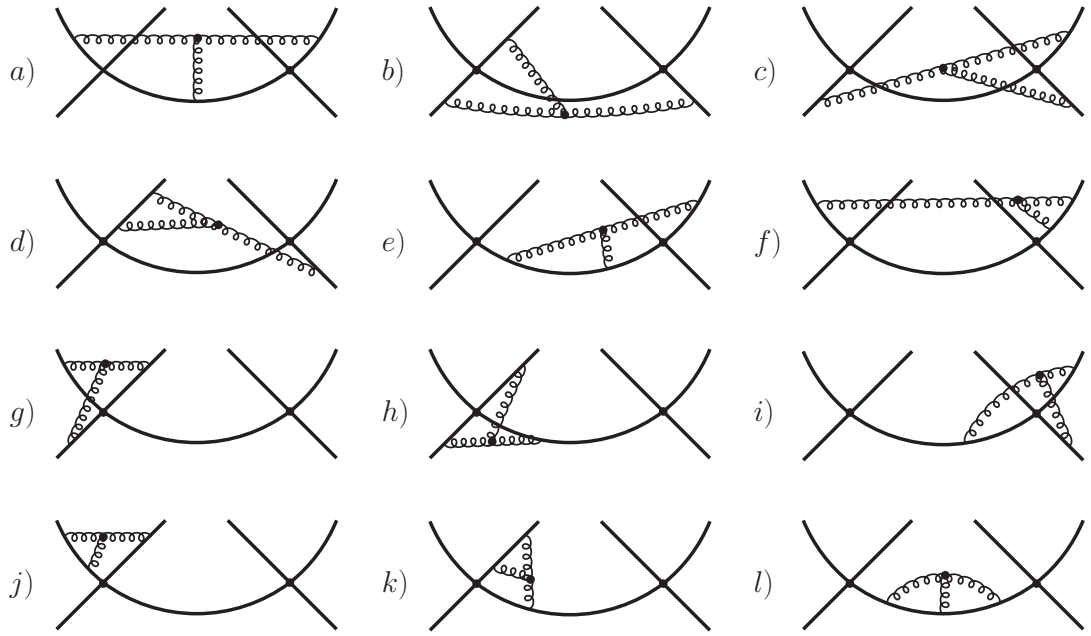

Figure 6.8: Typical examples of non-Abelian two-loop six-leg topologies with two ultrasoft gluons coupling to the heavy quark lines through $\psi^2\mathbf{A}$ and $\psi^2 A^0$ vertices. In total there are 78 topologies of this kind involved in the renormalization procedure of the six-quark operators $\mathcal{O}_{6i}$ at NLL level in Feynman gauge.

will hopefully address these issues.

Let us now concentrate on the facts. Similar as for the $\frac{1}{m^2}$ - potentials there are two classes of non-Abelian diagrams contributing to the running of $V_{k,\text{eff}}$ corresponding to classes 8 and 9 in table 6.2. In addition we now have a third class, which involves the next-to-leading order vertex of the multipole expanded Coulomb potential from Eq. (2.29). For the $\frac{1}{m^2}$ - potential topologies of Fig. 6.3 this class would produce terms proportional to the artificial off-shellness a of the external legs, but in case of the six-leg topologies in Fig. 6.8 and 6.9 there are non-vanishing contributions because of the additional internal heavy quark line and its physical off-shellness. Table 6.7 specifies the different types of contributions depending on class and topology of the non-Abelian diagrams in the way known from the previous sections.
To perform the corresponding non-Abelian two-loop integrals we need in addition to Eq. (6.17)-(6.19) an appropriate IBP recursion formula for another generic integral, which is defined as

$$I_3(\alpha,\beta,\gamma,\delta,\eta,\varphi) \;=\; \int\frac{d^dk}{(2\pi)^d}\int\frac{d^dl}{(2\pi)^d} \cdot\Big[(-k_0-a)^\alpha(-k_0-l_0+a)^\beta(-l_0-a)^\gamma(-k^2)^\delta(-l^2)^\eta(-(k+l)^2)^\varphi\Big]^{-1}. \quad (6.36)$$

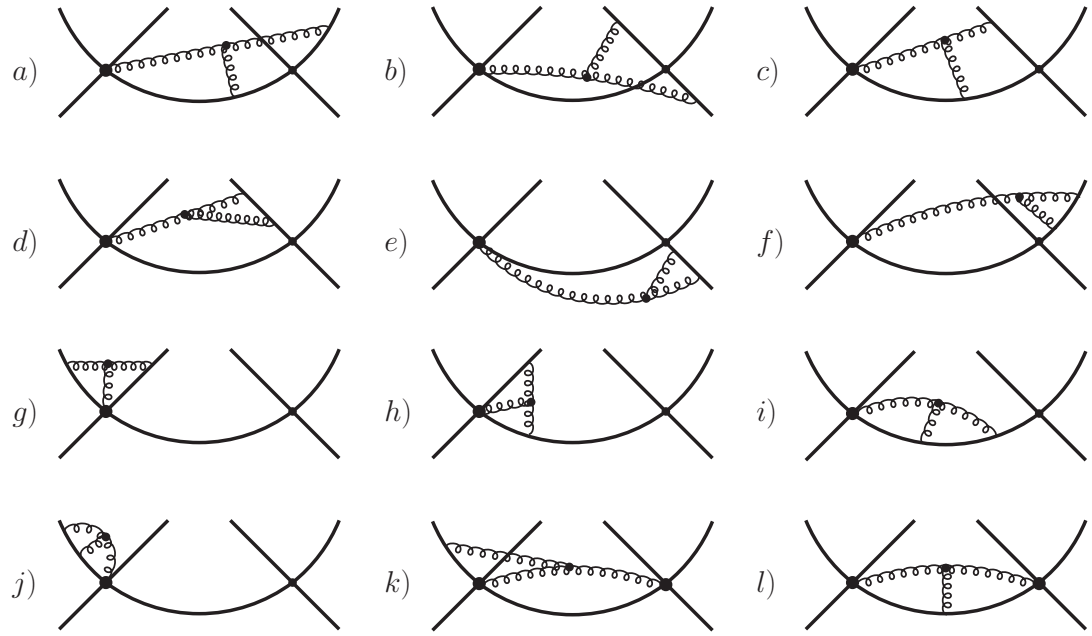

Figure 6.9: Some graphs representing the 63 different non-Abelian two-loop topologies, that include at least one $\psi^2\chi^2\mathbf{A}$ vertex and contribute to the ultrasoft NLL running of the $\mathcal{O}_{6i}$ operators.

We find the analogous relation as for I_2:

$$\begin{aligned} &I_3(\alpha,\beta,\gamma,\delta,\eta,\varphi) \;= \\ &= \frac{-\alpha\,\boldsymbol{\alpha^+\gamma^-} + \beta\,\boldsymbol{\beta^+}(\boldsymbol{\alpha^-}-\boldsymbol{\gamma^-}) + \delta\,\boldsymbol{\delta^+}(\boldsymbol{\eta^-}-\boldsymbol{\varphi^-}) + 2\varphi\,\boldsymbol{\varphi^+}(\boldsymbol{\delta^-}-\boldsymbol{\eta^-})}{d-\alpha-3\delta}\; I_3\;, \end{aligned} \tag{6.37}$$

where the operators $\boldsymbol{\alpha^\pm}$ etc. act on I_3 in accordance with Eq. (6.20). By shifting integration variables one also obtains useful identities like

$$I_3(\alpha,\beta,0,1,1,1) \;=\; (-1)^\beta I_3(0,\beta,\alpha,1,1,1)\;. \tag{6.38}$$

They help to reduce the non-Abelian two-loop integrals to a minimal number of the known one-loop integrals listed in the Appendix B.
Using the above relations for I_3 and the ones for I_1 and I_2 we were able to compute all integrals, that depend on only one off-shellness and are needed in the calculation of the contributions in table 6.7.
Furthermore we made use of the observation that the leading UV divergence of a dimensionless two-loop integral (in $d = 4$) must not depend on the involved (real) off-shellnesses[4]. Similarly a change of the (real) value of one off-shellness

[4]It may depend on the signs of the respective $i\epsilon$'s in the quark propagators, which are not explicitly displayed here, but by convention absorbed into the associated off-shellness with the same sign (see beginning of section 5.1).

Class \ Topologies	Fig. 6.8	Fig. 6.9
gluons: $1\times A^0$, $2\times \mathbf{A}$ no ins.	I	IV
gluons: $2\times A^0$, $1\times \mathbf{A}$ $1\times$ 	II	V
gluons: $2\times A^0$, $1\times \mathbf{A}$ $1\times$ 	III	VI

Table 6.7: Contributions (I-VI) of non-Abelian diagrams to the ultrasoft running of the $\mathcal{O}_{6i}$ operators at two-loop (NLL) level. For all vertices not specified explicitly again the lowest order standard versions are understood. Of course graphs with two vertices of a gluon directly coupling to a potential as e.g. in Fig. 6.9 k) and l) are not part of contributions V and VI, since a $\psi\psi^\dagger\chi\chi^\dagger A^0$ vertex does not exist in vNRQCD. For the sake of clarity we did however not make another distinction within the topologies here.

in an UV finite (non-zero) integral will not render it UV divergent. Therefore we have e.g.

$$\int\frac{d^dk}{(2\pi)^d}\int\frac{d^dl}{(2\pi)^d}\,\frac{1}{(k_0+2A)(k_0+l_0-a)\,k^2l^2(k+l)^2} \;=$$

$$=\;\int\!\!\int\,\frac{1}{(k_0+a)(k_0+l_0-a)\,k^2l^2(k+l)^2}+\mathcal{O}(\epsilon^0)\;=\;-\frac{1}{192\pi^2\epsilon}+\mathcal{O}(\epsilon^0) \qquad (6.39)$$

and

$$\int\frac{d^dk}{(2\pi)^d}\int\frac{d^dl}{(2\pi)^d}\,\frac{1}{(k_0+2A)(l_0-a)(k_0+l_0+a)\,k^2l^2(k+l)^2} \;=$$

$$=\;\int\!\!\int\,\frac{1}{(k_0+a)(l_0-a)(k_0+l_0+a)\,k^2l^2(k+l)^2}+\mathcal{O}(\epsilon^0)\;=\;\mathcal{O}(\epsilon^0)\,. \qquad (6.40)$$

A number of relations of this kind turns out to be enough to determine also the required two-loop integrals, that involve both off-shellnesses.
The determination of the color factors uses the methods described in the previous sections and follows the same lines.

All one-loop subdivergences cancel in the sum of the contributions I-VI as the non-Abelian quark-gluon vertex renormalization diagrams shown in Fig. 6.10 and

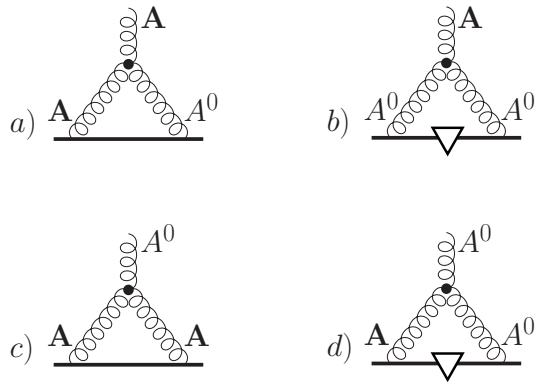

Figure 6.10: Non-Abelian quark-gluon vertex renormalization graphs. Mirror diagrams are understood.

the non-Abelian contributions to the $\psi\psi^\dagger\chi\chi^\dagger\mathbf{A}$ counterterm from the graphs in Fig. 6.11 do: Fig. 6.10 $a)+b)=0$, Fig. 6.10 $c)+d)=0$ and Fig. 6.11 $a)+b)=0$.

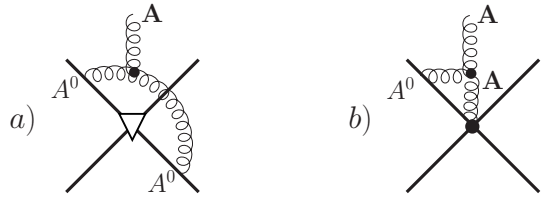

Figure 6.11: Non-Abelian corrections to the $\psi\psi^\dagger\chi\chi^\dagger\mathbf{A}$ vertex. Diagrams with all possible positions of the vertices on the heavy quark lines are understood.

The diagrams in Figs. 6.10 and 6.11 actually only have to be evaluated individually if one wants to get rid of the one-loop subdivergences in intermediate results as the ones given below. Their calculation is rather straightforward. The only thing to take care of are IR singularities from the two gluon propagators, which can be regulated in this (one loop) case easily e.g. by a gluon mass.
To subtract the two-loop subdivergences e.g. in diagrams with the topology in Fig. 6.8 g)-k) or Fig. 6.9 g), h) we have to add the tree-level diagram in Fig. 6.7 a) and only use the respective non-Abelian contributions (classes 8 and 9 in table 6.2) for the $\frac{1}{m^2}$ - potential countervertex. Diagrams with a two-loop self-energy subdivergence like in Fig. 6.8 l) vanish for the same reason as the corresponding counterterms in table 6.1.

Note that we have always chosen the same convention for the off-shellnesses so far. We have assigned the same artificial off-shellness a to every external leg

whereas the physical off-shellness on the internal quark line is $2A = 2(E - \frac{\mathbf{q}^2}{2m})$.[5] In principle however any configuration of artificial off-shellnesses should be allowed and it should not affect the result for the UV divergent part of a diagram, which contributes to the (observable) running of a potential, after subtraction of subdivergences.
So we could just as well choose different off-shellnesses a, b, etc. for each of the external legs in the above six-leg graphs. This is because the artificial off-shellnesses are only introduced to regulate potential IR singularities, i.e. to discriminate these from the relevant UV divergences, and are set to zero in the final result for the counterterms anyway.
However we will present an example in the following, where the divergence of a set of non-Abelian two-loop diagrams, that contributed already to the anomalous dimension of the $\frac{1}{m^2}$ - potentials and appear as subdiagrams in the current calculation, depends on the way of how the different artificial off-shell parameters a, b, etc. approach zero. There are different results if we take the on-shell limit for one leg after the other or first set all off-shellnesses equal and then to zero.
We are not sure about the interpretation of this phenomenon. It might very well be that it is connected to the above mentioned inconsistencies we encountered in the renormalization of $V_{k,\mathrm{eff}}$, but up to now we have not been able to clearly verify this statement.

Before continuing the discussion about possible sources of problems let us first take a look at the results for the contributions I-VI according to table 6.7 using the "standard" configuration for the off-shellnesses, where the same a is assigned to all external legs. They can be read off table 6.8.
The first observations are that the $\frac{1}{\epsilon^2}$ terms in III and (IV+V+VI) cancel in agreement with the cancellation of one-loop subdivergences mentioned above and that the results obviously do not take the simple Abelian form of Eqs. (6.33) and (6.34). The latter is actually not surprising, since there are no consistency constraints from any corresponding one-loop contributions to the RGE's as in the Abelian case (cf. section 6.4). We have found a similar behaviour already for the non-Abelian results related to the $\frac{1}{m^2}$ - potentials in section 6.2.
The most remarkable issue however is the soft momentum structure of the expression for (I+II) as well as of I and II separately. From a power counting w.r.t the ultrasoft scales only, we understand that one power of the physical off-shellness $A = \frac{\mathbf{p}^2+\mathbf{p}'^2-2\mathbf{q}^2}{4m}$, which is the only ultrasoft scale left after the external fields are set on-shell, must be in the denominator.
The propagator-like $\frac{1}{A}$ structure implies a non-local interaction w.r.t. to the soft three-momentum $\mathbf{q}$ carried from one potential to the other, which is however a

[5] Actually it must be $2A + a$ because of energy conservation, but since a is set to zero in the final results anyway, one can safely neglect it here.

Contribution	Result
I+II	$-\frac{i\,C_A \mathcal{V}_c^2 \alpha_U^2}{768\,A\,m^2\,\epsilon\,(\mathbf{p}'-\mathbf{q})^2(\mathbf{q}-\mathbf{p})^2}\cdot$ $\Big[C_F(C_A-2C_F)1\otimes\bar{1}\Big\{(C_A-2C_F)[58\mathbf{q}^2+30(\mathbf{p}+\mathbf{p}')\mathbf{q}+5(\mathbf{p}^2+\mathbf{p}'^2)]-24C_A\mathbf{q}^2\Big\}+$ $+T^A\otimes\bar{T}^A\Big\{(C_A-2C_F)^2\,[82\mathbf{q}^2+18(\mathbf{p}+\mathbf{p}')\mathbf{q}+5(\mathbf{p}^2+\mathbf{p}'^2)]+$ $+12C_A(C_A-2C_F)\,[-6\mathbf{q}^2+(\mathbf{p}+\mathbf{p}')\mathbf{q}]+24C_A^2\mathbf{q}^2\Big\}\Big]$
III	$\frac{i\,C_A\,\mathcal{V}_c^2\alpha_U^2}{16\,m\,\pi^2}\Big[-\frac{1}{\epsilon^2}\,C_A\,\Big[(C_A-2C_F)C_F(f_0+f_1)1\otimes\bar{1}+(C_A-4C_F)f_1T^A\otimes\bar{T}^A\Big]+$ $+\frac{1}{9\epsilon}\Big[C_F(C_A-2C_F)1\otimes\bar{1}\Big\{f_0[6C_A+(5C_A-18C_F)\pi^2]-2f_1[-3C_A+(2C_A-9C_F)\pi^2]\Big\}+$ $+T^A\otimes\bar{T}^A\Big\{18C_F(2C_F-C_A)\pi^2f_0+f_1[6C_A(C_A-4C_F)-4(C_A^2-4C_FC_A+9C_F^2)\pi^2]\Big\}\Big]\Big]$
IV+V+VI	$\frac{i\,C_A\,\mathcal{V}_c^2\alpha_U^2}{16\,m\,\pi^2}\Big[\frac{1}{\epsilon^2}\,C_A\,\Big[(C_A-2C_F)C_F(f_0+f_1)1\otimes\bar{1}+(C_A-4C_F)f_1T^A\otimes\bar{T}^A\Big]+$ $+\frac{1}{9\epsilon}\Big[C_F(C_A-2C_F)1\otimes\bar{1}\Big\{-5f_0[6C_A+(5C_A-18C_F)\pi^2]+10f_1[-3C_A+(2C_A-9C_F)\pi^2]$ $-4C_Af_2[12+\pi^2]\Big\}+$ $+T^A\otimes\bar{T}^A\Big\{90(C_A-2C_F)C_F\pi^2f_0+f_1[-30C_A(C_A-4C_F)+20(C_A^2-4C_FC_A+9C_F^2)\pi^2]+$ $+8C_Af_2[-3C_A+12C_F+(2C_A+C_F)\pi^2]\Big\}\Big]\Big]$

Table 6.8: Our results for the contributions defined in table 6.7 derived with the same off-shellness a assigned to all external legs and finally set to zero.

common feature of non-relativistic EFT operators and nothing to worry about[6]. Normally we expect those terms to be cancelled when subtracting the subdivergences associated with the renormalization of the $\frac{1}{m^2}$ - potentials, as e.g. observed for the Abelian diagrams of the previous subsection. In the current calculation this seems obviously not to be the case.
Therefore it is impossible to fully express the results for (I+II) in terms of a linear combination of the f_i functions defined in Eq. 5.15, as it was done for all other contributions to the renormalization of the $\mathcal{O}_{6i}$ ($\mathcal{O}_{ki}$) operators so far.

[6] A possible q_0 dependence would be problematic, but has already been eliminated by setting the external legs on-shell (apart from artificial off-shell parameters).

Moreover, a soft IR singularity is generated from the $\frac{1}{A}$ momentum structure when the heavy quark tadpole is closed and (or) the soft three-momentum ($\mathbf{q}$) integration is performed, see e.g. the Appendix of Ref. [65][7]. We must not subtract here any zero-bins related to the potential loop, which would convert this IR to an UV divergence by the pull-up mechanism described in section 3.7, because corresponding loops including ultrasoft heavy quarks are not part of the effective theory. Thus we are left with terms which are ultrasoft UV divergent and soft IR divergent at the same time.
Provided that they really exist, the physical meaning of such terms, or how to get rid of them in the prediction of physical quantities is not at all clear to us. That is why we tend to believe that the results shown in table 6.8, at least the one for (I+II), are not correct or not complete.

After an intensive search for calculational mistakes in our codes without success, we decided to carry out a cross check using the equivalence of the six-quark and sum operator approach, which has been pointed out in subsection 3.5.2.
Following this argument exactly the same results as in table 6.8 should be obtained, when setting the off-shellnesses of the two inner external lines, that close the potential loop when connected, to zero right from the start. I.e. already before the ultrasoft two-loop integrals have been evaluated.
The remaining four legs of the non-Abelian six-leg diagrams still carry an off-shellness a, that is set to zero after the evaluation of the integrals and the addition of the relevant counterdiagrams.
Intermediate ultrasoft IR singularities caused by loops involving the on-shell legs are supposed to cancel in the final results, because the corresponding three-loop diagrams with closed potential loop are expected to be free of ultrasoft IR divergences in any case, provided their four external legs are off-shell.
To perform the calculation with two on-shell legs we also need to compute non-Abelian two-loop integrals of the type in Eqs. (6.39) and (6.40), where one or two off-shellnesses in the integrand are replaced by zero[8]. Some of them can be derived from the integrals we know already by performing a partial fraction decomposition w.r.t. the off-shellnesses (a, A), e.g.

$$\begin{aligned}\int\frac{d^dk}{(2\pi)^d}\int\frac{d^dl}{(2\pi)^d}\,\frac{1}{l_0(k_0+a)\,k^2l^2(k+l)^2} &= -\frac{1}{2}\iint\frac{1}{(l_0-a)(k_0+a)\,k^2l^2(k+l)^2}\\ &= \frac{1}{768\,\pi^2\epsilon}+\mathcal{O}(\epsilon^0)\,, \qquad (6.41)\end{aligned}$$

where we used the IBP formula Eq. (6.18) to solve the integral with only off-shell propagators in the last step.

[7]The integrals in [65] imply the on-shell condition $\mathbf{p}^2=\mathbf{p}'^2$.

[8]The propagators in the integrands naturally have integer powers. Therefore the sign of the $i\epsilon$ of a propagator with zero off-shellness will not affect the result of the integral as can be checked easily by using the residue theorem to perform the first integration over k_0 (l_0). We can even drop the $i\epsilon$ in this case completely.

Among a few other non-Abelian integrals we used in this thesis the integral in Eq. (6.41) also can be found in Ref. [93]. Similar integrals with higher powers of the off-shell propagators are obtained by deriving w.r.t. to the off-shellness(es). The IBP recursion formula Eq. (6.19) still holds, when the off-shellness of the propagator associated with the parameter β is dropped. Together with algebraic identities similar to Eq. (6.38) and relations analogous to Eq. (6.39) and (6.40), we were thus able to solve almost all relevant integrals, or at least to identify their divergent parts, needed for the calculation of the diagrams with two on-shell legs. Fortunately we were able to determine the few remainig two-loop integrals indirectly by demanding left-right symmetry of the six-leg diagrams as it was stated in section 5.3.
The results of the calculation, where the artificial off-shellness of the two innermost legs of the graphs in Figs. 6.8 and 6.9 is initially set to zero are presented in table 6.9.

Contribution	Result
I+II	$\frac{i\,\mathbf{q}^2\,C_A\left[1\otimes\bar{1}(8C_F^3-6C_AC_F^2+C_A^2C_F)+T^A\otimes\bar{T}^A(C_A^2-6C_FC_A+12C_F^2)\right]\mathcal{V}_c^2\alpha_U^2}{96\,A\,m^2\epsilon\,(\mathbf{p}'-\mathbf{q})^2(\mathbf{q}-\mathbf{p})^2}$
III	$\frac{i\,C_A\,\mathcal{V}_c^2\alpha_U^2}{16\,m\,\pi^2}\Big[-\frac{1}{\epsilon^2}\,C_A\left[(C_A-2C_F)C_F(f_0+f_1)1\otimes\bar{1}+(C_A-4C_F)f_1T^A\otimes\bar{T}^A\right]+$ $+\frac{1}{9\epsilon}\Big[C_F(C_A-2C_F)1\otimes\bar{1}\Big\{f_0[6C_A+(2C_A-12C_F)\pi^2]-2f_1[-3C_A+(2C_A-6C_F)\pi^2]\Big\}+$ $+T^A\otimes\bar{T}^A\Big\{12C_F(2C_F-C_A)\pi^2f_0+f_1[6C_A(C_A-4C_F)-4(C_A^2-4C_FC_A+6C_F^2)\pi^2]\Big\}\Big]\Big]$
IV+V+VI	$\frac{i\,C_A\,\mathcal{V}_c^2\alpha_U^2}{16\,m\,\pi^2}\Big[\frac{1}{\epsilon^2}\,C_A\left[(C_A-2C_F)C_F(f_0+f_1)1\otimes\bar{1}+(C_A-4C_F)f_1T^A\otimes\bar{T}^A\right]+$ $+\frac{1}{9\epsilon}\Big[C_F(C_A-2C_F)1\otimes\bar{1}\Big\{-5f_0[6C_A+(2C_A-12C_F)\pi^2]+10f_1[-3C_A+(2C_A-6C_F)\pi^2]$ $-4C_Af_2[12-2\pi^2]\Big\}+$ $+T^A\otimes\bar{T}^A\Big\{60(C_A-2C_F)C_F\pi^2f_0+f_1[-30C_A(C_A-4C_F)+20(C_A^2-4C_FC_A+6C_F^2)\pi^2]+$ $+8C_Af_2[-3C_A+12C_F+(2C_A-2C_F)\pi^2]\Big\}\Big]\Big]$

Table 6.9: Results for the contributions defined in table 6.7 obtained by evaluating the corresponding six-leg diagrams with the off-shellness a assigned to the four outer legs and two on-shell inner legs. The inner legs correspond to a cut internal heavy quark line of a (three-loop) diagram with closed potential loop. Remarkably (only) the $\frac{\pi^0}{\epsilon}$-terms change in comparison to table 6.8.

If both were correct we would expect the results of table 6.8 and table 6.9 to agree. Obviously they do not, so at least one of them reflects a wrong or incomplete set of UV divergences of non-Abelian origin, which are to be absorbed by the counterterms of the six-quark (sum) operators $\mathcal{O}_{6i}$ ($\mathcal{O}_{ki}$).
The fact that both results for (I+II) contain this peculiar soft IR singularity mentioned above could as well mean, that none of them is correct. However the soft momentum structure of (I+II) in table 6.9 is much simpler than in table 6.8. Indeed we were able to trace back the origin of the "bad" $\frac{1}{A}$ term in this case to a single three-loop graph with closed potential loop, shown in Fig. 6.12, and the six-leg diagrams related to it by the residue theorem respectively. In table 6.8 also other diagrams contribute to that term.

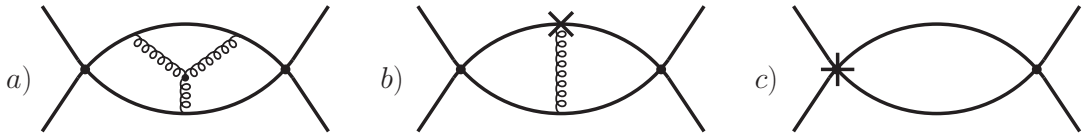

Figure 6.12: *a*) Three-loop topology with closed potential loop, that gives rise to the non-vanishing contribution (I+II) in table 6.9 after the associated one- and two-loop counterdiagrams illustrated in *b*) and *c*) have been added. Mirror graphs are understood. In the six-quark operator approach the potential loop is cut in all possible ways to generate the respective six-leg diagrams (see subsection 3.5.2).

For Abelian diagrams of the corresponding type (I and II in table 6.6) a set of diagrams analogous to Fig. 6.12 or the full set of the related six-leg diagrams the sum always gives a finite result. I.e. the three-loop UV divergences are completely cancelled by the associated counterdiagrams.

The reason why this cancellation does not occur among the non-Abelian type I and II diagrams of Fig. 6.12 is very likely connected to an issue in the context of the renormalization of the $\frac{1}{m^2}$ - potentials, that we discovered in the course of further investigating the problem.
We observed that the UV divergence of non-Abelian origin, which must be absorbed by the counterterms of V_2 and V_r, depends on the configuration of artificial off-shellnesses we use to regulate IR singularities. It rather makes a difference for the final results whether we send different off-shellness parameters to zero one after the other or set them equal and take their zero limit at the same time as

we did it in Ref. [33]. What we found concretely is e.g.

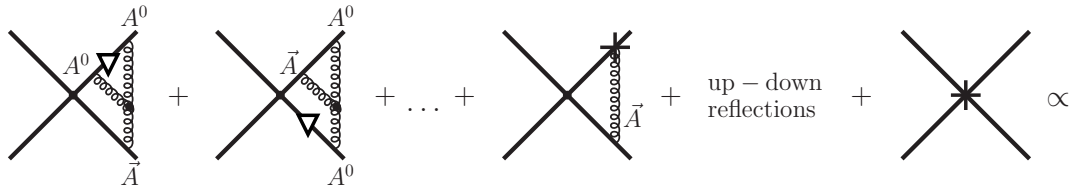

$$\propto \frac{(a-b)^2}{(a+b)^2}\frac{1}{\epsilon} \rightarrow \begin{cases} 0 & \text{for } b \rightarrow a \\ \frac{1}{\epsilon} & \text{for } b \rightarrow 0 \end{cases}, \tag{6.42}$$

where a and b are the off-shellness parameters of the two external legs involved in the loops. The crossed gluon interaction vertex denotes an insertion of a counterterm appropriate to remove the one-loop subdivergences. The crossed potential is the two-loop counterdiagram obtained by performing the calculation with equal off-shellnesses. For diagrams, where the loops also include the two legs on the left, the corresponding sum vanishes.

Obviously this behaviour causes problems, since as long as we do not find a clear reason, why one of the configurations is not allowed, we obtain ambiguous results for the running of the $\frac{1}{m^2}$ - potentials. Such a reason might perhaps be some symmetry, that is broken by the applied IR regularization and not properly restored in the limit of vanishing off-shellnesses. We are not aware of any at the moment, though.
Another scenario could be that the method of IR regularization by introducing artificial off-shellnesses generally fails for non-Abelian two-loop graphs of the above type, because of some subtle mechanisms we have not understood up to now. A way to check this would certainly be to recalculate the diagrams using a completely different IR regulator like e.g. a finite gluon mass. However the corresponding two-loop computations become way to complicated to perform them in practice.
After all there is of course the possibility, that we are missing contributions of diagrams we have not considered yet despite a careful analysis w.r.t. power counting.

Although we can not really be sure that it is correct we do trust the result with equal off-shellnesses before the on-shell limit [33] more then the other one in this particular case, because it is somehow the standard procedure and there is less risk to break a symmetry, which could spoil the result.
Furthermore setting one of the legs in Eq. (6.42) on-shell before performing the integrals produces a third result, that differs from the other two. The difference to the case, where the on-shell limits are taken one after the other could be explained by IR singularities that occur now because of the missing regulator.

The consequence of the ambiguous results in Eq. (6.42) for the renormalization of the six-quark (sum) operators $\mathcal{O}_{6i}$ ($\mathcal{O}_{ki}$) is rather obvious. Since in the six-leg

diagrams we naturally have at least two different off-shellnesses, one of which physical, we must not set all of them equal. The standard counterterms of the $\frac{1}{m^2}$ - potentials, determined in the previous section using the same off-shellness on all four legs, will therefore not be sufficient to subtract the respective two-loop subdivergences completely.
When calculating without any regulator on the inner legs however even two-loop counterterms allowing for two different off-shellnesses are not capable to remove the overall divergence in the sum of the six-leg diagrams associated with the three-loop graph in Fig. 6.12 *a*). As a result a $\frac{1}{A}$ term similar to (I+II) in table 6.9 is left. This might indicate that the three-loop diagrams with the topology Fig. 6.12 *a*) contain in addition to the soft also an ultrasoft IR singularity in contrast to our naive assumption. On the other hand there are to many open questions to draw a reliable conclusion.

Anyhow the ambiguities w.r.t. the non-Abelian renormalization of the $\frac{1}{m^2}$ - potentials V_r and V_2 cannot explain all the inconsistencies we have encountered so far. In order to clarify those issues we also performed the calculation of the contribution (I+II) with three different off-shellnesses, one physical ($2A$), one for the four outer (a) and one for the two inner legs (b). We found again different, but non-vanishing, results depending on how a and b approach zero. Even though we did not gain many new insights into the problem, we were at least able to cross check the non-Abelian two-loop integrals we are using. We did this by confirming that it does not matter for the result of a diagram, if two (or more) off-shellness parameters are set equal before or after the integration.
We also made the attempt to renormalize the six-quark operators off-shell, as we assigned the same off-shellness (A) as on the internal quark line to the two inner external legs in order to enforce the complete cancellation of subdivergences in the diagrams related to Fig. 6.12. But still we obtained a problematic $\frac{1}{A}$ term generated from other topologies.

All the problems described in this subsection seem to be specific to non-Abelian diagrams, since we have checked that the different methods of IR regularization applied above lead to the same result, which is moreover free of any $\frac{1}{A}$ terms, in the Abelian case (previous subsection).
This may give a hint that violation of gauge invariance might play a role and raises the question if we really have taken into account the complete gauge invariant set of Feynman graphs contributing to the NLL running of the six-quark (sum) operators or not. To be sure about that finally some further study is required.

To summarize the outcome of the current subsection, we state again, what we consider the most severe issues in our attempt of the non-Abelian renormalization of the six-quark (sum) operators, which are supposed to generate the effective

$\frac{1}{m|\mathbf{k}|}$ - potential in vNRQCD:

1. In any case we obtain peculiar divergent $\frac{1}{A}$ terms in our results, which do not give rise to the expected $\frac{1}{m|\mathbf{k}|}$ soft momentum structure, but to a soft IR singularity, when the heavy quark tadpole is closed and the integration over the potential loop three momentum ($\mathbf{q}$) is carried out respectively. We neither know how to treat this singularity in practice nor what its physical relevance and origin is in case it really exists.

2. The $\frac{\pi^0}{\epsilon}$ terms of our results depend on the specific configuration of artificial off-shellnesses, which are implemented in order to regulate ultrasoft IR singularities, and the conventions of how their zero limits are taken after subtraction of subdivergences. A proper regularization method applied to a gauge invariant set of diagrams must not exhibit such a behaviour.

3. The inconsistency of point 2. is not specific to the renormalization of the six-quark (sum) operators, but occurs already at the level of the $\frac{1}{m^2}$ - potentials, cf. Eq. (6.42). However it only concerns the diagrams with a non-Abelian triple gluon interaction considered in this work.

These issues might be due to one or more of the following possible reasons:

- The set of diagrams, that have been taken into account, is not complete. We have missed to include relevant contributions from diagrams, which have different topology or consist of different (new) vertices and conform to the respective velocity power counting conditions.

- The method we use to regularize ultrasoft IR singularities by introducing artificial off-shellnesses on the external heavy quark legs fails in the case of non-Abelian two-loop diagrams. Maybe it is not sufficient to remove all of the ultrasoft IR singularities in these diagrams, which are then wrongly interpreted as UV divergences, that have to be absorbed by the counterterms of the $\mathcal{O}_{6i}$ ($\mathcal{O}_{ki}$) operators.

- Some not yet identified symmetry is broken by our IR regularization procedure and not restored properly, when the off-shellness parameters are finally set to zero. That might spoil "Ward identity"-like relations between the diagrams, which could be important for consistency.

- In fact a soft IR singularity of unknown physical origin arises from the three-loop diagrams of Fig. 6.12. Of course this does not explain the inconsistencies of point 2. and 3..

- We made some (involved) mistake in the calculation of the two-loop integrals or in the generation of the amplitudes of the non-Abelian diagrams, which survived the various cross checks mentioned above.

Despite all the problems with the non-Abelian contributions we would still like to perform a preliminary analysis of the NLL running of the potentials derived in this section and see how it affects the total cross-section of $t\bar{t}$ production at threshold. Therefore we have to choose one of the two complete, but contradictory results we have displayed in tables 6.8 and 6.9 to continue with, while we just neglect the "bad" $\frac{1}{A}$ term. We decided in favor of

$$\begin{aligned}
&\mathrm{III}+\mathrm{IV}+\mathrm{V}+\mathrm{VI} \;=\\
&= \tfrac{i\,C_A\mathcal{V}_c^2\alpha_U^2}{18\,m\,\epsilon}\Big[1\otimes\bar{1}\big[-(C_A{-}2C_F)C_F\,(6C_F(f_1-f_0)+C_A(f_0-2f_1-f_2))\\
&\qquad -3\pi^{-2}C_A(C_A{-}2C_F)C_F(f_0+f_1+2f_2)\big]+\\
&\qquad T^A\otimes\bar{T}^A\big[2C_A^2(f_1+f_2)+2C_AC_F(3f_0-4f_1-f_2)+12C_F^2(f_1-f_0)\\
&\qquad -3\pi^{-2}C_A(C_A{-}4C_F)(f_1+f_2)\big]\Big] \qquad (6.43)
\end{aligned}$$

according to table 6.9, because the structure of the neglected (I+II) contribution is simpler and originates from a single set of diagrams related to Fig. 6.12 in that case.
In addition, we were able to check parts of the result by comparing the sum of a set of diagrams, that is supposed to reproduce the amplitude of a three-loop diagram with closed potential loop (see subsection 3.5.2), to the actual three-loop result. The latter is obtained by first performing the ultrasoft loop integrations (over k and l) and after that the q_0 integration from the potential loop. In practice however this calculation can only be carried out if one expands in the dimensional ϵ before the q_0 integration because of the complexity of the integrals. In all cases, where this is allowed, i.e. ϵ expansion and q_0 integration obviously commute, we indeed found agreement. A closer look shows that this check is unfortunately not applicable to the problematic contributions from the graphs in Fig. 6.12, since we must not interchange expansion and integration here.

Note that in Eq. (6.43) the terms proportional to π^{-2} have exactly the same soft momentum structure as the one-loop and Abelian two-loop results for the $\mathcal{O}_{6i}$ ($\mathcal{O}_{ki}$) counterterms in Eqs. (5.18), (6.33) and (6.34). We find the same expressions by summing the contributions in table 6.8. A corresponding observation was made in the context of the renormalization of the $\frac{1}{m^2}$ - potentials, cf. table 6.3. The π^{-2} contributions can be identified with the ones coming from two-loop diagrams that include one-loop subdivergences. They appear to be correct even in the case of the non-Abelian six-leg diagrams, since the cancellation of subdivergences by adding one-loop counterdiagrams obviously was successful leaving no logarithms of any off-shellness parameters whatsoever.

By all means we would like to stress again that no final reliable conclusion can be drawn from our results unless the problems listed at the end of this subsection are solved.

6.4 RGE's and Running

Since we are not going to consider corrections to the potentials $\sim \alpha_S^3 \ln \alpha_U$ in this work the inclusion of the soft mixing terms at the ultrasoft NLL level ($\sim \alpha_S^2 \alpha_U \ln \alpha_U$) follows exactly the lines of the LL procedure in sections 5.4 and 5.5 except for a little subtlety. Now that $\delta C_{2i} = \delta C_{2i}^{\text{1loop}} + \delta C_{2i}^{\text{2loop}}$ includes the corresponding two-loop contributions $\delta C_{2i}^{\text{2loop}} \sim \alpha_U^2$, we must not neglect the subleading term of $\nu \frac{d}{d\nu} V_c$ in the third term of Eq. 5.39. Furthermore we also have to keep the last term in order for this RGE to be consistent at $\mathcal{O}(\alpha_U^2)$. Therefore we end up with

$$\begin{aligned}
\nu \frac{d}{d\nu} \vec{V} &= \nu \frac{d}{d\nu} \big(V_c \, \vec{C}_{2i}\big) + 2 \frac{\alpha_S^2 \, \beta_0}{\mathbf{k}^2} \, \delta \vec{C}_{2i}^{\,\text{1loop}} - \frac{\alpha_S^2 \, \beta_0}{\mathbf{k}^2 \epsilon} \Big(\nu \frac{d}{d\nu} \delta \vec{C}_{2i}^{\,\text{1loop}} \Big) \\
&= \nu \frac{d}{d\nu} \big(V_c \, \vec{C}_{2i}\big) - 2 \frac{\alpha_S^2 \, \beta_0}{\mathbf{k}^2} \, \delta \vec{C}_{2i}^{\,\text{1loop}} - \Big(\nu \frac{d}{d\nu} \frac{\alpha_S^2 \, \beta_0}{\mathbf{k}^2 \epsilon} \Big) \delta \vec{C}_{2i}^{\,\text{1loop}} \\
&\quad - \frac{\alpha_S^2 \, \beta_0}{\mathbf{k}^2 \epsilon} \Big(\nu \frac{d}{d\nu} \delta \vec{C}_{2i}^{\,\text{1loop}} \Big) \\
&= \nu \frac{d}{d\nu} \big(V_c \, \vec{C}_{2i}\big) - 2\epsilon \Big(\frac{\alpha_S^2 \, \beta_0}{\mathbf{k}^2 \epsilon} \, \delta \vec{C}_{2i}^{\,\text{1loop}} \Big) - \nu \frac{d}{d\nu} \Big(\frac{\alpha_S^2 \, \beta_0}{\mathbf{k}^2 \epsilon} \, \delta \vec{C}_{2i}^{\,\text{1loop}} \Big) \, . \qquad (6.44)
\end{aligned}$$

On the other hand we consequently have to account for new diagrams, that contribute to the anomalous dimension at $\mathcal{O}(\alpha_S^2 \alpha_U)$:

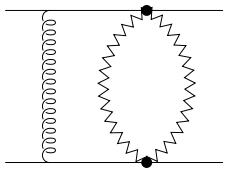

$$+ \quad \ldots \quad = \quad \frac{\alpha_S^2 \, \beta_0}{\mathbf{k}^2 \epsilon} \, \delta \vec{C}_{2i}^{\,\text{1loop}} \, . \qquad (6.45)$$

The amplitudes of the diagrams on the left hand side are understood as vectors in the $(1 \otimes \bar{1}, T^A \otimes \bar{T}^A)$ color space. The ellipses denote all other permutations of possible ultrasoft attachments including wavefunction diagrams (or equivalently the addition of wavefunction counterterms like in Eq. (5.24)) as well as the appropriate counterdiagrams to subtract the subdivergences.
Adding the contribution from Eq. (6.45) to the potential counterterm $\delta \vec{V}$ in Eq. (5.38) precisely cancels the last two terms in Eq. (6.44). We are therefore left with the original factorized form for the potential Wilson coefficients, that we have already found at ultrasoft LL level.
Analogous considerations show that the known factorization formula Eq. (5.41) is valid for the coefficients $\mathcal{V}_{ki}$ at ultrasoft NLL level as well.

As an aside we would like to mention here that the part of the result in Eq (6.45) generated only by the diagrams, where the soft modes are gluons, can also be inferred from related two-loop diagrams via the pull-up mechanism, see

section 3.7. Those diagrams with two ultrasoft gluons attached to a Coulomb potential have been calculated in section 6.2.
In addition to that the zero-bin subtraction at two-loop level also predicts purely soft UV divergences with opposite sign for every UV divergence from ultrasoft diagrams just as in the one-loop case [70]. So we will likewise assume the existence of soft pull-up terms by replacing $\alpha_U^2 \to \alpha_U^2 - \alpha_S^2$ in the results for the two-loop counterterms determined in this chapter.
Thus at two-loop precision the ultrasoft counterterms of the Wilson coefficients $C_{2i}^{(1,T)}$ and $C_{(6+2)i}^{(1,T)}$ introduced in section 5.4 together with their soft pull-up terms can be cast into the form

$$\delta C_i \;=\; A_i \,\frac{\alpha_U - \alpha_S}{\epsilon} \;+\; \tilde{A}_i \,\frac{\alpha_U^2 - \alpha_S^2}{\epsilon^2} \;+\; B_i \,\frac{\alpha_U^2 - \alpha_S^2}{\epsilon} \,. \tag{6.46}$$

From Eq. (6.46) we can derive the NLL anomalous dimension of the coefficient C_i using Eq. 5.43 for the running of the strong coupling constants:

$$\begin{aligned}
\nu\frac{d}{d\nu}C_i \;&=\; -\,\nu\frac{d}{d\nu}\delta C_i \;= \qquad\qquad (6.47)\\
&=\; -\frac{A_i}{\epsilon}\,\nu\frac{d}{d\nu}(\alpha_U - \alpha_S) \;-\; \left(\frac{\tilde{A}_i}{\epsilon^2} + \frac{B_i}{\epsilon}\right)\nu\frac{d}{d\nu}(\alpha_U^2 - \alpha_S^2)\\
&=\; \frac{A_i}{\epsilon}\left[2\epsilon(2\alpha_U - \alpha_S) + \frac{\beta_0}{2\pi}(2\alpha_U^2 - \alpha_S^2)\right] \;+\; \left(\frac{\tilde{A}_i}{\epsilon^2} + \frac{B_i}{\epsilon}\right)4\epsilon(2\alpha_U^2 - \alpha_S^2)\\
&=\; 2\,A_i\,(2\alpha_U - \alpha_S) + 4\,B_i\,(2\alpha_U^2 - \alpha_S^2) + \frac{\beta_0 A_i + 8\pi\tilde{A}_i}{2\pi\epsilon}\,(2\alpha_U^2 - \alpha_S^2)\,.
\end{aligned}$$

For this RGE to be consistent, i.e. finite in $d = 4$ dimensions, it is a necessary condition that the last term vanishes as

$$\tilde{A}_i \;=\; -\frac{\beta_0}{8\pi}\,A_i\,, \tag{6.48}$$

which represents a cross check of the $\frac{\alpha_U^2}{\epsilon^2}$ terms of the results derived in the previous sections. We already have referred to it several times earlier in the text in order to confirm our findings. Indeed all of the final expressions for two-loop counterterms determined in this work fulfil the consistency condition Eq. (6.48).

For $\delta C_{2i}^{(1,T)}$ and $\delta C_{(6+2)1,2}^{(1,T)}$ the corresponding one-loop constants A_i are given in Eqs. (5.26) and (5.33) and the two-loop constants B_i are determined from

Eqs. (6.28), (6.29), (6.33)-(6.35) and (6.43). They read[9]

$$
\begin{aligned}
B_{\mathbf{p}}^{(1)} &= -\frac{3}{8} C_A C_F (C_A - 2C_F)\,, \\
B_{\mathbf{p}}^{(T)} &= \frac{1}{72} C_A (60 C_F - 19 C_A) + \frac{C_A (47 C_A - 10 n_f T)}{54\pi^2}\,, \\
B_{\mathbf{k}}^{(1)} &= \frac{7}{72} C_A (C_A - 2C_F) C_F - \frac{(C_A - 2C_F) C_F (47 C_A - 10 n_f T)}{216\pi^2}\,, \\
B_{\mathbf{k}}^{(T)} &= \frac{1}{24} C_A (C_A - 2C_F) - \frac{(C_A - 2C_F)(47 C_A - 10 n_f T)}{72\pi^2}
\end{aligned}
\tag{6.49}
$$

and

$$
\begin{aligned}
B_1^{(1)} &= -\frac{C_A (C_A - 2C_F) C_F (47 C_A - 10 n_f T)}{108\pi^2}\,, \\
B_2^{(T)} &= \frac{C_A^3}{9} - \frac{C_A (C_A - 4C_F)(47 C_A - 10 n_f T)}{108\pi^2}\,.
\end{aligned}
\tag{6.50}
$$

To absorb all the divergences in Eq. (6.43) we have to extend the six-quark/sum operator basis at NLL level by new operators with appropriate soft momentum structure. We define the following (zero-matching) sum operators in addition to Eq. (3.36):

$$
\begin{aligned}
\mathcal{O}_{k3}^{(X)} &= \frac{\mu_S^{4\epsilon}}{m}\, X^A \otimes \bar{X}^A \sum_{\mathbf{p},\mathbf{p}',\mathbf{q}} (f_0 - f_1)\, \left[\psi_{\mathbf{p}'}^\dagger\, \psi_{\mathbf{p}}\, \chi_{-\mathbf{p}'}^\dagger\, \chi_{-\mathbf{p}}\right], \\
\mathcal{O}_{k4}^{(1)} &= \frac{\mu_S^{4\epsilon}}{m}\, 1 \otimes \bar{1} \sum_{\mathbf{p},\mathbf{p}',\mathbf{q}} (f_0 - 2f_1 - f_2)\, \left[\psi_{\mathbf{p}'}^\dagger\, \psi_{\mathbf{p}}\, \chi_{-\mathbf{p}'}^\dagger\, \chi_{-\mathbf{p}}\right], \\
\mathcal{O}_{k5}^{(T)} &= \frac{\mu_S^{4\epsilon}}{m}\, T^A \otimes \bar{T}^A \sum_{\mathbf{p}',\mathbf{p}',\mathbf{q}} (3f_0 - 4f_1 - f_2)\, \left[\psi_{\mathbf{p}'}^\dagger\, \psi_{\mathbf{p}}\, \chi_{-\mathbf{p}'}^\dagger\, \chi_{-\mathbf{p}}\right].
\end{aligned}
\tag{6.51}
$$

Thus the constants in the RGE's of the associated Wilson coefficients $C_{(6+2)3,4,5}^{(1,T)}$

[9] Note that the constants with index $\mathbf{p}$ differ from the ones given in Ref. [33] by a factor of two due to a different convention in the definition of the operators $\mathcal{O}_{2p}^{(2)}$.

are

$$\begin{aligned} A_{3,4,5}^{(1,T)} &= 0\,, \\ B_3^{(1)} &= \frac{1}{3} C_A (C_A - 2C_F) C_F^2\,, \\ B_3^{(T)} &= -\frac{2 C_A C_F^2}{3}\,, \\ B_4^{(1)} &= -\frac{1}{18} C_A^2 (C_A - 2C_F) C_F\,, \\ B_5^{(T)} &= \frac{C_A^2 C_F}{9}\,. \end{aligned} \tag{6.52}$$

To solve the NLL RGE in Eq. (6.47) we proceed in a similar way as in the LL case, Eq. (5.44), but allow for NLL running of α_S and α_U in the leading order terms:

$$\begin{aligned} dC_i &= 2\,A_i\,(2\alpha_U^{\rm NLL} - \alpha_S^{\rm NLL})\,d\ln\nu + 4\,B_i\left(2(\alpha_U^{\rm LL})^2 - (\alpha_S^{\rm LL})^2\right) d\ln\nu \\ &= -\frac{4\pi}{\beta_0}\,A_i \left(\left(1 - \frac{\beta_1}{4\pi\beta_0}\alpha_U^{\rm NLL}\right)\frac{d\alpha_U^{\rm NLL}}{\alpha_U^{\rm NLL}} - \left(1 - \frac{\beta_1}{4\pi\beta_0}\alpha_S^{\rm NLL}\right)\frac{d\alpha_S^{\rm NLL}}{\alpha_S^{\rm NLL}} \right) \\ &\quad -\frac{8\pi}{\beta_0}\,B_i\left(d\alpha_U^{\rm LL} - d\alpha_S^{\rm LL}\right) \\ &= -\frac{4\pi}{\beta_0}\,A_i \left(\frac{d\alpha_U}{\alpha_U} - \frac{d\alpha_S}{\alpha_S}\right) + \left(\frac{\beta_1}{\beta_0^2}\,A_i - \frac{8\pi}{\beta_0}\,B_i\right)\left(d\alpha_U - d\alpha_S\right)\,, \end{aligned} \tag{6.53}$$

where we used Eq. (3.18) to replace $d\ln\nu$ in the leading order term and Eq. (3.22) in the subleading term. In the last step we gave up the distinction between $\alpha_{U/S}^{\rm LL}$ and $\alpha_{U/S}^{\rm NLL}$, because it will be clear in the integrated result anyway.
Eq. (6.53) is now easy to integrate and respecting the (zero) matching conditions $C_i(\nu = 1) = 0$ we arrive at

$$C_i^{\rm NLL}(\nu) = -\frac{4\pi}{\beta_0}\,A_i\,\ln\frac{\alpha_U}{\alpha_S} + \left(\frac{\beta_1}{\beta_0^2}\,A_i - \frac{8\pi}{\beta_0}\,B_i\right)\left(\alpha_U - \alpha_S\right)\,. \tag{6.54}$$

Thus the ultrasoft NLL results for the evolution of $\mathcal{V}_2$, $\mathcal{V}_r$ and $\mathcal{V}_{ki}$ ($i = 1..5$) including (LL) soft mixing and pull-up contributions expressed in terms of the

running strong coupling constant are given by[10]

$$\begin{aligned}
\big(\mathcal{V}_2^{(1,T)}(\nu)\big)_{us}^{\rm NLL} &= -\frac{16\pi^2}{\beta_0} A_{\mathbf{k}}^{(1,T)}\, \alpha_S^{\rm LL} \left[\ln\frac{\alpha_U}{\alpha_S}\right]^{\rm NLL} \\
&\quad + \left[\frac{4\pi\beta_1}{\beta_0^2} A_{\mathbf{k}}^{(1,T)} - \frac{32\pi^2}{\beta_0} B_{\mathbf{k}}^{(1,T)}\right] \alpha_S^{\rm LL}\big(\alpha_U^{\rm LL} - \alpha_S^{\rm LL}\big)\,, \qquad (6.55)\\
\big(\mathcal{V}_r^{(1,T)}(\nu)\big)_{us}^{\rm NLL} &= -\frac{16\pi^2}{\beta_0} A_{\mathbf{p}}^{(1,T)}\, \alpha_S^{\rm LL} \left[\ln\frac{\alpha_U}{\alpha_S}\right]^{\rm NLL} \\
&\quad + \left[\frac{4\pi\beta_1}{\beta_0^2} A_{\mathbf{p}}^{(1,T)} - \frac{32\pi^2}{\beta_0} B_{\mathbf{p}}^{(1,T)}\right] \alpha_S^{\rm LL}\big(\alpha_U^{\rm LL} - \alpha_S^{\rm LL}\big)\,, \qquad (6.56)\\
\big(\mathcal{V}_{k1,2}^{(1,T)}(\nu)\big)_{us}^{\rm NLL} &= \frac{64\pi^3}{\beta_0} A_{1,2}^{(1,T)}\, (\alpha_S^{\rm LL})^2 \left[\ln\frac{\alpha_U}{\alpha_S}\right]^{\rm NLL} + \\
&\quad - \left[\frac{16\pi^2\beta_1}{\beta_0^2} A_{1,2}^{(1,T)} - \frac{128\pi^3}{\beta_0} B_{1,2}^{(1,T)}\right] (\alpha_S^{\rm LL})^2\big(\alpha_U^{\rm LL} - \alpha_S^{\rm LL}\big)\,, \qquad (6.57)\\
\big(\mathcal{V}_{k3,4,5}^{(1,T)}(\nu)\big)_{us}^{\rm NLL} &= \frac{128\pi^3}{\beta_0} B_{3,4,5}^{(1,T)}\, (\alpha_S^{\rm LL})^2\big(\alpha_U^{\rm LL} - \alpha_S^{\rm LL}\big)\,. \qquad (6.58)
\end{aligned}$$

To solve the RGE's for these potential coefficients without the soft mixing terms, that provide the nice factorized form of soft and ultrasoft contributions, is a bit more complicated due to mixed terms of α_S and α_U. In this case we have to substitute $\alpha_{S/U}^{\rm NLL}$ by Eq. (3.20) and express one of the LL coupling constants in terms of the other one using Eq. (3.17). The integration is then done w.r.t. $\alpha_{S/U}^{\rm LL}$. In Ref. [28] this is demonstrated at LL and for the fermionic (n_f) contributions also at NLL level.

With the new contributions from the sum operators $\mathcal{O}_{k3,4,5}$ or the respective six-quark operators $\mathcal{O}_{63,4,5}$ the Wilson coefficients $(\mathcal{V}_{k,\rm eff}^{(1/T)})_{us}$ of the effective $\frac{1}{m|\mathbf{k}|}$ potential now take according to Eq. (5.16) and Ref. [32] the form[11]

$$\begin{aligned}
\big(\mathcal{V}_{k,\rm eff}^{(1)}(\nu)\big)_{us}^{\rm NLL} &= -\frac{1}{8\pi^2}\left[\,3\mathcal{V}_{k1}^{(1)}(\nu) - \mathcal{V}_{k3}^{(1)}(\nu) - 3\mathcal{V}_{k4}^{(1)}(\nu)\,\right]^{\rm NLL}, \\
\big(\mathcal{V}_{k,\rm eff}^{(T)}(\nu)\big)_{us}^{\rm NLL} &= -\frac{1}{8\pi^2}\left[\,2\mathcal{V}_{k2}^{(T)}(\nu) - \mathcal{V}_{k3}^{(T)}(\nu) - 5\mathcal{V}_{k5}^{(T)}(\nu)\,\right]^{\rm NLL}. \qquad (6.59)
\end{aligned}$$

[10] As a technical aside we would like to remark that $\big[\ln\frac{\alpha_U}{\alpha_S}\big]^{\rm NLL}$ can also be expressed as $\big[\ln(\frac{z}{2-z}) - \ln(z) + \alpha_h\frac{\beta_1}{4\beta_0\pi}\,\frac{z}{2-z}\,\ln(\frac{z}{2-z}) - \alpha_h\frac{\beta_1}{4\beta_0\pi}\,z\ln(z)\big]$, where $z = \frac{\alpha_S^{\rm LL}}{\alpha_h}$. In this way LL and NLL terms can be easily distinguished in later numerical analysis.

[11] Remember the comments on our convention regarding the Wilson coefficients $\mathcal{V}_{ki}$ at the end of section 5.5.

Chapter 7

Numerical Analysis of the New Results

To evaluate the phenomenological effects of the new results for the running of the potential coefficients $\mathcal{V}_2$, $\mathcal{V}_r$ and $\mathcal{V}_{k,\text{eff}}$ obtained in this thesis we first have to transform them to the physical color singlet/octet basis by means of Eq. (2.26). Since for the prediction of $\sigma_{\text{tot}}(e^+e^- \to t\,\bar{t}\,)$ only the color singlet configuration is relevant, cf. Eq. (4.7), the numerical analysis in this chapter focusses on the NLL running of the coefficients

$$\mathcal{V}_i^{(s)} \;=\; \mathcal{V}_i^{(1)} \,-\, C_F \mathcal{V}_i^{(T)} \tag{7.1}$$

and their impact on the effective current Wilson coefficient $c_1(\nu)$.
For the application to the top-antitop threshold we adopt $\alpha_s(m_t) = 0.1074$ for the strong coupling constant and $m_t = 175$ GeV for the heavy quark mass in the following.

7.1 Results for $\frac{1}{m^2}$ - Potentials at NLL

The following discussion of $\mathcal{V}_2^{(s)}$ and $\mathcal{V}_r^{(s)}$ has already been published in Ref. [33]. In Fig. 7.1 *a*), *b*) the renormalization parameter (ν) dependence of $\mathcal{V}_2^{(s)}$ and $\mathcal{V}_r^{(s)}$ is shown at LL order (dashed black lines) including all soft and ultrasoft contributions [32, 54], and in addition including the full two-loop ultrasoft contributions of Eqs. (6.55) and (6.56) with (solid red lines) and without (dotted blue lines) the soft mixing contributions from the zero matching operators $\mathcal{O}_{2i}$ introduced in section 5.4.
To further illustrate the importance of the two-loop ultrasoft contributions we have displayed in Fig. 7.1 *c*), *d*) the evolution of the coefficients at LL order due to the one-loop ultrasoft contributions alone (dashed black lines), and in addition including the two-loop ultrasoft contributions analogous to Figs. 7.1 *a*) and *b*).

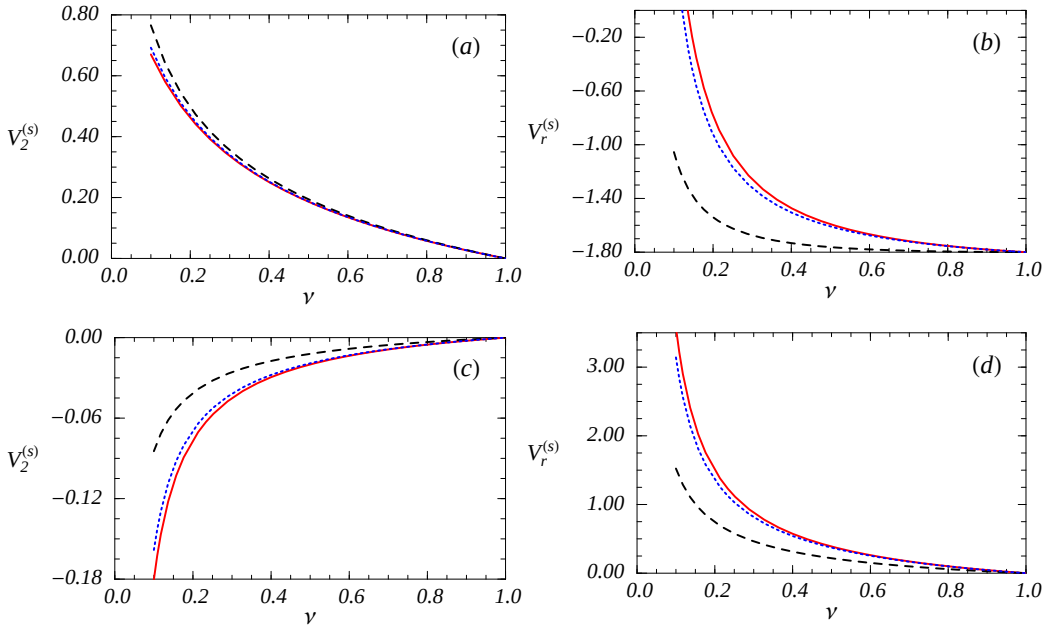

Figure 7.1: Renormalization scale dependence of $\mathcal{V}_2^{(s)}$ and $\mathcal{V}_r^{(s)}$. In *a*), *b*) the full LL results (soft + ultrasoft) (dashed lines), plus the NLL ultrasoft contributions with (solid lines) and without (dotted lines) the soft mixing terms are shown. In *c*), *d*) only the corresponding ultrasoft results are displayed omitting the known soft LL running. All of them include soft pull-up terms.

Comparing the behavior of the ultrasoft LL order and the NLL ultrasoft (two-loop) contributions in Fig. 7.1 *c*), *d*) we find that the NLL order corrections are of the same size as the ultrasoft LL order contributions. While for the potential $\mathcal{V}_2^{(s)}$ this is of no concern, since for $\mathcal{V}_2^{(s)}$ the ultrasoft contributions are suppressed by a small overall color factor compared to the soft LL contributions, the result for $\mathcal{V}_r^{(s)}$ shows that the two-loop ultrasoft corrections are indeed anomalously large, similar to the NNLL ultrasoft non-mixing contributions to the evolution of c_1 determined in Ref. [26]. From the dotted lines in Fig. 7.1 we also see that the correction arising from the mixing contributions are numerically small, which is consistent with the parametric counting we brought up in section 4.2.
At this point we would like to remark once again that we found in the course of this work different results for the non-Abelian two-loop contributions, when using different IR regularization setups, also for $\mathcal{V}_2$ and $\mathcal{V}_r$, as pointed out in subsection 6.3. All results displayed here agree with the ones published in Ref. [33] and were obtained in the "standard" off-shellness configuration using only one universal off-shellness.

7.2 Results for $\frac{1}{m|\mathbf{k}|}$ - Potentials at NLL

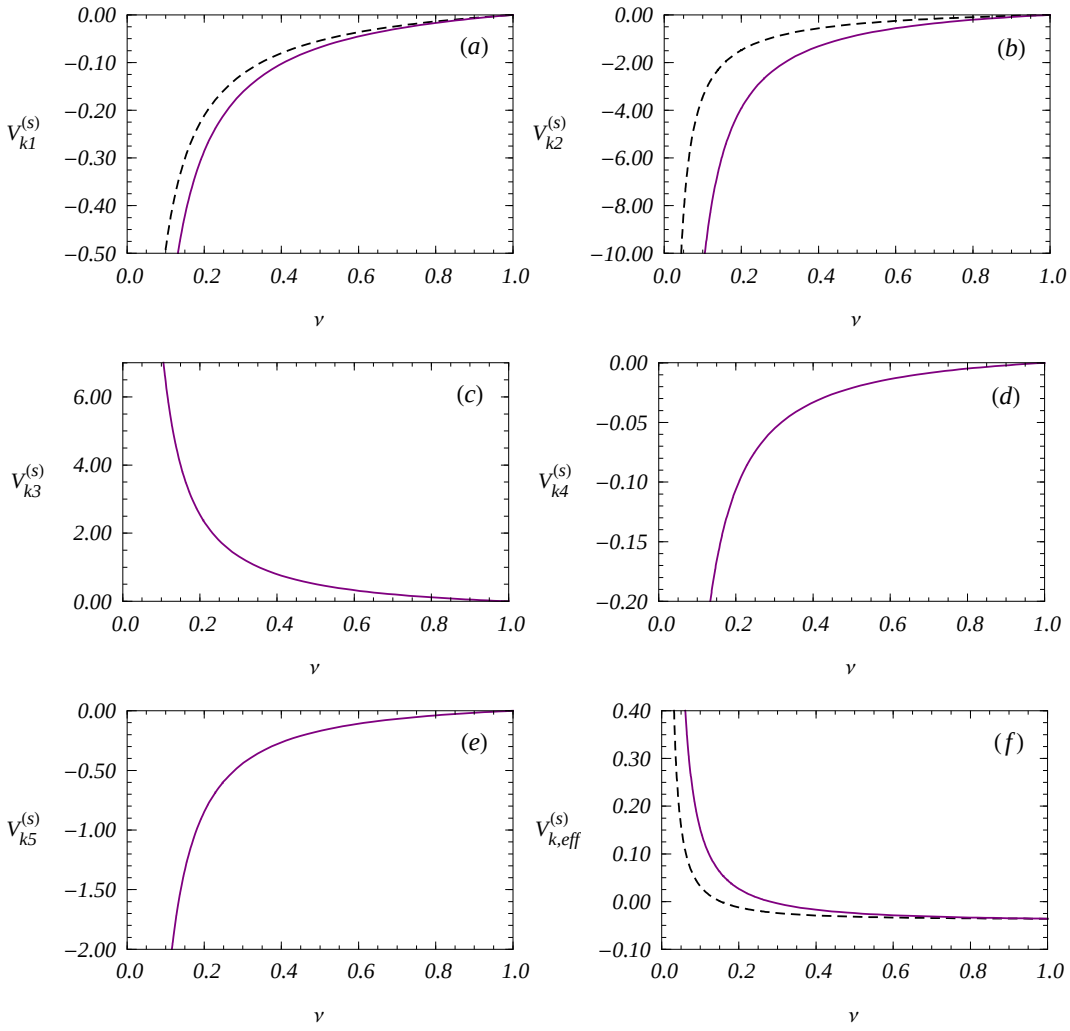

Figure 7.2: Renormalization scale dependence of the coefficients $\mathcal{V}_{ki}^{(s)}$ and $\mathcal{V}_{k,\text{eff}}^{(s)}$. In a) - e) all non-zero ultrasoft LL results (dashed lines), plus the ultrasoft NLL contributions (solid lines) are shown. Panel f) displays the corresponding results for $\mathcal{V}_{k,\text{eff}}^{(s)}$ and the full soft LL contributions are added to both curves. All plots include soft mixing and pull-up terms.

Concerning the complete two-loop running (violet solid lines) of the sum operator coefficients $\mathcal{V}_{k1}^{(s)}$ and $\mathcal{V}_{k2}^{(s)}$ in Eqs. (6.57) and (6.58) the qualitative statement, that the NLL contributions are sizable compared to the LL results (black dashed lines), obviously holds as well, see Fig. 7.2 a) and b). In this case like for the other coefficients $\mathcal{V}_{k3,4,5}^{(s)}$ displayed in Fig. 7.2 c), d), e) no pure soft contributions exist

apart from soft mixing and pull-up terms. Both of which are included everywhere in Fig. 7.2 and have a similar effect on the plotted curves as for $\mathcal{V}_2^{(s)}$ and $\mathcal{V}_r^{(s)}$ in Fig. 7.1.
The operators $\mathcal{O}_{k3,4,5}$ ($\mathcal{O}_{63,4,5}$) are first renormalized at two-loop level, see section 6.4. Therefore they do not run at LL and we can only roughly compare the size of their NLL coefficients to the one of the LL results for $\mathcal{V}_{k1,2}^{(s)}$ to estimate their numerical relevance.
Physically relevant for our purpose is anyway only the linear combination representing $\left(\mathcal{V}_{k,\text{eff}}^{(s)}\right)_{us}$ according to Eq. (6.59). In Fig. 7.2 f) we show the LL (black dashed lines) and NLL running (violet solid lines) of $\mathcal{V}_{k,\text{eff}}^{(s)}$ governed by the evolution of the $\mathcal{V}_{ki}$ in Eqs. (6.57) and (6.58). Both curves in addition imply the effects of the soft LL terms in Eq. (4.8), which are generated by sum operators that are introduced in Ref. [26] and receive quantum corrections from soft loops. This explains the offset on the vertical axis on the right-hand side of Fig. 7.2 f) representing the non-zero matching condition of those operators.
We observe again that in fact the ultrasoft NLL contributions are anomalously large and even exceed the LL contributions in Fig. 7.2 f) notably. Due to the small prefactor $\sim \frac{\mathcal{V}_c}{16\pi^2}$ in the anomalous dimension of c_1, Eq. (4.7), the $\mathcal{V}_2$ and $\mathcal{V}_r$ results are relatively suppressed against $\mathcal{V}_{k,\text{eff}}$. That is why the result in Fig. 7.2 f) has despite being numerically smaller an even larger impact on the evolution of c_1 than the ones in Fig. 7.1.

We will see below if the difference of LL and NLL evolution of $\mathcal{V}_{k,\text{eff}}^{(s)}$ is the effect, that can compensate for the large ultrasoft NNLL non-mixing contributions to c_1, and about which we were speculating in section 4.2.
All the analysis done here is preliminary, because we are not yet sure about the correctness of all the results in table 6.9, which we used as the non-Abelian contributions to the running of $\mathcal{V}_{k,\text{eff}}$.
In the next section we will also show the numerical effect on the final result for c_1 coming from the terms that are peculiarly affected by a change of the off-shellness configuration in the IR regularization procedure.

7.3 Results for $c_1(\nu)$ at NNLL

With the new ultrasoft NLL contributions to the potentials in Eqs. (6.55) - (6.58) the NNLL part of the integrated NLL anomalous dimension of c_1 in Eq. (4.7) reads

$$\begin{aligned}\xi^{\rm NNLL}_{\rm m,usoft} &= \frac{2\pi\beta_1}{\beta_0^3}\,\tilde{A}\,\alpha_s^2(m)\,\Big[-\frac{7}{4}+\frac{\pi^2}{6}+z\left(1-\ln\frac{z}{2-z}\right)+z^2\left(\frac{3}{4}-\frac{1}{2}\ln z\right)\\ &\qquad -\ln^2\left(\frac{z}{2}\right)+\ln^2\left(\frac{z}{2-z}\right)-2{\rm Li}_2\left(\frac{z}{2}\right)\Big]\\ &\quad +\frac{8\pi^2}{\beta_0^2}\,\tilde{B}\,\alpha_s^2(m)\,\Big[3-2z-z^2-4\ln(2-z)\Big], \qquad (7.2)\end{aligned}$$

where

$$\begin{aligned}\tilde{A} &= C_F\Big[A_{\mathbf{k}}^{(1)}+A_{\mathbf{p}}^{(1)}-C_F\big(A_{\mathbf{k}}^{(T)}+A_{\mathbf{p}}^{(T)}\big)\Big]+\Big[3A_1^{(1)}-2C_FA_2^{(T)}\Big],\\ \tilde{B} &= C_F\Big[B_{\mathbf{k}}^{(1)}+B_{\mathbf{p}}^{(1)}-C_F\big(B_{\mathbf{k}}^{(T)}+B_{\mathbf{p}}^{(T)}\big)\Big]+\\ &\quad +\Big[3B_1^{(1)}-B_3^{(1)}-3B_4^{(1)}-C_F\big(2B_2^{(T)}-B_3^{(T)}-5B_5^{(T)}\big)\Big],\\ z &\equiv \left(\frac{\alpha_s(m\nu)}{\alpha_s(m)}\right)^{\rm LL}=\left(1+\frac{\alpha_s(m)\beta_0}{2\pi}\ln\nu\right)^{-1}. \qquad (7.3)\end{aligned}$$

The constants $A_i^{(1,T)}$ and $B_i^{(1,T)}$ have been defined in Eqs. (5.26), (5.33) and Eqs. (6.49), (6.50) and (6.52) respectively.
For completeness we also give the form of the ultrasoft corrections to $\xi^{\rm NLL}$:

$$\xi^{\rm NLL}_{\rm usoft} = \frac{8\pi^2}{\beta_0^2}\,\tilde{A}\,\alpha_s(m)\,\Big[-1+z+(2-z)\ln(2-z)\Big]. \qquad (7.4)$$

The plot in Fig. 7.3 shows the evolution of the Wilson coefficient c_1 including all known contributions, among them Eq. 7.2 (black solid line), and represents an update of Fig.4.4 in section 4.2.
Note that the gap between NLL (blue dotted line) and NNLL curves shrinks to about half of its size, when the new ultrasoft mixing terms are included (black solid line). In particular the large raise close to threshold has vanished almost completely. This corresponds to a partial compensation among the anomalously large ultrasoft NNLL non-mixing contributions [26] and the ultrasoft NNLL mixing contributions in Eq. (7.2), that contains apart from purely ultrasoft also soft mixing and pull-up terms.
Translated to the total top-antitop production cross section $\sigma_{\rm tot}(e^+e^-\to t\,\bar{t}\,)$ at

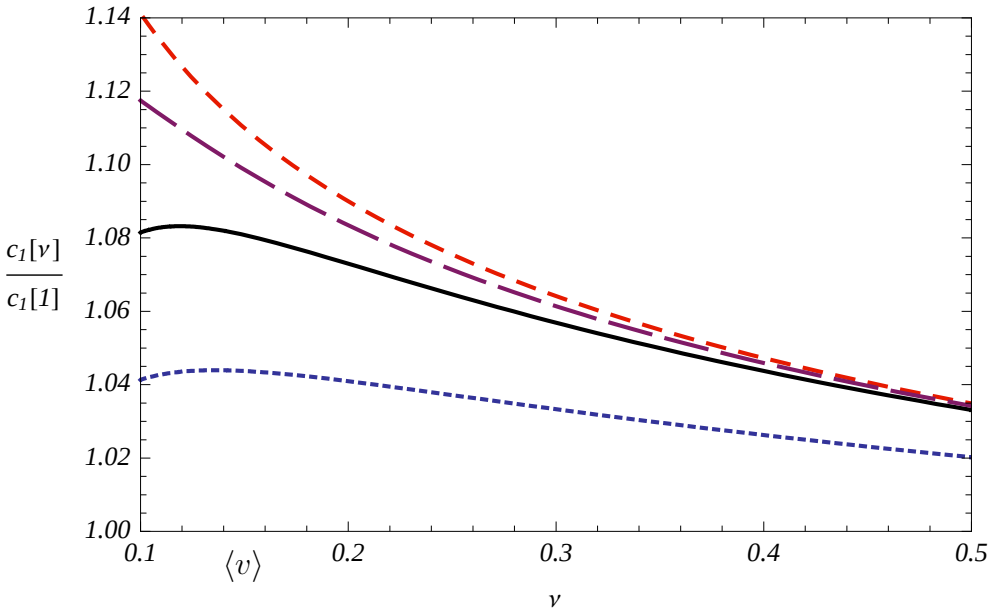

Figure 7.3: (Normalized) running of the current Wilson coefficient $c_1(\nu)$. The dotted (blue) line represents the full LL result $\exp[\xi^{\mathrm{NLL}}]$, the short-dashed (red) line includes in addition the NNLL non-mixing contributions: $\exp[\xi^{\mathrm{NLL}} + \xi^{\mathrm{NNLL}}_{\mathrm{nm}}]$. On top of that the solid (black) line allows also for the ultrasoft NNLL mixing contributions computed in this work: $\exp[\xi^{\mathrm{NLL}} + \xi^{\mathrm{NNLL}}_{\mathrm{nm}} + \xi^{\mathrm{NNLL}}_{\mathrm{m,usoft}}]$. To illustrate the effect of the non-Abelian two-loop corrections, which suffer from the problems described in subsection 6.3.3, we subtracted their contributions from the solid (black) curve to obtain the long-dashed (violet) line. $\langle v \rangle$ denotes a typical value for v in the threshold region.

threshold that means a substantial decrease of the theoretical uncertainty in the normalization ($\frac{\delta\sigma_{\mathrm{tot}}}{\sigma_{\mathrm{tot}}}$) to values, which are in the range of the proclaimed three percent aim, see chapter 4.
However we also realize from the distance between the (black) solid and the (violet) long-dashed curve that a large fraction of the promising compensation effect of $\xi^{\mathrm{NNLL}}_{\mathrm{m,usoft}}$ is caused by the non-Abelian $\frac{\pi^0}{\epsilon}$ - terms in Eq. (6.28) and table (6.9), which come along with some open questions.
Therefore it is too early to claim already a lower theoretical uncertainty $\frac{\delta\sigma_{\mathrm{tot}}}{\sigma_{\mathrm{tot}}}$ and further effort has to be undertaken to solve the problems encountered in subsection 6.3.3. Hopefully the current result will be at least qualitatively confirmed by subsequent work.

Appendix A

Feynman Rules of vNRQCD

In this Appendix we list the vNRQCD (momentum space) Feynman rules in Feynman gauge, that are used in this work.

Propagators

ultrasoft A^0 gluon:	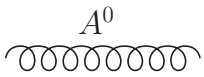	$\dfrac{-i\,\delta^{AB}}{k^2+i\epsilon}$
ultrasoft **A** gluon:	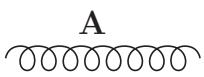	$\dfrac{i\,\delta^{ij}\,\delta^{AB}}{k^2+i\epsilon}$
heavy (anti)quark:		$\dfrac{i}{k_0-\frac{\mathbf{p}^2}{2m}+i\epsilon}$

(A.1)

Heavy Quark Kinetic Insertions

(soft and ultrasoft momenta point in the direction of the fermion flow)

$$-i\,\frac{\mathbf{p}\cdot\vec{k}}{m}$$

$$-i\,\frac{\vec{k}^2}{2m}$$

(A.2)

Heavy Quark - Ultrasoft Gluon - Vertices

(for antiquark vertices replace $T^A \to \bar{T}^A$, soft momenta point into the direction of the fermion flow)

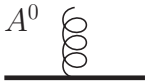

$$-i\,g\,T^A \tag{A.3}$$

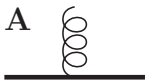

$$i\,g\frac{\mathbf{p}}{m}\,T^A$$

Triple Ultrasoft Gluon - Vertices

(all gluon four-momenta $k^\mu_{A,B,C}$ are incoming)

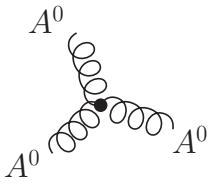

$$0$$

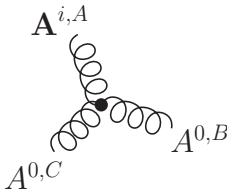

$$-g\,f^{ABC}(k^i_C - k^i_B) \tag{A.4}$$

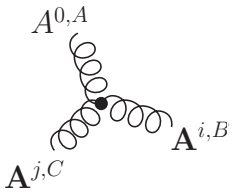

$$-g\,f^{ABC}\,\delta^{ij}\,(k^0_C - k^0_B)$$

Heavy Quark Potential - Vertices

(all soft and ultrasoft momenta point in the direction of the fermion flow)

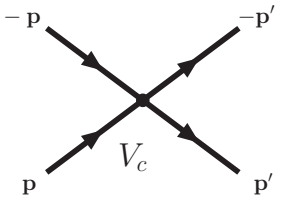

$$\frac{-i\,\mathcal{V}_c^{(T)}}{(\mathbf{p}'-\mathbf{p})^2}\;T^A\otimes\bar{T}^A$$

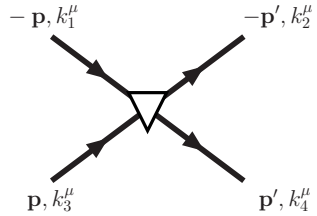

$$i\,\mathcal{V}_c^{(T)}\,T^A\otimes\bar{T}^A\;\frac{(\mathbf{p}'-\mathbf{p})\cdot[(\vec{k}_4-\vec{k}_3)-(\vec{k}_2-\vec{k}_1)]}{(\mathbf{p}'-\mathbf{p})^4} \tag{A.5}$$

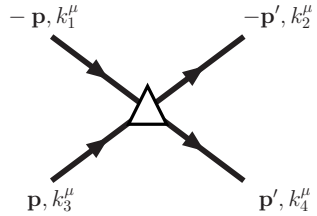

$$i\,\mathcal{V}_c^{(T)}\,T^A\otimes\bar{T}^A\left[\frac{(\vec{k}_4-\vec{k}_3)^2+(\vec{k}_2-\vec{k}_1)^2}{2\,(\mathbf{p}'-\mathbf{p})^4}\right.$$
$$\left.-\frac{2[(\mathbf{p}'-\mathbf{p})(\vec{k}_4-\vec{k}_3)]^2+2[(\mathbf{p}'-\mathbf{p})(\vec{k}_2-\vec{k}_1)]^2}{(\mathbf{p}'-\mathbf{p})^6}\right]$$

Heavy Quark Potential - Ultrasoft Gluon - Vertex

(all soft momenta point in the direction of the fermion flow)

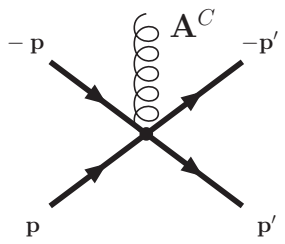

$$-2\,g\,\mathcal{V}_c^{(T)}\,f^{ABC}\,T^A\otimes\bar{T}^B\,\frac{(\mathbf{p}'-\mathbf{p})\cdot\mathbf{A}^C}{(\mathbf{p}'-\mathbf{p})^4} \tag{A.6}$$

Appendix B

Loop Integrals in Dimensional Regularization

This Appendix contains the standard (one-loop) integrals used in the calculations of one and two-loop amplitudes in this work as well as other useful integration formulas in d dimensions.

Tensor Integral

Relation between a tensor integral $\propto q^i q^j$, where $i, j = 1, 2, \ldots, d-1$, and a scalar integral:

$$\int d^d q \;\; q^i q^j \; f(q_0, \vec{q}^{\,2}) \;=\; \frac{\delta^{ij}}{d-1} \int d^d q \;\; \vec{q}^{\,2} \; f(q_0, \vec{q}^{\,2}) \tag{B.1}$$

All standard one-loop integrals listed at the end of the Appendix were determined by means of the following Feynman parameter formulas and d dimensional momentum integrals.

Feynman Parameters

$$\frac{1}{A^\alpha B^\beta} \;=\; \frac{\Gamma(\alpha+\beta)}{\Gamma(\alpha)\Gamma(\beta)} \int_0^1 dx \, \frac{x^{\alpha-1}(1-x)^{\beta-1}}{(xA+(1-x)B)^{\alpha+\beta}} \tag{B.2}$$

$$\frac{1}{A^\alpha B^\beta} \;=\; \frac{\Gamma(\alpha+\beta)}{\Gamma(\alpha)\Gamma(\beta)} \int_0^\infty d\lambda \, \frac{\lambda^{\alpha-1}}{(\lambda A+B)^{\alpha+\beta}} \tag{B.3}$$

Momentum Integrals

$$\int \frac{d^dq}{(2\pi)^d} \frac{1}{(-q^2+\Delta-i\epsilon)^n} = i\,(4\pi)^{-d/2} \frac{\Gamma(n-\frac{d}{2})}{\Gamma(n)} (\Delta-i\epsilon)^{\frac{d}{2}-n} \tag{B.4}$$

$$\int \frac{d^dq}{(2\pi)^d} \frac{1}{(-q^2\pm 2qp+\Delta-i\epsilon)^n} = i\,(4\pi)^{-d/2} \frac{\Gamma(n-\frac{d}{2})}{\Gamma(n)} (\Delta+p^2-i\epsilon)^{\frac{d}{2}-n} \tag{B.5}$$

Standard One-Loop Integrals

($a \to a+i\epsilon$ and $b \to b+i\epsilon$ are understood)

$$\int \frac{d^dk}{(2\pi)^d} \frac{1}{(-k^2-i\epsilon)^\alpha(-(k-q)^2-i\epsilon)^\beta} = \tag{B.6}$$

$$= \frac{i2^{-d}\pi^{-d/2}\,(-q^2)^{\frac{d}{2}-\alpha-\beta}\,\Gamma\left(\frac{d}{2}-\alpha\right)\Gamma\left(\frac{d}{2}-\beta\right)\Gamma\left(-\frac{d}{2}+\alpha+\beta\right)}{\Gamma(\alpha)\Gamma(d-\alpha-\beta)\Gamma(\beta)}$$

$$\int \frac{d^dk}{(2\pi)^d} \frac{1}{(-k_0-a)^\alpha(-k^2-i\epsilon)^\gamma} = \tag{B.7}$$

$$= \frac{i4^{-\gamma}(-a)^{d-\alpha-2\gamma}\pi^{-d/2}\Gamma\left(\frac{d}{2}-\gamma\right)\Gamma(-d+\alpha+2\gamma)}{\Gamma(\alpha)\Gamma(\gamma)}$$

$$\int \frac{d^dk}{(2\pi)^d} \frac{1}{(-k_0-i\epsilon)^\alpha(-k_0-a)^\beta(-k^2-i\epsilon)^\gamma} = \tag{B.8}$$

$$= \frac{i2^{1-a}(-d)^{a-\alpha-\beta-2\gamma}\pi^{\frac{1}{2}-\frac{a}{2}}\Gamma(a-\alpha-2\gamma)\Gamma(-a+\alpha+\beta+2\gamma)}{\Gamma(\beta)\Gamma\left(\frac{1}{2}(a-2\gamma+1)\right)\Gamma(\gamma)}$$

$$\int \frac{d^dk}{(2\pi)^d} \frac{1}{(+k_0-i\epsilon)^\alpha(-k_0-a)^\beta(-k^2-i\epsilon)^\gamma} = \tag{B.9}$$

$$= \frac{i4^{-\gamma}(-a)^{d-\alpha-\beta-2\gamma}\pi^{-d/2}\Gamma\left(\frac{d}{2}-\gamma\right)\Gamma(-d+2\gamma+1)\Gamma(-d+\alpha+\beta+2\gamma)}{\Gamma(\beta)\Gamma(\gamma)\Gamma(-d+\alpha+2\gamma+1)}$$

$$\cdot\,(\csc(\pi(d-\alpha-2\gamma))\sin(\pi\alpha)+1)$$

$$\int \frac{d^dk}{(2\pi)^d} \frac{1}{(+k_0-a)^\alpha (-k_0-a)^\beta (-k^2-i\epsilon)^\gamma} \;=\; \tag{B.10}$$

$$= \frac{i 2^{-\alpha-\beta-2\gamma+1} (-a)^{d-\alpha-\beta-2\gamma} \pi^{-d/2} \Gamma\left(\frac{d}{2}-\gamma\right) \Gamma(-d+2\gamma+1) \Gamma(-d+\alpha+\beta+2\gamma)}{\Gamma(\alpha)\Gamma(\beta)\Gamma(\gamma)}$$

$$\cdot \left(\Gamma(\beta)\, {}_2\tilde{F}_1\left(1-\alpha,-d+2\gamma+1;-d+\beta+2\gamma+1;-1\right) + \Gamma(\alpha)\, {}_2\tilde{F}_1\left(1-\beta,-d+2\gamma+1;-d+\alpha+2\gamma+1;-1\right) \right)$$

$$\int \frac{d^dk}{(2\pi)^d} \frac{1}{(-k_0-a)^\alpha (-k_0-b)^\beta (-k^2-i\epsilon)} \;=\; \tag{B.11}$$

$$= \frac{i(-b)^{d-\alpha-\beta-2} \pi^{-d/2} \Gamma\left(\frac{d}{2}-1\right) \Gamma(-d+\alpha+\beta+2)\, {}_2F_1\left(\alpha,-d+\alpha+\beta+2;\alpha+\beta;\frac{b-a}{b}\right)}{4\Gamma(\alpha+\beta)}$$

Furthermore the integral

$$\int \frac{d^dk}{(2\pi)^d} \frac{1}{(+k_0-a)^\alpha (-k_0-b)^\beta (-k^2-i\epsilon)} \tag{B.12}$$

has been used for $\alpha = 1, 2, 3, 4$ in several two-loop calculations. We have computed it with the same methods as the ones above. The expressions are however a bit lengthy and are therefore not displayed here.

Appendix C

Relations Among the SU(3) Generators

The T^A denote the SU(3) generators in the fundamental representation **3** and the $\bar{T}^A = -(T^A)^*$ the SU(3) generators in the anti-representation $\bar{\mathbf{3}}$.

$$\mathrm{tr}[T^A T^B] = \mathrm{tr}[\bar{T}^A \bar{T}^B] = T\,\delta^{AB}\,; \quad T = \frac{1}{2} \tag{C.1}$$

$$T^A T^A = C_F 1 \tag{C.2}$$
$$\bar{T}^A \bar{T}^A = C_F \bar{1} \tag{C.3}$$

$$\left[T^A, T^B\right] = i\,f^{ABC} T^C \tag{C.4}$$
$$\left[\bar{T}^A, \bar{T}^B\right] = i\,f^{ABC} \bar{T}^C \tag{C.5}$$

$$T^A T^B = \frac{1}{2}\left[\frac{1}{N_c}\delta^{AB}\,1 + d^{ABC}\,T^C + i\,f^{ABC}\,T^C\right] \tag{C.6}$$
$$\bar{T}^A \bar{T}^B = \frac{1}{2}\left[\frac{1}{N_c}\delta^{AB}\,\bar{1} - d^{ABC}\,\bar{T}^C + i\,f^{ABC}\,\bar{T}^C\right] \tag{C.7}$$

The f^{ABC} are totally antisymmetric and the d^{ABC} are totally symmetric.

$$f^{ABC} f^{ABD} = C_A\,\delta^{CD} \tag{C.8}$$
$$d^{AAB} = 0 \tag{C.9}$$
$$d^{ABC} f^{ABD} = 0 \tag{C.10}$$
$$d^{ABC} d^{ABD} = C_d\,\delta^{CD} \tag{C.11}$$

The basic color factors are:

$$C_A = N_c = 3 \tag{C.12}$$

$$C_F = \frac{N_c^2 - 1}{2N_c} \tag{C.13}$$

$$C_d = 8C_F - 3C_A \tag{C.14}$$

$$C_1 = \frac{1}{2}C_F(C_A - 2C_F) \tag{C.15}$$

$$\frac{1}{N_c} = (C_A - 2C_F) \tag{C.16}$$

Useful formulae:

$$T^B T^A T^B = (C_F - \tfrac{1}{2}C_A)\, T^A \tag{C.17}$$

$$\bar{T}^B \bar{T}^A \bar{T}^B = (C_F - \tfrac{1}{2}C_A)\, \bar{T}^A \tag{C.18}$$

$$if^{ABC} T^B T^C = -\tfrac{1}{2}C_A\, T^A \tag{C.19}$$

$$if^{ABC} \bar{T}^B \bar{T}^C = -\tfrac{1}{2}C_A\, \bar{T}^A \tag{C.20}$$

Fierz identity:

$$T^A_{ij} T^A_{kl} = \bar{T}^A_{ij} \bar{T}^A_{kl} = \frac{1}{2}\big(\delta_{il}\delta_{kj} - (C_A - 2C_F)\, \delta_{ij}\delta_{kl}\big) \tag{C.21}$$

Bibliography

[1] Tevatron Electroweak Working Group, "Combination of CDF and D0 Results on the Mass of the Top Quark," 2008.

[2] J. A. Aguilar-Saavedra *et al.*, "Tesla technical design report part iii: Physics at an e+e- linear collider," 2001.

[3] I. I. Y. Bigi, Y. L. Dokshitzer, V. A. Khoze, J. H. Kuhn, and P. M. Zerwas, "Production and Decay Properties of Ultraheavy Quarks," *Phys. Lett.*, vol. B181, p. 157, 1986.

[4] C. Farrell and A. H. Hoang, "The large Higgs energy region in Higgs associated top pair production at the linear collider," *Phys. Rev.*, vol. D72, p. 014007, 2005.

[5] C. Farrell and A. H. Hoang, "Next-to-leading-logarithmic QCD corrections to the cross section sigma(e+ e- –> t anti-t H) at 500-GeV," *Phys. Rev.*, vol. D74, p. 014008, 2006.

[6] M. J. Strassler and M. E. Peskin, "The Heavy top quark threshold: QCD and the Higgs," *Phys. Rev.*, vol. D43, pp. 1500–1514, 1991.

[7] R. Harlander, M. Jezabek, and J. H. Kuhn, "Higgs effects in top quark pair production," *Acta Phys. Polon.*, vol. 27, pp. 1781–1788, 1996.

[8] K. Fujii, T. Matsui, and Y. Sumino, "Physics at t anti-t threshold in e+ e- collisions," *Phys. Rev.*, vol. D50, pp. 4341–4362, 1994.

[9] M. Martinez and R. Miquel, "Multi-parameter fits to the t anti-t threshold observables at a future e+ e- linear collider," *Eur. Phys. J.*, vol. C27, pp. 49–55, 2003.

[10] J. Letts and P. Mattig, "Direct determination of the CKM matrix from decays of W bosons and top quarks at high energy e+ e- colliders," *Eur. Phys. J.*, vol. C21, pp. 211–223, 2001.

[11] W. Bernreuther, "Top quark physics at the LHC," *J. Phys.*, vol. G35, p. 083001, 2008.

[12] A. Djouadi *et al.*, "International Linear Collider Reference Design Report Volume 2: PHYSICS AT THE ILC," 2007.

[13] K. G. Chetyrkin and M. Steinhauser, "The relation between the MS-bar and the on-shell quark mass at order alpha(s)**3," *Nucl. Phys.*, vol. B573, pp. 617–651, 2000.

[14] A. H. Hoang, M. C. Smith, T. Stelzer, and S. Willenbrock, "Quarkonia and the pole mass," *Phys. Rev.*, vol. D59, p. 114014, 1999.

[15] A. H. Hoang and T. Teubner, "Top quark pair production close to threshold: Top mass, width and momentum distribution," *Phys. Rev.*, vol. D60, p. 114027, 1999.

[16] A. H. Hoang *et al.*, "Top-antitop pair production close to threshold: Synopsis of recent NNLO results," *Eur. Phys. J. direct*, vol. C2, p. 1, 2000.

[17] A. H. Hoang, "Heavy quarkonium dynamics," in *At the Frontier of Particle Physics/Handbook of QCD* (M. Shifman, ed.), vol. 4, World Scientific, Singapore, 2002.

[18] B. A. Kniehl, A. A. Penin, V. A. Smirnov, and M. Steinhauser, "Potential NRQCD and heavy-quarkonium spectrum at next-to- next-to-next-to-leading order," *Nucl. Phys.*, vol. B635, pp. 357–383, 2002.

[19] B. A. Kniehl, A. A. Penin, M. Steinhauser, and V. A. Smirnov, "Heavy-quarkonium creation and annihilation with O(alpha(s)**3 ln(alpha(s))) accuracy. ((V))," *Phys. Rev. Lett.*, vol. 90, p. 212001, 2003.

[20] A. A. Penin, V. A. Smirnov, and M. Steinhauser, "Heavy quarkonium spectrum and production / annihilation rates to order beta(0)**3 alpha(s)**3," *Nucl. Phys.*, vol. B716, pp. 303–318, 2005.

[21] M. Beneke, Y. Kiyo, and A. A. Penin, "Ultrasoft contribution to quarkonium production and annihilation," *Phys. Lett.*, vol. B653, pp. 53–59, 2007.

[22] M. Beneke, Y. Kiyo, and K. Schuller, "Third-order Coulomb corrections to the S-wave Green function, energy levels and wave functions at the origin," *Nucl. Phys.*, vol. B714, pp. 67–90, 2005.

[23] A. Pineda, "Next-to-leading-log renormalization-group running in heavy-quarkonium creation and annihilation," *Phys. Rev.*, vol. D66, p. 054022, 2002.

[24] A. H. Hoang, A. V. Manohar, I. W. Stewart, and T. Teubner, "A renormalization group improved calculation of top quark production near threshold," *Phys. Rev. Lett.*, vol. 86, pp. 1951–1954, 2001.

[25] A. H. Hoang, A. V. Manohar, I. W. Stewart, and T. Teubner, "The threshold t anti-t cross section at NNLL order," *Phys. Rev.*, vol. D65, p. 014014, 2002.

[26] A. H. Hoang, "Three-loop anomalous dimension of the heavy quark pair production current in non-relativistic qcd," *Phys. Rev.*, vol. D69, p. 034009, 2004.

[27] A. H. Hoang, "Top pair production at threshold and effective theories," *Acta Phys. Polon.*, vol. B34, pp. 4491–4509, 2003.

[28] M. Stahlhofen, Diploma Thesis, Technical University Munich, 2005.

[29] A. H. Hoang and C. J. Reisser, "Electroweak absorptive parts in nrqcd matching conditions," 2004.

[30] A. H. Hoang and C. J. Reisser, "On electroweak matching conditions for top pair production at threshold," *Phys. Rev.*, vol. D74, p. 034002, 2006.

[31] M. E. Luke, A. V. Manohar, and I. Z. Rothstein, "Renormalization group scaling in nonrelativistic QCD," *Phys. Rev.*, vol. D61, p. 074025, 2000.

[32] A. H. Hoang and I. W. Stewart, "Ultrasoft renormalization in non-relativistic QCD," *Phys. Rev.*, vol. D67, p. 114020, 2003.

[33] A. H. Hoang and M. Stahlhofen, "Two-Loop Ultrasoft Running of the $\mathcal{O}(v^2)$ QCD Quark Potentials," *Phys. Rev.*, vol. D75, p. 054025, 2007.

[34] H. Georgi, "Effective field theory," *Ann. Rev. Nucl. Part. Sci.*, vol. 43, pp. 209–252, 1993.

[35] I. Z. Rothstein, "TASI lectures on effective field theories," 2003.

[36] M. Neubert, "Effective field theory and heavy quark physics," 2005.

[37] A. V. Manohar, "Effective field theories," 1996.

[38] M. E. Peskin and D. V. Schroeder, *An Introduction to Quantum Field Theory*. Addison-Wesley Publishing Company, 1995.

[39] J. F. Donoghue, E. Golowich, and B. R. Holstein, *Dynamics of the standard model*, vol. 2. 1992.

[40] A. H. Hoang, "Lecture: Introduction to effective theories in particle physics." Graduate Lecture held at Technical University Munich, SoSe 2004.

[41] S. Weinberg, *The Quantum Theory of fields*, vol. 2. Cambridge University Press, 1996.

[42] T. Appelquist and J. Carazzone, "Infrared Singularities and Massive Fields," *Phys. Rev.*, vol. D11, p. 2856, 1975.

[43] H. Georgi, "An effective field theory for heavy quarks at low energies," *Phys. Lett.*, vol. B240, pp. 447–450, 1990.

[44] A. J. Buras, "Weak Hamiltonian, CP violation and rare decays," 1998.

[45] E. Witten, "Short Distance Analysis of Weak Interactions," *Nucl. Phys.*, vol. B122, p. 109, 1977.

[46] W. E. Caswell and G. P. Lepage, "Effective lagrangians for bound state problems in qed, qcd, and other field theories," *Phys. Lett.*, vol. B167, p. 437, 1986.

[47] G. T. Bodwin, E. Braaten, and G. P. Lepage, "Rigorous QCD analysis of inclusive annihilation and production of heavy quarkonium," *Phys. Rev.*, vol. D51, pp. 1125–1171, 1995.

[48] V. S. Fadin and V. A. Khoze, "Threshold Behavior of Heavy Top Production in e+ e- Collisions," *JETP Lett.*, vol. 46, pp. 525–529, 1987.

[49] M. B. Voloshin, "On Dynamics of Heavy Quarks in Nonperturbative QCD Vacuum," *Nucl. Phys.*, vol. B154, p. 365, 1979.

[50] H. Leutwyler, "How to Use Heavy Quarks to Probe the QCD Vacuum," *Phys. Lett.*, vol. B98, p. 447, 1981.

[51] V. S. Fadin and O. I. Yakovlev, "Nonperturbative correction to the cross-section of t anti- t quark pair production near threshold," *Sov. J. Nucl. Phys.*, vol. 53, pp. 688–691, 1991.

[52] P. Labelle, "Effective field theories for QED bound states: Extending nonrelativistic QED to study retardation effects," *Phys. Rev.*, vol. D58, p. 093013, 1998.

[53] A. Pineda and J. Soto, "Effective field theory for ultrasoft momenta in NRQCD and NRQED," *Nucl. Phys. Proc. Suppl.*, vol. 64, pp. 428–432, 1998.

[54] A. Pineda, "Renormalization group improvement of the NRQCD Lagrangian and heavy quarkonium spectrum," *Phys. Rev.*, vol. D65, p. 074007, 2002.

[55] A. V. Manohar, J. Soto, and I. W. Stewart, "The renormalization group for correlated scales: One-stage versus two-stage running," *Phys. Lett.*, vol. B486, pp. 400–405, 2000.

[56] N. Brambilla, A. Pineda, J. Soto, and A. Vairo, "Potential NRQCD: An effective theory for heavy quarkonium," *Nucl. Phys.*, vol. B566, p. 275, 2000.

[57] G. 't Hooft and M. J. G. Veltman, "Regularization and Renormalization of Gauge Fields," *Nucl. Phys.*, vol. B44, pp. 189–213, 1972.

[58] J. C. Collins, *Renormalization*. Cambridge University Press, 1984.

[59] M. Beneke and V. Smirnov, "Asymptotic expansion of Feynman integrals near threshold," *Nucl. Phys.*, vol. B522, p. 321, 1998.

[60] B. Grinstein and I. Z. Rothstein, "Effective field theory and matching in non-relativistic gauge theories," *Phys. Rev.*, vol. D57, pp. 78–82, 1998.

[61] H. Georgi, "On-shell effective field theory," *Nucl. Phys.*, vol. B361, pp. 339–350, 1991.

[62] A. V. Manohar and I. W. Stewart, "Running of the heavy quark production current and 1/v potential in qcd," *Phys. Rev.*, vol. D63, p. 054004, 2001.

[63] A. V. Manohar and I. W. Stewart, "Renormalization group analysis of the QCD quark potential to order v**2," *Phys. Rev.*, vol. D62, p. 014033, 2000.

[64] A. Manohar and M. Wise, "Heavy quark physics," *Camb. Monogr. Part. Phys. Nucl. Phys. Cosmol.*, vol. 10, pp. 1–191, 2000.

[65] A. V. Manohar and I. W. Stewart, "The qcd heavy-quark potential to order v**2: One loop matching conditions," *Phys. Rev.*, vol. D62, p. 074015, 2000.

[66] A. H. Hoang, A. V. Manohar, and I. W. Stewart, "The running coulomb potential and lamb shift in qcd," *Phys. Rev.*, vol. D64, p. 014033, 2001.

[67] A. Czarnecki and K. Melnikov, "Two-loop QCD corrections to the heavy quark pair production cross section in e+ e- annihilation near the threshold," *Phys. Rev. lett.*, vol. 80, pp. 2531–2534, 1998.

[68] M. Beneke, A. Signer, and V. A. Smirnov, "Two-loop Correction to the Leptonic Decay of Quarkonium," *Phys. Rev. lett.*, vol. 80, pp. 2535–2538, 1998.

[69] W. A. Bardeen, A. J. Buras, D. W. Duke, and T. Muta, "Deep Inelastic Scattering Beyond the Leading Order in Asymptotically Free Gauge Theories," *Phys. Rev.*, vol. D18, p. 3998, 1978.

[70] A. V. Manohar and I. W. Stewart, "The zero-bin and mode factorization in quantum field theory," *Phys. Rev.*, vol. D76, p. 074002, 2007.

[71] C. W. Bauer, D. Pirjol, and I. W. Stewart, "Soft-collinear factorization in effective field theory," *Phys. Rev.*, vol. D65, p. 054022, 2002.

[72] H. Lehmann, K. Symanzik, and W. Zimmermann, "On the formulation of quantized field theories," *Nuovo Cim.*, vol. 1, pp. 205–225, 1955.

[73] R. F. Streater and A. S. Wightman, *PCT, spin and statistics, and all that.* Redwood City, USA: Addison-Wesley, 1989.

[74] A. H. Hoang, "1S and MSbar Bottom Quark Masses from Upsilon Sum Rules," *Phys. Rev.*, vol. D61, p. 034005, 2000.

[75] J. D. Bjorken and S. D. Drell., *Relativistic Quantum Mechanics.* McGraw-Hill, 1964.

[76] E. H. Wichman and C. H. Woo *J. Math. Phys.*, vol. 2, p. 178, 1961.

[77] L. Hostler *J. Math. Phys.*, vol. 5, p. 591, 1964.

[78] J. Schwinger *J. Math. Phys.*, vol. 5, p. 1606, 1964.

[79] K. Melnikov and O. I. Yakovlev, "Top near threshold: All alpha-S corrections are trivial," *Phys. Lett.*, vol. B324, pp. 217–223, 1994.

[80] A. H. Hoang, Z. Ligeti, and A. V. Manohar, "B decays in the Upsilon expansion," *Phys. Rev.*, vol. D59, p. 074017, 1999.

[81] A. H. Hoang and T. Teubner, "Top quark pair production at threshold: Complete next-to- next-to-leading order relativistic corrections," *Phys. Rev.*, vol. D58, p. 114023, 1998.

[82] C. Reisser, PhD Thesis, Technical University Munich, 2008, ISBN 978-3-86727-607-8.

[83] N. Brambilla, A. Pineda, J. Soto, and A. Vairo, "The infrared behaviour of the static potential in perturbative QCD," *Phys. Rev.*, vol. D60, p. 091502, 1999.

[84] A. A. Penin, A. Pineda, V. A. Smirnov, and M. Steinhauser, "M(B/c*) - M(B/c) splitting from nonrelativistic renormalization group," *Phys. Lett.*, vol. B593, pp. 124–134, 2004.

[85] A. Pineda and A. Signer, "Heavy quark pair production near threshold with potential non-relativistic QCD," *Nucl. Phys.*, vol. B762, pp. 67–94, 2007.

[86] A. A. Penin, A. Pineda, V. A. Smirnov, and M. Steinhauser, "Spin dependence of heavy quarkonium production and annihilation rates: Complete next-to-next-to-leading logarithmic result," *Nucl. Phys.*, vol. B699, pp. 183–206, 2004.

[87] G. Heinrich and G. Leibbrandt, "Split dimensional regularization for the Coulomb gauge at two loops," *Nucl. Phys.*, vol. B575, pp. 359–382, 2000.

[88] A. G. Grozin, "Lectures on perturbative HQET. I," 2000.

[89] A. V. Manohar, "The HQET/NRQCD Lagrangian to order alpha/m^3," *Phys. Rev.*, vol. D56, pp. 230–237, 1997.

[90] T. Huber and D. Maitre, "HypExp, a Mathematica package for expanding hypergeometric functions around integer-valued parameters," *Comput. Phys. Commun.*, vol. 175, pp. 122–144, 2006.

[91] K. G. Chetyrkin and F. V. Tkachov, "Integration by Parts: The Algorithm to Calculate beta Functions in 4 Loops," *Nucl. Phys.*, vol. B192, pp. 159–204, 1981.

[92] R. Mertig, M. Böhm, and A. Denner, "Feyn Calc - Computer-algebraic calculation of Feynman amplitudes," *Comp. Phys. Comm.*, vol. 64, p. 345, 1991.

[93] V. Gimenez, "Two loop calculation of the anomalous dimension of four fermion operators with static heavy quarks," *Nucl. Phys.*, vol. B401, pp. 116–167, 1993.

Acknowledgements

I would like to thank

André Hoang
Edoardo Mirabella
Jianhui Zhang
Thomas Hahn
Felix Schwab
Maike Trenkel
Stefan Kallweit
Tobias Kasprzik
Christoph Reißer
Caillin Farrell
Arne Weber
Uli Meier
the MPPMUFA
the MPPMUBA
Antonio Pineda
my parents
and
Vanessa Candida

This work was supported in part by the EU network contract
MRTN-CT-2006-035482 (FLAVIAnet).